Inflammation triggers Zeb1-dependent escape from tumor dormancy

by

Jasmine M. De Cock

B.Sc. Biochemistry with Extra Mural Year
King's College London, 2010

SUBMITTED TO THE DEPARTMENT OF BIOLOGY
IN PARTIAL FULFILLMENT OF THE REQUIREMENTS
FOR THE DEGREE OF

DOCTOR OF PHILOSOPHY IN BIOLOGY
AT THE
MASSACHUSETTS INSTITUTE OF TECHNOLOGY

JUNE 2016

Signature of Author: …….....
Department of Biology
March 18, 2016

Certified by: ……..…….....…….……
Dr. Robert A. Weinberg
Professor of Biology
Thesis Supervisor

Accepted by: ……..…….....……
Dr. Michael Hemann
Professor of Biology
Chairperson, Biology Graduate Committee

Inflammation triggers Zeb1-dependent escape from tumor dormancy

by

Jasmine M. De Cock

Submitted to the Department of Biology on March 18, 2016
in Partial Fulfillment of the Requirements for the
Degree of Doctor of Philosophy in Biology

Abstract

Metastasis-related mortality for breast cancer patients often occurs many years after treatment of the primary tumor. Inflammation, through the orchestra of immune cells and released inflammatory cytokines, can predispose certain tissues to cancer development and can create a favorable environment for metastatic outgrowth. I evaluated whether lipopolysaccharide (LPS) could induce an inflammatory response, leading to the activation of the cell-biological epithelial-mesenchymal transition (EMT) program in dormant disseminated cancer cells *in vivo*, and subsequent metastatic outgrowth. To model metastatic cellular dormancy, I used a dormant subpopulation of cells (D2A1-d) that were enriched for *in vivo* from the highly metastatic carcinoma cell line D2A1, that was derived from spontaneous murine mammary tumor. The ability of the EMT program to awaken dormant disseminated D2A1-d cells was directly assessed *in vivo,* which resulted in the formation of macro-metastases following a transient induction of either the EMT-transcription factor Snail or Zeb1. Furthermore, the transient induction of Zeb1 led to the generation of $CD29^{+}$ $CD24^{-}$ metastasis-initiating cells. In mice bearing dormant disseminated D2A1-d cells, my findings demonstrated that LPS-treatment resulted in the awakening of D2A1-d cells and metastatic outgrowth in the lungs and bone. The awakening of dormant disseminated D2A1-d cells was dependent, albeit through unknown mechanism, on the presence of neutrophils. The LPS-mediated awakening of dormant disseminated cancer cells was also dependent upon the activation of the EMT-inducing transcription factor Zeb1 in the D2A1-d cells. In conclusion, my thesis work demonstrated that inflammation can trigger the escape of metastatic dormancy *in vivo*.

Thesis Supervisor: Robert A. Weinberg

Title: Professor of Biology, MIT; Member, Whitehead Institute for Biomedical Research

“ Science and everyday life cannot and should not be separated. Science, for me, gives a partial explanation of life. In so far as it goes, it is based on fact, experience and experiment.”

Rosalind Franklin, in a letter to her father (1940)

Dedication

To my great-great-grandmother, Carrie B. Morgan Dawson,
born eight years after the Emancipation Proclamation,
for her wisdom and vision
that a female child of her lineage would one day be allowed by law
to study at such a prestigious New England university.

Acknowledgements

I am forever indebted to my pillar of inspiration and encouragement, Dr Robert A. Weinberg: a true man of wisdom, class, charisma and integrity! Thank you so much for all that you have imparted to me from my very first interview with you at the MIT Biology Open House in the winter of 2010 and for your commitment to love for family, empowerment of nations through researchers to bring about change in the world. There are not enough words to say how much you have shaped my life, more importantly my vision of myself. Thank you for the numerous introductions you have made for me throughout the years. I am grateful to have met Richard Goldsby, Barbara Osborne and Lidia Villa-Komaroff and to have benefited from their wisdom.

I am grateful that I was able to share this experience with my fellow labmates in the Weinberg lab. In particular, I would like to thank Zuzana Keckesova, who is made of starlight watched me closely for the first six months and never strayed far off as I began to come into my own; Tsukasa Shibue, who patiently answered all my burning questions with grace and wisdom; Ferenc Reinhardt, for his skilled surgeon-like hands and warm and listening heart; Anushka Dongre, for her kind-nature and professional drive, Christine Chaffer, Cornelia Kroeger and Julia Froese for motivating me to keep moving whether it be in dance or strenuous exercise, Brian Bierie, Jordan Krall and Wai Leong Tam, my " late-night 309 mates" for being there whenever I needed. I thank my "laboratory" mothers, Elinor Ng Eaton, Mary Brooks, Joana Liu Donaher, Christine

Hickey, Sumiko Williams for always demonstrating excellence before me, both publicly and privately.

I would like to thank the MIT/ Cambridge community at large for providing me with support and safe-haven that I needed to thrive during my studies. I would like to thank my committee members Jacqueline Lees, Richard Hynes for their insightful advice and useful suggestions, and Paula Hammond for accepting to be my external thesis advisor. Dean Blanche Staton has advocated for me and has allowed me to participate in multiple initiatives at MIT, including MIT/Imperial College of London Global Fellows Program, Programming for Education and Advocacy of Cross Cultural Exchange (P.E.A.C.E), Mind Hand Heart initiative, MIT Summer Research Program (MSRP). I will be forever grateful to Anne Deconinck for giving me the opportunity of a lifetime to not only meet but to also present my research to the now King Philippe of Belgium! I am grateful to my church family at St Paul's AME Church for replenishing my soul each week, for my fellow missionaries of the Margaret Hazel Women's Missionary Society and for my fellow "dancing warriors" in the Liturgical Dance Ministry.

I thank my parents, Angela Victoria Shaw and Georges Julien De Cock for their sacrificial and unconditional love. My deepest gratitude to my brother Garrett Thomas De Cock, my sister-in-law Michelle O'keeffe, my brother Karel Alois De Cock, my sister-in-law Naambo Shivute for understanding my absence during family holidays and for missing birthdays and the births of my two nephews Esaiah Aurelio De Cock and

Dominic Shaw De Cock. I thank Warren Anthony Whyte for supporting me every step of the way, with patience, great insight, humor and love.

I have been blessed by the support of my loving friends through this journey. I am so grateful for my childhood friends Eline Van Uffelen, Veronique Herreweghe, Bintou Zerbo, Maita Gusiur, Sebastian Dahl, Nicholas Dechamps, Jivaan Bennett, and my closest adulthood friends Rumbi Manzou, Margaret Mutumba, Stephanie Adu, Obiageli Ofili, Akyini Apopa, Kiran Atwal, Sharla Duncan, Antonia Cuff, Uche Aniagwu, Nyasha Munjoma, Samuel Franklin Menoube and Christian Ngono for visiting me, checking-in on me and for making sure that I did not lose sight of who I am and kept smiling!

Lastly, I give thanks to the unseen and the unsung heroes who have contributed in making today possible. The completion of this gargantuan task is the culmination of many efforts, tears, sweat, disappointments, joys and praises.

Table of Contents

Chapter 1:

Introduction

Cancer Research at the forefront of an unmet global need

"The Emperor of all Maladies", "malignant tumor", "abnormal growth", "neoplasm": the saying that "a rose by any other name, would smell as sweet", can not be farther from the truth in regard to cancer. Cancer, a disease resulting from the uncontrolled division of abnormal cells, is the generic term describing the amalgamation of more than one hundred malignant growths that can affect almost any tissue. Of these, ~80% of life-threatening cancers are carcinomas, i.e. tumors arising from epithelial tissues, such as the skin, liver, breast and prostate. Taken together, cancer is the second leading cause of death worldwide, following closely behind heart disease, and it knows no boundaries: all familial lineages across time, geography, ethnicity, gender, class and age can be affected.

In 1938 James Ewing, a pioneer in the field cancer research and tumor pathology wrote: "public interest in the cancer problem is now at the highest point in history" (Eckhouse, S. *et al* 2008). However, since then, cancer research has expanded to a multi billion dollar global enterprise extending research funding from governmental agencies and industrial share holders to philanthropic funders (Eckhouse, S. *et al* 2008). In the United States, the National Cancer Institute accounts for the largest absolute spending; and there have been many political declarations made across the decades from President Richard Nixon declaring a national "War on Cancer" in 1971 to President Barack Obama announcing in his final State of the Union address that " with a new moonshot, America can cure cancer once and for all".

Despite decades of intense investigation, countless cancer-related discoveries, more remains to be learnt about the nature and the progression ofcancer. In as much as tangible progress in treating and preventing certain cancers has certainly been made through advances in surgical techniques, radiotherapy and the development of molecularly targeted therapies, a concerted effort must be made in ensuring global participation and access to cancer research studies. According to the World Health Organization's World Cancer Report of 2014, Africa, Asia, Central and South America account for 70% of the world's cancer-related deaths. Focusing our efforts on the cancer types that most afflict people from these regions will guarantee a more prosperous tomorrow.

The invasion-metastatic cascade, the modern day Charon crossing of the river Styx

The vast majority of cancer-related deaths can be attributed to metastases i.e., most cancer patients do not succumb to death from the primary tumor but from the outgrowth of tumors at distant sites (Steeg, P.S. 2006). Macroscopic metastases, also referred to as metastatic outgrowths, are dependent upon the successful completion of several sequential steps of the invasion-metastatic cascade. Thus, as the French gynecologist Jean Claude Recamier stated in 1829, "metastasis is the transfer of disease from one organ or part to another not directly connected to it"(Recamier, J.C. 1829). As depicted in Figure 1, the metastatic cascade begins with a confined primary tumor at the site of tumor origin and ends with metastatic outgrowth at a distant anatomical site. The steps of the metastatic cascade can be delineated as follows: 1) carcinoma cells at the tumor margin invade locally through the surrounding extracellular matrix (ECM) and into

the adjacent naïve tissue parenchyma, 2) disseminate in the hematogenous circulation, 3) survive the hemodynamic shear forces and predation by host immune cells in the vasculature, 4) arrest at a distant organ site, 5) extravasate into the parenchyma of distant tissues, 6) survive in the foreign microenvironment, 7) interact with the surrounding ECM, 8) re-initiate proliferation, 9) colonize the foreign microenvironment by forming clinically detectable metastases. Each step along the invasion-metastatic cascade possesses its own challenges and barriers that must be overcome. The overall efficiency of the process is very limited.

Figure 1: The invasion-metastatic cascade

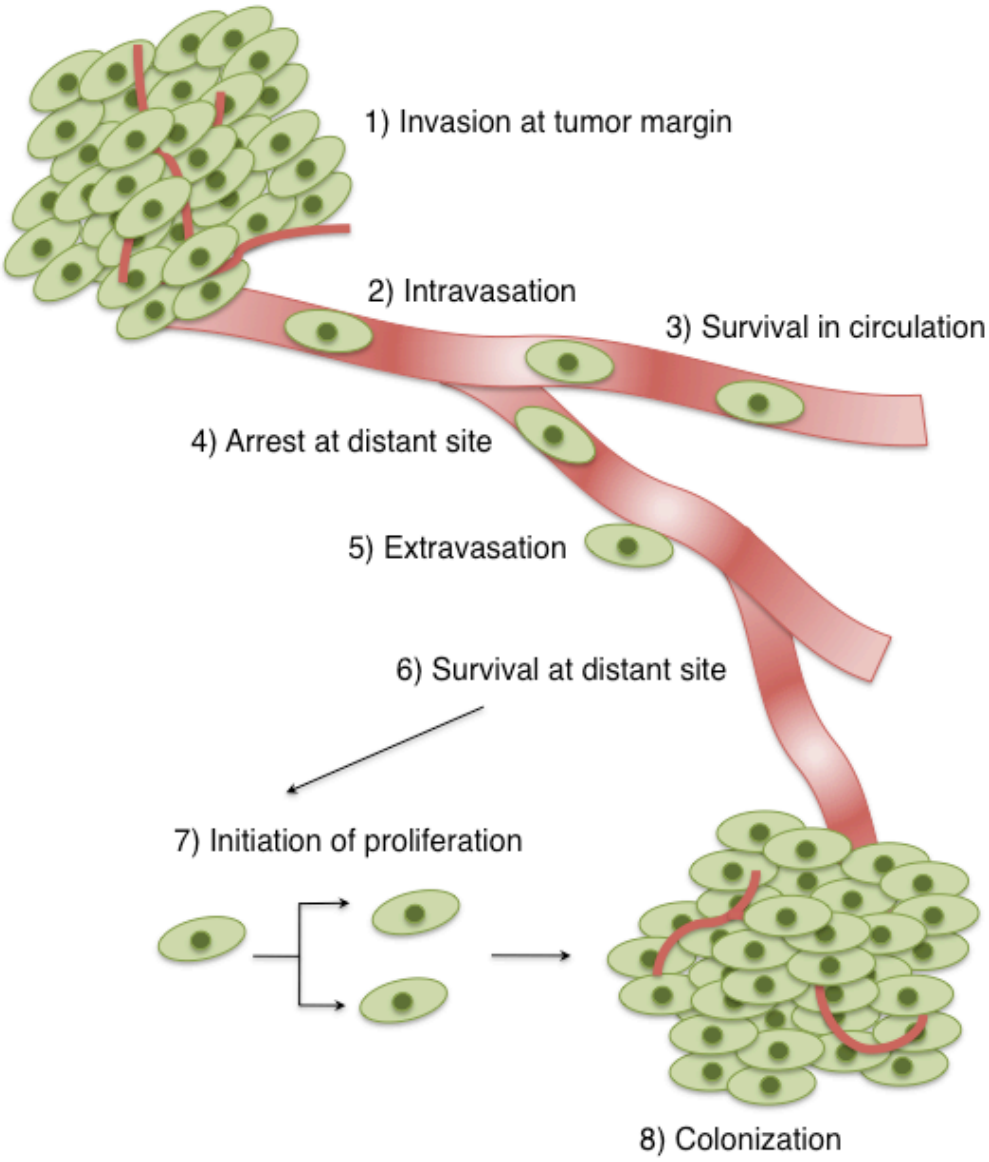

Figure 1. The invasion-metastatic cascade

Schematic depiction of the sequential steps in the invasion-metastatic cascade. (1) Once a primary tumor has formed, carcinoma cells at the margin of the tumor invade locally through the surrounding extracellular matrix (ECM) and into the adjacent naïve tissue parenchyma. (2) Carcinoma cells then enter into the hematogeneous circulation as single cells or as clusters of circulating tumor cells; (3) survive the mechanical and shear stresses in the circulation, and (4) arrest at distant site. (5) At the distant organ site, circulating tumor cells extravasate, potentially in a similar manner to leukocytes and extravasation may be facilitated by platelets and another leukocytes. (6) Once disseminated, carcinoma cells must survive at the distant site, (7) re-initiate proliferation, and (8) colonize i.e. grow from micro-metastases to macro-metastases. Adapted from Valastyan, S. & Weinberg, R. A. 2011.

The Epithelial-to-Mesenchymal Transition (EMT) at the heart of tumor dissemination

In order to overcome the intrinsic barrier that the normal epithelium present to invasion and potentially other barriers, carcinoma cells aberrantly re-activate the epithelial-to-mesenchymal transition (EMT) program, a cell-biological embryonic developmental program (Kalluri, R. & Weinberg, R.A. 2009; Thiery, J.P. *et al* 2009; Yang, J. & Weinberg, R.A. 2008; Hugo, H. *et al* 2007) (Figure 2). The onset of the EMT does not require additional genetic alterations in carcinoma cells, instead the EMT is controlled by various transcriptional and epigenetic regulators (Tam, W.L. & Weinberg, R.A. 2013). In particular, the EMT program is orchestrated by a set of pleiotropically acting transcription factors (TFs), such as Slug (Hajra, K.M. *et al* 2002), Snail (Battle, E. *et al* 2000), Twist (Yang, J. *et al* 2004) and Zeb1 (Eger, A. *et al* 2005). These EMT-TFs repress the expression of epithelial genes such as those encoding E-cadherin and occludin, while promoting the expression of mesenchymal genes such as those specifying N-cadherin and fibronectin.

Figure 2: The basics of the epithelial-mesenchymal transition

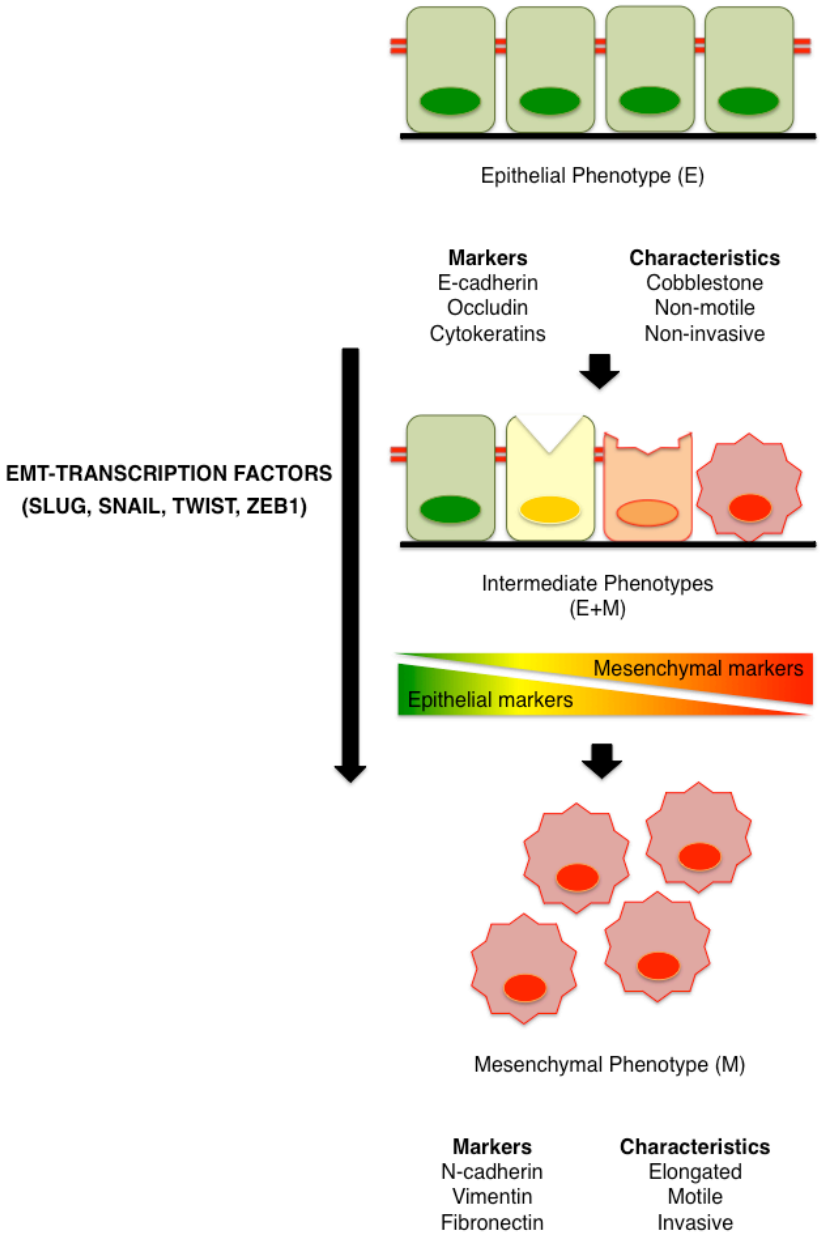

Adapted from Kalluri, R. & Weinberg, R.A. (2009)

Figure 2. The basics of the epithelial-to-mesenchymal transition (EMT)

During an EMT, polarized epithelial cells lose their organized phenotype and gain a scattered spindle-like, mesenchymal phenotype. The EMT is mediated by several transcription factors (including Slug, Snail, Twist, and Zeb1) and is characterized by a loss of tight junctional integrity, increased motility and *de novo* expression of mesenchymal markers, such as N-cadherin and vimentin, fibronectin. The commonly studied EMT transcription factors are listed. Co-expression of markers from both sets of cells defines intermediate or "partial" EMT phenotypes. Adapted from Kalluri, R. & Weinberg, R. A. 2009.

While the EMT program is first operative during implantation of the embryo to allow proper anchoring of the placenta, the EMT can re-occur at various stages of subsequent embryogenesis and, with great delay, in adulthood, such as during organ fibrosis (of the kidney, liver, lung and intestine), inflammation and tissue regeneration (Lopez-Novoa, J.M. & Nieto, M.A. 2009). The cellular response observed under inflammatory stresses within tissues provided the first evidence suggesting that cells could reside in a variety of phenotypic states arrayed along an epithelial to mesenchymal spectrum, thereby creating intermediate or "partial EMTs" (Kalluri, R. & Weinberg, R.A. 2009). Given the different biological processes that the EMT regulates, it is not surprising therefore that the EMT can be activated by heterotypic inductive signals, such as the canonical Wnt, fibroblast growth factor (FGF), bone morphogenetic protein (BMP) signaling pathways during embryonic development, as well as transforming growth factor-β (TGF-β), platelet-derived growth factor (PDGF), and epidermal growth factor (EGF), interleukin-6 (IL-6) and interleukin-1β (IL-1β) during inflammatory injury (Strutz, F. *et al* 2002; Kalluri, R. &Weinberg, R.A. 2009). The various versions of the EMT program are nonetheless mediated by a common set of EMT-TFs.

During the neoplastic EMT program, carcinoma cells detach from the primary tumor by losing their cell-cell interactions, invade into the neighboring normal parenchymal tissue, and enter the hematogenous circulation. Within the circulation, platelets can support the survival of carcinoma cells, maintain the activation of the EMT program, and promote extravasation at the distant metastatic site (Labelle, M. *et al* 2014). The signals that induce the neoplastic EMT program are an active area of research and

include cellular signals such as TGF-β, EGF, PDGF and hepatocyte growth factor (HGF) (Medici, D. *et al* 2008; Kokudo, T. *et al* 2008).

Since the EMT was first described by Elizabeth Hay, a pioneer in Cell Biology, as the "epithelial-mesenchymal transformation" when studying a model of embryonic gastrulation (Hay, E.D. 1968), the term "transformation" has been replaced with "transition" to emphasize the transient and reversible nature of this process. Indeed while the plasticity of the EMT has been widely accepted for both the classical type 1 EMT, seen during implantation, embryogenesis and organ development and the type 2 EMT, associated with tissue regeneration and organ fibrosis, this concept is only currently being explored and expanded to the neoplastic EMT.

Metastatic dormancy, an optional step delaying the ultimate kiss of death

Of the steps outlined above in the metastatic cascade, the most inefficient and crucial step that determines cellular fate (and currently the fate of the individual) is the ability of disseminated tumor cells (DTCs) to re-initiate proliferation at the metastatic site. Metastatic dormancy is the asymptomatic presence of DTCs in organs and tissues (Chambers, A.F. *et al* 2002; Folkman, J. & Kalluri, R. 2004) and is seen in carcinomas originating from the breast, kidney, prostate, and colon (Folkman, J. & Kalluri, R. 2004). Less than 0.01% of DTCs eventually succeed in forming macroscopic metastases, yet it is widely accepted that DTCs are the seeds for later tumor metastases (Fidler, I.J. 1970; Sosa, M.S. *et al* 2011). Indeed, while bone metastasis occurs at a frequency of 10-30% in prostate and breast cancers, (Pantel, K. & Brakenhoff, R.H. 2004; Gath, H.J. &

Brakenhoff, R.H. 1999), DTCs can be detected in >50% of patients (Wikman, H *et al* 2008).

In the specific case of breast cancer, metastases are typically detected within five years of surgery in patients with $HER2^+$ breast cancer, 10 years after surgery in patients with triple-negative breast cancer, and even up to 20 years after surgery in patients with ER^+ breast cancer (Kennecke, H. *et al* 2010; Smid, M. *et al* 2008). Metastases may be detected in patients with melanoma or renal cell carcinoma 10-15 years after initial clinical presentation or more than 15 years later in patients with prostate cancer (McNichols, D.W. *et al* 1981; Freedland, S. J. & Moul, J.W. 2007; Tsao, H. *et al* 1997).

Once extravasated, some carcinoma cells may undergo apoptosis, while other cells may enter a dormant state for several years or decades, presumably due to the inability to grow autonomously or due to unfavorable growth conditions in the metastatic site. The latter may represent an active stress or signaling barrier that DTCs must overcome (Gao, *et al* 2012) or an intrinsic cellular defect that inhibits DTCs from engaging productively with the surrounding ECM (Shibue, T. & Weinber, R. A. 2009; Karrison, T.G. *et al* 1999). Furthermore the cellular microenvironment at a distant site can actively suppress the survival of DTCs, for example by neutrophil-mediated killing of tumor cells (Granot, Z. *et al* 2011). Yet other DTCs may readily proliferate at the metastatic site (Figure 3a).

Figure 3: The fates of disseminated tumor cells

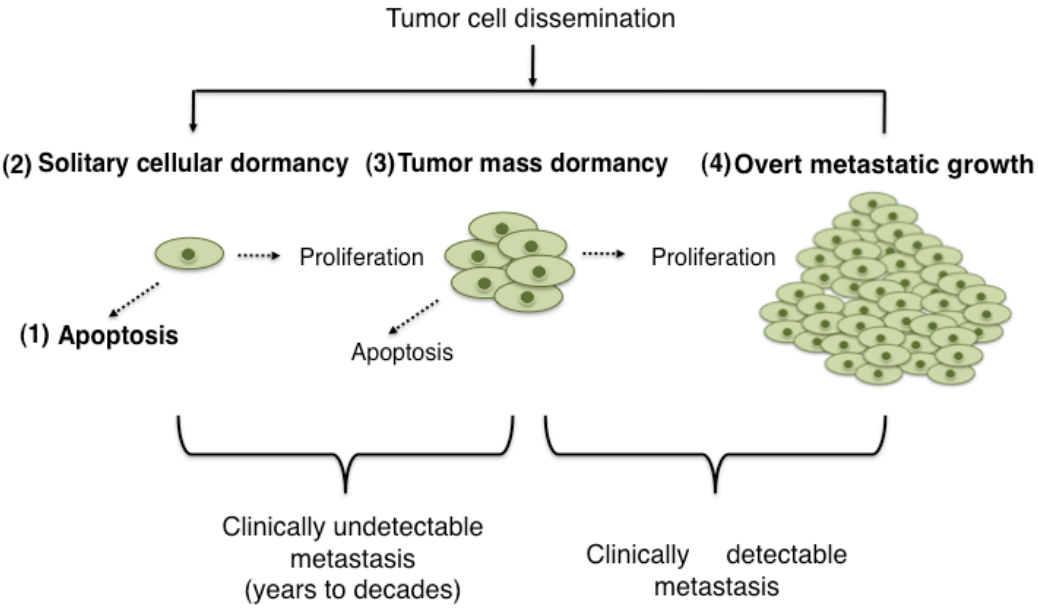

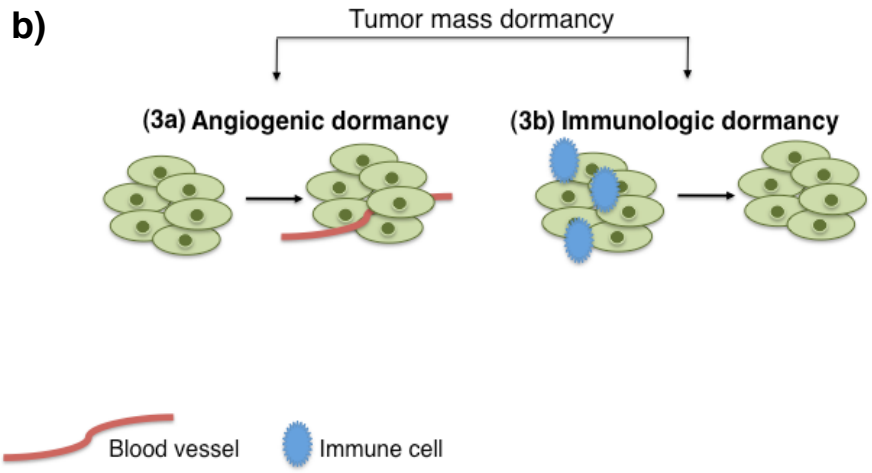

Adapted from Aguirre-Ghiso, J.A. (2007)

Figure 3. The fates of disseminated tumor cells (DTCs)

a) Once in circulation, carcinoma cells may extravasate into the tissue parenchyma or remain lodged intra-vascularly, where four potential fates may await them: (1) the vast majority of carcinoma cells will undergo apoptosis; while others will enter a state of dormancy, either as (2) single solitary cells or as (3) micrometastases i.e. clusters of thousands of cells; while yet (4) other carcinoma cells will resume proliferation and form macro-metastases. **b)** Micro-metastases may exist as a result of (3a) angiogenic dormancy, the balance of pro-and anti-angiogenic factors, or (3b) immunogenic dormancy, by which the tumor mass is actively maintained by the immune system. These forms of dormancy need not be mutually exclusive; it is possible that single solitary dormancy precedes tumor mass dormancy. Adapted from Aguirre-Ghiso, J.A. 2007.

The timing of dissemination may determine whether or not DTCs enter a dormant state. The rationale behind early dissemination leading to dormant DTCs stems from the notion that early-disseminated carcinoma cells may lack key genetic and/or epigenetic changes required for colonization. Evidence in support of dissemination being an early event in tumor progression can be collected from the analysis of bone marrow aspirates from patients with noninvasive lesions (Klein, C.A. 2009) and from preclinical studies using MMTV-Neu mice (Hüsemann, Y. *et al* 2008). In contrast, carcinoma cells that disseminate late in tumor progression, are likely to have acquired all the relevant genetic and/or epigenetic changes necessary for colonization. Working in the opposite direction, late DTCs may express metastasis suppressor genes, such as KISS1, MKK4 and Nm23-H1 (Taylor, J. *et al* 2008).

Types of metastatic dormancy: solitary cellular and tumor mass dormancy

At the sites of metastasis DTCs may exist as indolent micro-metastases, clusters of tens or hundreds of cancer cells persisting at some steady state through a balance between mitosis and apoptosis i.e., tumor mass dormancy (Aguirre-Ghiso, J. A. 2007). Two concepts support this notion: immuno-surveillance (Dunn, G.P. *et al* 2004; Koebel, C.M. *et al* 2007) and angiogenic dormancy (Holmgren, L. *et al* 1995) (Figure 3b). In the case where DTCs are scattered in isolation in the distant tissue, this type of dormancy is termed solitary cellular dormancy (Aguirre-Ghiso, J.A. 2007) and will be explored in greater detail in this thesis.

Angiogenic dormancy relates to the limited blood supply at the metastatic site; this insufficiency leads to the inability of tumors to grow beyond 1-2mm in diameter (Naumov, G.N. *et al* 2006), and has been observed in patients with retinoblastoma (Finkelstein, S. *et al* 1977). Escape from this type of dormancy is marked by the onset of angiogenesis, i.e. the "angiogenic switch" (Naumov, G.N. *et al* 2006). Studies have shown that the switch can occur by removing anti-angiogenic factors, such as TSP-1 (Hanahan, D. & Folkman, J 1996).

Independent of the influence of neoangiogenesis, in the 1950s, Burnet and Thomas recognized that tumors cells could be actively targeted and destroyed by the immune system by a process they termed immunosurveillance. A refinement of immunosurveillance, is immuno-editing i.e., the ability of immune cells to identify and selectively kill highly immunogenic tumor cells thereby allowing carcinoma cells expressing less immunogenic antigens to survive (Koebel, C.M. *et al* 2007). Under these conditions, the immune system actively retains the tumor at a constant mass (Koebel, C.M. *et al* 2007; Rabinovsky, R. *et al* 2007). There are individual case studies that have highlighted clinical evidence of immunosurveillance in immuno-compromised patients that have received transplants containing previously undetected occult tumor cells (Kimura, W. *et al* 1998).

Mechanisms to escape solitary cellular dormancy

In 1934 the Australian pathologist Rupert Willis first proposed the idea of "dormant tumor cells" and the British pathologist Geoffrey Hadfield explained two years

later the apparent paradox between the notion that cancer cells must proliferate uncontrollably by introducing the idea of "temporary mitotic arrest" (Klein, C.A. 2009; Hadfield, G. 1954). However, the mechanisms that regulate the transition between the dormant and proliferative states and markers of dormant DTCs remain largely unknown.

Solitary dormant DTC may exist in a non-proliferative state and lack markers of proliferation such as Ki67 (Pantel, K. *et al* 2009; Wikman, H. *et al* 2008). Indeed, dormant DTCs have been found in bone marrow aspirates in ~36-56% of patients at the time of clinical presentation, irrespective of lymph node status (Braun, S. *et al* 2000; Pierga, J.Y. *et al* 2003). While other organs may not be as readily accessible by pathological analysis, this does not preclude the possibility that DTCs may also reside in other anatomical sites. Therefore the presentation of DTCs in bone marrow aspirates may merely provide a snapshot of systemic behavior.

Current mechanisms to explain cancer dormancy invoke the absence of contextual signals that foster cancer growth or the presence of inhibitory signals that block proliferation and colonization (Dunn, G.P. *et al* 2004; Slaney, C. *et al* 2013). Aguirre-Ghiso, J.A. *et al* (2002) have determined that an $ERK^{low}/p38^{high}$ signaling ratio can induce dormancy, and that p38α/β kinase signaling regulates a "dormancy gene signature" (Adam, A.P. *et al* 2009). From this signature, TGF-$\beta 2^{high}$ microenvironments, such as in the bone, were shown to induce dormancy (Bragado, P. *et al* 2013).

However, much insight of dormant DTC-intrinsic factors has come from *in vitro* based three-dimensional (3D) cultures (Shibue, T. & Weinberg, R.A. 2009; Marlow, R. *et al* 2013) and *in vitro* organoid structures (Ghajar, C.M. *et al* 2013; Barkan, D. *et al* 2010). Indeed, reduced ligand-dependent signaling through adhesion molecules such as integrin α5β1 (Liu, D. *et al* 2002; White, D.E. *et al* 2004), or reduced receptor expression, such as urokinase plasminogen activator receptor and integrin β1 receptor results in cell cycle arrest and increase in p38 signaling disruption (Aguirre-Ghiso, J.A. 2007). Still, others proposed cell-autonomous mechanisms of cell cycle arrest that indicate high expression of p21 and p27 (Ducos, K. *et al* 2000; Pelayo, R. *et al* 2006).

Inflammation and cancer, an inseparable bond

The entrance into a dormant state may therefore be a natural response to an inhospitable microenvironment, as already proposed by the English surgeon Stephen Paget in 1889. Paget put forth the "seed and soil" hypothesis that suggests tumor cells have a predilection to disseminate ("seed") into preferred organs dependent upon the favorable interactions with the tissue microenvironment ("soil"). His hypothesis was made after postmortem examination of women with breast cancer (Paget, S. 1889). The concept that the microenvironment actively contributes to tumor growth has caused a radical shift in the way researchers view cancer biology. Indeed there is much more to cancer than a militia of tumor cells, instead cancer can be viewed as a philharmonic orchestra, in which the various stromal and immune cells are the musicians and the tumor cell is the conductor of the cacophony that the stromal compartment blares.

Inflammation has been tightly linked to tumor progression since its early portrayal as a "wound that never heals" (Dvorak, H.F. 1986; Pidgeon, G.P. *et al* 1999; Coussens, L.M. *et al* 2000; Shacter, E. & Weitzmann, S.A. 2002; Brigati, C. *et al* 2002; Coussens, H.F. & Werb, Z. 2002; Rao, V. P. *et al* 2006). Indeed in 1863 the German pathologist Rudolf Virchow proposed that infiltrating leukocytes were a hallmark of tumors (Balkwill, F. & Mantovani, A. 2001). Chronic inflammation is a causative agent of the initial formation of colon and hepatic cancers (Grivennikov, S.I. *et al* 2010). Intensive cross-talk can be seen between tumor cells and the tumor-associated stromal cells at the tumor margin and increasing evidence shows a dynamic interplay during the various steps of the metastatic cascade. In addition, inflammation has been identified as a crucial inducer of EMT during cancer progression (Mantovani, A. *et al* 2008; Lopez-Novoa, J. M. & Nieto, M.A. 2009; Grivennikov, S.I. *et al* 2010; Ricciardi, M. *et al* 2015). For example, within the primary tumor, infiltrating macrophages-derived TGF-β can cause an EMT in neighboring tumor cells (Bonde, A. K. *et al* 2012).

Thesis hypothesis and outline

Metastatic dormancy has been known for several decades and yet remains largely an unchartered research area. This highlights an unmet need and also underlies the difficulty that studying metastatic dormancy presents. If one delineates the steps required for dormant DTCs to successfully complete in order to form clinically-overt metastases, one might suggest that (1) dormant DTCs must engage with the ECM and with the cells of the adjacent normal tissue parenchyma, (2) dormant DTCs must have metastasis-initiating capabilities and (3) dormant DTCs must be able to establish a tumor that

resembles the primary tumor from which it arose at the histopathological level. In this thesis, I propose that the activation of the EMT program in dormant DTCs would satisfy these three conditions.

To begin, I note that Tsukasa Shibue, a post-doc in the Weinberg lab, has demonstrated that DTCs must extend filopodium-like-protrusions (FLPs) to ensure proliferation within the lung parenchyma soon after extravasation (Shibue, T. & Weinberg, R. A. 2009; Shibue, T. *et al* 2013). One can imagine that DTCs that fail to form FLPs may enter a dormant, non-proliferative state, in which they may persist indefinitely. Furthermore, the induced expression of EMT-TFs allows carcinoma cells that fail to generate FLPs to overcome this cell-intrinsic defect, in part because expression of proteins critical to FLP formation are induced by EMT-TFs. Second, seminal papers published by Mani, S.A. *et al* (2008) and Morel, A.P. *et al* (2008) taught that carcinoma cells that have undergone an EMT acquire the expression of stem cell markers and the ability to tumor-initiate by generating cells with cancer stem cell-like properties. This notion is of particular importance, as other have shown that not all cells are able to seed a tumor once isolated and re-implanted into mice. Indeed the cancer stem cell hypothesis provides an explanation for the existence of a heterogeneous population of malignant cells within a tumor and places cancer stem cells, capable of tumor-initiating, at the apex of the hierarchy (Coussens, L.M. & Werb, Z. 2002; Grivennikov, S.I. *et al* 2010; Atsumi, T. *et al* 2013). Last, given the reversible nature of the EMT, it is highly plausible that once carcinoma cells have begun proliferating, certain cells will re-

gain their epithelial characteristics, thereby enabling the established tumor to resemble the original primary tumor from which it arose.

With the understanding that the EMT program can be induced by multiple factors including inflammation, I hypothesized that both the EMT program and inflammation could be implicated in the escape from metastatic dormancy. While we know that normal epithelial cells can undergo the EMT program at distinct points during a human's lifetime, it is currently unknown whether carcinoma cells would similarly re-activate the EMT program over time as the demands and the environment of the cell change. Therefore, a greater understanding of the mechanisms regulating dormant DTCs is fundamental in understanding the metastatic process and will be an important guide for the development of novel therapeutic strategies that target these cancer cells.

In light of this, my thesis project can be divided into addressing and testing two specific hypotheses: 1) whether the induction of EMT-TFs can re-activate dormant DTCs in the lungs and 2) whether a localized inflammation can re-awaken dormant DTCs in the lungs (Figure 4).

Figure 4*:* Thesis Outline

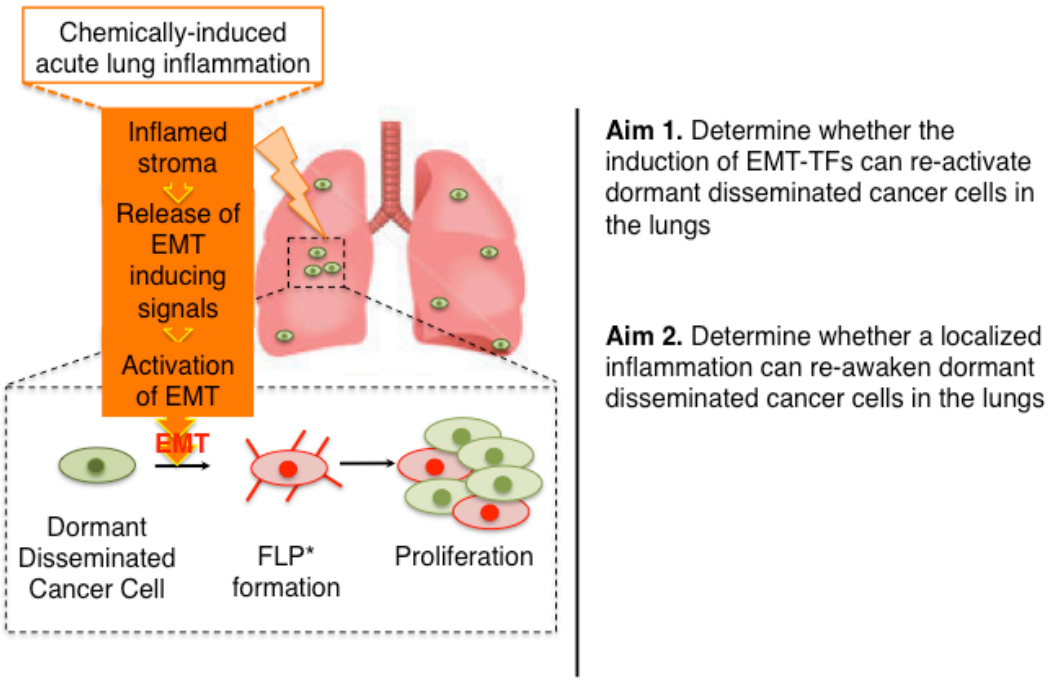

* FLP - *Filopodium-like protrusions*; *Shibue,T. et al.* (2013)

Figure 4. Thesis Outline

Schematic depiction of thesis outline and work plan.

To test the first hypothesis, I needed to develop a model of solitary metastatic dormancy *in vitro* and *in vivo* (Chapter 2). I intended to take advantage of the *in vitro* Matrigel-on-Top (MoT) 3D culture system that was previously developed in our lab (Shibue, T. & Weinberg, R.A. 2009). To model metastatic dormancy *in vivo*, I choose to inject carcinoma cells directly into the circulation via tail vein injection, thereby focusing on experimental metastasis in lungs. In Chapter 3, I studied the effects of the EMT program on the awakening of dormant DTCs in the lungs. Implicit in the outgrowth of metastases are dramatic perturbations of the tumor microenvironment from a non-permissive to permissive state, and the re-establishment of tumor cell heterogeneity. This aspect is explored in greater detail in Chapter 3.

To address my second hypothesis, I created an inflamed microenvironment in the vicinity of dormant DTCs and determined whether this could trigger the escape of metastatic dormancy. I proceeded to identify a potential mechanism by which inflammation may act. The findings related to the second aim are described in detail in Chapter 4 and the greater impact of these results is revealed in Chapter 5.

Chapter 2:

Generation and characterization of a model of metastatic dormancy

Introduction

Modeling metastatic dormancy is by no means a trivial matter. Primary tumor dormancy, also termed latency, which should be distinguished from metastatic dormancy, is the time that separates the malignant transformation of the founder cell from the establishment of a clinically detectable primary tumor (Aguirre-Ghiso, J.A. 2007). In the case of tumor latency, the delay in the formation of the primary tumor can be attributed to the slow accumulation of additional genetic mutations, necessary changes in the tumor microenvironment and the slow proliferation rate of carcinoma cells.

In contrast to tumor latency, which is restricted to the original site of malignancy, metastatic dormancy, as its name implies, occurs at an anatomically distant site of dissemination. These dormant cells would have migrated from the site of the primary tumor in response to various contextual signals, completing numerous steps along the metastatic cascade, as described in Chapter 1. Once arrived at this metastatic site, these particular cells would have had to persist in a quiescent state in this foreign milieu (cellular dormancy) or be controlled by a balance of cellular proliferation and apoptosis and remain clinically undetectable (tumor mass dormancy).

One could imagine that dormancy is only one of several fates that might await DTCs at distant sites: clearance, apoptosis, senescence or adaptation/proliferation. Plausible explanations for any one of these outcomes may be the contextual signals present at the site of dissemination (i.e., inhibitory or favorable) or may reflect cell-intrinsic limitations. However, while the majority of DTCs will not grow into overt

metastases, it is currently unknown which DTCs will be able to, nor is it known which molecular traits and mechanisms are required for this process.

Of note, for simplicity, metastatic dissemination is often conceptualized as occurring in a linear progression model i.e., once carcinoma cells have established a metastasis of a given size at one distant anatomical site, this metastasis can then propagate secondary metastases (Klein, C.A. 2009). Yet, it is highly plausible that carcinoma cells disseminated in parallel from the primary tumor and extravasated into different organ sites. This notion is highlighted in cases in which organ-transplant recipients developed metastatic disease originating from the donated organs. The organ donors were successfully treated for a primary tumor and deemed disease-free. Yet the donated organs harbored dormant DTCs, which grew out in the immunosuppressed recipients (Stephens, J.K. *et al* 2000). This observation also suggests that DTCs may not need to acquire additional genetic mutations beyond those present in the primary tumor in order to tumor initiate. Instead the DTCs may exist in a non-permissive microenvironment within the donor patient that is maintained by the host immune system (Chow, M. T. *et al* 2012).

This begins to paint a very complex picture in which it is not readily clear: 1) how one could re-create or model the metastatic tumor microenvironment *in vitro*, 2) how one could identify an appropriate cell model that could encompass all of these intricacies. Fortunately, an imperfect model can still be informative and insightful! In this chapter, I introduce the cell-model system that I chose to study metastatic dormancy.

To date, many studies of cancer dormancy have focused either on the spontaneous re-growth of tumors at the orthotopic site of implantation i.e. tumor relapse (Weinstein, I.B. 2002; Jain, M. *et al* 2002) or on the spontaneous metastasis of primary tumor cells to distant sites (Goss, P.E. & Chambers, A.F. 2010; Brabletz, T. 2012). The former studies relied heavily on oncogene addiction in inducible transgenic mouse models (Weinstein, I.B. 2002; Jain, M. *et al* 2002; Moody, S.E. *et al* 2002; Moody, S.E. *et al* 2008) The main limitations of these studies are the waiting time for tumor regression and the restriction to only studying localized orthotopic re-growths. The benefits of the latter studies are reduced by the requirement to surgically remove the primary tumors from the mice in order to study the later steps of tumor progression. Indeed, the interpretation of such studies is complicated by the fact that inflammation and wound healing at the site of tumor removal have been associated with enhanced tumor growth, and thus may influence the distant metastatic outgrowths (Hanahan, D. & Weinberg, R. A. 2011; Le Bitoux, M.A. & Stamenkovic, I. 2008; Demicheli, R. *et al* 1994; *unpublished data*). Furthermore, the surgical removal of the primary tumor could directly elicit the outgrowth of micro-metastases by removing the source of anti-angiogenic factors that prevented their metastatic outgrowth (O'Reilly, M.S. *et al* 1994).

Generation of an *in vivo* model to study metastatic dormancy in the lungs

I was able to extract much use from a cell-model system that was generated by a post-doc in our lab, Tsukasa Shibue[1]. To study metastatic dormancy, he took advantage

[1] Dr. Tsukasa Shibue developed this cell-model system and isolated the dormant sub-population of D2A1 cells that I have used for the remainder of this work. He performed one additional experiment that will be incorporated in this work and referenced at that point.

of a cell-enrichment technique, which was previously used to isolate metastatic cells with distinct organ-specific tropisms (Minn, A.J. *et al* 2005).

The highly metastatic murine mammary carcinoma D2A1 cell line used by Dr. Shibue forms tumors upon injection into the mammary fat pad of mice and can spontaneously metastasize to the lungs (Morris, V.L. *et al* 1993). Furthermore, upon injection into the tail vein of mice, which circumvents the aforementioned earlier steps in the metastatic cascade by allowing cancer cells to enter directly into hematogenous circulation, the D2A1 cells form macroscopic metastases. He therefore labeled the D2A1 cells *in vitro* with a cell-permeable vital dye, carboxyfluorescein succinimidyl ester (CFSE), which is diluted by a factor of two upon successive cycles of proliferation. He then proceeded by injecting 100,000 D2A1 cells into the tail vein of mice and harvested the lungs five days after injection. The subpopulation of label-retaining D2A1 cells was then isolated by fluorescence-activated cell sorting (FACS). Dr. Shibue performed ten successive rounds of *in vivo* selection and was able to enrich for a dormant sub-population of D2A1 cells, termed D2A1-d cells (Figure 5a). This sub-population of label-retaining D2A1 cells successfully extravasated into the lung parenchyma, persisted in the lungs, yet failed to proliferate. A lack of proliferation, hence retention of CSFE, indicated that these cells remained dormant following extravasation for at least five days. Subsequent experiments demonstrated that the D2A1-d cells remain dormant for at least six weeks following tail vein injection of 100,000 cells.

In vivo characterization of the D2A1-d cells

To fully characterize the metastasis-initiating potential of the D2A1-d cells, the D2A1-d cells were transduced with a lentiviral construct encoding the red fluorescent protein tandem dimer (td) Tomato, so that metastases could be imaged in tissues dissected from mice that had been injected with these cancer cells. I found that the D2A1-d cells fail to colonize the lungs six weeks after tail vein injection at dilutions of less than 100,000 cells, in sharp contrast to the parental D2A1 cells, which can form metastases with as few as 1000 cells within six weeks (Figure 5b). The D2A1-d cells can, however, readily form lung metastases within four weeks when injected in inocula of over 200,000 cells (Figure 5b). In cases where the D2A1-d cells can colonize the lungs, i.e., when injecting ≥ 200,000 cells into the tail vein, the D2A1-d cells are most likely traveling as clumps of cells rather than as single cells, which may allow them to maintain the cellular signals required for their proliferation. When the D2A1-d cells disseminate as solitary cells, they may not be able to perpetuate the signals required to proliferate in this otherwise-inhospitable environment. Keeping in mind that injecting ≥ 200,000 cells into the tail vein can lead to metastatic outgrowth, I used the D2A1-d cells as model of cellular dormancy by injecting 60,000-100,000 D2A1-d cells via the tail vein into mice for all subsequent experiments, as metastases rarely formed in the lungs at these numbers of injected cells.

Figure 5*: In vivo* enrichment strategy for dormant subpopulation of disseminated tumor cells

a

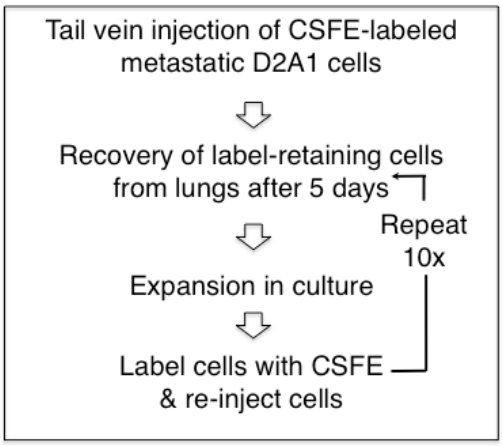

b

Tail Vein injection	D2A1 parental	D2A1-d
5×10^5	4/4	4/4
1×10^5	4/4	0/4
1×10^4	4/4	0/4
1×10^3	4/4	0/4

Figure 5. *In vivo* enrichment strategy for dormant subpopulation of disseminated tumor cells

(**a**) Schematic depiction of the *in vivo* strategy used to enrich for lung-specific dormant sub-populations of cells. Metastatic parental D2A1 cells were labeled *in vitro* with a cell-permeable vital dye carboxyfluorescein succinimidyl ester (CFSE). 100,000 of these labeled D2A1 cells were injected into mice via the tail vein. Five days later, mice were sacrificed and the lungs were harvested and dissociated. The sub-population of label-retaining D2A1 cells was isolated by fluorescence-activated cell sorting (FACS). The isolated cells were cultured *in vitro*, labeled once again *in vitro* using CFSE and re-introduced at 100,000 cells per tail vein into mice. This cycle was repeated ten times; **(b)** Incidence of metastasis formation in the lungs of mice injected via the tail vein with either D2A1-d or parental D2A1 cells at the indicated doses.

In order to determine whether the D2A1-d cells described above retained the potential to form primary tumors, I injected the D2A1-d cells at limiting dilutions into the mammary fat pads of mice (Figure 6a). As a control, the parental D2A1 cells were also injected at limiting dilutions into the mammary fat pads of mice. Both the D2A1-d and parental D2A1 cells were able to initiate tumors with comparable efficiencies and growth kinetics. However, a decrease in tumor forming ability was seen when 10^3 D2A1-d cells were injected, suggesting that there might be a slight reduction in tumor initiation ability (Figure 6a&b). Hematoxylin and eosin (H&E) staining of primary tumors formed by the implanted D2A1-d cells indicated circumscribed tumors (Figure 6c). In sharp contrast, the parental D2A1 cells form high-grade tumors with spindle-like cells and an invasive edge (Figure 6c). Interestingly, unlike the parental D2A1 cells, which can spontaneously metastasize from the primary tumor growing in the mammary fat pads to the lungs after four weeks, the D2A1-d cells failed to do so in the same time frame. This *in vivo* characterization demonstrates that the D2A1-d cells retained the potential to form primary tumors, failed to colonize the lungs and represent a model to study metastatic dormancy *in vivo* in the lungs.

Figure 6: D2A1-d cells retain tumorigenic potential at orthotopic site

a

	D2A1 parental		D2A1-d	
	T.I.	**Mets.**	**T.I.**	**Mets.**
5 x 10^5	5/5	3/5	5/5	0/5
1 x 10^5	5/5	2/5	5/5	0/5
1 x 10^4	6/8	0/2	6/8	0/2
1 x 10^3	6/8	0/2	3/8	0/2

T.I. – tumor incidence; Mets. – lung metastases

b

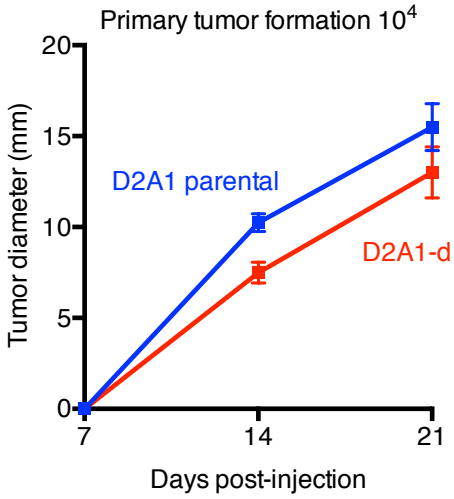

c

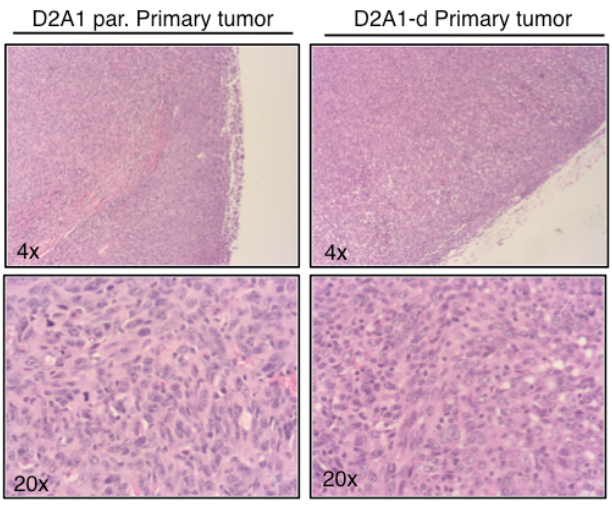

Figure 6. D2A1-d cells retain tumorigenic potential at orthotopic site

(a) Incidence of primary tumor formation and spontaneous metastasis in mice orthotopically implanted with either D2A1-d or parental D2A1 cells at the indicated doses. *T.I.* and *Mets* indicate primary tumor incidence and the number of mice with lung metastases, respectively; **(b)** Primary tumor growth curves *in vivo* of D2A1-d and parental D2A1 cell lines injected at 1.0×10^4 cells into the fourth mammary fat pad of mice; **(c)** Hematoxylin & eosin (H&E) staining of histological sections prepared from D2A1-d and parental D2A1 tumors.

In vitro characterization of the D2A1-d cells

Having determined certain characteristics of the D2A1-d cells *in vivo*, I proceeded to characterize these cells *in vitro*. Under 2-dimensional (2D) conditions, the D2A1-d cells proliferate at a rate that is not statistically different from the parental D2A1 cells (Figure 7a). This is consistent with their growth kinetics when implanted orthotopically into the mammary fat pads of mice.

In Chapter 1, I outlined the following mechanistic hypothesis to explain the awakening of dormant DTCs: an inflamed stroma might release EMT-inducing signals, which might in turn spawn the activation of the EMT program in nearby quiescent DTCs, leading to the extension of FLPs by these cells, and their active proliferation, resulting eventually in the formation of metastases. To test this hypothesized mechanism, it was necessary to determine whether or not the D2A1-d cells can extend FLPs under Matrigel-on-top (MoT) culture conditions, which is a confirmed readout for FLP formation *in vivo*, as defined in Shibue, T & Weinberg, R. A. 2009.

For this experiment, Dr. Shibue plated the parental D2A1 and the D2A1-d cells under MoT conditions. These cultures were then stained for F-actin as a marker for FLP formation. I found that both the parental D2A1 and the D2A1-d cells extended 5-6 FLPs/ cell under MoT conditions (Figure 7b). This finding suggests that the dormant behavior of the D2A1-d cells observed by Dr. Shibue and confirmed by me, as described above, is due to an FLP-independent mechanism, since the proposed mechanism would predict that the extension of FLPs should enable these cells to proliferate. This observation, however,

shed no light on the potential role of the EMT program in triggering the awakening of latent DTCs.

Prior to determining whether the activation of the EMT program in dormant DTCs could trigger metastatic outgrowth, I inspected the expression of key EMT-inducing TFs, such as Slug, Snail, Twist and Zeb1. By western blot analysis, I observed that the parental D2A1 cells express all of the above-mentioned EMT-TFs (Figure 7c). While the D2A1-d cells express Slug, the D2A1-d cells express low levels of Snail and fail to express Twist or Zeb1. The reduced expression of Snail, Twist and Zeb1 in the D2A1-d cells provided some initial insight into my revised hypothesis that the activation of the EMT program may awaken dormant DTCs.

Figure 7: *In vitro* characterization of D2A1-d cells

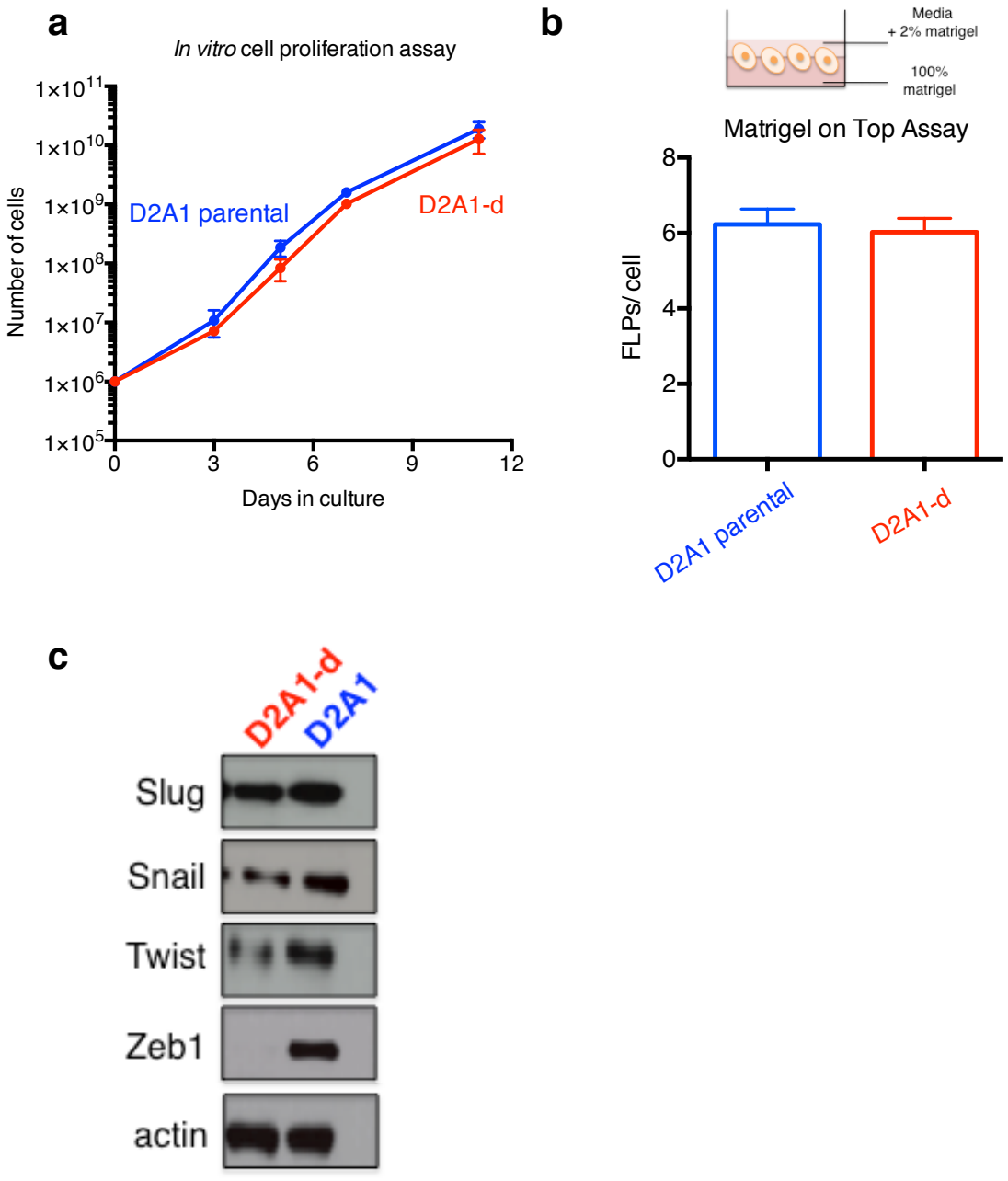

Figure 7. *In vitro* characterization of D2A1-d cells

(a) *In vitro* proliferation curves of D2A1-d and parental D2A1 cells. Data are representative of three independent experiments; **(b)** Matrigel-on-Top (MoT) cultures of D2A1-d and parental D2A1 cells were stained for the fluorescent actin marker lifeact-Ypet and 100 cells from each cell line were analyzed. Quantification of filopodium-like protrusions (FLPs) as determined by counting the number of FLPs per cell under fluorescent dissection microscope according to Shibue, T. & Weinberg, R. A. (2009). Data are represented as mean ± SEM; n=100; **(c)** Epithelial-to-mesenchymal transition (EMT-TFs) Slug, Snail, Twist and Zeb1 protein levels were determined by Western blot (WB) in the dormant D2A1 (D2A1-d) and parental D2A1 (D2A1) cell lines.

Discussion

To date, there are a handful of studies that have looked at modeling cellular dormancy. Much insight has been gained from studies that have cultured carcinoma cells under 3D conditions (Shibue, T. & Weinberg, R.A. 2009; Barkan, D. & Green, J.E. 2011). These studies looked at the cellular intrinsic defects that prevented dormant cells from interacting productively with their surrounding extra-cellular matrix. Another *in vitro* approach has been the use of 3D organoïd cultures (Ghajar, C.M., *et al* 2013). Organoïd cultures have the advantage of incorporating an additional level of complexity to the surrounding microenvironment of DTCs as stromal cells and the effect of their secreted proteins can be studied.

Despite the molecular insights that these *in vitro* approaches have provided, they remain approximations of the *in vivo* setting. Inoculating human carcinoma cell lines onto the chorioallantoic membrane of chick embryos has uncovered mechanisms pertaining to the induction of cellular cancer dormancy, such as stress signaling and the low activity ERK: p38 signaling ratio (Aguirre-Ghiso, J.A. 2002). Yet, other models of cellular dormancy used an experimental metastasis model in mice (Gao, H. *et al* 2012). While carcinoma cell lines are typically classified as non-metastatic or metastatic, this designation is determined by the ability of carcinoma cell lines to spontaneously metastasize from the primary tumor site. Rarely is this indicative of the ability of the carcinoma cell line to colonize a metastatic site when injected directly into circulation. Indeed, 99.9% of carcinoma cells injected the circulation do not survive the stress of dissemination and are cleared from the circulation (Chambers, A.F. *et al* 2002; see

appendix A). Therefore the carcinoma cell lines that have been used to study cellular dormancy may not fully represent all characteristics of dormant DTCs. It is highly plausible that better models of cellular dormancy have yet to be determined.

The experiments in this chapter validated and extended Dr Shibue's initial experiments that dormant disseminated cancer cells can be enriched by multiple rounds of *in vivo* selection. While the enriched sub-population of cells could not grow within the non-permissive environment of the lungs, these cells had not lost their tumorigenic potential, as demonstrated by their ability to form primary tumors upon inoculation in the mammary fat pad. However, given that these cells were isolated from a heterogeneous carcinoma cell line that can colonize the lungs, it is possible that this enriched sub-population of dormant cells only lacks few genetic or epigenetic alterations that would enable them to readily proliferate in the lungs.

Even though my initial hypothesis set out to test whether the activation of the EMT program in dormant DTCs would allow the carcinoma cells to extend FLPs, which would in turn allow the carcinoma cells to resume proliferation following extravasation and form macro-metastases, the results of the MoT experiment suggest that an alternative, FLP-independent mechanism. This also points to the existence of at least two mechanisms for the maintenance of cellular dormancy.

Of note, while the number of FLPs extended by the D2A1-d cells was similar to the number of FLPs extended by the parental D2A1 cells, the D2A1-d cells displayed a

distinct morphology under MoT conditions. Furthermore, it was possible to identify cell types within the parental D2A1 cells that resembled the D2A1-d cells under MoT conditions. This observation indicated that there might be additional factors that contribute to the dormant behavior of the D2A1-d cells in the lungs, as it pertains to the ability of the D2A1-d cells to interact with the surrounding extra-cellular matrix. However, I decided not to follow up on this.

The model system described above, while useful and of great interest, is far from ideal and may provide insight into only one model/mechanism of metastatic dormancy. First, the experimental enrichment of the dormant sub-population of carcinoma cells was performed directly at the metastatic site, and therefore these cells may not be able to complete all of the steps of the metastatic cascade, such as intravasation. One might imagine that the carcinoma cells that would have been collected at the metastatic site following spontaneous metastasis would have a different gene expression profile than the dormant sub-population of carcinoma cells that were collected following experimental metastasis. Next, an ideal model system for metastatic dormancy would more accurately mimic human cancer progression, including primary tumor formation, dissemination, surgical removal of the primary tumor mass or therapeutic treatment, rather than intravenously injected carcinoma cells.

Despite the ability of the D2A1-d cells to extend FLPs, the possibility remained that the EMT program might still play a role in awakening dormant disseminated cancer cells, doing so via an FLP-independent mechanism. As such, it remained possible that the

lack of expression of the master EMT-TF Snail, Twist and Zeb1 in the D2A1-d might play a role in maintaining the dormant state. This question is directly addressed in Chapter 3.

Materials and Methods

Cell Culture

All cells were cultured in 5% CO_2 humidified incubator at 37° C. The parental D2A1 and D2A1-d cell lines were grown in Dulbecco's Modified Eagle's Medium (DME) supplemented with 5% inactivated fetal bovine serum (IFS), 5% calf serum, 100 U/ml penicillin, and 100 μg/ml streptomycin (Invitrogen). The parental D2A1 cell line was a gift from P.L. Lollini (Rak J.W. *et al* 1992). Cells were passaged when confluence reached ~80% with 0.15% trypsin and re-seeded in a ratio of 1/12. Medium was always changed every third day.

Cell proliferation assay

Cells were seeded at 1.0 x 10^6 into 10 cm, split and counted using the automatic counter Vi-CELL Cell Viability Analyzer (Beckman Coulter) every three days for fourteen days.

Matrigel-on-top

The Matrigel on-top (MoT) culture was performed as described elsewhere (Shibue, T. & Weinberg, R. A. 2009). Briefly, the bottom of the well of 8-well chamber slides (NUNC), was coated with 40 ml/well of Matrigel (BD Biosciences) and incubated at 37 ˚C for 30 min to allow the gel to solidify. 400 cells were resuspended in 200 ml of 2D/3D-culture medium (DME/F12 medium supplemented with 2% horse serum, 0.5 mg/ml hydrocortisone, 50 ng/ml cholera toxin, 10 mg/ml insulin, 100 U/ml penicillin and 100 mg/ml streptomycin), containing 2% Matrigel, and added to the Matrigel-coated well.

Immunoblotting

Cells were harvested and lysed in RIPA buffer [25 mM Tris-HCL (ph 7.6), 150 mM NaCl, 1% Nonidet P-40, 1% sodium deoxycholate, O.1% SDS, 1x complete protease inhibitor mixture (Roche), 1x phosphatase inhibitors (Roche Diagnostics)]. The protein extracts were separated by 10% SDS-PAGE and were transferred to polyvinylidene fluoride (PVDF) membranes (Millipore). After one hour blocking in 5% non-fat milk, the membranes were incubated overnight with primary antibodies at 4'C. Blots were developed using ECL (Dura or Femto, Pierce). The types and dilutions of primary antibodies used were the following: Snail (Cell Signaling Technology 3879S; $1:10^3$), Twist (Abcam ab50887; $1:10^4$), Zeb1 (Cell Signaling Technology 3396S; $1:10^3$), E-cadherin (Cell Signaling Technology 3195S; $1:10^3$), Fibronectin (BD Biosciences 610078; 1: 10^3), N-cadherin (Cell Signaling 4061; $1:10^3$); Vimentin (Cell Signaling Technology 5741S; $1:10^3$), GAPDH (Cell Signaling Technology 2118S; $1:10^4$).

Animals

Balb/c mice were obtained from Jackson Laboratory (stock number 000651). All research involving animals was conducted in accordance with the Guide for the Care and Use of Laboratory Animals of the National Institute of Health. All animals were maintained according to the guidelines of the MIT Committee on Animal Care protocol (1014-109-17). All efforts were made to minimize suffering. Mice that had been dead by the end of experiments were excluded from the analysis.

For orthotopic tumor transplantations, 1.0 x 10^5 tumor cells, unless otherwise indicated, resuspended in 20 μL of their growth medium and 50% Matrigel were implanted bilaterally into the fourth mammary fat pad of 6 to 8-week old female syngeneic Balb/c mice. The tumor incidence was determined six to eight weeks post-injection.

For intravenous injections, 1.0 x 10^5 cells, unless otherwise indicated, resuspended in 100 μL of phosphate-buffered saline (PBS) were injected into the lateral tail vein. The lungs were examined for metastases four to six weeks post-injection.

Histology

Primary tumors were fixed in 10% neutral buffered formalin overnight and embedded in paraffin for sectioning; lungs were fixed in 4% paraformaldehyde and paraffin-embedded. Sections (5 μm thick) were cut from paraffin-embedded tissues and stained with haemotoxylin and eosin. Animals and In vivo tumorigenesis

Statistical Analysis

All data are represented as mean values ± standard errors of mean (SEM). *P* values of less than 0.05 were considered to be significant. Statistical analyses were carried out by two-tailed Student's t-test using Prism software (GraphPad Prism).

Chapter 3:

Role of the EMT program in awakening dormant DTCs

Introduction

Implicated in metastasis is the activation of the epithelial-to-mesenchymal transition (EMT) program, an embryonic developmental program that is aberrantly activated in cancer cells (Kalluri, R. &Weinberg, R.A. 2009). During the EMT program, cancer cells detach from the primary tumor by the loss of cell-cell interactions, increase their motility and invasive behavior, and acquire cancer stem cell (CSC) -like characteristics, such as self-renewal and drug resistance (Morel, A.P. *et al* 2008; Mani, S.A. *et al* 2008; Al-Hajj, M. *et al* 2003). This developmental and wound healing-associated program is aberrantly activated during tumor progression, and has been shown to be a responsible cause for the dissemination of cancer cells from the primary tumor (Thiery, J.P. *et al* 2009; Yang, J. & Weinberg, R.A. 2008). However, a role for the EMT program at the metastatic site has not yet been determined.

Once carcinoma cells have undergone an EMT and disseminated to sites such as the bone, liver, and lungs, it is believed that DTCs may undergo the reverse process termed mesenchymal-to-epithelial transition (MET). Histological staining of bone marrow-derived from cancer patients has shown the presence of epithelial cytokeratin-positive cells (Braun, S. *et al* 2000). Indeed the presence of such cytokeratin-positive cells in the bone marrow was associated with a significantly higher risk of distant metastases (Balic, M. *et al* 2006). Discovering the cellular signals and regulatory pathways involved in the MET is a topic of active research by those in the community. The MET may be a passive process through which carcinoma cells default in the absence of contextual EMT-maintaining cell signals, or there may be an active push for carcinoma

cells to undergo the MET at the metastatic site. While both scenarios are of equal interest for the establishment of metastatic dormancy, neither of these approaches will be explored in the present work.

As discussed in Chapter 2, the D2A1-d cells fail to express certain key EMT-TFs, such as Snail, Twist and Zeb1, unlike the parental D2A1 cells, which express all three EMT-TFs. While it is highly likely that other proteins are differentially expressed between the parental D2A1 and D2A1-d cells, I focused on this subset of transcription factors, as they are the master regulators of the EMT program. As mentioned in Chapter 1, the EMT program can be elicited by various cellular-signals and inflammatory mediators. As such, I chose to determine whether the EMT program as orchestrated by the EMT-TFs, could awaken dormant DTCs.

Generation and *in vitro* characterization of D2A1-d cells conditionally over-expressing EMT-TFs

To determine the possible effect of the EMT program on the awakening of dormant DTCs, I decided to transduce the D2A1-d cells with a doxycycline-inducible, HIV-based lentiviral vector encoding either Snail, Twist, Zeb1 or, as a vector control, the coding sequence of the firefly luciferase gene. This modified FUW lentiviral vector was constructed and donated by a previous graduate student in the Weinberg lab Dr. Kong-Jie Kah. Furthermore, I also stably expressed the firefly luciferase gene in the TdTomato^{+} D2A1-d cells in order to monitor outgrowth in mice by bioluminescence imaging. Accordingly, the growth of the D2A1-d cells could be studied *ex vivo* and *in vivo*.

Following *in vitro* exposure to doxycycline, the D2A1-d cells expressed the EMT-TFs (Figure 8a). Despite prolonged *in vitro* treatment with doxycycline for up to two weeks, the D2A1-d cells failed to undergo a complete EMT *in vitro*. Thus, D2A1-d cells expressing Snail or Zeb1 expressed fibronectin but failed to lose their expression of e-cadherin (Figure 8b). An incomplete induction of the EMT program *in vitro* has been observed by others in our lab and does not necessarily reflect the ability of these cells to undergo a complete EMT *in vivo*.

In re-activating dormant DTCs, one could presume that DTCs would awaken following stimulation of a mitogenic signal. To exclude a direct association of the EMT program with a mitogenic program, I conducted an *in vitro* cell-proliferation assay (Figure 8c). Upon over-expression of the EMT-TFs Snail, Twist or Zeb1, the proliferation of the D2A1-d cells was slightly reduced. This confirmed published results suggesting that the EMT program can in fact impair proliferation (Bierie, B. & Moses, H.L. 2006; Evdokimova, V. *et al* 2009; Vega, S. *et al* 2004). Hence, it was highly unlikely that the EMT-TFs had a mitogenic effect on the dormant DTCs.

Figure 8: *In vitro* induction of EMT-TFs in D2A1-d cells fails to induce a complete EMT and does not confer a proliferative advantage to cells

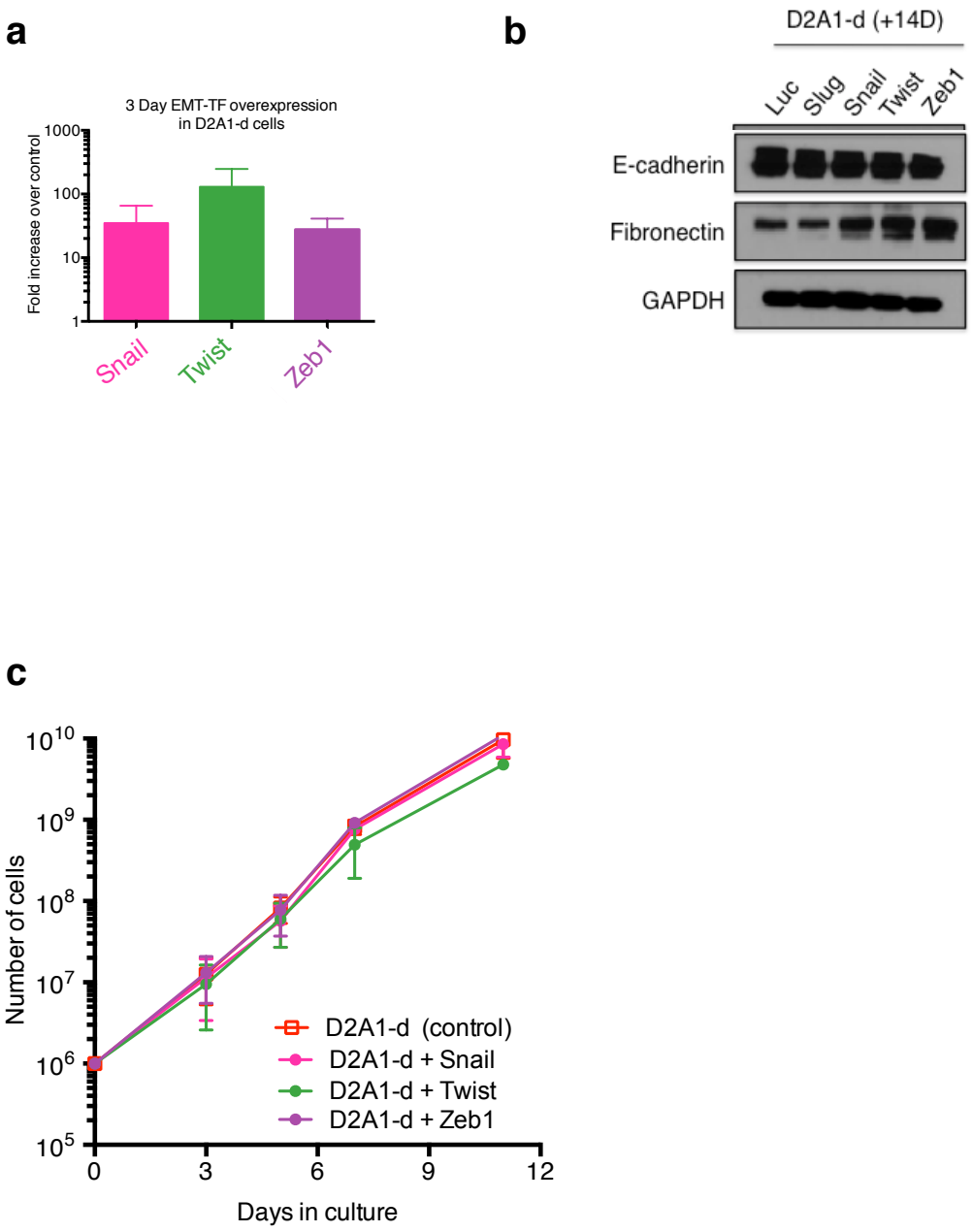

Figure 8. *In vitro* induction of EMT-TFs in D2A1-d cells fails to induce a complete EMT and does not confer a proliferative advantage to cells

(a) Relative increase of *Snail*, *Twist* and *Zeb1* mRNAs after three days of *in vitro* doxycycline treatment at 1 μg/mL as gauged by RT-PCR; **(b)** Cells treated for fourteen days with 1 μg/mL of doxycycline to induce EMT-TFs were harvested and proteins were extracted. The EMT status of cells was assessed by western blot. Fibronectin is a marker of mesenchymal cells; E-cadherin is a marker of epithelial cells; **(c)** *In vitro* proliferation curves of EMT-TF expressing D2A1-d cells. Proliferation assay was performed by plating 1 x 10^6 cells per 10 cm tissue culture plate, counted and re-plated at the same density every three days. Fresh doxycycline was added at 1 μg/mL every three days. Data are representative of three independent experiments.

Continuous induction of the EMT-TFs provokes weak metastatic outgrowth

Having sufficiently characterized the D2A1-d cells *in vitro* following the induction of the EMT-TFs (Snail, Twist or Zeb1), I tested one prediction of my original hypothesis i.e., that the activation of the EMT program could awaken dormant DTCs directly in BALB/C mice. BALB/C mice were injected via the tail vein with 100,000 untreated D2A1-d cells harboring either the doxycycline-inducible vector encoding Snail, Twist, Zeb1 or a luciferase control. Seven days later, all mice were fed doxycycline-treated water continuously for a fortnight. The seven-day period after tail vein injection was arbitrarily chosen to allow tumor cells to extravasate and become established in the lung parenchyma. Once the mice were taken off doxycycline-treated water, the mice were housed for an additional ten days (Figure 9). Four weeks after tail vein injection, all mice were sacrificed according to the approved guidelines of the MIT Committee on Animal Care.

Upon inspection of the harvested lungs under the fluorescent dissection microscope, very few, if any, metastases were seen (Figure 9). The mice that had been injected with the D2A1-d cells harboring the luciferase vector control (D2A1-d + Luc) did not display any metastases whatsoever; the same was true for the mice that had been injected with the D2A1-d cells harboring the doxycycline-inducible Twist vector (D2A1-d + Twist). However, the mice that had been injected with D2A1-d cells harboring the doxycycline-inducible Snail vector (D2A1-d + Snail) had on average one metastasis per mouse, while the mice that had been injected with the D2A1-d cells harboring the

doxycycline-inducible Zeb1 vector (D2A1-d + Zeb1) had on average 3 metastases per mouse (Figure 9; n=3).

Figure 9: Continuous induction of EMT-TFs provokes a weak awakening of dormant DTCs

a

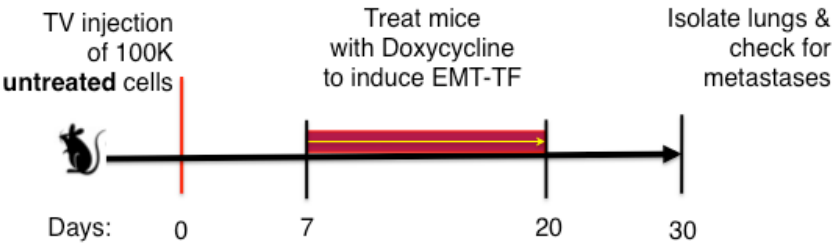

b

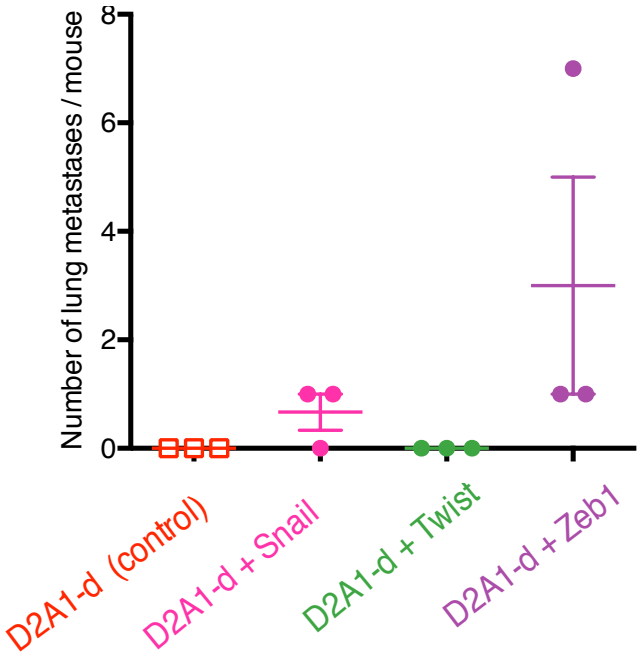

Figure 9. Continuous induction of EMT-TFs provokes a weak awakening of dormant DTCs

(a) Schematic depiction of the *in vivo* strategy used to continuously induce the EMT-TFs. On day 0, mice were injected with dormant D2A1 (D2A1-d) cells harboring either the doxycycline-inducible vector Snail, Twist, Zeb1 or a luciferase control. On day 7, all mice received doxycycline-treated water continuously for two weeks. Doxycycline-treated water was refreshed every three days. On day 21, mice were taken off doxycycline-treated water, and were housed for an additional ten days; **(b)** Quantification of lung metastases as determined by numbers of metastatic nodules visible under fluorescent dissection microscope at 0.8x magnification. Each data point represents the number of lung metastases in an individual mouse. *D2A1-d (control)* – D2A1-d cells harboring a luciferase control vector; *D2A1-d + Snail* - D2A1-d cells harboring a doxycycline-inducible vector expressing Snail; *D2A1-d + Twist* - D2A1-d cells harboring a doxycycline-inducible vector expressing Twist; *D2A1-d + Zeb1* - D2A1-d cells harboring a doxycycline-inducible vector expressing Zeb1. Data are represented as mean ± SEM (n=3).

The ability of only Snail and Zeb1, and not Twist, to provoke a weak awakening of dormant DTCs was not surprising as it would appear that not all EMT-TFs can induce the EMT program to the same extent, and that the individual EMT-TFs can modulate different forms of the EMT program. Furthermore, the results from this experiment provided some evidence that the EMT program is involved in the escape of metastatic dormancy, it was entirely possible that a continuous induction of the EMT program had detrimental effects on the metastasis-initiating potential of these cells. Indeed, unpublished results from other studies in the lab showed that a prolonged induction of the EMT program pushed the carcinoma cells into an irreversible mesenchymal cell state. Within this irreversible mesenchymal state or "extreme-EMT state", carcinoma cells are unable to tumor-initiate and have lost their CSC-like traits. In light of these combined observations, I altered the experimental strategy as it pertained to the induction of EMT *in vivo*.

Transient induction of the EMT-TFs provokes robust metastatic outgrowth

While an extreme-EMT state proved to be less advantageous to the metastatic outgrowth, I hypothesized, as an alternative, that a transient induction of the EMT program would allow carcinoma cells to maintain their cellular plasticity and retain CSC-like traits. Therefore, in my next set of experiments, I decided to pulse feed the mice with doxycycline-treated water (Figure 10a). Seven days after tail vein injection of 100,000 cells, all mice were fed doxycycline-treated water for three days. The doxycycline-treated water was then replaced with normal water for two days, and replaced with doxycycline-treated water for another three days. This cycle of three-days on/ two-days off was

repeated once more. The entire period of doxycycline-treatment spanned two weeks. At the end of this period, the mice were housed for an additional ten days and sacrificed four weeks after tail vein injection. I omitted the D2A1-d + Twist cells from further study, as the mice injected with these cells had previously failed to display any metastases, and I therefore focused exclusively on the D2A1-d + Snail and D2A1-d + Zeb1 cells.

On this occasion, what I observed under the fluorescent dissection microscope was unlike what I had previously described following continuous EMT-induction (Figure 10b-d). Of ten mice that were injected with D2A1-d + Luc control cells, only one mouse had developed metastases. The lungs of the remaining nine mice were entirely devoid of metastases. Three out of ten mice from the group of mice injected with D2A1-d + Snail cells developed metastases, 15 metastases on average per mouse. Six out of ten mice from the group of mice injected with D2A1-d + Zeb1 cells developed 23 metastases on average per mouse.

Figure 10: Transient induction of EMT-TFs provokes a robust awakening of dormant DTCs

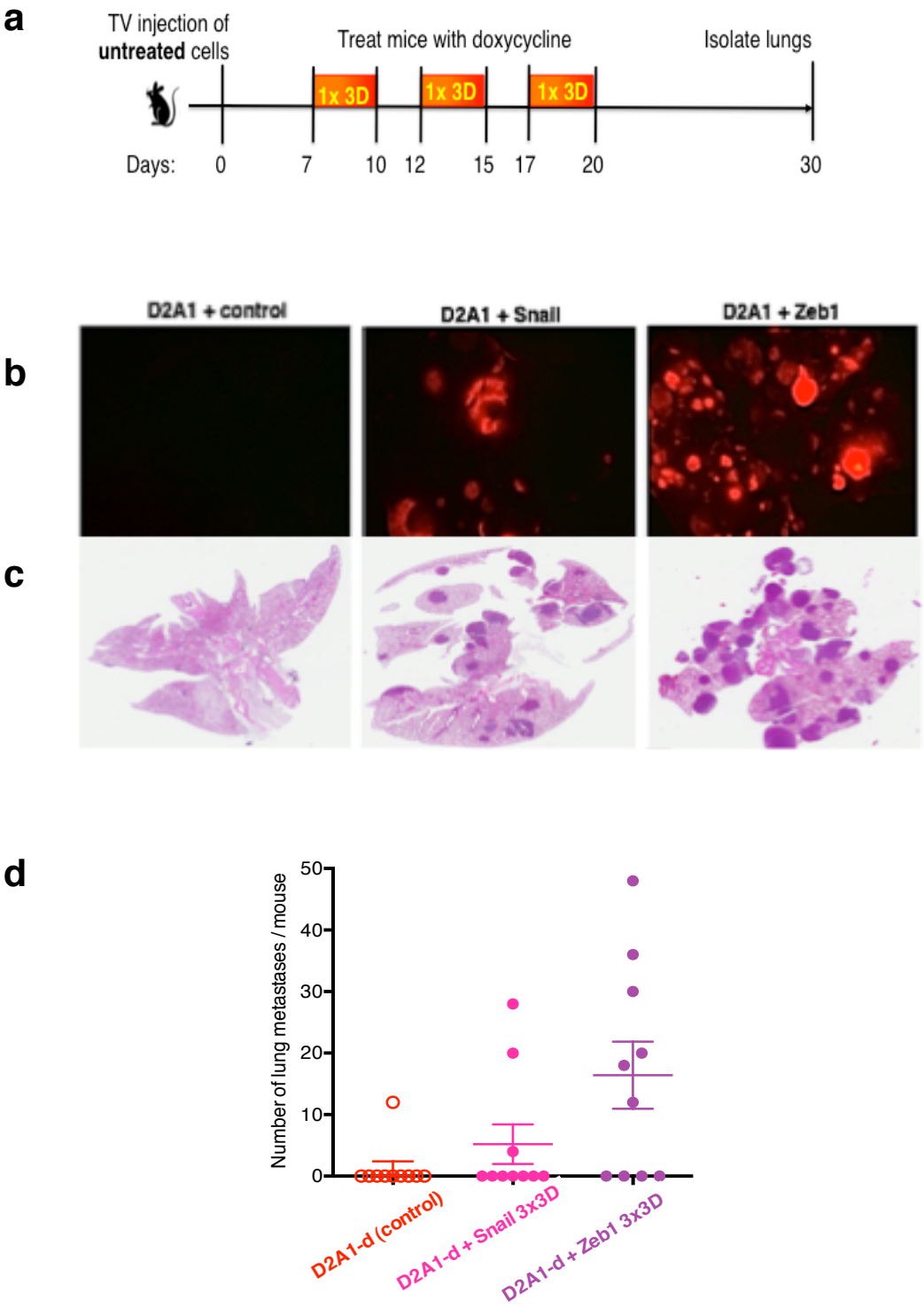

Figure 10. Transient induction of EMT-TFs provokes a robust awakening of dormant DTCs

(a) Schematic depiction of the *in vivo* strategy used to transiently induce the EMT-TFs. On day 0, mice were injected with D2A1-d harboring either the doxycycline-inducible vector Snail, Zeb1 or a luciferase control. On day 7, all mice received doxycycline-treated water for three days (1x3D). On day 10, doxycycline-treated water was replaced with regular water. On day 13, all mice received doxycycline-treated water for another three days. On day, 16, doxycycline-treated water was replaced with regular water. This pulse of doxycycline-treated water was repeated once more. In total the mice received three pulses of doxycycline-treated water. After the final day of the third pulse treatment of doxycycline-treated water, the mice were housed for an additional ten days. The dot plot shows the number of lung metastases per mouse. *D2A1-d (control)* – dormant D2A1 cells harboring a luciferase control vector; *D2A1-d + Snail* – D2A1-d cells harboring a doxycycline-inducible vector expressing Snail; *D2A1-d + Zeb1* – D2A1-d cells harboring a doxycycline-inducible vector expressing Zeb1. Data are representative of three independent experiments; (**b**) Representative fluorescent images of whole lungs taken at 0.8x magnification under dissection microscope; (**c**) Representative H&E staining of histological sections of whole lungs following *in vivo* strategy outlined in Panel a; (**d**) Quantification of lung metastases as determined by numbers of metastatic nodules visible under fluorescent dissection microscope at 0.8x magnification. Each data point represents the number of lung metastases in an individual mouse. Data show mean ± SEM (n=10).

From this experiment, it was clear that both the EMT-TFs Snail and Zeb1 could in fact cause the awakening of dormant DTCs in the lungs, although the effect of the EMT-TF Zeb1 was far more profound that Snail. Furthermore, this result validated the speculation that a transient induction of the EMT program was beneficial to carcinoma cells albeit for reasons that were still unclear at this point.

The MoT experiment conducted in Chapter 2 (Figure 7) demonstrated that both the D2A1-d and parental D2A1 cells could extend FLPs. However, this does not obviate the possibility that the activation of the EMT program in dormant DTCs would allow the carcinoma cells to extend FLPs, which may be required to form macro-metastases. To fully test my initial hypothesis, as outlined in Chapter 2, I infect the D2A1-d + Zeb1 cells with short hairpin RNAs against ILK messenger RNAs (shILK) and short hairpin RNAs against β-parvin (sh β-parvin), two key regulators of FLP formation (Shibue, T. *et al* 2013; Figure 11a). Both sets of shRNA constructs had been validated by Shibue, T. *et al* 2013. I then proceeded to inject groups of five mice via the tail vein with D2A1-d + Zeb1 cells, D2A1-d + Zeb1 cells that harbored either shILK_E or the shILK_F and D2A1-d + Zeb1 cells that harbored either sh β-parvin _J or the sh β-parvin _L. Seven days later, I treated these mice with two three-day pulses of doxycycline-treated water separated by a two-day interval of regular water. Two weeks later I sacrificed these mice, harvested their lungs and counted the number of metastases under the fluorescent dissection microscope (Figure 11b).

The mice that had been injected with the D2A1-d + Zeb1 cells developed on average ten metastases per mouse. The mice that had been injected with the D2A1-d + Zeb1+ shILK_E cells had 43 metastases per mouse, while the mice that had been injected with the D2A1-d + Zeb1 + shILK_F cells had an average of 36 metastases per mouse. The mice that had been injected with the D2A1-d + Zeb1+ shβ-parvin _J cells had 30 metastases per mouse, while the mice that had been injected with the D2A1-d + Zeb1 + shβ-parvin _L cells had an average of 25 metastases per mouse. Overall the mice that had been injected with D2A1-d + Zeb1 cells harboring the shRNA constructs of the key regulators of FLP formation developed significantly more lung metastases per mouse than the mice that had been injected with the D2A1-d + Zeb1 cells alone (Figure 11c). By western blot, I was able to confirm that the respective protein knockdowns were maintained in the D2A1-d cells that were extracted from lung metastases (Figure 11d). Taken together, these results confirmed that my initial hypothesis needed to be revised. While the activation of the EMT program in dormant DTCs can lead to the formation of macro-metastases, this occurs through a FLP-independent mechanism.

Figure 11: EMT-mediated awakening of dormant DTCs is not dependent upon the expression of key regulators of FLP formation

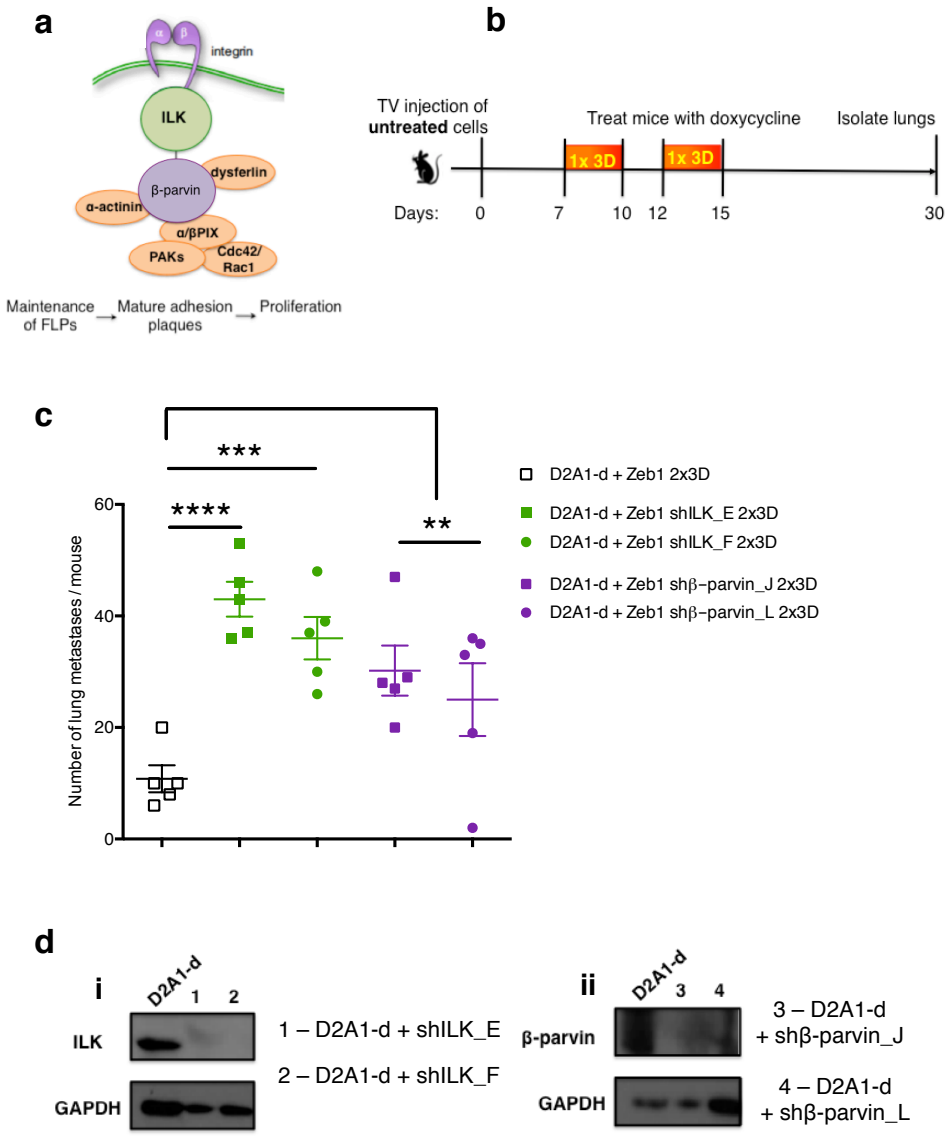

Figure 11. EMT-mediated awakening of dormant DTCs is not dependent upon the expression of key regulators of FLP formation

(**a**) Schematic depiction of signaling cascade Adapted from Shibue, T. *et al* (2013); **(b)** Schematic depiction of the *in vivo* strategy. On day 0, mice were injected with D2A1-d + Zeb1 cells harboring ILK shRNAs or β-parvin shRNAs. On day 7, all mice received doxycycline-infused water for three days (1x3D). On day 10, doxycycline-infused water was replaced with regular water. On day 13, all mice received doxycycline-infused water for another three days. On day, 16, doxycycline-infused water was replaced with regular water; the mice were housed for an additional two weeks; (**c**) Knockdown of key regulators of FLP formation in D2A1-d + Zeb1 cells with either shILK or shβ-parvin subsequently does not reduce metastatic outgrowth. Quantification of lung metastases as determined by numbers of metastatic nodules visible under fluorescent dissection microscope at 0.8x magnification at thirty days post-tail vein injection in BALB/c mice. Each data point represents the number of lung metastases in an individual mouse. Data are represented as mean ± SEM; n=5. The *P*-values were calculated by Student's t-test. (**) $P < 0.006$; (***) $P < 0.0005$; (****) $P < 0.0001$; (**d**) (**i**) Knockdown of two ILK shRNAs was determined by Western Blot in D2A1-d cells isolated from mice that were injected with D2A1-d + Zeb1 with either shILK; (**ii**) Knockdown of two β-parvin shRNAs was determined by Western Blot in D2A1-d cells isolated from mice that were injected with D2A1-d + Zeb1 with either β-parvin.

To further explore the metes and bounds of the transient EMT-induction required for metastatic outgrowth, I repeated the above experiment using both the D2A1-d cells + Snail and D2A1-d cells + Zeb1 and a more transient *in vivo* doxycycline-regimen (Figure 12a). This would allow me to determine how a transient EMT-induction could provoke the awakening of dormant DTCs. The transient nature of this *in vivo* pulse would also help model the transient nature of an acute inflammatory response *in vivo*. Thus, I injected mice via the tail vein with untreated D2A1-d cells + Snail or D2A1-d cells + Zeb1. Seven days later, I divided the mice into groups of five mice per group: mice that were to be maintained untreated for the remainder of the experiment, mice that were to be fed doxcycycline-treated water for one single day, mice that were to be fed doxcycycline-treated water for three consecutive days, and mice that were to be fed doxcycycline-treated water according to the initial pulse treatment (three three-day pulses). At the end of the doxycycline treatment, these mice were housed for an additional ten days.

I observed that none of the control mice that had been injected with D2A1-d + Zeb1 cells developed a single metastasis. From the group that received a single day of doxycycline-treated water, mice developed on average six metastases; from the group that received three days of doxycycline-treated water, mice developed on average fifteen metastases. The mice that received three three-day pulses of doxycycline-treated water developed on average fifty metastases (Figure 12b-d). This experiment confirmed my previous results and also showed that even a single day of EMT-induction could have a profound positive impact on metastatic outgrowth.

All experiments described thus far entailed awakening dormant DTCs after seven days of dormancy in mice, equivalent to eight months in humans. While this time scale facilitated experimentation, it was by no means representative of the length of dormancy that may be seen in patients following initial diagnosis, which in the case of breast cancer, can extend to decades. I therefore expanded my modeling of dormancy to three weeks, which is the equivalent to two years in humans.

To determine whether the transient induction of the EMT program can awaken disseminated cancer cells that have been dormant for a more extended period of time, I injected mice via the tail vein with D2A1-d cells + Snail and waited three weeks before doxycycline-treatment (Figure 12e). Three weeks after the tail vein injection, I fed these mice with a single three-day pulse of doxycycline-treated water. These mice were sacrificed eight weeks following tail vein injection. At the end of the experiment, control mice developed lung metastases, on average fifteen lung metastases per mouse. All mice that had been treated with doxycycline-water developed on average twenty-nine lung metastases per mouse (Figure 12e). The ability of the doxycycline-untreated mice to spontaneously develop metastases suggests that there is a delay in tumor growth, once injected the D2A1-d cells slowly form lung metastases after four weeks. While the control mice were able to develop metastases in the absence of Snail induction, these results suggest, nevertheless, that a transient induction of Snail is able to accelerate the awakening of DTCs that had been dormant for an extended period of time.

Figure 12: A three-day induction of Snail or Zeb1 provokes a robust awakening of dormant DTCs after seven or twenty-one days of dormancy

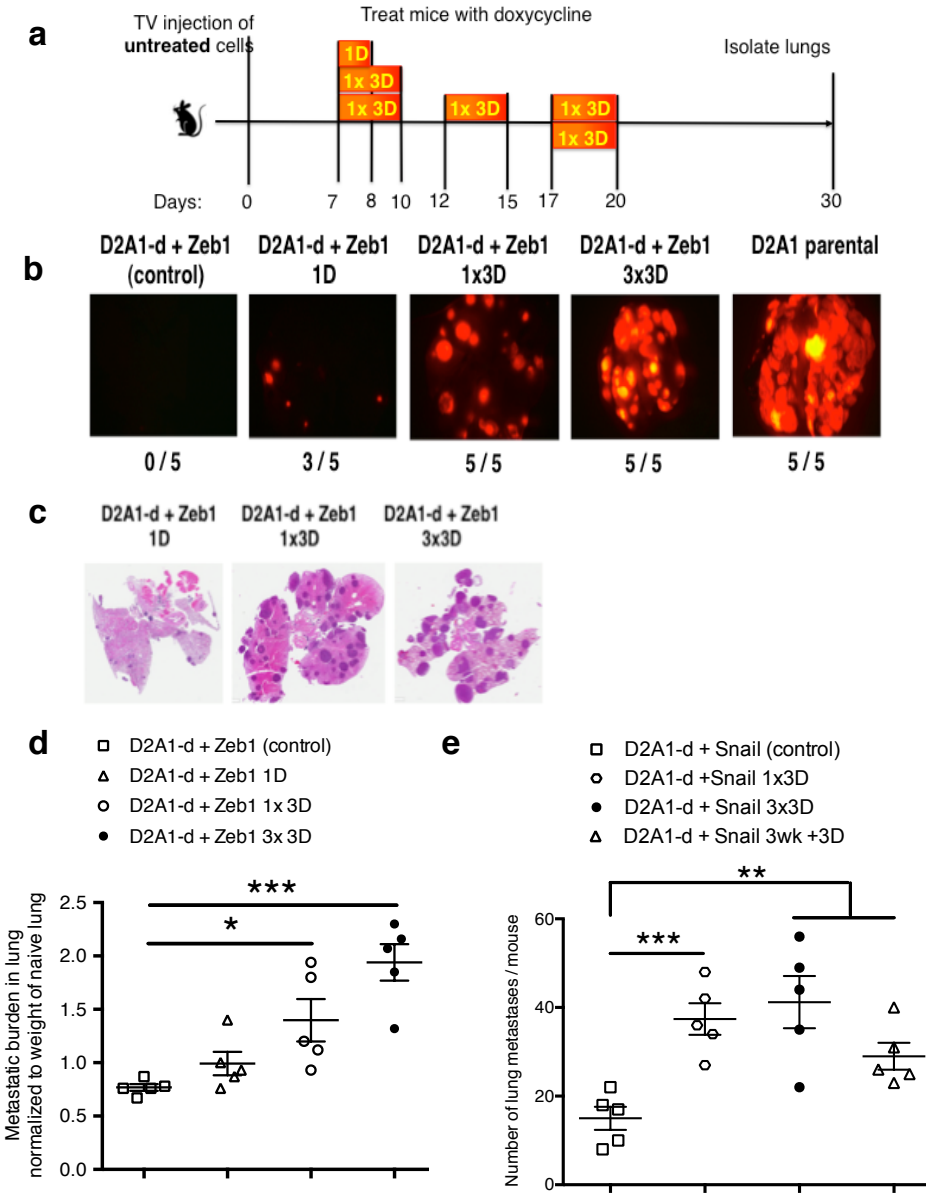

Figure 12. A three-day induction of Zeb1 provokes a robust awakening of dormant DTCs after seven or twenty-one days of dormancy

(a) Schematic depiction of the *in vivo* strategy used to determine the limitations of the transient EMT-TF induction. On day 0, mice were injected with dormant D2A1 (*D2A1-d*) cells harboring either the doxycycline-inducible vector Snail or Zeb1. On day 7, mice were randomly divided into groups: mice that were never to receive doxycycline-treated water (*D2A1-d + Snail_control* or *D2A1-d + Zeb1_control*), mice that were to be fed doxycycline-treated water for a single day (*D2A1-d + Zeb1_1D*), mice that were to be fed doxycycline-treated water for three consecutive days (*D2A1-d + Snail_3D* or *D2A1-d + Zeb1_3D*), mice that were to be fed doxycycline-treated water for three three-day pulses (*D2A1-d + Zeb1_3x3D* or *D2A1-d + Zeb1_3x3D*), or mice that were to be fed doxycycline-treated water after three weeks of dormancy for three consecutive days (*D2A1-d + Snail_3w+3D*). At the end of the respective doxycycline-regimen, the mice were given normal water until the end of the experiment; **(b)** Representative fluorescent images of whole lungs taken following *in vivo* strategy outlined above of mice injected with D2A1-d + Zeb1 cells; **(c)** Representative H&E staining of histological sections prepared from lungs of mice as in Panel b; **(d)** Quantification of Zeb1-induced lung metastases as determined by metastatic burden normalized to weight of naïve lung. Each data point represents the number of lung metastases in an individual mouse; **(e)** Quantification of Snail-induced lung metastases as determined by numbers of metastatic nodules visible under fluorescent dissection microscope at 0.8x magnification. Each data point represents the number of lung metastases in an individual mouse. Data are

represented as mean ± SEM. The *P*-values were calculated by Student's t-test. (*) $P < 0.05$; (**) $P < 0.004$; (***) $P < 0.001$.

Zeb1 expression is necessary for the awakening of dormant disseminated cancer cells

The above experiments demonstrate that transient Snail or Zeb1 expression is sufficient to cause the awakening of dormant disseminated cancer cells after various periods of dormancy. A key question that-remained unanswered was whether Zeb1 expression is necessary for the awakening of cancer cells from dormancy.

A previous graduate student in our lab, Kong Jie Kah, studied the relationship between the different EMT-TF that were known at that time and developed an EMT core expression signature, i.e., an expression signature that was shared by cells transformed by these various EMT-TFs. He found that Zeb1 was a central mediator of the EMT, functioned downstream to EMT-TFs such as Slug, Snail and Twist, and that the Snail protein can bind to the Zeb1 promoter thereby activating Zeb1 expression. I confirmed the ability of Snail expressing cells to also express Zeb1 by western blot analyses. Indeed D2A1-d cells that had been induced to express Snail after seven days of doxycycline began to express Zeb1 protein (Figure 13a). To determine whether the Snail-induced metastatic outgrowth was in part mediated by the endogenous up-regulation of Zeb1, I decided to infect the D2A1-d + Snail cells with short hairpin RNAs against Zeb1 messenger RNAs (shZeb1). The shZeb1 constructs were efficient at knocking down the expression of Zeb1 following Snail induction in the D2A1-d + Snail cells (Figure 13a). Of the two short hairpins that I used, only one of them, shZeb1_B, was able to confer a 90% knockdown of the Zeb1 protein, while shZeb1_A conferred a 50% knockdown of the Zeb1 protein.

I proceeded to inject five mice via the tail vein with D2A1-d + Snail cells harboring a control shRNA and ten mice via the tail vein with D2A1-d + Snail cells that harbored either shZeb1_A or the shZeb1_B. Seven days later, I treated these mice with two three-day pulses of doxycycline-treated water separated by a two-day interval of regular water. Two weeks later I sacrificed these mice, harvested their lungs and counted the number of metastases under the fluorescent dissection microscope (Figure 13b).

The mice that had been injected with the D2A1-d + Snail cells harboring a control shRNA developed on average 16 metastases per mouse. The mice that had been injected with the D2A1-d + Snail + shZeb1_B cells, which completely knocked-down Zeb1 expression, had five metastases per mouse, while the mice that had been injected with the D2A1-d + Snail + shZeb1_A cells, which had an incomplete knockdown of Zeb1 expression, had an average of seven metastases per mouse. Overall the mice that had been injected with D2A1-d + Snail cells harboring the shZeb1 constructs developed on average six metastases per mouse. Since Snail and Zeb1 both control the expression of a common subset of genes, it is not surprising that a complete loss of Zeb1 expression did not entirely abrogate metastatic outgrowth. Nonetheless, this 2.5-fold reduction in the total number of lung metastases suggests that Zeb1 contributes to optimal awakening of dormant DTCs.

Figure 13: Knockdown of Zeb1 in Snail-expressing D2A1-d cells inhibits metastatic outgrowth

a

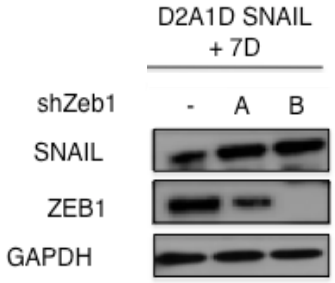

b

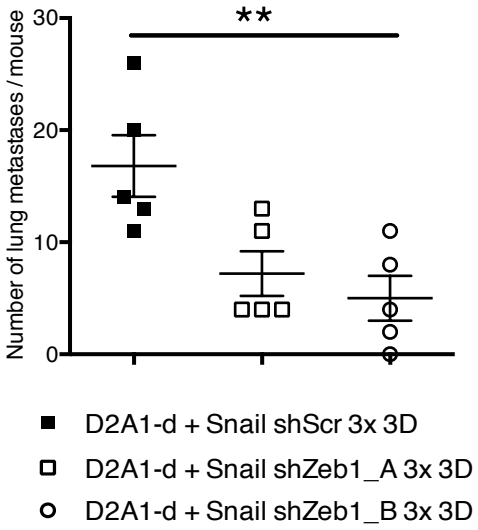

Figure 13. Knockdown of Zeb1 in Snail-expressing D2A1-d cells inhibits metastatic outgrowth

(a) D2A1-d cells expressing Snail and transduced with control- or Zeb1-shRNAs were treated for seven days with 1 μg/mL of doxycycline and whole-cell lysates were analyzed using Western blot to gauge Zeb1 protein knockdown; **(b)** Quantification of lung metastases as determined by numbers of metastatic nodules visible under fluorescent dissection microscope at 0.8x magnification. Each data point represents the number of lung metastases in an individual mouse. Data are represented as mean ± SEM. The *P*-values were calculated by Student's t-test. (*) $P < 0.05$; (**) $P < 0.009$. *D2A1-d + Snail + shScr* - D2A1-d cells harboring a doxycycline-inducible vector expressing Snail and a control shRNA; *D2A1-d + Snail + shZeb1_A* - D2A1-d cells harboring a doxycycline-inducible vector expressing Snail and shRNA against Zeb1 A vector; *D2A1-d + Snail + shZeb1_B* - D2A1-d cells harboring a doxycycline-inducible vector expressing Snail and shRNA against Zeb1 B vector.

Transient expression of Zeb1 generates metastasis-initiating cells (MICs)

The experiments above converge on the notion that induced Zeb1 expression is sufficient to induce metastatic outgrowth of otherwise-dormant carcinoma cells in the lungs. To determine whether the transient induction of EMT-TFs had re-programmed the D2A1-d cells in a cell-heritable manner, I isolated D2A1-d + Snail and D2A1-d + Zeb1 cells from the pooled lung metastases of individual mice that had been treated with three three-day pulses of doxycycline by FACS. I then injected 100,000 of these cells into the tail vein of naïve mice after a week of culture *in vitro* (Figure 14a). Three weeks later all mice had developed lung metastases to the same extent as mice that had been injected with parental D2A1 cells i.e., ≥100 metastases per mouse (Figure 14b&c). This was in sharp contrast to what is observed when mice are injected with 100,000 of D2A1-d cells that had not been previously awoken *in vivo,* which yielded no metastases. This result suggested that the EMT-awoken D2A1-d that had been previously isolated from lung metastases had undergone cell-heritable changes in gene expression.

Figure 14: Tumor cells isolated from EMT-awoken lung metastases readily form macro-metastases

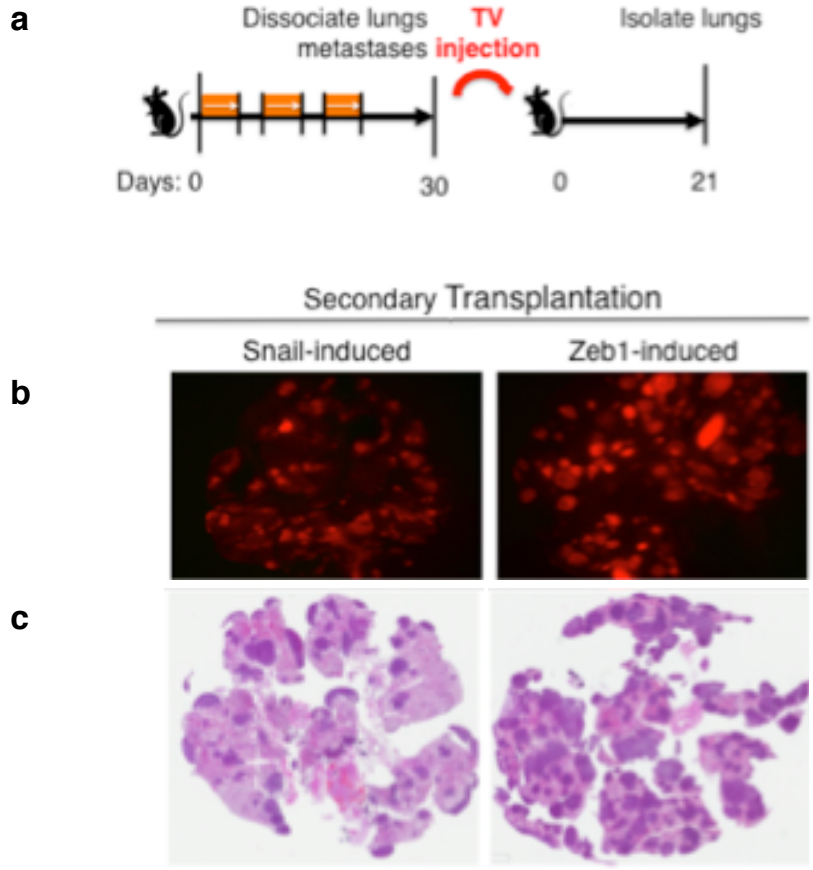

Figure 14. Tumor cells isolated from EMT-awoken lung metastases readily form macro-metastases

(a) Schematic depiction of *in vivo* strategy; (**b)** Representative fluorescent images of whole lungs were taken from representative mice immediately at necropsy; Data are representative of two independent experiments; n=8; **(c)** Representative H&E staining of histological sections prepared from lungs of mice. Data are representative of two independent experiments.

From the literature and from work published in our lab, the EMT program has been proven to generate CSCs (Morel, A.P. *et al* 2008; Mani, S.A. *et al* 2008). These EMT-induced CSCs have been characterized by several traits, such as 1) their ability to form tumorspheres *in vitro*, 2) their cell-surface marker profile by flow cytometry, 3) their ability to initiate tumors when implanted at limiting dilutions *in vivo*, and 4) their elevated resistance to certain therapeutics (Polyak, K. & Weinberg, R.A. 2009; Thiery, J.P. *et al* 2009). The majority of these studies, however, have been carried out using human cells. As such, the cell-surface markers relevant to murine cells have not been as well established.

To determine if the parental D2A1 cells and the D2A1-d cells differentially expressed certain cell-surface markers, I stained both cell types with a combination of known murine cell-surface markers (Visvader, J.E. & Smith, G.H. 2011; Shibue, T. *et al* 2013). Of the cell-surface markers that I tested, only the CD24 marker yielded an expression profile that was significantly different between the two cell types (Figure 15a). Thus, the parental D2A1 cells were largely $CD24^-$ while the D2A1-d cells were $CD24^+$**.** Furthermore, when the D2A1-d + Zeb1 cells were treated *in vitro* with doxycycline for seven days, there was a marked shift from a $CD24^+$ to $CD24^-$ expression state (Figure 15a).

Remarkably, when the cells isolated from the metastases of the D2A1-d + Zeb1 cells that had transiently been treated with doxycycline *in vivo* for three days or three days with doxycycline were examined for their CD24 profile, the majority of cells were

$CD24^-$ (Figure 15b). This suggests that even *in vivo*, there is a shift in the CD24 profile of D2A1-d cells.

To determine whether the shift in CD24 expression was functionally meaningful, I determined the metastatic potential of the isolated $CD24^-$ and $CD24^+$ populations from the doxycycline-treated D2A1-d + Zeb1 cells. After five days of *in vitro* doxycycline-treatment, I isolated the $CD24^-$ and $CD24^+$ populations from the D2A1-d + Zeb1 cells by FACS and injected them via the tail vein into mice (Figure 15c).

For this experiment, mice were divided into four groups, with all mice in these groups receiving 100,00 cells per tail vein injection: 1) mice were injected with untreated D2A1-d + Zeb1 cells, 2) mice were injected with unsorted D2A1-d + Zeb1 cells that had been treated with doxycycline for five days *in vitro*, 3) mice were injected with the sorted $CD24^+$ D2A1-d + Zeb1 cells that had been treated with doxycycline for five days *in vitro,* 4) mice were injected with the sorted $CD24^-$ D2A1-d + Zeb1 cells that had been treated with doxycycline for five days *in vitro*. Following tail vein injection these mice were housed for four weeks at which time the mice were sacrificed and lungs were harvested (Figure 15d).

The mice that had been injected with the doxycycline-untreated D2A1-d + Zeb1 developed on average three metastases per mouse; the mice that were injected with unsorted D2A1-d + Zeb1 cells that had been treated with doxycycline for five days *in vitro* developed on average fifteen metastases per mouse; the mice that were injected with

the sorted $CD24^+$ D2A1-d + Zeb1 cells that had been treated with doxycycline for five days *in vitro* developed on average two metastases per mouse; the mice that were injected with the sorted $CD24^-$ D2A1-d + Zeb1 cells that had been treated with doxycycline for five days *in vitro* developed on average thirty-six metastases per mouse.

There was a 16-fold increase in the metastatic potential of the $CD24^-$ cells compared to the $CD24^+$ cells. Of note, by western blot, I was able to confirm that Zeb1 was expressed in both sub-populations of cells (Figure 15e). This result was suggestive that low CD24 cell-surface expression can serve as marker of putative MICs.

The question remained, however, whether the difference in metastatic potential between the $CD24^-$ and $CD24^+$ expressing D2A1-d + Zeb1 cells was restricted to their ability to colonize the lungs or whether, alternatively there also existed a difference in their ability to form primary tumors. I therefore injected the same four groups of D2A1-d + Zeb1 cells into the mammary fat pad of mice at limiting dilutions (Figure 15f&g). Following fat pad injection, all four groups of D2A1-d + Zeb1 cells were able to tumor initiate at the same frequency (Figure 15f&g). This result therefore suggests that both the $CD24^-$ and $CD24^+$ cells had CSC-like traits, while only the $CD24^-$ had MIC-like traits. Therefore, MICs may represent a subset of CSCs.

Figure 15: Transient Zeb1 expression generates "metastasis-initiating cells" (MICs)

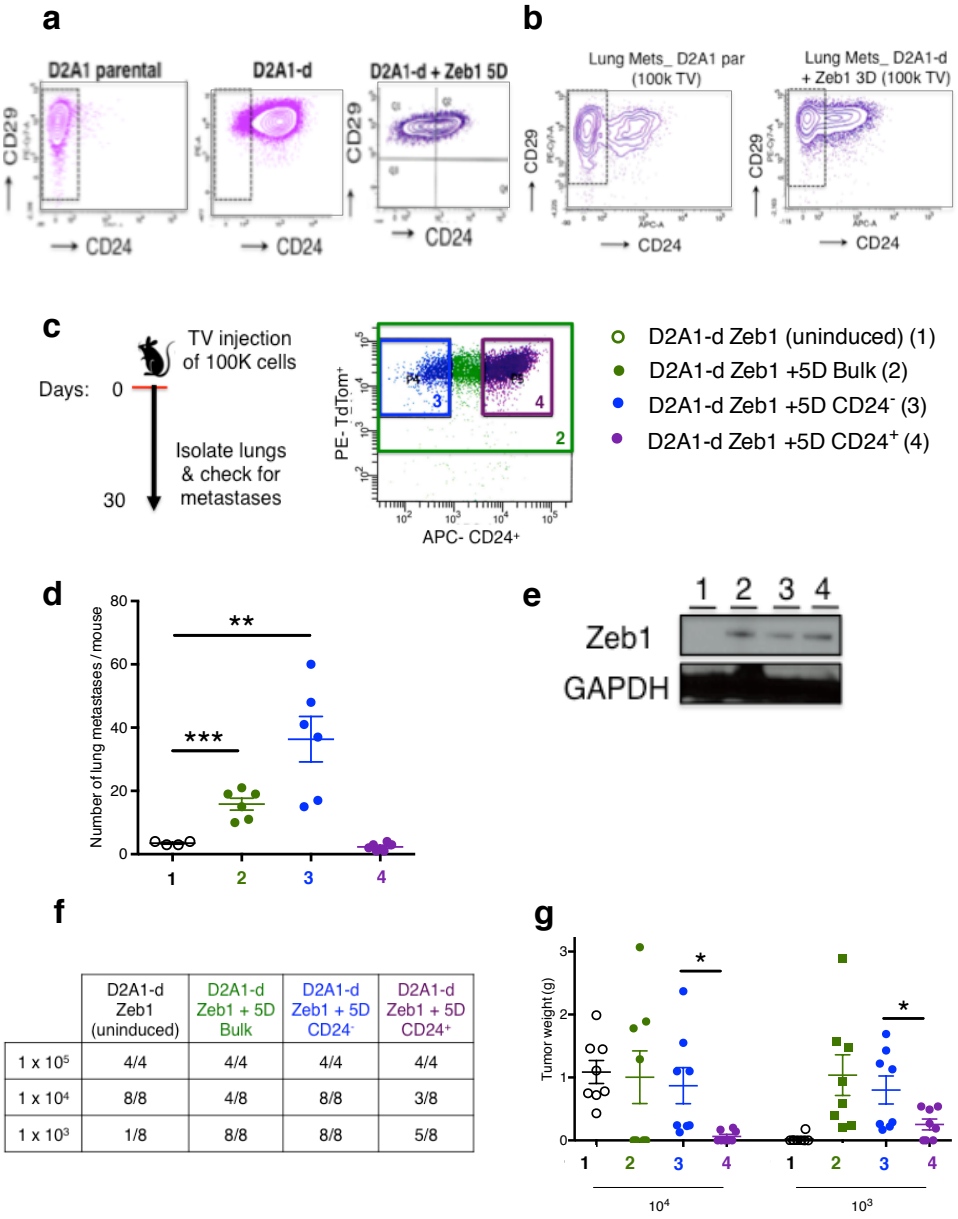

	D2A1-d Zeb1 (uninduced)	D2A1-d Zeb1 + 5D Bulk	D2A1-d Zeb1 + 5D CD24⁻	D2A1-d Zeb1 + 5D CD24⁺
1 x 10^5	4/4	4/4	4/4	4/4
1 x 10^4	8/8	4/8	8/8	3/8
1 x 10^3	1/8	8/8	8/8	5/8

Figure 15. Transient Zeb1 expression generates "metastasis-initiating cells" (MICs)

(a) Flow cytometry analysis of the CD29 and CD24-cell surface expression of D2A1-d, D2A1 cells and D2A1-d + Zeb1 after five days of doxycycline treatment; **(b)** Flow cytometry analysis of the CD29 and CD24-cell surface expression of tumor cells isolated from D2A1-d + Zeb1 lung metastases and parental lung metastases; **(c)** Schematic depiction of the *in vivo* strategy used to determine whether the EMT program generates MICs. On the fifth day of doxycycline treatment *in vitro*, D2A1-d + Zeb1 cells were sorted by FACS based on their CD24-cell surface expression. Untreated D2A1-d + Zeb1, D2A1-d + Zeb1 +5D bulk, sorted $CD24^-$ D2A1-d + Zeb1 +5D and sorted $CD24^+$ D2A1-d + Zeb1 +5D cells were each injected at 100,000 cells into the tail vein of BALB/c mice; **(d)** Quantification of lung metastases as determined by numbers of metastatic nodules visible under fluorescent dissection microscope at 0.8x magnification. Each data point represents the number of metastases in an individual mouse. Data are represented as mean ± SEM. Data are representative of three independent experiments, n=10; **, P< 0.07; ***, P< 0.001 by Student's *t* test; **(e)** Whole-cell lysates of cells described above were immunoblotted for Zeb1. GAPDH served as loading control; **(f)** Table of incidence of primary tumor formation in mice orthotopically implanted with the groups of cells isolated as described in Panel c; (**g**) Quantification of primary tumor weights at indicated doses six weeks post-injection. Data are represented as mean ± SEM. The *P*-values were calculated by Student's t-test. (*) $P < 0.05$; (**) $P < 0.01$; (***) $P < 0.001$.

Discussion

Based on these experiments, I propose a novel mechanism by which dormant DTCs can colonize the lungs. Transient Snail- or Zeb1-expression, in contrast to constitutive expression, enables cancer cells to maintain their cellular plasticity, which they need to re-initiate the tumor. Support for the role of the EMT program at the metastatic site comes from recent publications, which have shown that transient Snail expression is necessary for initiating metastatic outgrowth (Wendt, M.K. *et al* 2011; Tran, H.D. *et al* 2014; Moody, S.E. *et al* 2008). Indeed loss of e-cadherin is required for the initiation of metastastic outgrowth either by direct knockdown of protein levels (Wendt, M.K. *et al* 2011) or by hypermethylation of the *CDH1* promoter and histone modification (Lyu, T. *et al* 2013).

At first glance my findings might appear contradictory to those of Ocaña, O.H. *et al* (2012) and Tsai, J. H. *et al* (2012), both of which suggest that it is the MET program, and not the EMT program, that precedes re-activation of dormant cancer cells. However, I believe that these studies as well as my own, converge on the notion that cancer cells must acquire tumor-initiating-like qualities in order colonize the metastatic site. This will be discussed in greater detail in the following paragraph. Cancer cells that are trapped in a more mesenchymal state lack the plasticity (and the ability to generate via MET) more epithelial cells that are equally important components of metastatic outgrowths. To date, however, there has been no indication that the MET program can generate CSCs.

There is a growing understanding that the EMT program cannot be divided into two distinct cell states: epithelial versus mesenchymal. Instead, the EMT program involves a range of intermediate states. It is my belief that a "partial EMT", which is currently very loosely defined as cancer cells having maintained some epithelial-like traits while having gained certain mesenchymal-like traits, is the ideal cell-state for tumor initiation and generates cells that may become CSCs (Figure 16).

Figure 16: The EMT is a dynamic process and a manifestation of epithelial plasticity

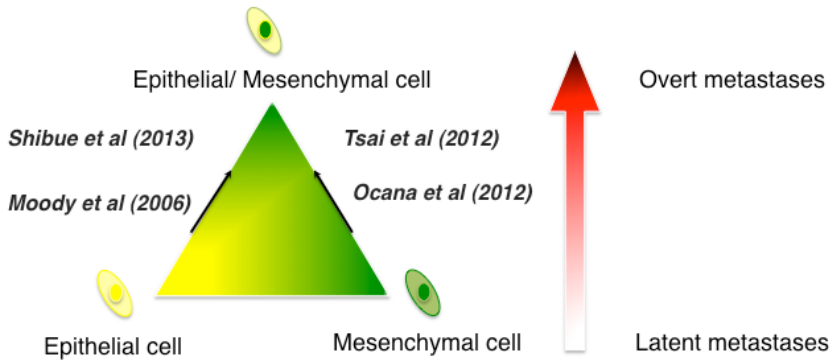

Figure 16. The EMT is a dynamic process and a manifestation of epithelial plasticity

Schematic depiction of the intermediate EMT states along with their plausible tumor-initiating capabilities. The extent of EMT varies (indicated by triangle) from a transient loss of cell polarity to total reprogramming of the cell, thus generating a spectrum of metastable phenotypic states. It is currently believed that a "partial EMT", accessible by either the EMT program or the mesenchymal-to-epithelial transition (MET) program, is associated with the acquisition of stemness properties and tumor-initiation, while a complete epithelial or mesenchymal state is unfavorable for tumor initiation.

In the 2012 Ocaña, O.H. et al. paper, the authors use the human BT-549 mammary cancer cell line, which can be defined as mesenchymal, as it expresses vimentin and lacks E-cadherin expression. Following knockdown of the EMT-inducer PRRX1 using short hairpin RNAs in the BT-549 cells (BT-549 + shPRRX1), the observed MET was indicated by the gain of expression of E-cadherin at the cell-to-cell junctions and a shift from the $CD44^{+}CD24^{+}$ cell state to a $CD44^{+}$ $CD24^{-}$ cell state. Furthermore in this study, only the BT-549 + shPRRX1 cells were able to form lung metastases following tail vein injection into mice. Therefore, despite the need of the EMT to be inhibited in the BT-549 cells, metastatic outgrowth in this cell line was associated with a shift in the cell surface expression of CD24, validating an observation that was made in the present work.

Tsai, J.H. et al. (2012) utilized a 7,12-dimethylbenz[a]anthracene (DMBA)/ 12-O-tetradecanoulphorbol-13-acetate (TPA) skin tumor model to study the impact of irreversible and reversible induction of Twist1 on metastasis. As revealed by this model, mice that had a reversible induction of Twist1 developed lung metastases and significantly more metastatic lesions than mice that had an irreversible induction of Twist1. While the authors did not conduct additional experiments to identify the regulators modulating cellular plasticity, these results would seem to confirm the findings demonstrated in the present work that a transient induction of the EMT program, rather than a continuous induction, is necessary experimentally to create cells that are capable of colonization. Interestingly, BT-549 cells harboring short RNA hairpins against Twist messenger RNAs are unable to form any lung metastases (Ocaña, O.H. *et al* 2012).

Taken together these two reports appear to conflict in their evidence as to whether Twist1 may facilitate colonization. From my own *in vitro* and *in vivo* experiments using Twist, I conclude that Twist is not involved in metastatic outgrowth. However, I believe it is rather premature to make generalization about the EMT program based on a single EMT-TF and cell-line. It would be more prudent to suggest that the induction of the EMT or MET program following extravasation may be highly dependent on the cell type and where the cells reside on the epithelial-mesenchymal spectrum (Figure 16).

As a whole, the body of work presented in this chapter reveals that transient induction of the EMT program, and not a continuous induction, through controlled expression of Snail or Zeb1, is sufficient to awaken dormant DTCs. The transient induction of Zeb1 causes these previously dormant DTCs to generate MICs that are capable of colonizing the lungs. The transient induction allows endogenous Zeb1 to turn on which is important for metastases formation (Guo, W. *et al* 2012). In the next chapter, I will discuss my efforts at identifying stimuli that could activate the endogenous EMT program in cancer cells *in vivo* and thereby provide a more realistic picture of how dormant cancer cells could be awoken in a clinical setting.

Materials and Methods

Cell Culture

All cells were cultured in 5% CO_2 humidified incubator at 37° C. Parental D2A1 and D2A1-d cells were grown in Dulbecco's Modified Eagle's Medium (DME) supplemented with 5% inactivated fetal bovine serum (IFS), 5% calf serum, 100 U/ml penicillin, and 100 μg/ml streptomycin (Invitrogen). Mouse mammary carcinoma cell line D2A1 was a gift from P.L. Lollini. Cells were passaged when confluence reached ~80% with 0.15% trypsin and re-seeded in a ratio of 1/12. Medium was always changed every third day.

Cell proliferation assay

Cells were seeded at 1.0 x 10^6 into 10 cm, split and counted using the automatic counter Vi-CELL Cell Viability Analyzer (Beckman Coulter) every three days for fourteen days.

Plasmids and lenti-viral infections

Mouse Snail, Twist1, Zeb1 cDNAs obtained from Open Biosystems were subcloned into FUW-LPT2 tetracycline-inducible lentiviral vector (modified from FUW-tetO by Kong-Jie Kah) with puromycin resistance gene. pMMP-LucNeo, carrying coding sequences for luciferase and neomycin phosphotransferase, were obtained from Dr. Segal.
pLKO-puro was used as backbones for the lentiviral vectors expressing short hairpin RNAs (shRNAs). The shRNA sequences for Zeb1 were: (sh Zeb1 A) GTCGACAGTCAGTAGCGTTTA and CCGCCAACAAGCAGACTATTC (sh Zeb1 B). Cells were seeded at 5.0 x 10^5 cells per 10 cm dish and transduced 24 hours later with concentrated virus in the presence of 5 μg/ml polybrene (EMD Millipore #TR-1003-G).

The selection of cells that were successfully infected with lentivirus or retrovirus was performed with medium containing 4 μg/ml of puromycin. The infection efficiency was routinely greater than 80%.

Quantitative RT-PCR

Total RNA was isolated directly from cultured cells using the RNeasy Plus Mini kit (Qiagen #74136). Reverse transcription was performed with High Capacity cDNA Reverse Transcription Kit (Life Technologies #4368814). mRNA levels were measured with gene-specific primers using SYBR Green I master mix (Roche) on a Roche LightCycler 480 system (Roche). Relative expression levels were normalized to β-actin. The PCR primer sequences are listed in the table below and were used as described previously (Shibue, T. & Weinberg, R.A. 2009).

Snail	forward	GCTGCTTCGAGCCATAGAACTAAA
	reverse	TTGAGGGAGGTAGGGAAGTGG
Twist	forward	CCTGTGGACTGGCTCCATTTT
	reverse	CCAGTTTGATCCCAGCGTTT
Zeb1	forward	GTCTTCCTTTAGTTGATCAGGATGG
	reverse	TGTAGGGGCTGGGATTTCTTT
β-actin	forward	ACCGTGAAAAGATGACCCAGA
	reverse	AGGCATACAGGGACAGCACA

Immunoblotting

Cells were harvested and lysed in RIPA buffer [25 mM Tris-HCL (ph 7.6), 150 mM NaCl, 1% Nonidet P-40, 1% sodium deoxycholate, O.1% SDS, 1x complete protease

inhibitor mixture (Roche), 1x phosphatase inhibitors (Roche Diagnostics)]. The protein extracts were separated by 10% SDS-PAGE and were transferred to polyvinylidene fluoride (PVDF) membranes (Millipore). After one hour blocking in 5% non-fat milk, the membranes were incubated overnight with primary antibodies at 4'C. Blots were developed using ECL (Dura or Femto, Pierce). The types and dilutions of primary antibodies used were the following: Snail (Cell Signaling Technology 3879S; $1:10^3$), Twist (Abcam ab50887; $1:10^4$), Zeb1 (Cell Signaling Technology 3396S; $1:10^3$), E-cadherin (Cell Signaling Technology 3195S; $1:10^3$), Cytokeratin 5 (Covance PRB-160P; $1:10^3$); Fibronectin (BD Biosciences 610078; 1: 10^3), N-cadherin (Cell Signaling 4061; $1:10^3$); Vimentin (Cell Signaling Technology 5741S; $1:10^3$), GAPDH (Cell Signaling Technology 2118S; $1:10^4$).

Animals

Balb/c mice were obtained from Jackson Laboratory (stock number 000651). All research involving animals was conducted in accordance with the Guide for the Care and Use of Laboratory Animals of the National Institute of Health. All animals were maintained according to the guidelines of the MIT Committee on Animal Care protocol (1014-109-17). All efforts were made to minimize suffering. Mice that had been dead by the end of experiments were excluded from the analysis.

For intravenous injections, 1.0 x 10^5 cells, unless otherwise indicated, resuspended in 100 μL of phosphate-buffered saline (PBS) were injected into the lateral tail vein. The lungs were examined for metastases four to six weeks post-injection. The *in vivo*

doxycycline treatment was administered through drinking water containing 2 mg/mL doxycycline and 10 mg/mL sucrose.

For orthotopic tumor transplantations, 1.0 x 10^5 tumor cells, unless otherwise indicated, resuspended in 20 μL of their growth medium and 50% Matrigel were implanted bilaterally into the fourth mammary fat pad of 6 to 8-week old female syngeneic Balb/c mice. The tumor incidence was determined six to eight weeks post-injection.

Quantification of lung metastases

Whole lung images were taken using a fluorescence dissection microscope (Leica MZ12). Colonies visible at 0.8x magnification of objective lens under fluorescence microscopy were counted as macro-metastases.

Histology

Primary tumors were fixed in 10% neutral buffered formalin overnight and embedded in paraffin for sectioning; lungs were fixed in 4% paraformaldehyde and paraffin-embedded. Sections (5 μm thick) were cut from paraffin-embedded tissues and stained with haemotoxylin and eosin. Entire tissue sections were imaged at 20x with the Aperio slide scanner (Leica Biosystems), and the number of metastases per section quantified using ImageScope analysis software (Leica Biosystems).

Flow cytometry

Lungs were minced using a razor blade and incubated in a DME based dissociation solution containing DNAse and 1.5 mg/ml Collagenase A (Roche) rotating at 37ºC for two hours. The dissociated lungs were then washed twice with PBS + 0.1% bovine serum albumin (BSA) , and filtered through a 70 μm and 40 μm cell strainer. To sort the D2A1 cells by the cell-surface expression of CD29 and CD24 markers, cells were detached from the culture dish and were incubated with CD29 (Affimetrix 25-0291-80; 1:200) and CD24 (Affimetrix 17-0242-80; 1:200) diluted in PBS. After incubating on ice for 45 minutes, cells were washed twice in PBS and sorted with a BD FACSAria (BD Biosciences).

Statistical Analysis

All data are represented as mean values ± standard errors of mean (SEM). *P* values of less than 0.05 were considered to be significant. Statistical analyses were carried out by two-tailed Student's t-test using Prism software (GraphPad Prism).

Chapter 4:

Inflammation triggers Zeb1-dependent escape from tumor dormancy

Introduction

In the previous chapter I have shown that the induction of the EMT program by the experimental activation of the Snail and Zeb1 EMT-TFs can cause dormant cancer cells to escape metastatic dormancy. To this extent, my work closely aligns with other studies that have focused on the cell-intrinsic traits that must be overcome to form overt-metastases (Oskarsson, T. *et al* 2011; Wendt, M.K. *et al* 2011; Gao, H. *et al* 2012). Nevertheless, yet other observations would indicate that both cell-autonomous and -non-autonomous changes must occur in order for cancer cells to exit dormancy and elicit metastatic relapse.

In fact the EMT program can be activated by heterotypic signals received by normal and neoplastic epithelial cells under various physiological and pathological states (Thiery, J.P. *et al* 2009). Indeed Lopez-Novoa, J.M. *et al* (2009) placed the EMT program at the centre of the crossing-point between cancer progression and inflammation. The importance of inflammation in cancer progression is widely recognized as inflammation is portrayed as one of the original hallmarks of cancer (Hanahan, D. & Weinberg, R.A. 2000).

Chronic inflammation, a hallmark of non-healing wounds, has been shown to predispose certain tissues, such as the colon, the liver and the pancreas to cancer development via ulcerative colitis, hepatitis and chronic pancreatitis (Junttila, M.R. & de Sauvage, F. J. 2013). Striking parallels have been described between the tumor microenvironment and the wound healing process, leading to the description of tumors as

"wound healing gone awry" (Dvorak, H.F. 1986). Despite the immense collection of studies that have outlined the role of inflammation and immune cells from primary tumor formation to intra-luminal survival and extravasation at the metastatic site (Joyce, J.A. & Pollard, J.W. 2009; see Appendix A), far less is known of the role of inflammation in metastatic colonization, i.e. the fate of extravasated cells within the parenchyma of a distant tissue. While there have been studies that have suggested that a pre-inflamed microenvironment in the lungs, can enhance the ability of DTC to colonize the metastatic site (Bouchard, G. *et al* 2013; Cox, T.R. *et al* 2013; El Rayes, T. *et al* 2015), to our knowledge, this is the first study that seeks to determine whether an inflamed microenvironment in the vicinity of dormant DTCs causes the escape cellular dormancy.

As such, I hypothesized that a localized inflammatory microenvironment in the vicinity of dormant DTCs can provoke the activation of the previously silent EMT program in dormant DTCs, thereby causing proliferation and metastatic outgrowth. This hypothesis was revised, as described in Chapter 2, to occur in the absence of any necessary involvement of FLPs in this awakening.

Numerous models of lung injury in mice exist (Matute-Bello, G. *et al* 2008). Of these, I decided to commence my study using lipopolysaccharide (LPS) as the agent that induces lung inflammation. LPS is an abundant glycoprotein expressed within the cell wall of the Gram-negative bacteria, such as *E. Coli*. Following injection into mice via intra-peritoneal (i.p.) injection or intra-tracheal (i.t.) instillation, mice readily develop a strong inflammatory response. Once entered into the circulation, LPS binds to the Toll-

Like receptor-4 (TLR4) displayed on the luminal surfaces of nearby endothelial cells, and this binding leads to the activation of NF-ϰB through the recruitment and activation of MyD88, IL-1R kinase (IRAK) (Ulevitch, R. J. & Tobias, P.S. 1995) in these cells. This activation culminates in the secretion of inflammatory mediators, such as tumor necrosis factor-alpha (TNF-α), IL1-β and IL-6 (Figure 17).

Figure 17: Signaling pathway of TLR4 receptor

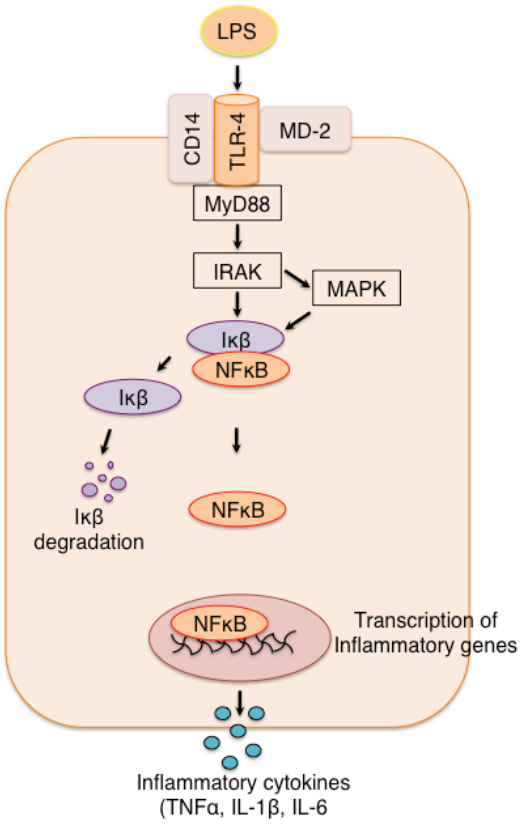

Figure 17. Signaling pathway of TLR4 receptor

Lipopolysaccharide (LPS) forms a complex with lipopolysaccharide-binding protein (LBP), which binds to cell surface CD14. This then forms a complex with Toll-like receptor 4 (TLR4) and MD2. The TLR4 signaling cascade is initiated after binding with the adaptor protein myeloid differentiation protein 88 (MyD88). The activation leads to a complex formation involving MyD88, IRAK4, IRAK2/1, TRAF6. This chain of events triggers the activation and translocation of NF-ϰB and results in the transcription of cytokines, such as TNF-α, IL-1β and IL-6. Adapted from Nahid, M.A. *et al* (2011).

The inflammatory response following a single dose of LPS is rather transient and is resolved within seventy-two hours (Su, X. *et al* 2011). Neutrophils are the first immune cell type to arrive at the site of injury (Andonegui, G. *et al* 2003). Shortly thereafter, macrophages are recruited by neutrophils. Of the released inflammatory cytokines, TNF-α, IL-6, IL-1β are abundantly secreted, as detected by the enzyme-linked immunosorbent assay (ELISA) from bronchoalveolar lavage fluid (Su, X. *et al* 2011). This set of released cytokines was of particular interest to me as these particular signaling molecules have been associated with inducing the EMT program (Thiery, J.P. *et al* 2009).

***In vitro* characterization of the effects of LPS on D2A1-d cells**

Prior to determining the effect of LPS-induced inflammation on the awakening of dormant DTCs *in vivo*, I undertook to characterize and rule out any potential direct effects of LPS on 1) the proliferation of D2A1-d *in vitro* and 2) the EMT status of the D2A1-d cells.

By western blot analyses, I confirmed the expression of TLR4 in D2A1-d cells following *in vitro* LPS treatment (Figure 18a). To determine whether LPS conferred a proliferative advantage to D2A1-d cells, I plated 500 D2A1-d cells with various concentrations of LPS (0.5 μg/mL; 2 μg/mL; 5 μg/mL) *in vitro* and monitored their proliferation (Figure 18b). Even at 5 μg/mL of LPS, with fresh LPS added daily, LPS did not confer proliferative advantage to the D2A1-d cells.

To determine whether TLR4 mediated LPS-induced activation of *NF-κB*, I transduced the D2A1-d cells with a NF-κB -luciferase reporter plasmid generated by Dr. Brian Bierie, a post-doc in the lab. Dr. Bierie cloned a fragment of the NF-κB promoter into a luciferase reporter plasmid (Figure 18c). As a negative control, I also transduced the D2A1-d cells with a viral vector expressing shRNAs targeted against TLR4 and the NF-κB-luciferase reporter. As shown in Figure 18c, the relative luciferase activity was three-fold higher in the D2A1-d + NF-κB-luciferase reporter cells after 2-6 hours of LPS treatment, as compared with the untreated D2A1-d cells and the D2A1-d cells expressing shTLR4 that had been treated with LPS. 24 hours after LPS treatment, no statistically significant difference was observed between LPS-treated and untreated D2A1-d cells. These results indicated that LPS signaling was active in D2A1-d, but that the signal was lost within 24 hours.

Furthermore western blot analysis for proteins associated with the EMT program such as Zeb1, keratin 8 remained unexpressed or failed to alter in their expression after two weeks of LPS treatment *in vitro (*Figure 18d). This result suggested that LPS had no direct effect on the proliferation or EMT status of the D2A1-d cells *in vitro*. However, these observations could not rule out a direct mitogenic effect *in vivo*.

Figure 18: LPS activates NF-κB through TLR4 but does not confer a proliferative advantage or induce EMT *in vitro*

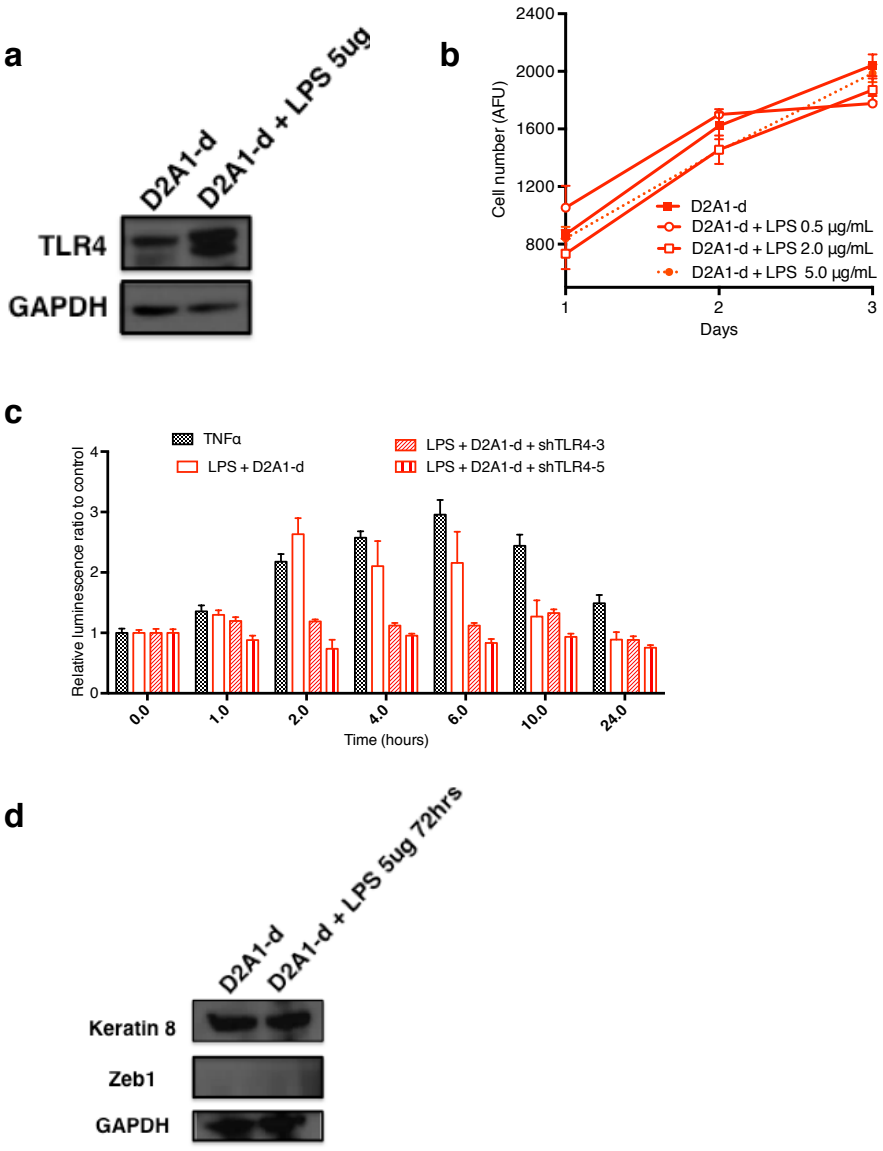

Figure 18. LPS activates NF-κB through TLR4 but does not confer a proliferative advantage or induce EMT *in vitro*

(a) TLR4 protein levels were analyzed by Western blotting. 5 μg/mL of LPS was added daily to D2A1-d cells. After 72 hours cells were harvested and proteins were extracted; **(b)** *In vitro* proliferation assay of D2A1-d in the presence or absence of 0.5, 2 and 5 μg/mL of LPS as gauged in a luminometer. Data are representative of three independent experiments; **(c)** D2A1-d cells integrated with NF-κB-dependent luciferase reporter were treated with 5 μg/mL of LPS for 1, 2, 4, 6, 10, or 24 hours. D2A1-d cells co-transfected with shTLR4 and NF-κB-dependent luciferase reporter served as a control of TLR4 receptor activity. TNFα served as a positive control; **(d)** Effect of LPS on EMT in D2A1-d cells. Cells were incubated in the presence of 5 μg/mL LPS for 14 days and whole-cell lysates were immunoblotted for Zeb1 and keratin 8 expression. GAPDH served as loading control.

LPS as a model of pulmonary inflammation

As previously stated, LPS is a commonly used inflammation-inducing agent. To confirm the existence of an inflammatory response in mice following LPS treatment, I collected blood from LPS-treated mice at 4, 8, 24, 48 and 72 hours post-LPS treatment and analyzed the blood cell counts (Figure 19a). At 4 hours post-LPS treatment, there was a 20% increase in the number of circulating neutrophils; at 8 hours post-LPS treatment, this increase reached its peak and returned to baseline levels by 72 hours post-LPS treatment. At 8 hours post-LPS treatment, there was a modest 10% increase in the percent of circulating monocytes found in the blood. However, the percentage of circulating monocytes returned to baseline levels within 24 hours in the blood. These findings confirmed reports made by others in the field (Su, X. et al. 2011).

LPS-induced inflammation can awaken dormant DTCs

To directly address whether inflammation could cause the outgrowth of dormant DTCs, I first injected the D2A1-d cells into the tail vein of mice. One week later, I treated these mice with 2mg/kg of LPS via i.p. or 50 μg i.t. injection (Figure 19b). Within four weeks, mice exposed to LPS carried on average fifteen metastases per lungs, while the control mice solely injected with D2A1-d cells had at most one metastasis per lung (Figure 19c-d).

To determine whether this result was idiosyncratic to the D2A1-d cells, I sought to confirm this result using other murine carcinoma cell lines. Given the initial challenge to identify cancer cell lines that would become dormant following tail vein injection, I

sought to inject non-metastatic or weakly metastatic murine carcinoma cell lines, such as 67NR, 168FARN and TS/A-d, into the tail vein of mice and determine the presence of macro-metastases following LPS injection. (TS/A-d cells are another *in vivo* enriched dormant subpopulation of cells that were generated by Dr. Shibue.)

Since I had not fully characterized these cell lines, I decided to inject 100,000 TdTomato$^+$ 67NR cells and 100,000 TdTomato$^+$ 168FARN cells into mice via the tail vein, thereby using the same conditions as previously used for the D2A1-d cells. One week post-tail vein injection, I treated these mice with 2mg/kg of LPS via i.p. injection. Four weeks post-tail vein injection, I sacrificed these mice and counted the number of lung metastases under the fluorescent microscope. Mice injected with 168FARN or TS/A-d cells did not form any metastases, whether or not they had been treated with LPS. In contrast, untreated mice injected with 67NR cells developed an average of four metastasis per mouse, while LPS-treated mice injected with 67NR cells formed an average twelve metastases per mouse (Figure 19e). This result suggested that LPS could awaken not only D2A1-d cells but also 67NR cells. The failure to awaken the 168FARN cells may be due to the fact that they cannot be awakened regardless of the protocol tried, i.e., the 168FARN might be intrinsically refractory to awakening. I confirmed by *in vitro* LPS treatment of 67NR cells that LPS on its own did not confer a proliferative advantage to cells (Figure 19f).

Figure 19: LPS can awaken dormant DTCs *in vivo*

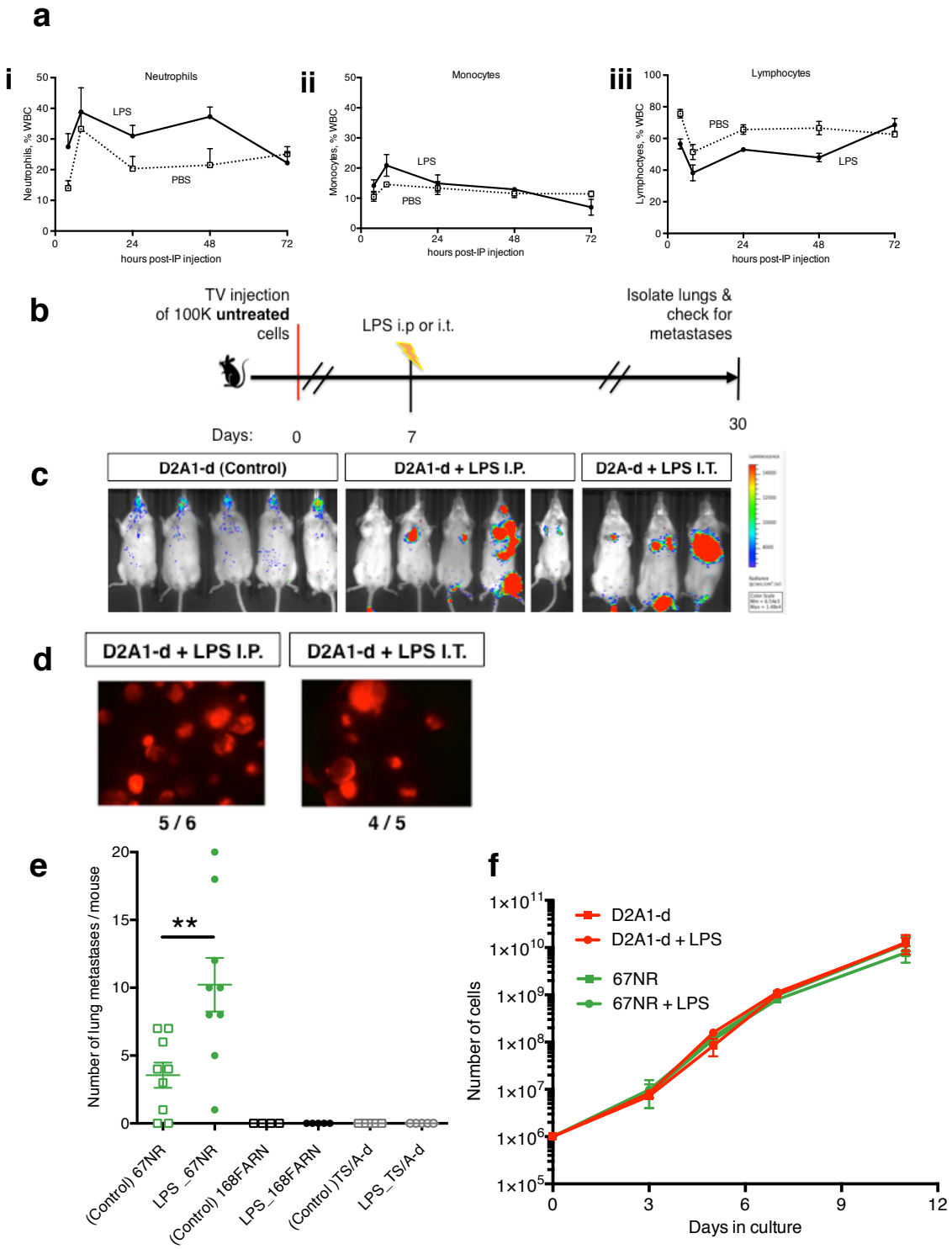

Figure 19. LPS can awaken dormant DTCs *in vivo*

(a) Time-dependent changes in differential cell counts after LPS challenge (2mg/kg i.p.) in BALB/c mice. **(i)** neutrophils, **(ii)** monocytes, **(iii)** lymphocytes were monitored at 4, 8, 24, 48 and 72 hours after treatment. Blood samples for hematological studies were collected at the selected time intervals. Data represent the means ± SEM of 4 mice in each treatment group; **(b)** Schematic depiction of the *in vivo* strategy used to treat mice with LPS. On day 0, mice were injected via the tail vein with D2A1-d cells. On day 7, mice received 2mg/mL LPS i.p. or i.t.; **(c)** Representative luminescent images of mice previously injected with D2A1-d cells and that received LPS intraperitoneally as detected with an IVIS Spectrum. The animals were sacrificed thirty days later; **(d)** Representative fluorescent images of the above mice taken at 0.8x magnification under the fluorescent detection microscope. Data are representative of three independent experiments; **(e)** Mice were injected with 100,000 67NR, 168FARN or TS/A-d cells. Quantification of lung metastases as determined by numbers of metastatic nodules visible under fluorescent dissection microscope at 0.8x magnification. Each data point represents the number of lung metastases in an individual mouse. Data are represented as mean ± SEM (n=9). The *P*-values were calculated by Student's t-test. (*) $P < 0.05$; (**) $P < 0.008$; **(f)** Cell proliferation assay *in vitro* of D2A1-d and 67NR cells in the presence or absence of 5 μg/mL of LPS.

To conclusively determine whether the LPS-induced metastatic outgrowth was the byproduct of the inflamed microenvironment that was created upon LPS treatment and not the direct result of the D2A1-d cells responding to LPS *in vivo*, I purchased C.C3-TLR4$^{Lps\text{-}d}$/J mice from the Jackson Laboratory. This congenic BALB/c mouse strain was developed by Vogel, S.N. *et al* (1994) and has since then been widely used (Andonegui, G. et al. 2003). Aside from their unresponsiveness to LPS, the C.C3-TLR4$^{Lps\text{-}d}$/J mice are developmentally and immunologically normal. More than 50 years ago, the C3H/HeJ mouse strain was found to carry a codominant allele (Lps^{d}), which was responsible for its defective response to bacterial endotoxin (Sultzer, B.M. *et al* 1968; Watson, J. & Riblet, R. 1974). In 1998, this codominance was shown to be the result of a Proline to Histidine point mutation at position 712 in the amino acid sequence of TLR4 protein which had a dominant negative effect on LPS signal transduction (Poltorak, A. *et al* 1998).

I injected the C.C3-TLR4$^{Lps\text{-}d}$/J mice with 100,000 D2A1-d cells via the tail vein and treated these mice one week later with LPS. None of the mice that had been injected with D2A1-d cells and then treated with LPS developed lung metastases after six weeks, suggesting that the awakening of dormant DTCs is dependent upon the inflammatory signals released in the inflamed microenvironment in response to TLR4-mediated signaling (Figure 20a&b).

To control for the possibility that tumor growth is inhibited in C.C3-TLR4$^{Lps\text{-}d}$/J mice, I also injected D2A1-d cells into the mammary fat pads of C.C3-TLR4$^{Lps\text{-}d}$/J mice.

D2A1-d cells were able to form primary tumors, thereby excluding the possibility that C.C3-TLR4$^{Lps\text{-}d}$/J mice harbor additional genetic alterations that inhibit tumor growth (Figure 20c).

Figure 20: Stromal TLR4 is important for LPS-induced awakening of dormant DTCs

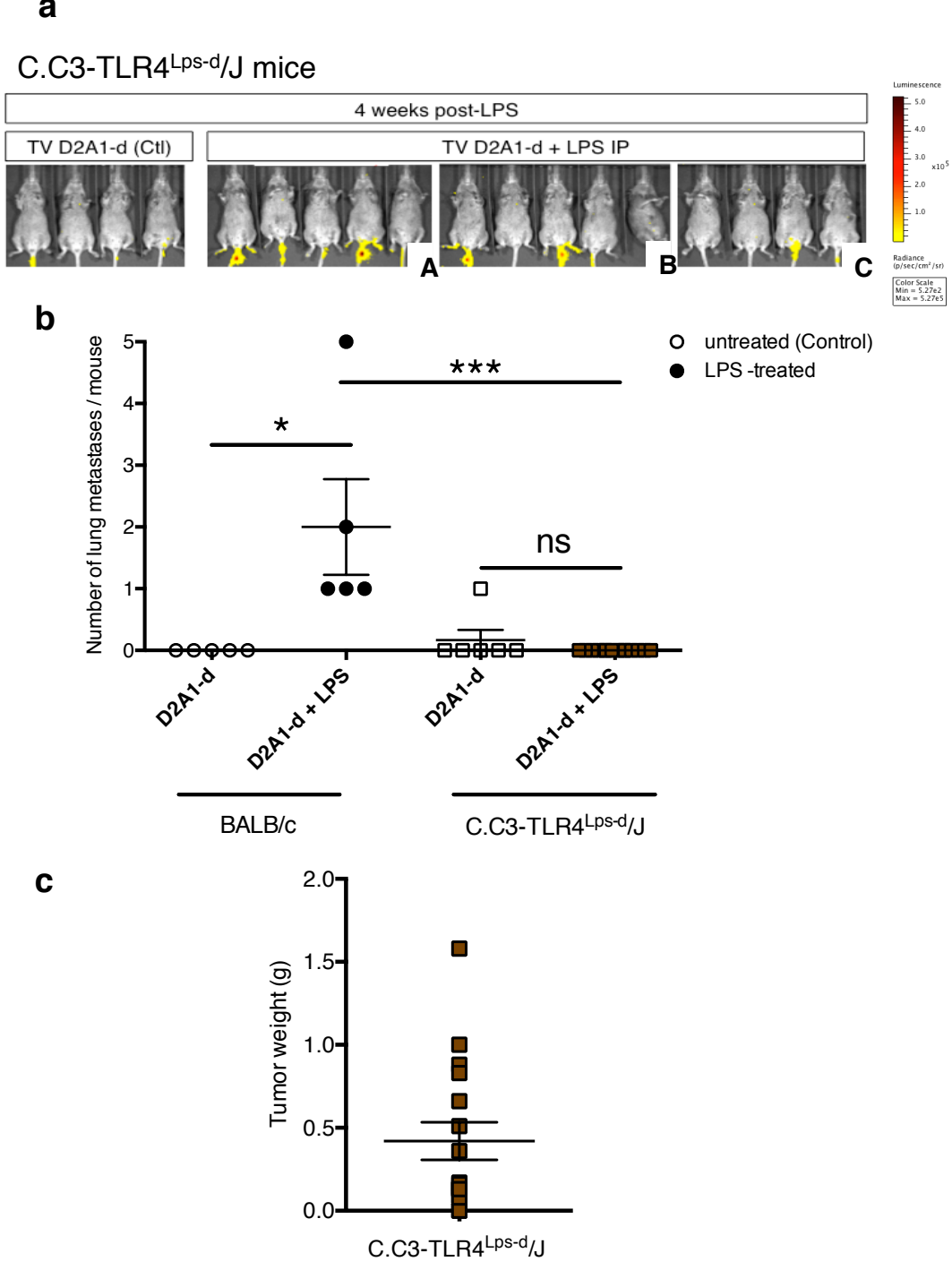

Figure 20. Stromal TLR4 is important for LPS-induced awakening of dormant DTCs

(**a**) Luminescent signals detected thirty days post-tail vein injection of D2A1-d cells in C.C3-TLR4$^{Lps\text{-}d}$/J mice treated with 2 mg/kg of LPS via i.p. injection. Data are representative of two independent experiment; (**b**) 100,000 D2A1-d cells were injected intravenously into either wild-type BALB/c mice or C.C3-TLR4$^{Lps\text{-}d}$/J mice, one week later mice were treated with 2 mg/kg LPS. Quantification of lung metastases as determined by numbers of metastatic nodules visible under fluorescent dissection microscope at 0.8x magnification at thirty days post-tail vein injection. Each data point represents the number of metastases in an individual mouse. The *P*-values were calculated by Student's t-test. (*) $P < 0.05$; (**) $P < 0.01$; (***) $P < 0.0004$; (**c**) Quantification of primary tumor weights at 10^5 D2A1-d cells five weeks post-injection into C.C3-TLR4$^{Lps\text{-}d}$/J mice. Data are represented as mean ± SEM.

In greater detail, LPS is known to activate neutrophils, macrophages and endothelial cells. Within four hours of i.p. administration of LPS, neutrophils preferentially congregate into the lungs and thereafter recruit monocytes to the lungs (Andonegui, G. *et al* 2003). To determine the specific subset of immune cells that mediated the observed escape from metastatic dormancy, I undertook to perform experiments in different immuno-deficient mouse backgrounds and to deplete specific subsets of immune cells.

To exclude the contribution of the adaptive immune system, I injected the D2A1-d cells via the tail vein in NOD-SCID mice, which lack B and T lymphocytes. One week later I treated these mice with LPS. Treating NOD-SCID mice that had been injected with D2A1-d cells with LPS provoked metastatic outgrowth, on average ten metastases per lungs, while the LPS-untreated mice developed on average three metastases per lungs (Figure 21). Hence, LPS-induced awakening of dormant DTCs is not significantly dependent on the presence of the adaptive immune system.

Figure 21: Adaptive immunity is not required for LPS-induced awakening of dormant DTCs

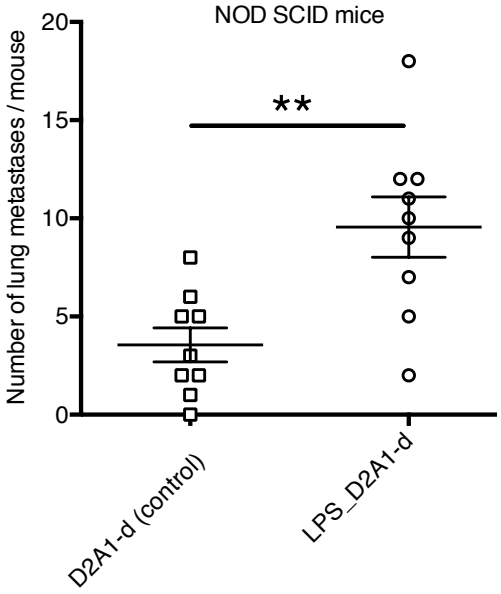

Figure 21. Adaptive immunity is not required for LPS-induced awakening of dormant DTCs

100,000 D2A1-d cells were injected intravenously into NOD-SCID mice, one week later mice were treated with 2 mg/kg LPS via i.p. injection. Quantification of lung metastases as determined by numbers of metastatic nodules visible under fluorescent dissection microscope at 0.8x magnification at thirty days post-tail vein injection. Each data point represents the number of metastases in an individual mouse. Data are represented as mean ± SEM. The *P*-values were calculated by Student's t-test. (*) $P < 0.05$; (**) $P < 0.01$; (***) $P < 0.001$.

Prior to determining the effect of neutrophil depletion on metastatic outgrowth, I confirmed the efficiency of the neutrophil elimination forty-eight hours after a single administration of the anti-Ly6G clone 1A8 monoclonal antibody (Figure 22a). After forty-eight hours, $Ly6G^{+}CD11b^{+}$ were depleted over 90% (Figure 22b&c). Furthermore over 80% of $Ly6G^{+}Ly6C^{-}$ neutrophils were depleted (Figure 22d&e). The specificity of the antibody was confirmed by looking at the $Ly6G^{-}Ly6C^{+}$ cells, which were not depleted (Figure 22f).

Figure 22: Neutrophils can be depleted for at least 48 hours following a single antibody adminstration

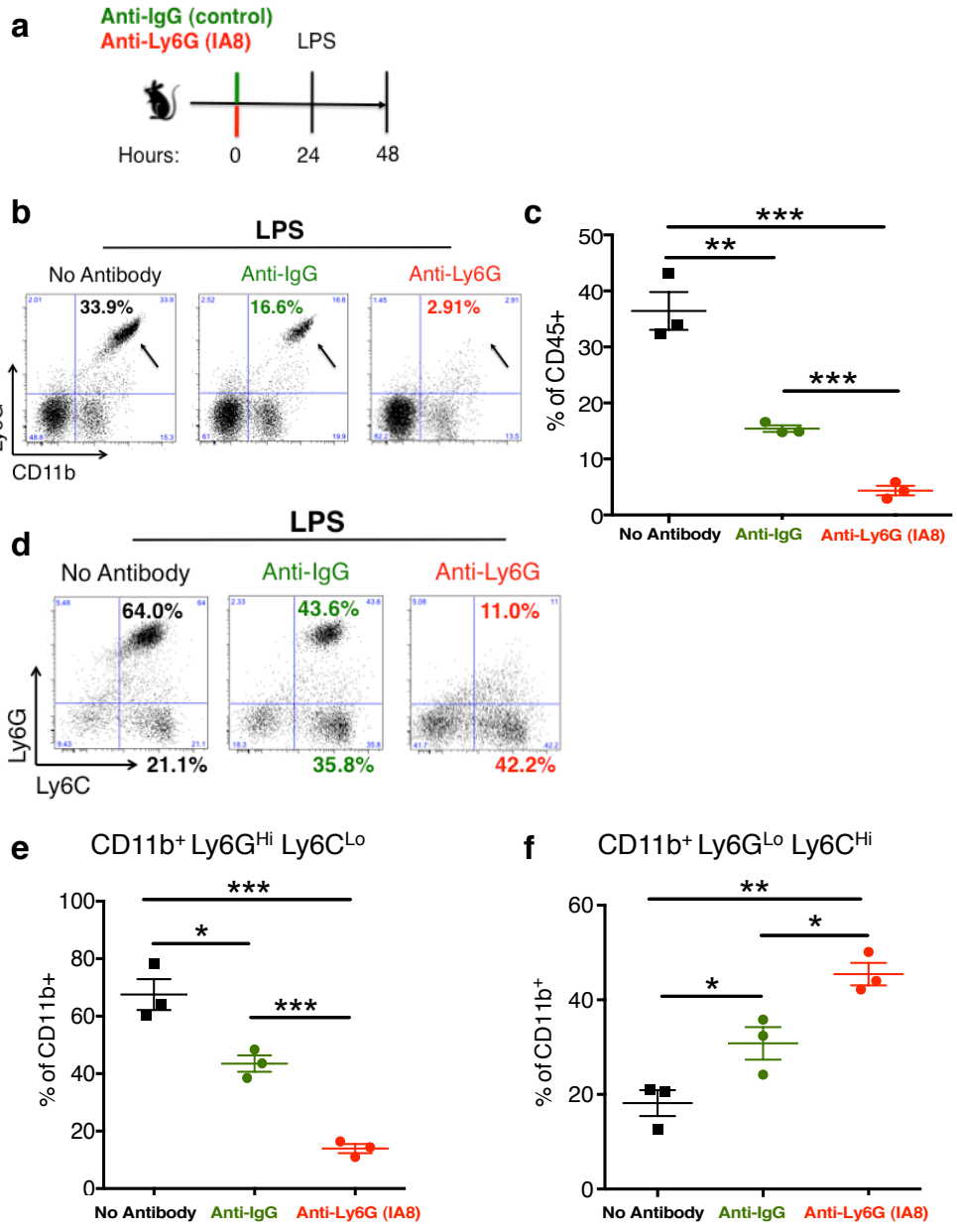

Figure 22. Neutrophils can be depleted for at least 48 hours following a single antibody administration

(a) Schematic of depletion of neutrophils in the lungs following a single injection of anti-Ly6G (1A8) antibody after 48 hours; (**b**) Flow cytometry plot of $Ly6G^{+}$ $CD11b^{+}$ cells in total $CD45^{+}$ hematopoietic cells in lungs 48 hours after matched-control IgG antibody or anti-Ly6G (1A8) antibody administration. Arrows indicate expected position of $Ly6G^{+}$ $CD11b^{+}$ cells; **(c)** Percentage of $Ly6G^{+}$ $CD11b^{+}$ cells in total $CD45^{+}$ hematopoietic cells in lungs 48 hours after matched-control IgG antibody or anti-Ly6G (1A8) antibody administration; **(d)** Representative flow cytometry plots outlining Ly6G expression and Ly6C expression on $CD45^{+}$ $CD11b^{+}$ hematopoietic cells; **(e)** Percentage of $Ly6G^{Hi}$ $Ly6C^{Lo}$ cells in total $CD45^{+}$ $CD11b^{+}$ hematopoietic cells in lungs 48 hours after matched-control IgG antibody or anti-Ly6G (1A8) antibody administration; **(f)** Percentage of $Ly6G^{Lo}$ $Ly6C^{Hi}$ cells in total $CD45^{+}$ $CD11b^{+}$ hematopoietic cells in lungs 48 hours after matched-control IgG antibody or anti-Ly6G (IA8) antibody administration. Each dot represents an individual mouse. Data show mean ± SEM. The *P*-values were calculated by Student's t-test. (*) $P < 0.02$(**) $P < 0.004$; (***) $P < 0.0008$; n = 3.

Next I injected 100,000 D2A1-d cells into the tail vein of BALB/c mice, and six days later I injected these mice with 200 μg of anti-Ly6G (Clone IA8) via i.p. injection. The following day, these mice were treated with 2mg/kg of LPS via i.p. injection; the next day these mice were again treated with 200 μg of anti-Ly6G (Clone IA8) via i.p. injection (Figure 23a). None of the mice that had been injected with D2A1-d cells + neutralizing antibody against neutrophils and treated thereafter with LPS developed lung metastases, while the mice that had been injected with D2A1-d cells and treated with LPS developed on average four lung metastases per mouse (Figure 23c).

To determine whether macrophages contributed to the LPS-induced metastatic outgrowth, I depleted circulating macrophages by administrating either anti-CCL2 neutralizing antibody or clodronate liposomes via the intravenuous route (Koay, M.A. *et al* 2002). The experimental plan that I used was as follows: 100,000 D2A1-d cells were injected into the tail vein of BALB/c mice, seven days later I treated the mice with 2mg/kg of LPS. Six hours after LPS treatment, I injected one group of mice with clodronate liposomes or PBS liposomes via intravenous injection to deplete circulating macrophages, while another group of mice were injected with anti-CCL2 or control anti-IgG antibody via i.p. injection (Figure 23b). However, both groups of mice developed on average four lung metastases per mouse, thereby suggesting that neutrophils, and not macrophages, are required for LPS-induced metastatic outgrowth.

Figure 23: Neutrophil inhibition, not macrophage inhibition blocks LPS-induced awakening of dormant DTCs

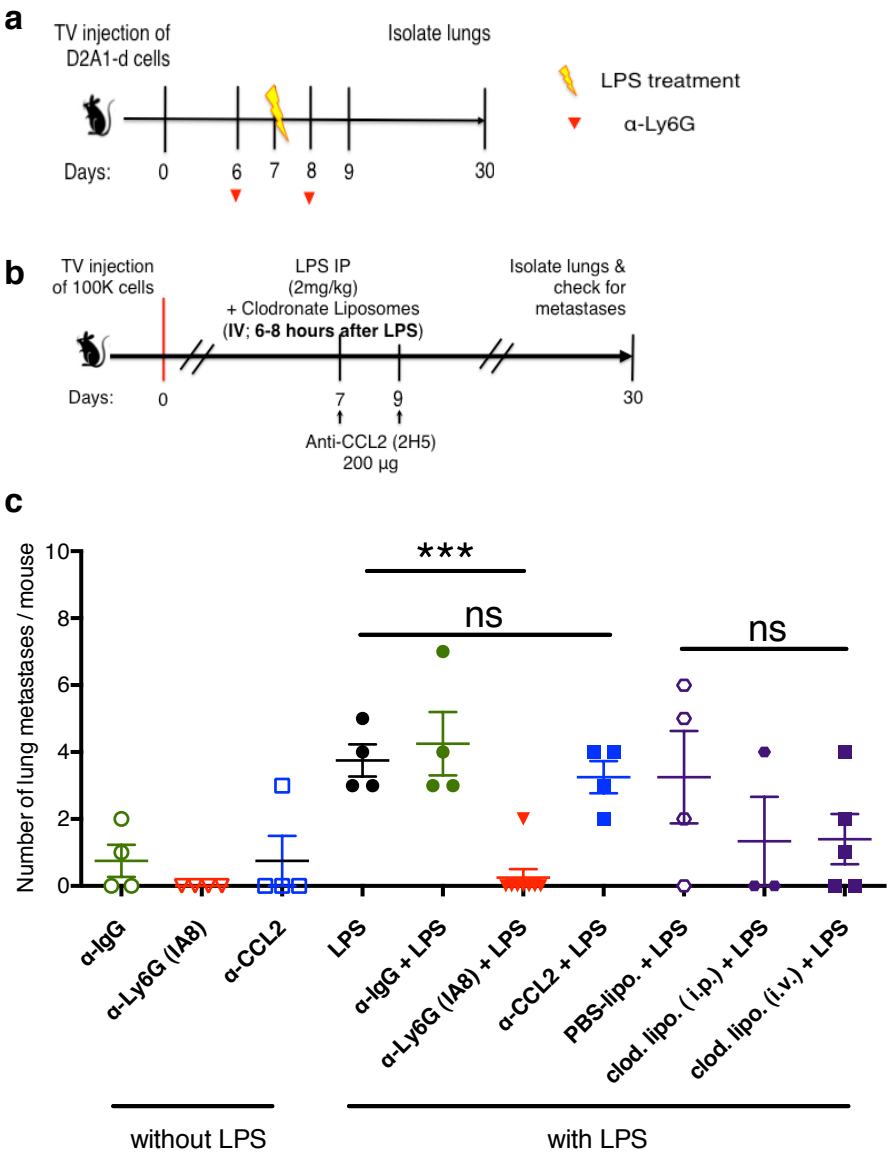

Figure 23. Neutrophil inhibition, not macrophage inhibition blocks LPS-induced awakening of dormant DTCs

(a) Schematic depiction of the experimental strategy used to deplete neutrophils following LPS treatment in mice previously inoculated with D2A1-d cells. On day 0, mice were injected via the tail vein with D2A1-d cells. Mice to be depleted for neutrophil were treated on day 6 and 8 with anti-Ly6G (IA8) antibody. On day 7, mice received 2mg/mL LPS i.p.; (**b**) Schematic depiction of the experimental strategy used to deplete macrophages following LPS treatment in mice previously inoculated with D2A1-d cells. On day 0, mice were injected via the tail vein with D2A1-d cells. Mice to be depleted for macrophages were either treated six hours after LPS with anti-CCL2 antibody and again on day 9 or the mice received 0.1 mL/10g of clodronate liposomes via intravenous injection six hours after LPS and again on day 9. Control IgG served as a negative control for antibody depletion. PBS liposomes were a control for the clodronate liposomes; (**c**) Quantification of lung metastases as determined by numbers of metastatic nodules visible under fluorescent dissection microscope at 0.8x magnification at thirty days post-tail vein injection. Each data point represents the number of metastases in an individual mouse. Data are the sum of two independent experiments; n=4-8; ***, P< 0.0003 by Student's *t* test.

LPS-induced awakening of DTCs is dependent upon activation of the EMT program

Having shown thus far that LPS can awaken DTCs via the infiltration of neutrophils, it was vital to determine whether the awakening of DTCs occurred via the activation of the endogenous EMT program in the dormant DTCs. Therefore, I isolated the TdTomato^{+} D2A1-d cells from the lung metastases of LPS-treated mice by FACS and assessed the activation of EMT-TFs in these cells by western blot analyses (Figure 24a). The D2A1-d cells isolated from the lung metastases of LPS-treated mice expressed Twist and Zeb1; this is consistent with a causal association of the EMT program with metastatic outgrowth but did not provide direct evidence.

To test whether the LPS-induced metastatic outgrowth was dependent upon the activation of an EMT program within the latent tumor cells, I first injected mice via the tail vein with D2A1-d cells that had been infected with a viral vector expressing shRNA against Zeb1 (D2A1-d + shZeb1_A or D2A1-d + shZeb1_B); one week later, I treated these mice later with LPS. (I used the same shRNAs against Zeb1 as described in Chapter 3. These shRNAs were able to knockdown Zeb1 expression by 50-100% (Figure 24b) 20% of mice injected with the D2A1-d + shZeb1_A or D2A1-d + shZeb1_B cells developed metastases upon LPS-treatment, while 70% of the mice injected in parallel with control shRNAs developed metastases (Figure 24c). The mice that were injected with D2A1-d + shZeb1_A cells, which had 50% reduction of Zeb1 protein levels, developed on average six metastases, while the mice that were injected with D2A1-d + shZeb1_B cells, which had 100% reduction of Zeb1 protein levels, developed at most one metastasis (Figure 24c).

To control for any cytostatic or mitogenic effect the knockdown of Zeb1 might have on cell proliferation *in vivo*, I also injected D2A1-d + shZeb1_A and D2A1-d + shZeb1_B cells into the mammary fat pads of mice. D2A1-d cells expressing either shZeb1 construct were able to form primary tumors at limiting dilutions, thereby excluding the possibility that Zeb1 knockdown was cytostatic for the D2A1-d cells (Figure 24d&e). Taken together, these results demonstrate that LPS-induced awakening of dormant DTCs is mediated by the EMT-TF Zeb1.

Figure 24: LPS-induced awakening of dormant DTCs is dependent upon Zeb1 expression

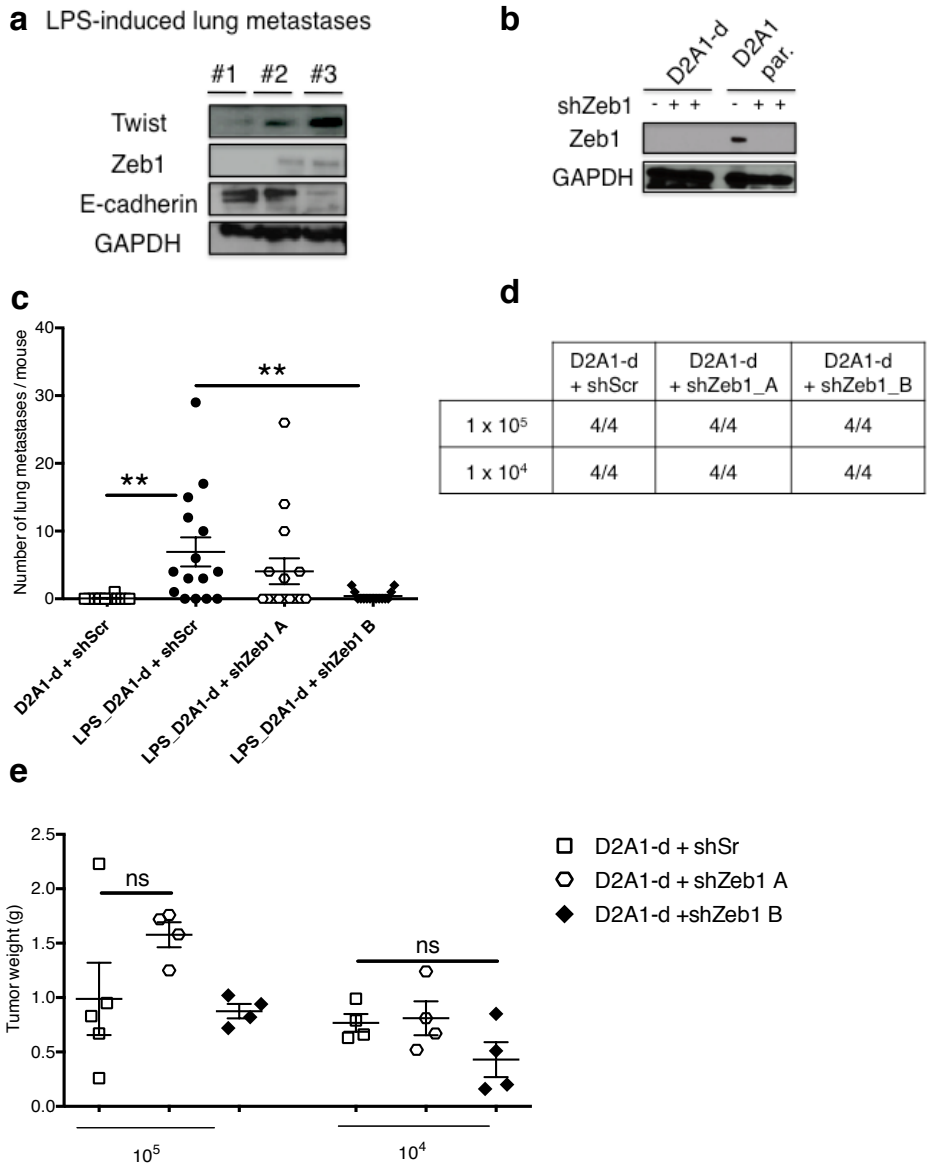

	D2A1-d + shScr	D2A1-d + shZeb1_A	D2A1-d + shZeb1_B
1 x 10^5	4/4	4/4	4/4
1 x 10^4	4/4	4/4	4/4

Figure 24. LPS-induced awakening of dormant DTCs is dependent upon Zeb1 expression

(a) TdTomato^{+} tumor cells isolated from lung metastases of three independent mice harboring metastases following LPS treatment were analyzed for the indicated expression of E-cadherin and the EMT-TFs (Twist and Zeb1) by Western blot; **(b)** Knockdown of two Zeb1 shRNAs was determined by Western Blot in parental D2A1; **(c)** Mice were injected with D2A1-d cells harboring Zeb1 shRNAs or control shRNAs. One week later mice were treated with 2 mg/kg of LPS. Knockdown of Zeb1 in D2A1-d cells with either shZeb1_A or shZeb1_B subsequently reduces metastatic outgrowth following LPS treatment. shScrambled (shScr) is a control shRNA. Quantification of lung metastases as determined by numbers of metastatic nodules visible under fluorescent dissection microscope at 0.8x magnification at thirty days post-tail vein injection. Each data point represents the number of lung metastases in an individual mouse; **(d)** Incidence of primary tumor formation in mice orthotopically implanted with either D2A1-d cells harboring Zeb1 shRNAs or control shRNAs at the indicated doses; (**e**) Quantification of primary tumor weights at indicated doses six weeks post-injection. Each data point represents the number of metastases in an individual mouse. Data are represented as mean ± SEM (n=8). The *P*-values were calculated by Student's t-test. (*) $P < 0.05$; (**) $P < 0.0005$

Awoken DTCs secrete CCL2 into the tumor microenvironment

The experiments described above indicated the involvement of immune cells triggering the awakening of DTCs. However, it was plausible that, once awoken, DTCs actively contributed to maintaining an inflamed microenvironment. This may parallel the behavior of carcinoma cells in the primary tumor, which actively recruit inflammatory cells to the tumor microenvironment (Joyce, J.A. & Pollard, J.W. 2009).

To this end, I sought to determine, in an unbiased approach, whether inflammatory cytokines were secreted by D2A1-d cells upon expression of Zeb1. I collected conditioned medium of cultured parental D2A1, D2A1-d, and D2A1-d cells expressing Zeb1 and analyzed the conditioned media of these cells in a commercially available cytokine array (Figure 25a).

From this cytokine array, I determined that all three cell-lines secreted interferon gamma-inducible protein 10 (IP-10/CXCL10), growth-regulated alpha protein precursor (GROα/CXCL1), macrophage colony-stimulating factor (M-CSF) and tissue metalloproteinase inhibitor 1 precursor (TIMP1). The secretion of granulocyte colony-stimulating factor (G-CSF), stromal cell-derived factor 1 precursor (SDF-1/CXCL12) and regulated on activation normal T cell expressed and secreted (RANTES) was unique to the parental D2A1 cells; the secretion of interleukin 1-alpha (IL1-α) and granulocyte macrophage colony-stimulating factor (GM-CSF) was unique to the D2A1-d cells; the secretion of TNFα and growth-regulated beta protein precursor (GROβ/CXCL2) was unique to the D2A1-d cells expressing Zeb1.

Of greatest interest, however, was the list of cytokines that were secreted solely by the parental D2A1 cells and the D2A1-d cells expressing Zeb1, since both the parental D2A1 cells and the D2A1-d cells expressing Zeb1 were capable of colonizing the lungs. The only cytokine that was secreted by both the parental D2A1 and the D2A1-d cells expressing Zeb1 was: monocyte chemotactic protein 1 (MCP1/CCL2). I confirmed the secretion of CCL2 by the D2A1 parental and D2A1-d cells expressing Zeb1 by ELISA (Figure 25b). As shown in Figure 23, CCL2 was not required for the initiation of LPS-induced recruitment of macrophages. This observation did not preclude the possibility that once awoken, DTCs would secrete CCL2 and actively recruit CCL2-responding immune cells to the nascent tumor microenvironment. While the *in vitro* experiments revealed that D2A1-d cells expressing Zeb1 secrete CCL2, it is unknown whether or not the CCL2/CCR2 signaling pathway was active *in vivo* and further experimentation would be necessary to determine this.

Figure 25: Cytokine array reveals distinct cytokine secretion patterns in D2A1-d, parental D2A1 and D2A1-d expressing Zeb1 cells

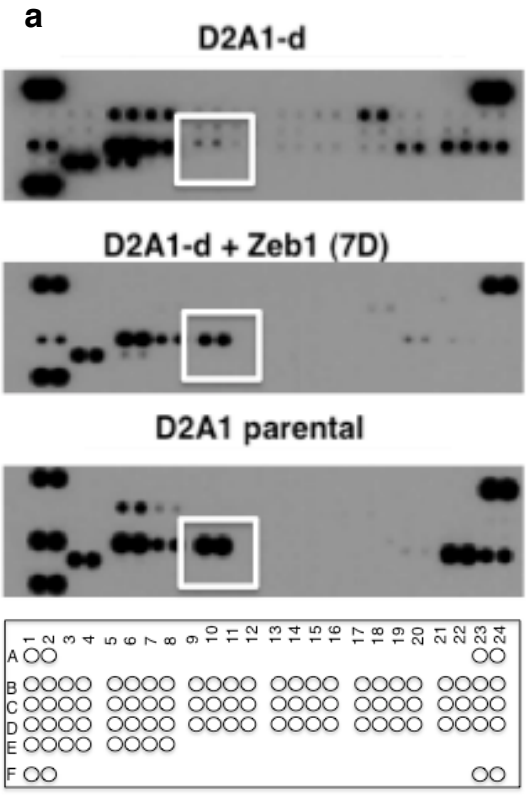

Coordinate	Target	Coordinate	Target
A1,A2	Reference spot	**D9,D10**	MCP1/CCL2
B5,B6	G-CSF	**D19,D20**	GROβ/CXCL2
B7,B8	GM-CSF	**D21,D22**	RANTES
B17,B18	IL1-α	**D23,D24**	SDF-1/CXCL12
D1,D2	IP-10, CXCL10	**E3,E4**	TIMP-1
D5,D6	GROα,CXCL1	**E5,E6**	TNF-α
D7,D8	M-CSF	**F1,F2**	Reference spot

Figure 25. Cytokine array reveals distinct cytokine patterns in D2A1-d, parental D2A1 and D2A1-d expressing Zeb1 cells

(a) (*above*) A mouse cytokine protein array was used to profile 40 cytokines in conditioned medium. Each cytokine was detected in duplicate. Differentially expressed cytokines (defined as only be secreted by D2A1-d expressing Zeb1 and parental D2A1 cells) are highlighted with a black box; (*below*) Array template of analytes represented **(b)** CCL2 concentrations in D2A1-d, untreated D2A1-d + Zeb1, D2A1-d + Zeb1 +3D – D2A1-d cells expressing Zeb1 after three days of doxycycline treatment, parental D2A1 cells as determined by ELISA. Data are represented as mean ± SEM. The *P*-values were calculated by Student's t-test. (*) $P < 0.05$; (**) $P < 0.01$; (***) $P < 0.001$. Data are representative of three independent experiments.

LPS-induced inflammation is required for colonization of the bone

Having demonstrated that LPS can awaken dormant DTCs in the lungs, I wanted to determine whether this finding was specific to the lungs. I therefore injected 80,000 D2A1-d cells into mice via intra-cardiac injection, a commonly used experimental route to study metastasis all over the body. One week later, I treated mice with 2mg/kg of LPS via ip injection. Following intra-cardiac injection of D2A1-d cells, there was no difference in the number of adrenal metastases formed by untreated and LPS-treated mice. However, only mice that were treated with LPS developed bone metastases (Figure 26). Therefore LPS-induced inflammation did not enhance or inhibit the growth of adrenal gland metastases, but LPS-induced inflammation was required for awakening of otherwise-dormant DTCs in the colonization of the bone.

Figure 26: LPS-induced inflammation triggers awakening of dormant DTCs in the bone

a

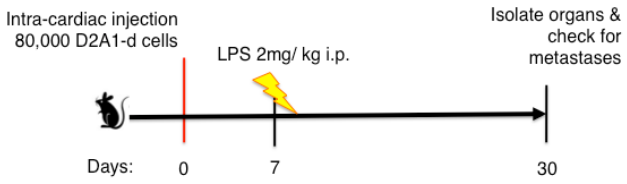

b

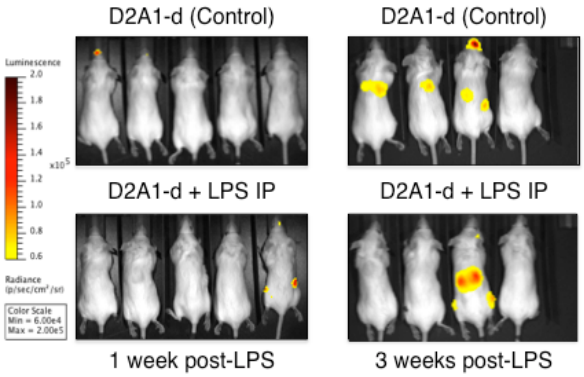

c

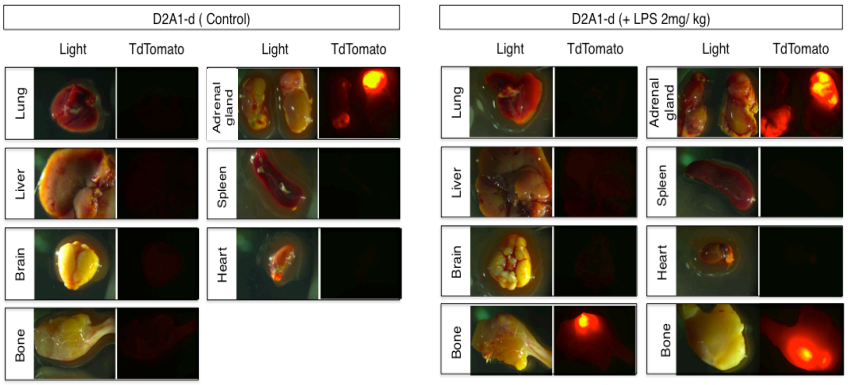

Figure 26. LPS-induced inflammation triggers awakening of dormant DTCs in the bone

(a) Schematic depiction of the *in vivo* strategy used to determine whether LPS-induced inflammation can awaken dormant DTC in other organs. 80,000 D2A1-d cells were injected into the left ventricle of the heart of BALB/c mice. One week later, mice were treated via i.p. injection with 2mg/kg of LPS; **(b)** Mice inoculated via intra-cardiac injection with TdTomato^{+} D2A1-d cells and left untreated or treated with LPS one week later. Representative bioluminescent images of mice bearing metastases; (**c**) Representative images of whole-body tumor distribution of a single mouse untreated or LPS-treated mouse revealed using fluorescent dissection microscopy (n=12).

Discussion

The experiments outlined in this chapter indicate that 1) LPS can awaken dormant DTCs in the lungs and in the bone marrow; 2) LPS-induced awakening of DTCs is dependent upon the recruitment of neutrophils; 3) LPS-induced awakening of DTCs causes the activation of endogenous Zeb1 in DTCs.

Hepatitis viruses, papillomavirus, and *Helicobacter pylori* are responsible for most of the malignancies arising in the liver, cervix and stomach respectively and are attributable to infections (de Martel, C. *et al* 2012). However, to our knowledge this is the first example of a study exploring the effects of inflammation on dormant DTCs that have been previously seeded, i.e., not looking at the effects of a pre-inflamed stroma on the outgrowth of DTCs. While I demonstrated that LPS-induced inflammation could awaken dormant DTCs, it is highly plausible that other inflammatory stimuli can also trigger the awakening of DTCs. I attempted to explore this idea by inducing inflammation by the administration of bleomycin into mice. After administration of bleomycin, there is an onset of an acute inflammatory response lasting up to eight days, followed by fibrogenic changes resulting in the deposition of matrix and distortion of the lung structure up to thirty-five days post-administration (Chaudhary, N.I. *et al* 2006). Furthermore, the immune cells responsible for the acute inflammatory response and the factors retrieved in the bronchoalveolar lavage fluid (IL-1, IL-6, INF-γ, TNF-α) were identical to those found in the inflammatory microenvironment following LPS administration (Chaudhary, N.I. *et al* 2006). For these reasons, I believed bleomycin would also be able to provoke the awakening of dormant DTCs.

Unfortunately, the BALB/c mouse strain (to which my cell model system is syngeneic) is highly resistant to the effects of bleomycin, unlike the strongly responding mice of the C57BL/6-strain (Phan, S. H. & Kunkel, S. L. 1992). However, BALB/c mice can overcome this resistance by the administration of 100 mg/ kg cyclophosphamide via i.p. injection twenty-four hours prior to the administration of 150mg/ kg of bleomycin via i.p. injection (Schrier, D. J. & Phan, S.H. 1984).

I therefore used this experimental plan to determine whether bleomycin-mediated inflammation could awaken previously disseminated D2A1-d cells in the lungs. Unfortunately, none of the mice developed lung metastases *(n=5)*. Considering that cyclophosphamide is a known chemotherapeutic, it was highly possible that the disseminated D2A1-d cells had undergone apoptosis following this treatment.

As a second approach to test my hypothesis, I injected the D2A1-d cells via the tail vein into the first filial (F1) generation of offspring of BALB/c and CB57BL/6 mice, and treated these mice one week later with 150 mg/kg of bleomycin. The rationale for this approach was that the F1 offspring would have acquired the responsiveness to bleomycin from the parental CB57BL/6 mouse, while still retaining the ability to form tumors with the sufficient BALB/c background. By using this strain, I could also forego the use of cyclophosphamide to sensitize the mouse to the effects of bleomycin and its potential chemotherapeutic effects. Unfortunately, none of the mice developed lung metastases *(n=14)*. Cox, T.R. *et al* (2013), however, demonstrated that a bleomycin-induced fibrosis enhanced metastatic colonization of 4T1 murine mammary carcinoma

cells that were injected into the fibrotic tissue. I therefore believe that bleomycin could cause the awakening of dormant DTCs but further optimization is required.

In this chapter, I was able to demonstrate the importance of neutrophils in the awakening of dormant DTCs in the lungs. From this finding, one can imagine that the activation of the EMT program leading to the onset of metastatic outgrowth might have been as a result of 1) direct cell-signaling between the dormant DTCs and neutrophils, 2) release of neutrophil-derived proteases following degranulation of neutrophils, or 3) macrophages-recruited by the neutrophils.

To address the possibility of direct cell-mediated signaling between the dormant DTCs and neutrophils, one could propose to conduct *in vitro* co-culture experiments with both cell-types differentially labeled with a fluorescent protein and determine whether the neutrophils are able to cause the activation of the EMT program in the tumor cells. One major caveat to this approach, however, is that the tumor cells are not dormant under *in vitro* culture conditions. Thus, this will not model the behavior of the tumor cells *in vivo*. Furthermore, current experimental practices used to distinguish between juxtacrine and paracrine signaling will not be useful in this context, as these assays are not amenable to dormant cells. Lastly, the ratio of neutrophils to tumor cells required for the activation of the EMT program is not readily apparent.

Histological analyses of lung sections of LPS-treated mice that had been previously injected with D2A1-d cells would also provide little insight into the nature of

this interaction. Even if immuno-fluorescent staining of histological sections of the lungs of LPS-treated mice that had previously been injected with D2A1-d cells did show neutrophils in close proximity to DTCs, this would only provide a snapshot of the potential interaction between these two cell-types. Immunofluorescent staining for cell-signaling molecules is not easily achieved. Therefore, a better *in vitro* model is required to adequately address the potential direct cell-signaling events between the neutrophils and dormant tumor cells.

For the most part it is highly plausible that multiple EMT-inducing signals are present within this LPS-induced inflammatory microenvironment and that a single EMT-inducing signal is often insufficient to cause the awakening of dormant DTCs. If true, this would represent a formidable task of teasing apart the individual cell-signals required to act in concert to stimulate expression of an EMT program. Regardless of the complexity of the heterotypic signaling cascades, my study suggests that these signals converge on the activation of Zeb1 in dormant DTCs.

El Rayes, T. *et al* (2015) published a study looking at the effects of a pre-inflamed lung on metastatic outgrowth. In this paper, they established that LPS-induced lung inflammation did not have any effect on tumor cell extravasation or seeding into the lungs, but that the pre-inflamed lung caused tumor cells to more rapidly colonize the lung tissue. The authors attributed this increase in metastatic outgrowth to neutrophil released-proteases. Through a series of *in vitro* and *in vivo* bone marrow transplantation assays, they showed that upon LPS-administration, neutrophils degranulate and secrete various

proteases, such as cathepsin G and elastase, which in turn, degrade thrombospondin-1 (Tsp-1). The degradation of Tsp-1 renders the lung microenvironment conducive to metastatic outgrowth. While I have not confirmed the loss of Tsp-1 in my model system following LPS-treatment, it is plausible that neutrophils behave in a similar manner and cause the awakening of dormant DTCs.

Taken together, two other studies, one from the same group mentioned above and the other published by Ghajar, C.M. *et al* (2013), Tsp-1 can be secreted by both myeloid cells and endothelial cells and may contribute in the maintenance of DTCs in a dormant state. If proven to be true in my model system, the dormant disseminated D2A1-d cells can extend FLPs, yet are retained in the dormant state, as they are unable to degrade Tsp-1. To test this idea, it would be of interest to determine whether or not Tsp-1 is degraded in the lungs of mice that had been injected with the parental D2A1 cells.

However, not all studies report that loss of Tsp-1 is associated with metastatic outgrowth. Kudo-Saito, C. *et al* (2009) reported that Tsp-1 could be an EMT inducer through TGF-β activation and that inhibition of Tsp-1 leads to the inhibition of primary tumor growth and metastasis. While this study suggests a potential association between the EMT program and Tsp-1, others have noted that cleaved Tsp-1 can affect the activity of TGF-β (Iruela-Arispe, M. L. *et al* 2004). Indeed multiple proteases can cleave Tsp-1, which may lead to its ability to act as an EMT inducer. The ability of cleaved Tsp-1 to induce the EMT program in dormant DTCs would still support the idea that loss of Tsp-1 is required for metastatic outgrowth in the lungs. The ability of Tsp-1 to inhibit tumor

growth relates to the concept that Tsp-1 in an angiogenesis inhibitor. Over-expression of Tsp-1 by tumor cell lines leads to a reduction in tumor burden due to a decrease in vascular density in comparison to control tumors (Iruela-Arispe, M. L. *et al* 2004). These studies would suggest that in some settings a particular function of Tsp-1 is highlighted, and that depending on its interaction with other proteins or cleavage-status this particularly large protein may or may not display anti-tumorigenic effects. Furthermore, the ability of TGF-β to act as an inducer or inhibitor of the EMT program appears to be highly context-dependent.

When I first started working on the re-activation of dormant DTCs, most studies had focused on the reduced tumor cell-microenvironment cross-talk that might induce dormancy. In the cited studies, the gene expression of cells that were able to colonize the lungs was compared to the gene expression of cells that were not able to colonize the lungs either in 3D culture conditions or using gain-of-function screens (Aguirre-Ghiso, J. A. 2002; Aguirre-Ghiso, J.A. *et al* 2004; Shibue, T. & Weinberg, R. A. 2009; Barkan, D. & Green, J.E. 2011; Gao, H. *et al* 2012). There was little to suggest how tumor cells could escape dormancy without genetic manipulation. Inflammation at the metastatic site became more widely studied during the course of my research, and a microenvironment that was inflamed prior to the arrival of DTCs was demonstrated to enhance the likelihood of subsequent metastatic outgrowth (Bouchard, G. *et al* 2013; Cox, T.R. *et al* 2013; El Rayes, T. *et al* 2015). I provided evidence to suggest that dormant DTCs can be re-activated by an inflamed microenvironment, and that these dormant DTCs require Zeb1 activation for metastatic outgrowth.

Materials and Methods

Cell Culture

All cells were cultured in 5% CO_2 humidified incubator at 37° C. Mouse mammary carcinoma cell lines D2A1, TS/A, 67NR, 168FARN were grown in Dulbecco's Modified Eagle's Medium (DME) supplemented with 5% inactivated fetal bovine serum (IFS), 5% calf serum, 100 U/ml penicillin, and 100 μg/ml streptomycin (Invitrogen). Mouse mammary carcinoma cell lines D2A1 and TS/A were gifts from F. R. Miller and P.L. Lollini, respectively (Rak, J.W. *et al* 1992; Nanni, P. *et al* 1983). Cells were passaged when confluence reached ~80% with 0.15% trypsin and re-seeded in a ratio of 1/12. Medium was always changed every third day.

Plasmids and lenti-viral infections

Mouse Snail, Twist1, Zeb1 cDNAs obtained from Open Biosystems were subcloned into FUW-LPT2 tetracycline-inducible lentiviral vector (modified from FUW-tetO by Kong-Jie Kah) with puromycin resistance gene. pMMP-LucNeo, carrying coding sequences for luciferase and neomycin phosphotransferase, were obtained from Dr. Segal (3). pLKO-puro was used as backbones for the lentiviral vectors expressing short hairpin RNAs (shRNAs). The shRNA sequences for Zeb1 were: (sh Zeb1 A) GTCGACAGTCAGTAGCGTTTA and CCGCCAACAAGCAGACTATTC (sh Zeb1 B). Cells were seeded at 5.0 x 10^5 cells per 10 cm dish and transduced 24 hours later with concentrated virus in the presence of 5 μg/ml polybrene (EMD Millipore #TR-1003-G). The selection of cells that were successfully infected with lentivirus or retrovirus was

performed with medium containing 4 μg/ml of puromycin. The infection efficiency was routinely greater than 80%.

Cell proliferation assay

Cells were seeded at 1.0 x 10^6 into 10 cm, split and counted using the automatic counter Vi-CELL Cell Viability Analyzer (Beckman Coulter) every three days for fourteen days. For Figure 18b, 1.0 x 10^3 cells were seeded onto 96-well plates in triplicate. Cell viability was measured using CellTiter-Glo (Promega) according to the manufacturer's instructions.

Immunoblotting

Cells were harvested and lysed in RIPA buffer [25 mM Tris-HCL (ph 7.6), 150 mM NaCl, 1% Nonidet P-40, 1% sodium deoxycholate, O.1% SDS, 1x complete protease inhibitor mixture (Roche), 1x phosphatase inhibitors (Roche Diagnostics)]. The protein extracts were separated by 10% SDS-PAGE and were transferred to polyvinylidene fluoride (PVDF) membranes (Millipore). After one hour blocking in 5% non-fat milk, the membranes were incubated overnight with primary antibodies at 4'C. Blots were developed using ECL (Dura or Femto, Pierce). The types and dilutions of primary antibodies used were the following: Snail (Cell Signaling Technology 3879S; 1:10^3), Twist (Abcam ab50887; 1:10^4), Zeb1 (Cell Signaling Technology 3396S; 1:10^3), E-cadherin (Cell Signaling Technology 3195S; 1:10^3), Cytokeratin 5 (Covance PRB-160P; 1:10^3); Fibronectin (BD Biosciences 610078; 1: 10^3); N-cadherin (Cell Signaling 4061;

1:10^3); Vimentin (Cell Signaling Technology 5741S; 1:10^3), GAPDH (Cell Signaling Technology 2118S; 1:10^4).

NF-kB reporter assay

NF-kB-WT promoter luciferase construct was pGreenFire-NF-kB (System Biosystems Inc., #TR012PA-1). *Firefly* and *Renilla* luciferase activities were measured with the Dual-Luciferase Reporter system (Promega). Cells were seeded 1.0 x 10^4 into a 96-well plate in 50 μL with 10 μg/mL of LPS at the indicated time points. Media and LPS were freshly replaced after 24 hours. The data generated were expressed as relative to vector control after normalization to *Renilla* luciferase readings. All experiments were performed in triplicate.

Animals

BALB/c mice and C.C3 $TLR4^{Lps\text{-}d}$ were obtained from Jackson Laboratory (stock numbers 000651 and 002930 respectively). A colony of NOD-SCID mice was maintained in-house. All research involving animals was conducted in accordance with the Guide for the Care and Use of Laboratory Animals of the National Institute of Health. All animals were maintained according to the guidelines of the MIT Committee on Animal Care protocol (1014-109-17). All efforts were made to minimize suffering. Mice that had been dead by the end of experiments were excluded from the analysis.

For orthotopic tumor transplantations, 1.0 x 10^5 tumor cells, unless otherwise indicated, resuspended in 20 μL of their growth medium and 50% Matrigel were implanted

bilaterally into the fourth mammary fat pad of 6 to 8-week old female syngeneic BALB/c mice. The tumor incidence and weight was measured six to eight weeks post-injection.

For intravenous injections, 1.0 x 10^5 cells, unless otherwise indicated, resuspended in 100 μL of phosphate-buffered saline (PBS) were injected into the lateral tail vein. The lungs were examined for metastases four to six weeks post-injection.

For intracardiac injections, 8.0 x 10^4 cells, resuspended in 100 μL of PBS were injected into the left ventricle of six- to eight-week old BALB/c mice. Three weeks later, mice were sacrificed for harvesting the brain, lungs, liver, bone and adrenal glands. Metastasis formation was examined and scored using a dissection microscope (Leica MZ12).

Acute Lung Injury

Escherichia coli LPS type 055:B5 (Sigma Aldrich L2880) was used for animal exposures. LPS was delivered by i.p. injection 2mg/kg unless otherwise stated. Mice were sacrificed twenty-one days later.

To obtain peripheral white blood cell counts following LPS treatment at indicated times, mice were bled retro-orbitally. For white blood cell counts, an aliquot was diluted 1:5 in 1X PBS and processed at the MIT Division of Comparative Medicine.

Neutrophil depletion

To deplete neutrophils, anti-Ly6G antibody (200 μg per mouse, clone 1A8; Bioxcell BE0117) was injected i.p. one day prior LPS treatment and twenty-four hours after LPS treatment. Matching isotype Hamster IgG (Bioxcell BE0091) served as a control antibody.

Circulating monocyte and macrophage depletion

To deplete circulating monocytes and macrophages, anti-CCL2 antibody (200 μg per mouse, clone 2H5; Bioxcell BE0185) was injected i.p. six hours after LPS treatment and again twenty-four hours after LPS treatment. Matching isotype Hamster IgG (Bioxcell BE0091) served as a control antibody.

Clodronate treatment

Treatment with clodronate liposomes was performed as described elsewhere (Hitchcock, J.R. *et al* 2015). Liposomes encapsulated with clodronate to deplete macrophages and control liposomes containing PBS only were purchased from Nico van Rooijen, Netherlands. Clodronate-liposomes and PBS-liposomes (0.1ml/10g body weight) were injected intravenously into six- to eight-week old BALB/c mice six hours after LPS treatment.

Quantification of lung metastases

Whole lung images were taken using a fluorescence dissection microscope (Leica MZ12). Colonies visible at 0.8x magnification of objective lens under fluorescence microscopy were counted as macro-metastases.

Histology

Primary tumors were fixed in 10% neutral buffered formalin overnight and embedded in paraffin for sectioning; lungs were fixed in 4% paraformaldehyde and paraffin-embedded. Sections (5 μm thick) were cut from paraffin-embedded tissues and stained with haemotoxylin and eosin. Entire tissue sections were imaged at 20x with the Aperio slide scanner (Leica Biosystems), and the number of metastases per section quantified using ImageScope analysis software (Leica Biosystems).

Bioluminescent imaging

Mice were anaesthetized with 2.5% isoflurane and injected i.p with 165mg/kg of body weight D-luficerin (Caliper Life Sciences). Mice were imaged in an IVIS 100 chamber ten minutes after D-luficerin injection, and data were recorded and analyzed using Living Image Software version 4.3.1 (Caliper Life Sciences). To measure lung colonization, photon flux was calculated for each mouse by using a circular region of interest. Photon flux was normalized by subtracting a background value obtained from the average photon flux of mice from the control group.

ELISA and protein array

Conditioned media from cell lines were analyzed for the secretion of various proteins using mouse cytokine array panel A (ARY006; R&D Systems) according to manufacturer's instructions. Levels of CCL2 were determined by commercially available sandwich enzyme-linked immunosorbent assay (ELISA) kit according to manufacturer's protocols (MJE00; R&D Systems). The absorbance was measured on Multiskan EX (Thermo Electron Corporation).

Flow cytometry

Lungs were minced using a razor blade and incubated in a DME based dissociation solution containing DNAse and 1.5 mg/ml Collagenase A (Roche) rotating at 37ºC for two hours. The dissociated lungs were then washed twice with PBS + 0.1% BSA, and filtered through a 70 μm and 40 μm cell strainer. Cells were stained with the following fluorophore-conjugated antibodies for thirty minutes at 4ºC: for tumor-associated macrophages: CD45 FITC (eBioscience 11-0451-82; 1:400), CD11b PerCP-Cyanine 5.5 (eBioscience 45-0112-80; 1:400); F480 PE-Cyanine7 (Affimetrix 25-4801-82; 1:400); CCR2 APC-Cy7 (BioLegend 150603; 1:400); Ly6C e450 (Affimetrix 48-5932-80; 1:200); for myeloid cells: CD45 PE-Cyanine7 (Affimetrix 25-0451-81; 1:400); CD11b PerCP-Cyanine5.5 (eBioscience 45-0112-80; 1:400); Ly6C e450 (Affimetrix 48-5932-80; 1:200); Ly6G FITC (BioLegend 127606; 1:200). Cells were acquired on a Fortessa (BD Biosciences) and analyzed using FACSDiva (BD Biosciences).

To sort the D2A1 cells by the cell-surface expression of CD29 and CD24 markers, cells were detached from the culture dish and were incubated with CD29 (Affimetrix 25-0291-80; 1:200) and CD24 (Affimetrix 17-0242-80; 1:200) diluted in PBS. After incubating on ice for 45 minutes, cells were washed twice in PBS + 0.1% BSA and sorted with a BD FACSAria (BD Biosciences).

Statistical Analysis

All data are represented as mean values ± standard errors of mean (SEM). *P* values of less than 0.05 were considered to be significant. Statistical analyses were carried out by two-tailed Student's t-test using Prism software (GraphPad Prism).

Chapter 5:

Conclusion and Future Directions

Despite significant improvements in diagnostic screening and the development of innovative and targeted cancer therapeutics, metastatic relapse following long-periods of post-therapy remission remains a threat to patients. In previous chapters, I described a particular model of cellular dormancy that is created by multiple rounds of *in vivo* enrichment for non-proliferative cells in the lung parenchyma. I discussed new insights revealing that the EMT program induced by Snail or Zeb1 can cause the awakening of dormant DTCs and proposed that this awakening was accompanied by the generation of MICs capable of colonizing the lung tissue. To our knowledge, this is the first model of cancer dormancy that demonstrated that an inflamed microenvironment could provoke the escape of cellular dormancy. Attesting to the possible generality of the identified mechanism, LPS-induced inflammation enabled not only colonization of the lungs, but also of the bone.

Inflammatory oncotaxis

The present results validate a previously untested speculation made nearly forty years ago that "inflammation is only one potential cause for facilitating metastases formation but one with which physicians should be acquainted" (DerHagopian, R.P. *et al* 1978). Inflammatory oncotaxis postulates that metastatic cancer cells are attracted to sites of inflammation. This encompasses both the notion of 1) a pre-metastatic niche, a pre-inflamed microenvironment to which tumor cells will migrate, and 2) dormant DTCs already present may respond to localized inflammation. Evidence for inflammatory oncotaxis after years of disease-free survival exists as individual case reports for various tumor types (Walter, N.D. *et al* 2011). Furthermore, the clinical recommendation of non-

steroidal anti-inflammatory drugs to cancer patients that have undergone surgery to inhibit local recurrence and metastasis attests to the clinical association of inflammation and cancer progression (de Groot, D.J. *et al* 2007; Rothwell, P.M. *et al* 2012).

Although my work focused on one inflammatory agent, LPS, others who have looked at the effect of a pre-inflamed microenvironment on facilitating metastatic outgrowth, have been able to substantiate their findings using LPS and bleomycin (Cox, T.R. *et al* 2013) or LPS and a transgenic mouse model for IL-1β–induced inflammation (El Rayes, T. *et al* 2015). The underlying reason for selecting these particular models of inflammation by the authors of the studies mentioned above may have been the similarity of the immune response generated as compared to the inflammatory response elicited by LPS. While I did not have time to determine the effects of these inducers of inflammation on the outgrowth of dormant DTCs, it is highly plausible that metastatic outgrowth would be noted. Indeed, IL-1 β has been shown to upregulate Zeb1 in hepatic carcinoma cell lines (Dohadwala, M. *et al* 2010). This suggests that IL-1β–induced inflammation might provoke the awakening of dormant DTCs in a similar Zeb1-dependent manner.

However, it is highly plausible that other pro-inflammatory stimuli that provoke an alternative inflammatory response to LPS could ignite the escape of metastatic dormancy. Indeed a recent study has shown that irradiation of the lungs of mice that had been previously injected with the dormant D2.0R cells readily form metastasis under these conditions albeit through an undetermined mechanism (Bouchard, M. *et al* 2013). In this study, the authors primarily collected the conditioned medium of irradiated

fibroblasts and lung epithelial cells and added it to *in vitro* 3D-cultures of dormant D2.0R cells. This allowed the authors to focus on secreted mediators from an irradiated lung microenvironment, as direct irradiation of the D2.0R 3D-cultures had no effect on tumor cell proliferation. In addition, mice that had been injected with D2.0R cells and irradiated four days later developed lung metastases after forty-two days. While Bouchard, G. *et al* (2013) provides evidence for inflammation to awaken dormant DTCs, the authors focused solely on inflammatory signaling pathways and did not entertain the notion that radiation might activate dormant DTCs by eliminating natural killer cells and other immune cells that had been suppressing tumor growth. The question also remains as to whether this observation can be extended to different cancer types. Indeed, while D2.0R cells do not readily proliferate in the lungs following tail vein injection, D2.0R cells were able to switch to a proliferative state upon injection into fibrotic collagen I-rich lungs (Barkan, D. *et al* 2010). Yet, the injection of melanoma cells into a fibrotic collagen I-rich microenvironment induced quiescence (Ossowski, L. *et al* 2010).

My thesis work is of particular interest when one considers the possibility of comorbidity in patients i.e. the co-existence of diseases or disorders in addition to a primary disease of interest, especially in aging patients as age is believed to be "the single most important risk factor for the development of cancer" (Extermann, M. 2007). Comorbidities include diseases such as heart disease, osteoporosis, diabetes, lung infections, pneumonia and often involve inflammation. Indeed comorbidity can affect risk, detection and treatment (Read, W.L. *et al* 2004; Tammemagi, C. *et al* 2005). Furthermore, numerous studies have suggested that high levels of comorbidity are

associated with poorer survival (Houterman, S. *et al* 2004; Griffiths, R.I. *et al* 2014). With more than 60% of cancer patients diagnosed later in life, many patients may have comorbidities that favor cancer progression. According to one study, comorbidity is prevalent in 20-35% of patients with breast cancer (Søgaard, M. *et al* 2013) and cohort studies have reported up to five-fold higher mortality rates for breast cancer patients with comorbidity compared to patients with no comorbidity (Jørgensen, T.L. *et al* 2012). Even in the absence of overt diseases, aging is associated with an increase in several inflammatory markers (Desai, A. *et al* 2010), which may predispose patients with dormant DTCs to metastatic awakening.

LPS and the macroenvironment

LPS administration can mimic inflammatory disease as well as metabolic disorders, such as metabolic endotoxemia when administered at low dose for an extensive amount of time (Boutagy, N.E. *et al* 2015). Indeed LPS has been identified as a causative factor of the onset of insulin resistance, obesity and diabetes. In addition, studies have used a continuous administration of low doses of LPS in mice to mimic a high-fat diet (Guo, H. *et al* 2016). Nutritional fatty acids can activate TLR4 signaling in adipocytes to induce inflammatory signaling. The change in global cultural norms to adopt a more Western fat-enriched diet has led to obesity becoming an epidemic. While wheat gluten can cause gut inflammation, the induced secretion pattern of cytokines and chemokines is distinct from the classic pro-inflammatory mediators produced following LPS administration (Nikulina, M. *et al* 2004). This suggests that a continuous administration of low doses of LPS may cause the awakening of dormant DTCs, and indicates that a

systemic inflammatory response might also trigger the escape of tumor dormancy.

Furthermore, with the increased interest in studying the trillions of microbiota with which we coexist, in particular commensal microbiota, it is plausible, through an imbalance of the microbiota homeostasis, that inflammation can arise and potentiate the outgrowth of dormant DTCs. Rao, V.P. *et al* (2006) demonstrated that the enteric bacteria *Helicobacter hepaticus* can induce mammary adenocarcinoma and required neutrophils to promote tumorigenesis (Lakritz, J.R. *et al* 2015). In addition the host microbiome has been shown to modulate the tumor-macroenvironment, i.e. the whole host immune system (Al-Zhoughbi, W. *et al* 2014) and even in extra-intestinal sites (Erdman, S.E. & Poutahidis, T. 2014).

The Lung- and Bone-microenvironments make strange bedfellows

While LPS-induced inflammation caused the outgrowth of dormant DTCs in the lungs and in the bone, it is not readily apparent why this would happen in these two sites specifically. One hypothesis comes from the description of the perivascular niche in which dormant DTCs may reside according to Ghajar, C.M. *et al* (2013). In this study, the authors found that dormant DTCs reside on the microvascular endothelium in the lungs and in the bone. The lung and bone microvascular endothelium maintain the DTCs in a dormant state through the secretion of Tsp-1. Only upon the loss of Tsp-1 are these dormant DTCs able to proliferate. By extrapolating upon the results of El Rayes, T. *et al* (2015), one can hypothesize that neutrophils recruited by LPS-induced inflammation can degrade endothelial-derived Tsp-1, and thus allow the DTCs to escape dormancy.

However, experiments will have to be designed to test this directly.

Regardless of the contribution of Tsp-1, other factors might be involved in causing the awakening of dormant DTCs at these two distinct sites. Indeed, Mock, K. *et al* (2015) suggest that TGF-β-released during bone remodeling can stabilize an EMT. Furthermore the expression of the EMT-inducer Zeb1 in carcinoma cells can induce osteoclast formation and inhibit osteoblast differentiation for bone resorption through the activation of genes associated with breast cancer bone metastasis, as defined by a previously determined bone metastasis gene signature (Mock, K. *et al* 2015; Kang, Y. *et al* 2003). Thus this particular study confirms an important role of Zeb1 in metastatic outgrowth. One could also envision looking for similarities between the extra-cellular matrices and the stromal cell types of both the lungs and the bone to uncover additional regulatory molecules of metastatic awakening.

Of MICs and CSCs

While the majority of cancer-related deaths are caused by metastatic disease, little is known about the identity of the responsible founder cells that are most likely already present, albeit undetectable, at the distant site at the time of primary tumor diagnosis. The metastatic founder cell might be a disseminated quiescent MIC or a non-MIC that can display MIC-like properties. While much effort has been devoted into identifying markers of CSCs, the markers and functional assays to identify MICs have yet to be properly determined and evaluated. Are MICs identical to CSCs? Do they have overlapping properties?

In this thesis, I demonstrated that the transient induction of Zeb1 in D2A1-d cells led to generation of putative MICs. Both the putative MICs and non-MICs were able to form primary tumors at limiting dilutions, and thus both cells types would qualify as CSCs. However, following tail vein injection, only the putative MICs readily colonized the lungs. This suggests that MICs are a specialized subset of CSCs. Therefore it would appear that a therapeutic approach designed to target MICs would be of some benefit. As such, further study and characterization of MICs would provide novel targetable signaling molecules and proteins.

Metastatic dormancy, a window of therapeutic opportunities

The mere presence of latent tumorigenic cells in patients deemed cancer-free puts a dark cloud above the notion that one can be "cured" of cancer and offers new challenges that must be addressed by cancer therapeutics. Part of the difficulty in "curing" patients is that during the "hidden" phase, DTCs can't be targeted using drugs that exclusively recognize proliferating cells. Therefore the resistance of dormant DTCs may stem from the fact that they are non-proliferating and are, in this sense, indistinguishable from normal differentiated cells in their responsiveness to drug therapies. Thus, the identification of markers unique to dormant DTCs may provide useful targets; the ultimate therapeutic goal would be to eradicate dormant DTCs, especially those with metastasis-initiating capabilities.

It is worth noting that in dormancy, proliferation may be uncoupled from survival and dormant DTCs may activate unique survival mechanisms. Alternatively, based on the

assumption that the dormant state is reversible, discovering mechanisms by which only dormant DTCs can be re-activated, i.e. without adversely affecting normal quiescent cells, may provide opportunities for combined drug treatments with existing therapeutics that target proliferating cells (Figure 27). Furthermore, given the importance of neutrophils as indicated by this work, neutrophils may represent an attractive therapeutic target (Quail, D.F. & Joyce, J.A. 2013).

Figure 27: Tumor dormancy, a potential therapeutic target

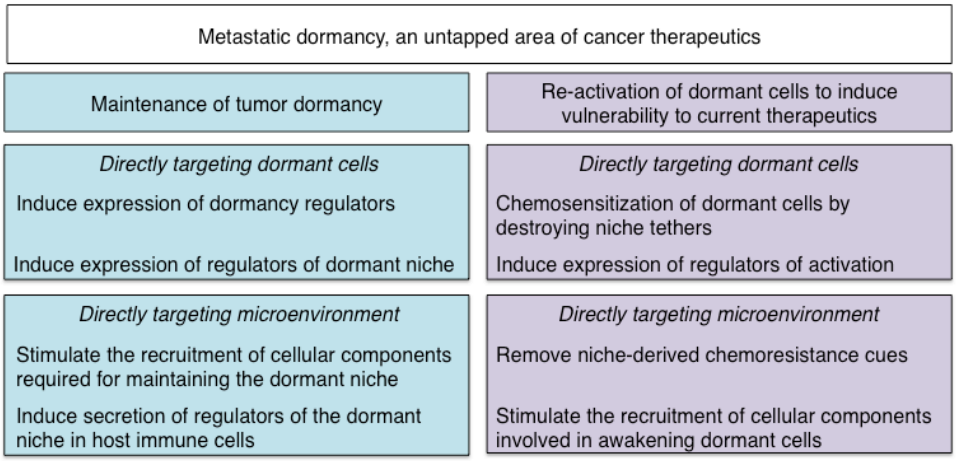

Figure 27. Tumor dormancy, a potential therapeutic target

Two distinct strategies emerge to treat dormant DTCs (1) chronic dormancy management to sensitize dormant DTCs to cytotoxic treatment, for example, by inducing the expression of key regulators of tumor dormancy or key dormant niche components, or (2) activate dormant DTCs to allow sensitization to commonly used therapeutics.

In conclusion, the future of studying metastatic dormancy is promising as novel techniques and imaging capabilities are being discovered, as well as offering novel therapeutic prospects for metastatic dormancy. Moreover, the present work may represent only the first of a number of diverse experimental models of DTC awakening that will be developed in the future, some of which may depend on quite different molecular mechanisms and signaling pathways to trigger the eruption of previously inapparent metastatic deposits. Given that interest in studying metastatic dormancy has been exponentially growing over the past decade, it is highly likely that new insights will rapidly be made.

References

Adam, A.P. *et al* (2009) Computational identification of a p38SAPK-regulated transcription factor network required for tumor cell quiescence. *Cancer Research*. **69(14)**, 5664-72.

Aguirre-Ghiso, J.A. (2002) Inhibition of FAK signaling activated by urokinase receptor induces dormancy in human carcinoma cells in vivo. *Oncogene*. **21 (16)**, 2513-24.

Aguirre-Ghiso, J.A., Ossowski, L. & Rosenbaum, S.K. (2004) Green fluorescent protein tagging of extracellular signal-regulated kinase and p38 pathways reveals novel dynamics of pathway activation during primary and metastatic growth. *Cancer Research*. **64**, 7336-7345.

Aguirre-Ghiso, J.A. (2007) Models, mechanisms and clinical evidence for cancer dormancy. *Nature Reviews Cancer*. **7**, 834-46.

Al-Hajj, M., Wicha, M.S., Benito-Hernandez, A., Morrison, S.J. & Clarke, M.F. (2003) Prospective identification of tumorigenic breast cancer cells. *Proceedings of the National Academy of Sciences*. **100 (7)**, 3983-8.

Al-Zhoughbi, W. *et al* (2014) Tumor macroenvironment and metabolism. *Seminars in Oncology*. **41(2)**, 281-295.

Andonegui, G. *et al* (2003) Endothelium-derived Toll-like receptor-4 is the key molecule in LPS-induced neutrophil sequestration into lungs. *Journal Clinical Investigation*. **111(7)**, 1011-20.

Atsumi, T. *et al* (2013) Inflammation amplifier, a new paradigm in cancer biology. *Cancer Research*. **74(1)**, 8-14.

Balic, M. *et al* (2006) Most early disseminated cancer cells detected in bone marrow of breast cancer patients have a putative breast cancer stem cell phenotype. *Clinical Cancer Research*. **12(19)**: 5615-21.

Balkwill, F. & Mantovani, A. (2001) Inflammation and cancer: back to Virchow? *Lancet*. **357**, 539-545.

Barkan, D. *et al* (2010) Metastatic growth of dormant cells by a col-I-enriched fibrotic environment. *Cancer Research*. **70(14)**, 5706-16.

Barkan, D. & Green, J.E. (2011) An in vitro system to study tumor dormancy and the switch to metastatic growth. *Journal Visualized Experiments*. **54**, 2914.

Batlle, E. *et al* (2000) The transcription factor snail is a repressor of E-cadherin gene expression in epithelial tumour cells. *Nature Cell Biology*. **2(2)**, 84-9.

Bierie, B. & Moses, H.L. (2006) Tumor microenvironment: TGFbeta: the molecular Jekyll and Hyde of cancer. *Nature Reviews Cancer*. **6**, 506-520.

Bonde, A.K., Tischier, V., Kumar, S., Soltermann, A. & Schwendener, R.A. (2012) Intratumoral macrophages contribute to epithelial-mesenchymal transition in solid tumors. *BioMed Central Cancer*. **12**, 35.

Bouchard, G. *et al* (2013) Pre-irradiation of mouse mammary gland stimulates cancer cell migration and development of lung metastases. *British Journal of Cancer*. **109 (7)**, 1829-38.

Boutagy, N.E., McMillan, R.P., Frisard, M.I. & Hulver, M.W. (2015) Metabolic endotoxemia with obesity: Is it real and is it relevant? *Biochimie*. S0300-9084

Brabletz, T. (2012) To differentiate or not--routes towards metastasis. *Nature reviews Cancer*. **12(6)**, 425-36.

Bragado, P. *et al* (2013) TGF-β2 dictates disseminated tumor cell fate in target organs through TGF-β-RIII and p38α/β signaling. *Nature Cell Biology*. **15(11),** 1351-61.

Brandolini, L. *et al* (2000) Lipopolysaccharide-induced lung injury in mice. II. Evaluation of functional damage in isolated parenchyma strips. *Pulmonary Pharmacology & Therapeutics*. **13**, 71-78.

Braun, S. *et al* (2000) Cytokeratin-positive cells in the bone marrow and survival of patients with stage I, II, or III breast cancer. *New England Journal of Medicine*. **342 (8)**, 525-33.

Brigati, C., Noonan, D.M., Albini, A. & Benelli, R. (2002) Tumors and inflammatory infiltrates: friends or foes? *Clinical Experimental Metastasis*. **19**, 247-258.

Chambers, A.F., Groom, A.C. & MacDonald, I.C. (2002) Dissemination and growth of cancer cells in metastatic sites. *Nature Reviews Cancer*. **2**, 563-572.

Chaudhary, N.I., Schnapp, A. & Park, J.E. (2006) Pharmacologic differentiation of inflammation and fibrosis in the rat bleomcyin model. *American Journal of Respiratory and Critical Care Medicine*. **73(7)**, 769-76.

Chow, M.T., Moller, A. & Smyth, M.J. (2012) Inflammation and immune surveillance in cancer. *Seminars in Cancer Biology*. **22**, 23-32.

Coussens, L.M. *et al* (2000) Inflammatory mast cells up-regulate angiogenesis during squamous epithelial carcinogenesis. *Genes & Development*. **13**, 1382-1397.

Coussens, L.M. & Werb, Z. (2002) Inflammation and cancer. *Nature*. **420**, 860-867.

Cox, T.R. *et al* (2013) LOX-mediated collagen crosslinking is responsible for fibrosis-enhanced metastasis. *Cancer Research*. **73(6**), 1721-32.

Daley, J., Tomay, A.A., Connolly, M.D., Reichnner, J.S. & Albina, J.E. (2008) Use of Ly6G-specific monoclonal antibody to deplete neutrophils in mice. *Journal of Leukocyte Biology*. **83 (1)**, 64-70.

de Groot, D.J., de Vries, E.G., Groen, H.J. & de Jong, S. (2007) Non-steroidal anti-inflammatory drugs to potentiate chemotherapy effects: from lab to clinic. *Critical Reviews in Oncology/Hematology*. **61(1)**, 52-69.

de Martel, C. *et al* (2012) Global burden of cancers attributable to infections in 2008: a review and synthetic analysis. *Lancet Oncology*. **13**, 607–615.

Demicheli, R. *et al* (1994) Local recurrences following mastectomy: support for the concept of tumor dormancy. *Journal of the National Cancer Institute*. **86(1)**, 45-8.

DePalma, M. & Lewis, C.E. (2013) Macrophage regulation of tumor responses to anticancer therapies. *Cancer Cell*. **23(3**), 277-286

DerHagoPian, R.P., Sugarbaker, E.V. & Ketcham, A. (1978) Inflammatory oncotaxis. *Journal of the American Medical Association*. **240(4)**, 374-5.

Desai, A., Grolleau-Julius, A. & Yung, R. (201) Leukocyte function in the aging immune system. *Journal of Leukocyte Biology*. **87**, 1001–1009.

Diamnod, C.E., Khameneh, H. J., Brough, D. & Mortellaro, A. (2015) Novel perspectives on non-canonical inflammasome activation. *Dove Medical Press*. **4**, 131-141.

Dohadwala, M. *et al* (2010) The role of ZEB1 in the inflammation-induced promotion of EMT in HNSCC. Otolaryngology - *Head and Neck Surgery*. **142(5)**, 753-9.

Ducos, K., Panterne, B., Fortunel, N., Hatzfeld, A., Monier, M.N. & Hatzfeld, J. (2000) p21 (cip1) mRNA is controlled by endogenous transforming growth factor-beta1 in quiescent human hematopoietic stem/progenitor cells. *Journal of Cell Physiology*. **184(1),** 80-5.

Dunn, G.P., Old, L.J. & Schreiber, R.D. (2004) The immunobiology of cancer immunosurveillance and immunoediting. *Immunity*. **21(2)**, 137-48.

Dvorak, H.F. (1986) Tumors: wounds that do not heal. Similarities between tumor stroma generation and wound healing. *New England Journal of Medicine*. **315(26)**, 1650-9.

Eckhouse, S., Lewison, G. & Sullivan, R. (2008) Trends in the global funding and activity of caner research. *Molecular Oncology*. **2(1**), 20-32.

Eger, A. *et al* (2005) DeltaEF1 is a transcriptional repressor of E-cadherin and regulates epithelial plasticity in breast cancer cells. *Oncogene*. **24(14)**, 2375-85.

El Rayes, T. *et al* (2015) Lung inflammation promotes metastasis through neutrophil protease-mediated degradation of Tsp-1. *Proceedings of the National Academy of Sciences*. **112(52)**, 16000-5.

Eming, S.A., Krieg, T. & Davidson, J.M. (2007) Inflammation in wound repair: molecular and cellular mechanisms. *Journal Investigative Dermatology*. **3**, 514-25.

Erdman, S.E. & Poutahidis, T. (2014) The microbiome modulates the tumor macroenvironment. *Oncoimmunology*. 3.

Evdokimova, V. *et al* (2009) Translational activation of snail1 and other developmentally regulated transcription factors by YB-1 promotes an epithelial-mesenchymal transition. *Cancer Cell*. **15**, 402-415.

Extermann, M. (2007) Interaction between comorbidity and cancer. *Cancer Control*. **14(1)**, 13-22.

Fidler IJ. (1970) Metastasis: quantitative analysis of distribution and fate of tumor emboli labeled with 125 I-5-iodo-2'-deoxyuridine. *Journal of the National Cancer Institute*. **45**, 773–82.

Fidler IJ. (2003) The pathogenesis of cancer metastasis: the 'seed and soil' hypothesis revisited. *Nat Reviews Cancer*. **3**, 453–458.

Finkelstein, D., Brem, S., Patz, A., Folkman, J., Miller, S. & Ho-Chen, C. (1977) Experimental retinal neovascularization induced by intravitreal tumors. *American Journal of Ophthalmology*. **83(5)**, 660-4.

Folkman, J. & Kalluri, R. (2004) Cancer without disease. *Nature*. **427(6977)**, 787.

Freedland, S.J. & Moul, J.W. (2007) Prostate specific antigen recurrence after definitive therapy. *Journal of Urology*. **177**, 1985–91.

Gao, H. *et al* (2012) The BMP inhibitor Coco reactivates breast cancer cells at lung metastatic sites. *Cell*. **150(4)**, 764-79.

Gath, H.J. & Brakenhoff, R.H. (1999) Minimal residual disease in head and neck cancer. *Cancer Metastasis Reviews*. **18(1)**, 109-26.

Ghajar, C.M. *et al* (2013) The perivascular niche regulates breast tumour dormancy. *Nature Cell Biology*. **15(7)**, 807-17.

Giancotti, F. (2013) Mechanisms governing metastatic dormancy and reactivation. *Cell*. 1**55**, 750-764.

Goss, P.E. & Chambers, A.F. (2010) Does tumour dormancy offer a therapeutic target? *Nature reviews Cancer*. **10(12)**, 871-7.

Granot, Z. *et al* (2011) Tumor entrained neutrophils inhibit seeding in the premetastatic lung. *Cancer Cell*. **20**, 300-314.

Griffiths, R.I., Gleeson, M.L., Valderas, J.M. & Danese, M.D. (2014) Impact of undetected comorbidity on treatment and outcomes of breast cancer. *International Journal of Breast Cancer*. 970780.

Grivennikov, S.I., Greten, F.R. & Karin, M. (2010) Immunity, inflammation, and cancer. *Cell*. **140**, 883-899.

Guo, H., Diao, N., Yuan, R., Chen, K., Geng, S, Li, M. & Li, L. (2016) Subclinical-dose endotoxin sustains low-grade inflammation and exacerbates steatohepatitis in high-fat diet-fed mice. *Journal of Immunology*. **196(5)**, 2300-8.

Guo, W., Keckesova, Z., Donaher, J.L., Shibue, T., Tischler, V., Reinhardt, F., Itzkovitz, S., Noske, A., Zürrer-Härdi, U., Bell, G., Tam, W.L., Mani, S.A., van Oudenaarden, A. & Weinberg, R.A. (2012) Slug and Sox9 cooperatively determine the mammary stem cell state. *Cell* **148(5)**, 1015-28.

Guo, Y., Li, P., Biedsoe, G., Yang, Z.R., Chao, L. & Chao, J. (2015) Kallistatin inhibits TGF—induced endothelial-mesenchymal transition by differential regulation of micrRNA-21 and eNOS expression. *Experimental Cell Research*. **337(1)**, 103-10.

Gurpinar, E., Grizzle, W.E. & Piazza, G. (2014) NSAIDS inhibit tumorigenesis, but how? *Clinical Cancer Research*. **20**, 1104-1113.

Hadfield, G. (1954) The dormant cancer cell. *British Medical Journal*. **4888**, 607-610.

Hajra, K.M., Chen, D.Y. & Fearon, E.R. (2002) The SLUG zinc-finger protein represses E-cadherin in breast cancer. *Cancer research*. **62(6)**, 1613-8.

Hanahan, D. & Folkman, J. (1996) Patterns and emerging mechanisms of the angiogenic switch during tumorigenesis. *Cell*. **86(3)**, 353-64.

Hanahan, D. & Weinberg, R.A. (2000) The hallmarks of cancer. *Cell*. **100(1)**, 57-70.

Hanahan, D. & Weinberg, R.A. (2011) Hallmarks of cancer: the next generation. *Cell*. **144(5)**, 646-74.

Hay, E.D. (1968) Organization and fine structure of epithelium and mesenchyme in the developing chick embryo. In Epithelial-mesenchymal interactions. R. Fleischmajer and R.E. Billingham, editors. Williams & Wilkins. Baltimore, Maryland, USA. 31–55.
Hitchcock, J.R. *et al* Cunningham, A.F. (2015) Inflammation drives thrombosis after Salmonella infection via CLEC-2 on platelets. *Journal of Clinical Investigation*, **125**: 4429-4446.
Holmgren, L., O'Reilly, M.S. & Folkman, J. (1995) Dormancy of micrometastases: balanced proliferation and apoptosis in the presence of angiogenesis suppression. *Nature Medicine*.**1(2)**, 149-53.

Houterman, S., Janssen-Heijnen, M.L., Verheij, C.D., Louwman, W.J., Vreugdenhil, G., Sangen, M.J. & Coebergh, J.W. (2004) Comorbidity has negligible impact on treatment and complications but influences survival in breast cancer patients. *British Journal of Cancer*. **90(12)**, 2332–2337.

Hu, Y. & Smyth, G.K. (2009) ELDA: Extreme limiting dilution analysis for comparing depleted and enriched populations in stem cell and other assays. *Journal of Immunological Methods*. **347**, 70-78.

Hugo, H. *et al* (2007) Epithelial-mesenchymal and mesenchymal-epithelial transitions in carcinoma progression. *Journal of Cellular Physiology*. **213(2)**, 374-83.

Hüsemann, Y. *et al* (2008) Systemic spread is an early step in breast cancer. *Cancer Cell*. **13**, 58–68.

Iruela-Arispe, M. L., Luque, A. & Lee, N. (2004) Thrombospondin modules and angiogenesis. *International Journal of Biochemistry & Cell Biology*. **36**, 1070-1078.

Jain, M. *et al* (2002) Sustained loss of a neoplastic phenotype by brief inactivation of MYC. *Science*. **297(5578)**, 102-4.

Jørgensen, T.L., Hallas, J., Friis, S. & Herrstedt, J. (2012) Comorbidity in elderly cancer patients in relation to overall and cancer-specific mortality. *British Journal of Cancer*. **106(7)**, 1353–1360.

Joyce, J.A. & Pollard, J.W. (2009) Microenvironmental regulation of metastasis. *Nature Reviews Cancer*. **9(4)**, 239-252.

Juntilla, M.R. & de Sauvage, F.J. (2013) Influence of tumor micro-environment heterogeneity on therapeutic response. *Nature*. **501(7467)**, 346-54.

Kalluri, R. & Neilson, E.G. (2003) Epithelial-mesenchymal transition and its implications for fibrosis. *Journal of Clinical Investigation*. **112(12)**, 1776-1784.

Kalluri, R. & Weinberg, R.A. (2009) The basics of epithelial-mesenchymal transition. *Journal of Clinical Investigation*. **119(6)**, 1420-8.

Kang, Y., Siegel, P.M., Shu, W., Drobnjak, M., Kakonen, S.M., Cordón-Cardo, C., Guise, T.A. & Massagué. (2003) A multigenic program mediating breast cancer metastasis to bone. *Cancer Cell*. **3(6)**, 537-49.

Karrison, T.G., Ferguson, D.J. & Meier, P. (1999) Dormancy of mammary carcinoma after mastectomy. *Journal of the National Cancer Institute*. **91(1)**, 80-5.

Kennecke, H. (2010) Metastatic behavior of breast cancer subtypes. *Journal of Clinical Oncology*. **28(20)**, 3271-7.

Kimura, W., Morikane, K., Esaki, Y., Chan, W.C. & Pour, P.M. (1998) Histologic and biologic patterns of microscopic pancreatic ductal adenocarcinomas detected incidentally at autopsy. *Cancer*. **82**, 1839–49.

Klein, C. A. (2009) Parallel progression of primary tumours and metastases. *Nature Reviews Cancer*. **9**, 302-312.

Koay, M.A., Gao, X., Washington, M.K., Parman, K.S., Sadikot, R.T., Blackwell, T.S. & Christman, J.W. (2002) Macrophages are necessary for maximal nuclear factor-ϰB activation in response to endotoxin. *American Journal of Respiratory Cell and Molecular Biology*. **26**, 572-578.

Koebel, C.M. *et al* (2007) Adaptive immunity maintains occult cancer in an equilibrium state. *Nature*. **450(7171)**, 903-7.

Kokudo, T., Suzuki, Y., Yoshimatsu, Y., Yamazaki, T., Watabe, T. & Miyazono, K. (2008) Snail is required for TGFbeta-induced endothelial-mesenchymal transition of embryonic stem cell-derived endothelial cells. *Journal of Cell Science*. **121(20)**, 3317-24.

Kudo-Saito, C., Shirako, H., Takeuchi, T. & Kawakami, Y. (2009) Cancer metastasis is accelerated through immunosuppresion during Snail-induced EMT of cancer cells. *Cancer Cell*. **15(3)**, 195-206.

Labelle, M., Begum, S. & Hynes, R.O. (2014) Platelets guide the formation of early metastatic niches. *Proceedings of the National Academy of Sciences*. **111(30)**, E30353-61.

Lakritz, J.R. *et al* (2015) Gut bacteria require neutrophils to promote mammary tumorigenesis. *Oncotarget*. **6(11)**, 9387-96.

Le Bitoux, M.A. & Stamenkovic, I. (2008) Tumor-host interactions: the role of inflammation. *Histochemistry and cell biology*. **130(6)**, 1079-90.

Liu, D., Aguirre-Ghiso, J., Estrada, Y. & Ossowski, L. (2002) EGFR is a transducer of the urokinase receptor initiated signal that is required for in vivo growth of a human carcinoma. *Cancer Cell*. **1(5)**, 445-56.

Lopez-Novoa, J.M. & Nieto, M.A. (2009) Inflammation and EMT: an alliance towards organ fibrosis and cancer progression. *EMBO Molecular Medicine*. **(6-7)**, 303-14.

Lu, H. *et al* (2014) A breast cancer stem cell niche supported by juxtracrine signaling from monocytes and macrophages. *Nature Cell Biology*. **16(11)**, 1105-17.

Lyu, T. *et al* (2013) Expression and epigenetic regulation of angiogenesis-related factors during dormancy and recurrent growth of ovarian carcinoma. *Epigenetics*. **8(12)**, 1330-46.

Mani, S.A. *et al* (2008) The epithelial-mesenchymal transition generates cells with properties of stem cells. *Cell*. **133(4)**, 704-15.

Mantovani, A. Allavena, P., Sica, A. & Balkwill, F. (2008) Cancer-related inflammation. *Nature*. **454(7203)**, 436-44.

Marlow, R. *et al* (2013) A novel model of dormancy for bone metastatic breast cancer cells. *Cancer Research*. **73(23)**, 6886-99.

Matute-Bello, G., Frevert, C. & Martin T. (2008) Animal models of acute lung injury. *American Journal Physiology Lung Cell Molecular Physiology*. **295**, L379-L399.

McNichols, D.W., Segura, J.W. & DeWeerd, J.H. (1981) Renal cell carcinoma: longterm survival and late recurrence. *Journal of Urology*. **126**, 17–23.

Medici, D., Hay, E.D. & Olsen, B.R. (2008) Snail and Slug promote epithelial-mesenchymal transition through beta-catenin-T-cell factor-4-dependent expression of transforming growth factor-beta3. *Molecular Biology of Cell*. **19(11)**, 4875-87.

Minn, A.J. *et al* (2005) Distinct organ-specific metastatic potential of individual breast cancer cells and primary tumors. *Journal of Clinical Investigation*. **115 (1)**, 44-55.

Mock, K., Preca, B.T., Brummer, T., Brabletz, S., Stemmler, M.P. & Brabletz, T. (2015) The EMT-activator Zeb1 induces bones metastasis associated genes including BMP-inhibitors. *Oncotarget*. **6(16)**, 14399-412.

Moody, S.E. *et al* (2002) Conditional activation of Neu in the mammary epithelium of transgenic mice results in reversible pulmonary metastasis. *Cancer Cell*. **2(6)**, 451-61.

Moody, S.E. *et al* (2008) The transcriptional repressor Snail promotes mammary tumor recurrence. *Cancer Cell*. **8(3)**, 197-209.

Moore, B.B. & Hogaboam, C.M. (2008) Murine models of pulmonary fibrosis. *American Journal of Physiology Lung Cellular Molecular Physiology*. **294**, L152–160.

Morel, A.P., Lievre, M., Thomas, C., Hinkal, G., Ansieau, S. & Puisieux, A. (2008) Generation of breast cancer stem cells through epithelial mesenchymal transition. *PloS one*. **3(8)**, e2888.

Morris, V.L., Tuck, A.B., Wilson, S.M., Percy, D. & Chambers, A.F. (1993) Tumor progression and metastasis in murine D2 hyperplastic alveolar nodule mammary tumor cell lines. *Clinical & experimental metastasis*. **11(1)**,103-12.

Nahid, M.A, Satoh, M. & Chan, E.K.L. (2011) MicroRNA in TLR signaling and endotoxin tolerance. *Cellular & Molecular Immunolog*. **8**, 388-403.

Nanni, P., de Giovanni, C., Lollini, P.L., Nicoletti, G. & Prodi, G. (1983) TS/A: a new metastasizing cell line from a BALB/c spontaneous mammary adenocarcinoma. *Clinical Experimental Metastasis*, **1**:373–80.

Naumov, G.N., Akslen, L.A. & Folkman, J. (2006) Role of angiogenesis in human tumor dormancy: animal models of the angiogeneic switch. *Cell Cycle*. **5**, 1779-1787.

Nikulina, M., Habich, C., Flohe, S.B., Scott, F.W. & Kolb, H. (2004) Wheat gluten cuases dendritic cell maturation and chemokine secretion. *Journal of immunology*. **173(3)**, 1925-33.

Ocaña, O.H. *et al* (2012) Metastatic colonization requires the repression of the epithelial-mesenchymal transition inducer Prrx1. *Cancer Cell*. **22(6)**, 709-24.

O'Reilly, M.S. *et al* (1994) Angiostatin: a novel angiogenesis inhibitor that mediates the suppression of metastases by a Lewis lung carcinoma. *Cell*. **79(2)**, 315-28.

Oskarsson, T. *et al* (2011) Breast cancer cells produce tenascin C as a metastatic niche component to colonize the lungs. *Nature Medicine*. **17**, 867-874.

Ossowski, L. & Aguirre-Ghiso, J.A. (2010) Dormancy of metastatic melanoma. *Pigment Cell Melanoma Research*. **23(1)**, 41-56.

Paget S. (1989) The distribution of secondary growths in cancer of the breast. 1889. *Cancer Metastasis Review*. **8**, 98–101.

Pantel, K. & Brakenhoff, R.H. (2004) Dissecting the metastatic cascade. *Nature Reviews Cancer*. **4(6)**, 448-56.

Pantel, K. Alix-Panabières, C. & Riethdorf, S. (2009) Cancer micrometastases. *Nature Reviews Clinical Oncology*. **6(6)**, 339-51.

Pelayo, R., Miyazaki, K., Huang, J., Garrett, K.P., Osmond, D.G. & Kincade, P.W. (2006) Cell cycle quiescence of early lymphoid progenitors in adult bone marrow. *Stem Cells*. **24(12)**, 2703-13.

Phan, S.H. & Kunkel, S.L. (1992) Lung cytokine production in bleomycin-induced pulmonary fibrosis. *Experimental Lung Research*. **18(1)**, 29-43.

Pidgeon, G.P., Harmey, J.H., Kay, E., Da Costa, M., Redmond, H.P. & Bouchier-Hayes, D.J. (1999) The role of endotoxin/lipopolysaccharide in surgically induced tumor growth in a murine model of metastatic disease. *British Journal of Cancer*. **81(8)**, 1311-1317.

Pierga, J.Y. *et al* (2003) Clinical significance of proliferative potential of occult metastatic cells in bone marrow of patients with breast cancer. *British Journal of Cancer*. **89**, 539–545.

Poltorak, A. *et al* (1998) Defective LPS signaling in C3H/HeJ and C57BL/10ScCr mice: mutations in *TLR4* gene. *Science*. **282**, 2085-2088.

Polyak, K. & Weinberg, R.A. (2009) Transitions between epithelial and mesenchymal states: acquisition of malignant and stem cells traits. *Nature Reviews Cancer*. **9**, 265-273.

Puisieux, A., Brabletz, T. & Caramel, J. (2014) Oncogenic roles of EMT-induced transcription factors. *Nature Cell Biology*. **16**, 488-494.

Qian, B. *et al* (2009) A distinct macrophage population mediates metastatic breast cancer cell extravasation, establishment and growth. *PLoS ONE*. **4(8)**, e6562.

Quail, D.F. & Joyce, J.A. (2013) Microenvironmental regulation of tumor progression and metastasis. *Nature Medicine*. **19(11)**, 1423-37.

Rabinovsky, R., Uhr, J.W., Vitetta, E.S. & Yefenof, E. (2007) Cancer dormancy: lessons from a B cell lymphoma and adenocarcinoma of the prostate. *Advances in Cancer Research* . **97**, 189-202.

Rak J.W., McEachern, D. & Miller, F.R. (1992) Sequential alteration of peanut agglutinin binding-glycoprotein expression during progression of murine mammary neoplasia. *British Journal of Cancer*, **5**, 641–8.

Rao, V.P. *et al* (2006) Innate immune inflammatory response against enteric bacteria *Helicobacter hepaticus* induces mammary adenocarcinoma in mice. *Cancer Research* **66(15),** 7395-7400.

Read, W.L. *et al* (2004) Differential prognostic impact of comorbidity. *Journal of Clinical Oncology***. 22(15)**, 3099-3103.

Recamier, J.C. (1829) Recherches sur le traitement du cancer sur la compression methodique simple ou combinee et sur l'histoire generale de la meme maladie. 2nd ed.

Ricciardi, M. *et al* (2015) Epithelial-to-mesenchymal transition (EMT) induced by inflammatory priming elicits mesenchymal stromal cell-like immune-modulatory properties in cancer cells. *British Journal of Cancer*. **112(6)**, 1067-75.

Rojas, M., Woods, CR., Mora, AL., Xu, J. & Brigham, KL. (2005) Endotoxin-induced lung injury in mice: Structural, functional, and biochemical responses. *American Journal of Physiology Lung Cellular Molecular Physiology*. **288***, L333-341*.

Rothwell, P.M., Wilson, M., Price, J.F., Belch, J.F., Meade, T.W. & Mehta, Z. (2012) Effect of daily aspirin on risk of cancer metastasis: a study of incident cancers during randomized controlled trials. *Lancet*. **379(9826)**, 1591-601.

Sarfarti, D., Koczwara, B. & Jackson, C. (2016) The impact of comorbidity on cancer and its treatment. *CA Cancer Journal Clinical*. 21342.

Schmidt, J.M. *et al* (2015) Stem-cell like properties and epithelial plasticity arise as stable traits after transient Twist1 activation. *Cell Reports*. **10(2)**, 131-9.

Schrier, D.J. & Phan, S.H. (1984) Modulation of bleomycin-induced pulmonary fibrosis in the BALB/c mouse by cyclophosphamide-sensitive T cells. *American Journal of Pathology*. **116(2)**, 270-8.

Shacter, E. & Weitzman, S.A. (2002) Chronic inflammation and cancer. *Oncology*. **15**, 217-226.

Shibue, T. & Weinberg, R.A. (2009) Integrin beta1-focal adhesion kinase signaling directs the proliferation of metastatic cancer cells disseminated in the lungs. *Proceedings of the National Academy of Sciences of the United States of America*. **106(25)**, 10290-5.

Shibue, T., Brooks, M.W. & Weinberg, R.A. (2013) An integrin-linked machinery of cytoskeletal regulation that enables experimental tumor initiation and metastatic colonization. *Cancer Cell*. **4**, 381-98.

Slaney, C.Y., Rautela, J. & Parker, B.S. (2013) The emerging role of immunosurveillance in dictating metastatic spread in breast cancer. *Cancer Research*. **73(19)**, 5852-7.

Smid, M. *et al* (2008) Subtypes of breast cancer show preferential site of relapse. *Cancer Research*. **68(9)**, 3108-14.

Søgaard, M., Thomsen, R.W., Bossen, K.S., Sørensen, H.T. & Nørgaard, M. (2013) The impact of comorbidity on cancer survival: a review. *Clinical Epidemiology*. **5(Suppl 1)**, 3-29.

Sosa, M.S., Avivar-Valderas, A., Bragado, P., Wen, H.C. & Aguirre-Ghiso, J.A. (2011) ERK1/2 and p38α/β signaling in tumor cell quiescence: opportunities to control dormant residual disease. *Clinical Cancer Research*. **17(18)**, 5850-7.

Steeg, P.S. (2006) Tumor metastasis: mechanistic insights and clinical challenges. *Nature Medicine*. **12**, 895-904.

Stephens, J.K. *et al* (2000) Fatal transfer of malignant melanoma from multiorgan donor to four allograft recipients.*Transplantation*. **70**, 232-6.

Strutz, F. *et al* (2002) Role of basic fibroblast growth factor-2 in epithelial-mesenchymal transformation. *Kidney international*. **61(5)**, 1714-28.

Su, X., Looney, M.R., Hang, S., Lee, J.W., Song, Y. & Matthay, M.A. (2011) Role of CFTR expressed by neutrophils in modulating acute lung inflammation and injury in mice. *Inflammation Research*. **60(7)**, 619-632.

Sultzer, B.M. (1968) Genetic control of leucocyte responses to endotoxin. *Nature*. **219(5160)**, 1253-4.

Tam, W.L. & Weinberg, R.A. (2013) The epigenetics of epithelial-mesenchymal plasticity in cancer. *Nature Medicine*. **19(11)**, 1438-49.

Tammemagi, C., Nerenz, D., Neslund-Dudas, C., Fedkamp, C. & Nathanson, D. (2005) Comorbidity and survival disparities among black and white patients with breast cancer *JAMA*. **294(14)**, 1765-1772.

Tan, B.T., Park, C.Y., Ailles, L.E. & Weissman, I.L. (2006) The cancer stem cell hypothesis: a work in progress. *Laboratory Investigation*. **86**, 1203-1207.

Taylor, J., Hickson, J., Lotan, T., Yamada, D.S. & Rinker-Schaeffer, C. (2008) Using metastasis suppressor proteins to dissect interactions among cancer cells and their microenvironment. *Cancer Metastasis Reviews*. **27(1)**, 67-83.

Thiery, J.P., Acloque, H., Huang, R.Y.J. & Nieto, M.A. (2009) Epithelial-mesenchymal transitions in development and disease. *Cell*. **139**, 871-890.

Tran, H.D., Luitel, K., Kim, M., Zhang, K., Longmore, G.D. & Tran, D. (2014) Transient SNAIL1 expression is necessary for metastatic competence in breast cancer. *Cancer Research*. **74(21)**, 6330-6340.

Tsai, J.H., Donaher, J.L., Murphy, D.A., Chau, S. & Yang, J. (2012) Spatiotemporal regulation of epithelial-mesenchymal transition is essential for squamous cell carcinoma metastasis. *Cancer Cell*. **22(6)**, 725-36.

Tsao, H., Cosimi, A.B. & Sober, A.J. (1997) Ultra-later recurrence (15 years or longer) of cutaneous melanoma. *Cancer*. **79**, 2361-70.

Ulevitch, R.J. & Tobias, P.S. (1995) Receptor-dependent mechanisms of cell stimulation by bacterial endotoxin. *Annual Review Immunology*. **13**, 437-57.

Valastyan, S. &Weinberg, R.A. (2011) Tumor metastasis: molecular insights and evolving paradigms. *Cell*. **147(2)**, 275-92.
Vega, S., Morales, A.V., Ocana, O.H, Valdes, F., Fabregat, I. & Nieto, M.A. (2004) Snail blocks the cell cycle and confers resistance to cell death. *Genes & Development*. **18**, 113101143.

Visvader, J.E. & Smith, G.H. (2011) Murine mammary epithelial stem cells: discovery, function and current status. *Cold Spring Harb Perspective Biology*. **3(2)**, a004879.

Vogel, S.N., Wax, J.S., Perera, P.Y., Padian, C., Potter, M. & Mock, B.A. (1994) Construction of a BALB/C congenic mouse, C.C3H-Lpsd, that expresses the Lpsd allele: analysis of chromosome 4 markers surrounding the Lps gene. *Infection & Immunity*. **62(10)**, 4454-9.

Walter, N.D. *et al* (2011) Wound healing after traume may predispose to lung cancer metastasis: review of potential mechanisms. *American Journal of Respiratory Cell and Molecular Biology*. **44(5)**, 591-6.

Watson, J. & Riblet, R. (1974) Genetic control of responses to bacterial lipopolysaccharides in mice. *Journal Experimental Medicine*. **140(5)**, 1147-1161.

Weinstein, I.B. (2002) Cancer. Addiction to oncogenes – the Achilles heal of cancer. *Science*. **297(5578)**, 63-4.

Wendt, M.K., Taylor, M.A., Schiemann, B.J. & Schiemann, W.P. (2011) Down-regulation of epithelial cadherin is required to initiate metastatic outgrowth of breast cancer. *Molecular Biology of Cell*. **22(14)**, 2423-2435.

White, D.E. *et al* (2004) Targeted disruption of beta1-integrin in a transgenic mouse model of human breast cancer reveals an essential role in mammary tumor induction. *Cancer Cell*. **6(2)**, 159-70.

Wikman, H., Vessella, R. & Pantel, K. (2008) Cancer micrometastasis and tumour dormancy. *APMIS*. **116(7-8)**, 754-70.

Yang, J. *et al* (2004) Twist, a master regulator of morphogenesis, plays an essential role in tumor metastasis. *Cell*. **117(7)**, 927-39.

Yang, J. & Weinberg, R.A. (2008) Epithelial-mesenchymal transition: at the crossroads of development and tumor metastasis. *Developmental Cell*. **14(6)**, 818-29.

Ye, X., Tam, W.L., Shibue, T., Kaygusuz, Y., Reinhardt, F., Eaton, E. & Weinberg, R.A. (2015) Distinct EMT programs control normal mammary stem cells and tumor-initiating cells. *Nature*. **525**, 256-260.

Yeh, A.C & Ramaswamy, S. (2015) Mechanisms of Cancer Cell Dormancy – Another Hallmark of Cancer? *Cancer Research*. **75(23)**, 5014-5022.

Appendix I:

Neutrophils suppress intraluminal NK-mediated tumor cell clearance and enhance extravasation of disseminated carcinoma cells

Asaf Spiegel[1], Samin Houshyar[1], Mary Brooks[1], Ferenc Reinhardt[1], Michele Ardolino[2], Evelyn Fessler[1], Jasmine DeCock[1], Ioannis K. Zervantonakis[3], Alexandre Ianello[2], Yoshiko Iwamoto[4], Virna Cortez-Retamozo[4], Mikael J. Pittet[4], David H. Raulet[2] and Robert A. Weinberg[1,5,6,*]

[1]Whitehead Institute for Biomedical Research, Cambridge, MA 02142, USA

[2]Department of Molecular and Cell Biology and Cancer Research Laboratory, Division of Immunology, University of California at Berkeley, Berkeley, CA 94720, USA

[3]Department of Mechanical Engineering, Massachusetts Institute of Technology, Cambridge, MA 02139, USA

[4]Center for Systems Biology, Massachusetts General Hospital and Harvard Medical School, Boston, MA 02114, USA

[5]Department of Biology, Massachusetts Institute of Technology, Cambridge, MA 02142, USA

[6]Massachusetts Institute of Technology Ludwig Center for Molecular Oncology, Cambridge, MA 02139, USA

Personal Contribution to the Project

This chapter is the result of collaboration with Asaf Spiegel on work that is currently under review with *Cancer Discovery*. Asaf requested assistance in performing bioluminescent imaging experiments and determining the rate of carcinoma cell clearance. I performed the bioluminescent imaging experiments and the relevant data analysis, which is described in this appendix.

Abstract

Immune cells promote the initial metastatic dissemination of carcinoma cells from primary tumors. In contrast to their well-studied functions in the initial stages of metastasis, the specific roles of immunocytes in facilitating progression through the critical later steps of the invasion-metastasis cascade remain poorly understood. Here we define novel functions of neutrophils in promoting intraluminal survival and extravasation at sites of metastatic dissemination. We show that CD11b$^+$/Ly6G$^+$ neutrophils enhance metastasis formation via two distinct mechanisms. First, neutrophils inhibit natural killer cell function, which leads to a significant increase in the intraluminal survival time of tumor cells. Thereafter, neutrophils operate to facilitate extravasation of tumor cells through the secretion of IL-1b and matrix metalloproteinases. These results identify neutrophils as key regulators of intraluminal survival and extravasation through their crosstalk with host cells and disseminating carcinoma cells.

The metastatic spread of tumor cells to distant sites is estimated to be responsible for at least 90% of cancer-related mortality, but the mechanisms leading to these secondary growths are incompletely understood. Evidence accumulated in recent years demonstrates that the invasive and metastatic traits of cancer cells are often governed by complex interactions between cancer cells and surrounding stromal cells of host origin. This crosstalk extends across multiple stages of the invasion-metastasis cascade - the sequence of events that commences with locally invasive primary tumor cells, proceeds through their intravasation, transport and survival in the circulation, extravasation into the

parenchyma of distant tissues, formation of micrometastases, and finally their colonization of these tissues, yielding macroscopic metastases [1]. While the tumor-promoting effects of immune cells acting at the primary tumor site have been studied extensively [2-6], relatively little is known about how circulating immune cells affect the dynamics of the later phases of the invasion-metastasis cascade.

Among the various immune cell populations of the host, studies of the contributions of neutrophils to cancer biology have been overshadowed by examinations of other cell types, most notably macrophages. Furthermore, the role of neutrophils in cancer has been a subject of controversy, as both tumor-promoting and -suppressing effects have been reported [7-15]. Neutrophils have been implicated in cancer pathogenesis because of their ability to secrete cytokines, such as IL-1b, which is known to activate endothelial cells [16], and proteases, such as matrix metalloproteinases (MMPs), which can cleave components of the extracellular matrix (ECM) as well as cell-surface adhesion molecules [17]. In addition, MMPs can liberate growth factors that are bound in an inactive state either to the ECM or to the plasma membrane, thereby making these factors readily available to cancer cells [18, 19]. Acting in these ways, MMPs have been shown to contribute to the local invasion and intravasation steps of the invasion-metastasis cascade [20-24].

Independent of the localized interactions between cancer cells and neutrophils, neutrophils can play a role in the systemic response to tumorigenesis. For example the systemic effects of tumors on host physiology, including neutrophilia, are often observed

in murine models of cancer as well as in cancer patients [3, 5, 25-28]. Moreover, elevated levels of circulating neutrophils represent a marker of poor prognosis in cancer patients [29, 30].

In the present study, we demonstrate that the systemic effects initiated by neoplastic cells residing in the primary tumor profoundly impact their vascular intraluminal survival and extravasation at distant metastatic sites. More specifically, our results demonstrate that neutrophils, mobilized by the primary tumors, have the ability to prevent NK cell-mediated clearance of tumor cells from initial sites of dissemination while concurrently facilitating the extravasation of tumor cells into the lung parenchyma.

RESULTS

Tumor metastasis is facilitated by neutrophils

In order to study systemic mechanisms that facilitate tumor progression, we employed an established *in vivo* experimental system using the previously described murine mammary carcinoma 4T1 cells [31, 32]. When injected subcutaneously (s.c.) into syngeneic BALB/c hosts, 4T1 cells form vigorously growing primary tumors and are able to complete all steps of the metastatic cascade, resulting in the formation of large numbers of visible metastatic nodules in the lungs [31]. We confirmed earlier reports using the 4T1 tumor model [12-14, 33], and observed a 100-fold elevation in the number of circulating white blood cells (WBCs) in 4T1 tumor-bearing mice (hereafter termed 4T1 mice; 4 weeks post-implantation) relative to normal control hosts; neutrophils accounted largely for this expansion of the WBC compartment (Fig.1A). Of note,

implantation of 4T1 tumors either orthotopically or subcutaneously yielded similar effects in terms of neutrophilia as well as splenomegaly (Supplementary Fig. 1A). Accordingly, we proceeded with subcutaneous implantation of 4T1 cells since this method eliminates the significant immune effects that result from the far more invasive orthotopic surgery and post-surgical wound healing. ELISA analysis demonstrated that cultured 4T1 cells secreted high levels of G-CSF (1.14$\pm$ 0.35 ng/ml /10^6 cells), a cytokine that has been shown to cause the expansion and mobilization of neutrophils [12]. Furthermore, given that the expression of the G-CSF receptor was undetectable in this tumor cell line (Supplementary Fig. 1B), it was unlikely that the secreted G-CSF acted in an autocrine manner. Hence, the 4T1 tumor model and its associated neutrophilia provided the necessary platform to study the role of neutrophils in cancer progression.

We also noted a 10-fold increase in spleen weight of 4T1 mice, (Fig. 1B) and wished to determine whether this splenomegaly contributed in any way to the metastatic ability of the 4T1 cells, since the spleen can serve as an important reservoir of myeloid cells such as neutrophils [34]. To test this notion we removed the spleens of BALB/c mice prior to implanting 4T1 tumor cells s.c.. We chose splenectomy because post-surgical recovery is rapid and there are few systemic side-effects on host physiology. In splenectomized mice relative to non-splenectomized 4T1 mice, we observed a 50% reduction in the total number of circulating WBCs, which was paralleled by a similar reduction in the number of neutrophils at the time the experiments were terminated (4-5 weeks post- 4T1 cell implantation; Supplementary Fig. 1C). While there was no reduction in the weights of primary tumors in splenectomized mice (Fig. 1C),

splenectomy prior to subcutaneous injection of 4T1 tumor cells led to a 56% reduction in the number of pulmonary metastases formed relative to those in the control, sham-operated mice (Fig. 1D, 1E).

We wished to further verify that the efficient metastasis of 4T1 tumor cells depended in significant part on systemic physiologic effects. To address this possibility, we asked whether implantation of 4T1 tumors would affect the spontaneous metastasis of D2A1 murine mammary carcinoma cells implanted subcutaneously on the contralateral flank of a syngeneic host BALB/c mouse. When implanted on their own, D2A1 primary tumors rarely spawn pulmonary metastases [35]. However, D2A1 cells are able to form macroscopic metastases in the lung when injected in large numbers intravenously [36]. (Of note, the number of neutrophils in D2A1 tumors was 5-fold lower than that found in 4T1 tumors - 1,634$\pm$318/gram of tumor and 8,127$\pm$1762/gram of tumor, respectively.) While no significant change in D2A1 primary tumor weight was noted in response to contralateral implantation of 4T1 cells (Fig. 1F), a 22-fold increase in the number of D2A1-derived lung metastases was observed relative to D2A1 tumors implanted contralaterally to control Matrigel implants (Fig. 1G). These results indicated that 4T1 cells could create a systemic environment that enabled metastasis of otherwise-non-metastatic or weakly metastatic carcinoma cells. (Of note, the contralateral implantation of D2A1 cells did not affect the number of 4T1 metastatic lesions). Importantly, splenectomy substantially reduced the ability of 4T1 tumors to induce the metastasis of contralaterally implanted D2A1 tumors, as evidenced by a 67% decrease in D2A1 pulmonary metastases (Fig. 1H). Hence, optimal expression of the systemic effects

wrought by 4T1 cells depended on an intact spleen, which ostensibly served as a reservoir for myeloid cells mediating these effects.

Next we ectopically expressed G-CSF in D2A1 cells which do not on their own ordinarily express this cytokine. G-CSF overexpression in D2A1 cells (secreted levels were comparable and even slightly higher than 4T1 cells; Supplementary Fig 1D), was able to phenocopy the systemic neutrophilia provoked by 4T1 tumors (Fig. 1I) and yielded a 54-fold increase of D2A1 metastases formed in the lungs (Fig. 1J). Collectively, these experiments demonstrated that the G-CSF-driven expansion of neutrophils is both necessary and sufficient for this response.

While the mechanism of the systemic potentiation of metastasis was still undefined, its effects on D2A1 cells were transient and reversible. Thus, when we isolated D2A1 tumor cells that had successfully metastasized to the lungs of contralaterally implanted 4T1 mice and re-injected these cells into naive mice, the previously metastasized D2A1 cells were no more able, on a per cell basis, to metastasize than parental cells that had not experienced the systemic environment present in a 4T1-bearing host (data not shown).

These results pointed to an important role for neutrophils in driving metastasis. To further explore the contributions of neutrophils to this process, we asked whether normal, physiologic levels of neutrophils, rather than the dramatic neutrophilia observed in 4T1-bearing hosts, might also function to promote tumor metastasis. To address this question,

we depleted neutrophils in non-tumor bearing mice by injecting the 1A8 monoclonal antibody, which depletes specifically $Ly6G^+$ neutrophils but not granulocyte receptor-1 $(Gr\text{-}1)^+$ monocytes [37]. This depletion of neutrophils prior to intravenous injection (a route that allows them to form metastatic lesions as cited earlier) of D2A1 cells led to a 56% decrease in metastases in the lungs of these animals (Fig. 1K). Thus, even normal levels of circulating neutrophils could indeed promote metastasis, and enhancing these levels could serve as a useful experimental tool to better understand the role of immune cells in tumor metastasis. Furthermore, the results of this experiment suggested that neutrophils might primarily impact post-intravasation processes, an issue that we address in more detail below.

Neutrophils facilitate intermediate steps of the invasion-metastasis cascade

Responding to the above-described results, we attempted to delineate the specific step(s) of the invasion-metastasis cascade that were affected by the neutrophils. To address whether mobilized neutrophils might infiltrate the primary tumor and affect cells within these growths, D2A1 cells were co-mixed with splenocytes from 4T1-bearing mice and co-injected subcutaneously into BALB/c mice. No metastatic D2A1 nodules were observed in these mice, indicating that direct heterotypic interactions between the splenocytes and the tumor cells within the primary tumor were unlikely to increase metastasis (data not shown).

We next tested whether the systemic environment in 4T1 mice affected the ability of D2A1 tumor cells to intravasate. When D2A1 cells were implanted contralaterally to

4T1 tumors, only a marginal (2-fold) increase was observed in the number of circulating D2A1 tumor cells 4-5 weeks post implantation of the primary tumors (relative to control mice in which D2A1 cells had been implanted contralaterally to Matrigel plugs; Supplementary Fig. 2A). These results suggested that the >20-fold increase in D2A1 metastasis triggered by 4T1 primary tumors (Fig. 1H) was not likely to result from differences in the ability of D2A1 primary tumor cells to intravasate at increased rates in the presence of distant 4T1 tumors.

Collectively, the above experiments suggested that the metastasis-promoting role of neutrophils act on the post-intravasation steps of the invasion-metastasis cascade. To directly test this notion, we asked whether the systemic environment of a 4T1-bearing host would promote the metastasis of intravenously injected D2A1 cells that have bypassed the early steps of invasion and intravasation because of their route of introduction into mice. We injected a relatively small number of D2A1 cells ($2x10^4$), as this size of inoculum more closely mimics conditions of spontaneous metastasis. Under these conditions we found that mice bearing already-established subcutaneous 4T1 tumors experienced a 12-fold increase in the number of D2A1 lung foci relative to naïve mice.

We extended these analyses to both MDA-MB-231 human breast cancer cells and B16-F10 mouse melanoma cells (both injected into immune-deficient NOD/SCID mice) and observed similarly strong metastasis promotion in 4T1-bearing mice (Fig. 2A) upon i.v. injection of 2×10^4 cells. These results provided direct evidence that the previously

observed systemic effects of primary 4T1 tumors could be ascribed largely, if not entirely, to facilitation of the later (i.e., post-intravasation) steps of the invasion-metastasis cascade.

We reasoned that the observed metastasis-promoting effects of established 4T1 primary tumors on intravenously injected tumor cells could result from two alternative mechanisms: i) tumor cells disseminated by the 4T1 primary tumors reached the lungs earlier than the D2A1 cells and persisted in this tissue, thereby creating a favorable microenvironment for subsequent metastasis formation by D2A1 cells; or ii) the G-CSF released by 4T1 cells induced mobilization of neutrophils that facilitate the metastasis of D2A1 cells.

To address the first possibility, we injected $2x10^4$ 4T1 cells intravenously, one day before injection of D2A1 cells. However, no increase in the number of D2A1 metastases formed was detected under these conditions (Supplementary Fig. 2B), eliminating direct interactions in the lungs as a cause for the increased metastasis of D2A1 cells in 4T1-bearing mice

Wishing to critically test the second hypothesized mechanism, we determined whether the splenocytes induced by 4T1 primary tumors sufficed, on their own, to increase the metastasis of D2A1 cells. We therefore performed adoptive transfer of splenocytes isolated from 4T1-bearing mice into naïve, non-tumor-bearing mice. One hour after introduction of these splenocytes, D2A1 cells were injected intravenously into

these mice. As depicted in Figure 2B, adoptive transfer of splenocytes prior to intravenous injection of D2A1 cells led to a 6.6-fold increase in eventual metastasis formation by D2A1 cells.

Taken together, these results indicated that the observed increase in metastasis elicited by 4T1 tumors was mediated primarily, and possibly entirely, by 4T1-mobilized neutrophils that could, on their own, drive enhanced metastasis formation. Conversely, a significant contribution of disseminated 4T1 carcinoma cells that had arrived previously in the lungs and created a "niche" for subsequently arriving D2A1 cells was ruled out.

Localization of the effects of 4T1 tumors to the later steps of the invasion-metastasis cascade allowed us to further resolve the effects of G-CSF. Treating mice with 5 daily injections of G-CSF prior to the intravenous injection of D2A1 cells resulted in a 48-fold increase in the number of D2A1 lung metastases (Fig. 2C). Hence, subcutaneously introduced G-CSF could essentially phenocopy the effects of 4T1 primary tumors.

Wishing to ensure that G-CSF acts via the mobilization of neutrophils rather than by alternative mechanisms, we repeated the above experiment using the adoptive transfer of splenocytes from tumor-free mice that had been treated with G-CSF (5 daily injections). The number of D2A1 pulmonary metastases was 9-fold higher in recipients of splenocytes from these G-CSF-treated mice relative to injection of the same number of splenocytes from control PBS-treated mice (Fig. 2D). Hence, these effects in enhancing

metastasis formation operated after the entrance of the immune cells into the general circulation and once again appeared to be confined to the later stages of the invasion-metastasis cascade. Moreover, this effect could be achieved by cells that accumulated in large numbers in the spleens following systemic G-CSF treatment.

We addressed post-extravasation effects of 4T1-induced splenocytes by examining the effects of circulating immune cells on colonization, i.e., the outgrowth of micrometastases in the lung parenchyma into macroscopic deposits. Thus, we injected D2A1 cells intravenously into naïve mice and allowed them 48 hours to extravasate (D2A1 cells extravasate in less than 48 hours [38]), thereby enabling us to focus solely on post-extravasation events. When we thereafter injected splenocytes from 4T1-bearing mice into these mice, we observed no increase in the number of lung macro-metastases formed by the previously extravasated D2A1 cells relative to control mice that had not been treated with adoptive transfer of splenocytes (Supplementary Fig. 2C). These observations, when taken together, indicated that the G-CSF-induced neutrophils acted to foster metastasis after intravasation but before post-extravasation colonization.

Neutrophils increase accumulation of cancer cells in the lungs

We attempted to delineate with even more precision the specific post-intravasation steps of metastasis that were facilitated by neutrophils. When comparing survival of D2A1 tumor cells in control and 4T1-bearing hosts, we found that 24 hours after i.v. injection of D2A1 cells, the number of these cells that were present in the lungs of 4T1 tumor-bearing mice was greatly increased (50 fold) compared to the D2A1 cells

detected in naïve hosts (Fig. 2E). We further tested whether primary tumors derived from either D2A1 or B16-F10 cells, engineered in both cases to express ectopic G-CSF, would be able to promote retention of D2A1 cells in the lungs after i.v. injection. As mentioned above (Supplementary Fig. 1D) for D2A1 cells, this forced expression of G-CSF in B16-F10 cells resulted in secreted levels of this cytokine that were comparable to those secreted by 4T1 cells (Supplementary Fig. 2D). The number of D2A1 cells retained in the lungs was increased 20-fold in mice bearing D2A1-G-CSF primary tumors and 11-fold in mice bearing B16-F10-G-CSF primary tumors relative to corresponding control tumors that did not secrete this cytokine (Fig. 2F). Hence, in both cases, the forced expression of G-CSF resulted in greatly increased retention of disseminated cells within the lungs.

We proceeded to assess a specific role for neutrophils in mediating tumor cell retention in the lung. In fact, the spleens of 4T1-mice are populated by heterogenous populations of cells. In order to test for the specific involvement of neutrophils, we conducted adoptive transfer experiments in which $Ly6G^{+}$-enriched neutrophils were injected into naïve, non-tumor-bearing mice. One hour after introduction of the neutrophils, D2A1 cells were injected intravenously into these mice. This led to a 3.5–fold increase in the number of D2A1 cells retained in the lung (Fig. 2G).

We further verified that tumor cell retention in the lungs was mediated specifically by neutrophils by treating 4T1 tumor-bearing mice with the neutrophil-depleting 1A8 antibody. This resulted in a 54% reduction in the number of D2A1 cells found in the lungs of 4T1 mice 24 hours after i.v. injection, relative to untreated or IgG-

treated controls (Fig. 2H). Furthermore, physiological levels of neutrophils present in naïve, non-tumor-bearing mice were also important in facilitating retention of intravenously-injected tumor cells, as evidenced by the fact that depletion of these neutrophils (using anti-Ly6G antibodies) resulted 24 hours later in a 58% reduction (relative to untreated or IgG- treated controls) in the number of i.v. injected D2A1 cells found in the lungs of mice (Fig. 2I). Hence, even the normally present circulating neutrophils are intrinsically capable of facilitating metastasis by increasing the accumulation of tumor cells in the lungs within the short time period after introduction of the tumor cells into the venous circulation.

Neutrophils inhibit NK-mediated clearance of tumor cells

The observed increased accumulation of carcinoma cells in the lungs was compatible, in principle, with three alternative neutrophil-mediated mechanisms: more efficient physical trapping of intravasated carcinoma cells in the lung microvessels, enhanced intraluminal survival of intravasated cells, or elevated extravasation of these cells. Thus, we further explored the trapping of D2A1 cells in the lung capillary beds using *in vivo* bioluminescent measurements conducted 10 min after i.v. injection; in this instance, we found no significant differences in the numbers of D2A1 cells found in the lungs of naïve mice or 4T1-bearing mice. This indicated that initial physical trapping of cells in pulmonary microvessels was not affected by the presence of splenocytes (Fig. 3B).

A significant difference in the number of D2A1 cells in the lungs was apparent, however, soon after this initial trapping. Thus, 70% of D2A1 cells injected into naïve

mice had been cleared from the lungs within 4 hours (Fig. 3A, 3B). In contrast, in mice bearing 4T1 primary tumors, only 20% of the D2A1 cells were cleared from the lungs of 4T1 mice by this time. These results suggested that the systemic changes in mice bearing 4T1 primary tumors acted to reduce the otherwise-rapid attrition of D2A1 cells initially trapped in the lungs (Fig. 3B).

We hypothesized that the neutrophils might protect cancer cells from rapid intraluminal clearance from pulmonary microvessels by inhibiting the natural killer (NK) cells that normally perform this function [39, 40]. By depleting NK cells in BALB/c mice using the anti-asialo-GM-1 antibody [41], we determined that NK cell do, in fact, clear D2A1 cells from the circulation. Thus, ablation of NK cells prior to injection of D2A1 cells resulted in a 5.5-fold increase in the number of D2A1 cells found in the lung 4 hours after i.v. injection of these tumor cells (Fig. 3C).

Similarly, depletion of NK cells in a C57BL/6 background using the strain-specific antibody NK1.1 resulted in a 7-fold increase in the number of B16-F10 melanoma cells found in the lung 4 hours after intravenous injection of the tumor cells (Supplementary Fig. 3A). These observations indicated that NK cells play a major role in preventing tumor cell accumulation in the lungs, ostensibly by reducing the intraluminal survival time of the tumor cells. Importantly, when NK cells were depleted 24 hours after injection of D2A1 cells -- a time when tumor cells have either extravasated or been cleared from the vasculature -- no increase in lung metastases was observed (Fig. 3D),

indicating that NK cells acted while the cancer cells were still within the lumina of microvessels, not thereafter.

We wished to further validate that the increased survival of intraluminal D2A1 cells promoted by neutrophils in 4T1-bearing hosts was due to protection of these cells from NK-mediated clearance and not by some other neutrophil-induced, NK-independent mechanism. To distinguish between these possibilities, we depleted NK cells from 4T1 mice (by treating with anti-asialo-GM1) prior to intravenous injection of D2A1 cells. As depicted in Figure 3E, this antibody treatment did not result in further reduction of D2A1 cell clearance relative to the reduction observed in 4T1 mice that had not been depleted of NK cells. Accordingly, the ability of NK cells to kill the intraluminal tumor cells was already significantly impaired in 4T1 mice in a manner that could not be further reduced by the NK-depleting antibody.

Yet other observations provided further support for the notion that neutrophils protect cancer cells in intraluminal sites from NK-mediated clearance. In particular, we made use of YAC-1 cells, which are established targets of NK-mediated clearance [42], and indeed found YAC-1 clearance was NK cell-dependent, since depletion of NK cells using anti-asialo-GM-1 antibodies resulted in a 4.5-fold increase in the number of YAC-1 cells found in the lung 4 hours after intravenous injection (Fig. 3F). Moreover, the clearance of YAC-1 cells was inhibited when injected into 4T1-bearing mice relative to control mice (Fig. 3F). Importantly, consistent with our results with D2A1 cells (Fig. 2G), the protection of YAC-1 cells from NK-mediated clearance in 4T1-bearing mice

was dependent upon neutrophils, as neutrophil depletion abrogated any protective effects in these mice (Fig. 3G). These observations, when taken together, allowed us to conclude that neutrophils mobilized in 4T1-bearing mice protect tumor cells from NK-mediated clearance, thereby prolonging their survival in the circulation and increasing the number of cells that could, in principle, subsequently form metastases.

We also undertook to further characterize the mechanism by which neutrophils inhibited the NK-mediated clearance of circulating D2A1 cells. The observed differences in NK activity between 4T1 mice and control non-tumor-bearing hosts did not result from a reduction in the numbers of circulating NK cells, as we detected similar numbers of NK cells in the lungs of both groups of mice. This strongly suggested that the reduced NK-mediated clearance resulted from a decrease in the functionality of individual NK cells.

To address this possibility, we employed a commonly used measure to gauge NK cell function by examining NK cell responsiveness ex vivo. This was assayed by functional activation of NK cells obtained from the lungs and spleens of 4T1 tumor-bearing mice and from control naïve mice using plate-bound antibodies specific for the NKG2D or NKp46 NK-activating receptors, or control IgG, followed by flow cytometry to assess intracellular IFN-γ production and degranulation (indicated by CD107a expression) [43, 44]. As depicted in Figure 3H, 5% of the NK cells of control naïve mice were $CD107^{+}/IFN\text{-}\gamma^{+}$ in response to NKG2D stimulation and 10-12% of the NK cells were $CD107^{+}/IFN\text{-}\gamma^{+}$ in response to NKp46 stimulation. In contrast, in NK cells obtained from spleens or lungs of 4T1 mice a 3-6 fold reduction in the percent of cells that were

responsive to receptor stimulation was observed; <1.5% of NK cells were $CD107^+/IFN\text{-}\gamma^+$ in response to NKG2D stimulation (similar to baseline levels obtained from stimulation with IgG control) and <4% of the NK cells were $CD107^+/IFN\text{-}\gamma^+$ in response to NKp46 stimulation (Fig. 3H). Together with earlier data, these results argued that the unique systemic response provoked by 4T1 tumors, namely the expansion and mobilization of neutrophils, led in turn to inhibition of the ability of NK cells to undergo functional activation and thereby attenuated the NK cell-mediated clearance of intraluminal tumor cells.

Neutrophils promote extravasation of intraluminal tumor cells

Extravasation is a crucial step in metastasis formation [45]. Having confined the effects of neutrophils on metastasis to stages after intravasation and prior to colonization of the lung parenchyma, we considered whether neutrophils might facilitate extravasation of tumor cells from the lumina of pulmonary microvessels. We had previously observed that neutrophils increase the number of D2A1 cells surviving in the lungs 24 hours after their intravenous injection (Fig. 2G), but the proportion of extravasated carcinoma cells relative to those retained within the lumina of microvessels remained unknown. To examine this in more detail, we injected human breast cancer cells (MDA-MB-231) intravenously into NOD/SCID mice. Two hours later, we intravenously injected a human-specific HLA-A2 antibody that binds to class I MHC displayed by MDA-MB-231 cells. This protocol enabled us to label only cells of human origin, and only those present in the vascular lumen, but not breast cancer cells that had already extravasated.

Two hours after their injection, 70% of the MDA-MB-231 cells that were still present in the lungs of 4T1 mice were unstained by the antibody, suggesting that they had already extravasated from intraluminal sites and had therefore invaded the lung parenchyma. In contrast, only 30% of cancer cells retained in the lungs of the naïve mice had escaped from the lumina and arrived in the parenchyma (Fig. 4A). This indicated that within two hours of i.v. injection, a significantly higher proportion of the MDA-MB-231 tumor cells had extravasated from the luminal to the parenchymal side of endothelial walls in the 4T1 mice relative to their behavior in naïve mice. Hence, neutrophils mobilized by 4T1 cells accelerated the kinetics of extravasation of carcinoma cells that had previously lodged within pulmonary microvessels.

Neutrophils facilitate extravasation of tumor cells in an MMP-dependent manner

We undertook to study in more detail the mechanism(s) by which extravasation of intraluminal carcinoma cells was enhanced by the presence of splenocytes. Thus, we asked whether conditioned medium from splenocytes would enhance transendothelial migration in an *in vitro* model, in which transwell-permeable filter inserts were coated with either bEnd.3 murine endothelial cells or human umbilical vein endothelial cells (HUVECs). Conditioned medium from splenocytes of tumor-free mice slightly increased the transendothelial migration of D2A1 cells relative to unconditioned medium, whereas medium conditioned by splenocytes from 4T1-tumor-bearing mice led to a 3-fold increase in the ability of D2A1 cells to traverse the endothelial sheet of HUVECs (Fig. 4B, 4C). Similar results were obtained when the transwell membranes were coated with bEnd.3 murine endothelial cells and when the migration of B16-F10 tumor cells was

tested (Fig. 4D). These observations demonstrated that splenocytes from 4T1-bearing mice secrete soluble factors that enhance transendothelial migration of cancer cells.

The work described above had allowed us to associate most of the systemic effects of 4T1 cells to the mobilization specifically of neutrophils. Moreover, the percentage of $CD11b^+/Ly6G^+$ neutrophils within the splenocyte population was substantially elevated (21 fold) in 4T1 mice relative to naïve mice (Supplementary Fig. 4A). Accordingly we wished to confirm that neutrophils were responsible for facilitating transendothelial migration of cancer cells. To do so, we enriched for $Ly6G^+$ neutrophils from the spleens of 4T1 mice and collected conditioned medium from these cells as well as from unfractionated splenocytes containing an equal number of neutrophils. In fact, the medium conditioned by the $Ly6G^+$-enriched splenocytes from control mice increased transendothelial migration of D2A1 cells to a similar extent as the medium conditioned by unfractionated splenocytes prepared from 4T1 mice (Fig. 4E). Hence, $Ly6G^+$ neutrophils present in the spleens of 4T1 mice were indeed responsible for the lion's share of the observed enhanced transendothelial migration.

We undertook to determine whether neutrophils from 4T1-bearing mice were qualitatively different from normal neutrophils in their ability to promote transendothelial migration. To do so, we enriched splenocytes from non-tumor-bearing naïve mice for $Ly6G^+$ neutrophils. Conditioned medium from these cells increased transendothelial migration of D2A1 cells to the same extent as did medium conditioned by comparable numbers of $Ly6G^+$ cells prepared from 4T1-mice (Fig. 4F). Therefore, individual

neutrophils from tumor-bearing and non-tumor-bearing mice were equally competent to facilitate extravasation, and the cell-biological effects of splenocytes from tumor-bearing mice, including the enhanced transendothelial migration described above (Fig. 4D), reflected an expansion in the numbers of neutrophils and therefore a corresponding amplification of their normal intrinsic biological properties.

We proceeded to examine whether soluble factors were secreted by the neutrophils that enhanced the transendothelial migration of the tumor cells. Using antibody arrays, we found higher levels of secretion of two proteases, MMP-8 and MMP-9, in splenocytes from 4T1 mice relative to the medium conditioned from the same number of splenocytes extracted from naïve mice. These findings were further verified by ELISA (Fig. 4G). Inhibition of MMP-8 with either a specific small molecule inhibitor or a neutralizing antibody reduced the rate of transendothelial migration to basal levels observed in unconditioned medium (Fig. 4H). An anti-MMP-9 antibody also reduced by more than 50% the ability of splenocyte-conditioned medium to enhance transendothelial migration (Fig. 4H). Overall, these results indicated that splenocyte-secreted MMP-8 and MMP-9 played an important role in mediating the *in vitro* trans-endothelial cell migration of tumor cells. Importantly, the high levels of MMP-8 and MMP-9 were secreted into the medium by $Ly6G^+$ neutrophils (data not shown), further emphasizing the key role of neutrophils in promoting metastasis by aiding tumor cell extravasation.

As reported by others [11, 12, 33] , we noted the abundant expression of MMP-9 in the lungs of 4T1 tumor-bearing mice but not in those of control mice. Furthermore, the

MMP-9 is expressed by $Ly6G^+$ neutrophils (Fig. 4I). We employed MMP-9 knockout (KO) mice [46] to further dissect the contribution of this particular protease to metastasis using isogenic B16-F10-G-CSF rather than 4T1 cells to mobilize neutrophils in the C57BL/6 genetic background. Equal numbers of the splenocytes from these tumor-bearing wild type (WT) and MMP-9 KO host mice were then injected into recipient mice followed by i.v. injection of B16-F10-GFP^+ cells (1 hour later). As expected, the adoptive transfer of WT splenocytes into WT recipient mice resulted in a 5-fold increase in metastasis relative to control mice that did not receive splenocytes. In contrast, no significant increase was observed following adoptive transfer of MMP-9 KO splenocytes into MMP-9 KO recipient mice. Importantly, when MMP-9 wild-type splenocytes were transferred into MMP-9 KO recipient mice - a 5-fold increase in B16-F10 lung metastases was noted, similar to the effect achieved by adoptive transfer of WT splenocytes into WT recipient mice (Fig. 4J). This indicated that the splenocyte-derived protease MMP-9 played a major role in facilitating transendothelial migration both *in vitro* and, more importantly, *in vivo*, the latter process contributing to enhanced formation of metastases. These data collectively argue that, in addition to their role in inhibiting NK cell-mediated clearance of tumor cells, neutrophils promote metastasis by enhancing the extravasation of these cells.

Neutrophil-secreted IL-1b activates endothelial cells and facilitates migration

The enhanced extravasation clearly involves an interplay between three cell types – the extravasating tumor cells, the neutrophils, and the endothelial cells. To further dissect components of this crosstalk, we first looked for a direct effect of the neutrophils

on either the tumor cells or the endothelial cells individually. To test this, we conducted experiments in which only the tumor cells or the endothelial cells were pre-treated with the 4T1 splenocyte-conditioned medium for 3 hours. The pre-treated cells were washed to remove any residue of the conditioned medium prior to the addition of D2A1 cells to the top chamber of transwells in which the membranes had been coated with endothelial cells. This protocol contrast with that employed in the experiments depicted in Figure 4B, in which the migration occurred in the presence of conditioned medium. As indicated in Fig. 5A, pretreatment of the D2A1 cells alone did not increase their ability to migrate through the endothelial cell layer. In stark contrast, pre-treatment of murine endothelial bEnd.3 cells with the 4T1-splenocyte-conditioned medium indeed sufficed to increase transendothelial migration of D2A1 cells (Fig. 5B). Furthermore, incubation of bEnd.3 cells with 4T1-splenocyte-conditioned medium induced expression and secretion of MMP-9 by the endothelial cells, augmenting that initially produced by the neutrophils (Fig. 5C, and Supplementary Fig. 5A, 5B). These results suggest that the enhanced extravasation does not result from a direct effect of the neutrophils on the migrating tumor cells but instead through the modulation of the endothelial cell barrier.

Immune cells impact their surroundings through the secretion of cytokines and chemokines. More specifically, IL-1b is a cytokine that is known to be secreted by neutrophils, to activate endothelial cells, and to increase leukocyte extravasation [16]. We therefore tested whether IL-1b plays a role in the activation of the endothelial cells in our system, and indeed, a 2-fold increase in transendothelial migration of D2A1 cells was observed when IL-1b was added to RPMI medium (Supplementary Fig 5C).

Furthermore, higher (4-fold) levels of IL-1b were secreted into the conditioned medium by splenocytes from 4T1 mice compared to splenocytes from control Balb/c mice (Fig. 5D). Importantly, the levels of IL-1b secreted by $Ly6G^+$ neutrophils (enriched from spleens of 4T1 mice) were similar to those secreted by the 4T1 splenocyte population, pointing to the important role neutrophils play in IL-1b-mediated responses. Moreover, transendothelial migration *in vitro* was reduced when an IL-1 receptor antagonist was added to conditioned medium from splenocytes obtained from 4T1 mice (Fig. 5E). Furthermore, upon addition of an IL-1 receptor antagonist to the conditioned medium, MMP-9 secretion by endothelial cells following treatment with 4T1 splenocyte-conditioned medium was inhibited (Fig. 5F). Taken together, these observations indicated that neutrophil-secreted IL-1b acts directly to activate the endothelial cells, ostensibly amplifying the effects of the already-high levels of MMP-9 found in the 4T1-splenocyte-conditioned medium.

Activated endothelial cells enable expedited protrusion formation by intraluminal tumor cells

To further decipher the mechanism underlying the transendothelial migration of the tumor cells, and more specifically how activated endothelial cells enable enhanced migration, we employed an in vitro assay featuring perfusible microvasculature formed in micro-devices [47]. In this model, HUVECs are suspended in a fibrin/collagen type I matrix and interconnected vascular networks are formed via a vasculogenic-like process over a period of 4 to 5 days in micro-devices. In this assay, tumor cells can be infused and are found to arrest via physical trapping, mimicking the *in vivo* process.

Extravasation rate is quantified via confocal microscopy at 20X and scored as cells that have completely cleared the endothelial barrier (Fig 6A).

HUVEC networks were treated with 4T1-splenocyte-conditioned medium (or control RPMI) for 4 hours prior to addition of human MDA-MB-231 to the devices. We found that 16.2% of MDA-MB-231 human breast cancer cells extravasated from the microvessels formed by control HUVECs within 3 hours. This extravasation efficiency (i.e. the fraction of cells that had migrated across the endothelial layer) was increased ~2.5 fold when HUVEC cells were pre-treated with 4T1-splenocyte-conditioned medium (Fig. 6A and 6B).

In order to study and understand the transendothelial migration of the tumor cells in further detail, we tracked the transendothelial migration of MDA-MB-231 cells using time-lapse confocal microscopy. We first noted that the initial sign of transendothelial crossing of tumor cells appeared as small protrusions extending from the cell bodies of these cells through the endothelial layer.

Analysis of image sequences of transmigrating MDA-MB-231 revealed that the time required for tumor cells to extend the first initial discernible protrusion past the lumen was significantly shorter when HUVECs were pre-treated with 4T1-splenocyte conditioned medium (compared to RPMI control). Thus, following pretreatment of HUVECs with 4T1-splenocyte-conditioned medium, ~ 5% of MDA-MB-231 had already extended protrusions after 15 minutes following tumor perfusion, whereas the same

degree of protrusion formation occurs in control treated devices only after 1 hour (Fig. 6B). When individual tumor cells were tracked, it was found that the average time for the first observed protrusion was ~ 30 minutes for 4T1- conditioned medium treated HUVECs, compared to ~ 90 minutes for the control RPMI (Fig. 6C). However, the length of time required for MDA-MB-231 cells to migrate across the endothelial cell layer – i.e., the amount of time required for a cell from the first observable protrusion until complete translocation across the endothelial barrier was not different between treated vs. un-treated HUVEC cells (~ 50 minutes) (Fig. 6D).

These results further strengthen the findings reported above demonstrating that the neutrophils facilitate the migration of tumor cells in an indirect manner – not through a direct effect on the tumor cells but rather through their activation of endothelial cells, which in turn expedite the initiation of transendothelial crossing by tumor cells.

DISCUSSION

As the biological complexity of tumor growth and metastasis is explored in greater detail, it has become apparent that key aspects of tumor biology can only be explained by a detailed understanding of how various types of host cells contribute to tumor progression. The work presented here describes how recruited host cells can affect the behavior of cancer cells that have traveled from primary tumors to a distant anatomical site, specifically the lungs. Such effects, by necessity, reflect changes in the systemic physiology of tumor-bearing hosts and govern later steps of the invasion-metastasis cascade. More specifically, we find that $Ly6G^+$ neutrophils can increase

metastatic seeding in at least two distinct ways: (i) by inhibiting NK cell cytotoxic activity, the neutrophils can protect intraluminally trapped tumor cells from rapid clearance by these innate immune cells, and (ii) by expediting extravasation. Both of these mechanisms contribute to the ultimate formation of metastases by increasing the pool of tumor cells that succeed in entering the lung parenchyma, placing them in sites where they are poised to generate micrometastases and, subsequently, macroscopic metastases (Fig. 6E).

Previous reports have suggested that tumors are able to modify the distant microenvironment prior to arrival of metastatic cells, doing so by creating a 'pre-metastatic niche' [48-50]. In this 'pre-metastatic niche' model, bone marrow-derived cells were reported to arrive in the lung parenchyma days before tumor cells and create a more hospitable environment that facilitates colonization and subsequent formation of macroscopic metastases. We demonstrate here a quite different mechanism, in which the accessory effects of neutrophils operate only in a relatively short window of time during which neutrophils suppress the otherwise-rapid NK-mediated clearance of intraluminally trapped carcinoma cells and facilitate the extravasation of these cells through effects on endothelial cells.

Our observations demonstrate a clear pro-metastatic role for the $Ly6G^+$ neutrophils and are supported by other reports showing that $Gr1^+$-$CD11b^+$ cells alter the overall landscape of the metastatic lung and tip the balance of immune protection in favor of tumor promotion [12, 33]. Others have shown an anti-metastatic effect for neutrophils

in 4T1 tumor bearing mice [11]. These anti-metastatic properties were demonstrated in neutrophils that accumulate in the lung prior to metastasis formation (i.e., up to day 10 after initial 4T1 tumor implantation), whereas our own work examines these dynamics in a later phase when implanted tumor cells have already formed significant primary tumors and have proceeded to seed and colonize distant tissues (14-31 days after 4T1 tumor implantation). The role of neutrophils in metastasis may be context dependent, and it is plausible that the early tumor-entrained neutrophils and their later counterparts exert opposite functions on metastatic progression in the lungs. Further studies may shed light on the role of neutrophils in the formation of various types of metastases.

While our present results demonstrate that $Ly6G^+$ neutrophils directly promote pulmonary metastasis of cancer cells through at least two distinct mechanisms, it remains possible that other types of innate immune cells promote metastasis in other cancers and anatomical sites by acting through alternative mechanisms. For example, recent studies have reported a role for the cytokine CCL2 in promoting metastasis in models of breast and colon carcinoma through recruitment of monocytes to the lung [51, 52] as well as by activating endothelial cells, doing so by signaling through their CCR2 receptors [53]. Platelets have also been shown to play a role in facilitating metastasis through the secretion of CXCL5 and CXCL7 which recruit granulocytes to sites of intraluminally trapped tumor cells [54]. Altogether, these results point to the complexity of the intraluminal survival and extravasation steps, in which different types of immune cells, cytokines and proteases appear to participate.

Tumor cells have been shown to recruit immune-suppressive cells that erect a protective barrier against immune attack [55-58]. These suppressive actions have been studied mostly in the context of the monocyte/macrophage subset of $CD11b^+/Gr1^+$ myeloid cells and their role in suppression of T-cell-mediated responses [59, 60]. The fact that we observed comparable effects in immune-competent mice as well as immune-deficient NOD/SCID mice indicates that the mechanism of action in our model system utilizes a different type of immune suppression. Furthermore, our data highlight an immunosuppressive role that is unique in two aspects: 1) the immune cells involved – neutrophils – act through their inhibition of NK-mediated clearance of cancer cells; and 2) the time frame of the immunosuppression – a transient effect occurring during the intravascular stages of the multistep invasion-metastasis cascade.

The present results show that the neutrophils activate and induce changes in endothelial cells leading to increased extravasation through the action of MMP-9. An additional mechanism for this direct activation of endothelial cells might well be mediated through vascular endothelial growth factor (VEGF). While several proteinases are capable of releasing VEGF from the extracellular matrix, MMP-9 is especially efficient in this regard [61, 62]. Along these lines, the increase in MMP-9 levels that we observed in splenocyte-conditioned medium from 4T1 mice was accompanied by a concomitant increase in the levels of VEGF (compared to splenocyte-conditioned medium from control naïve mice; data not shown). This crosstalk between neutrophils and endothelial cells and the specific roles of MMP-9 and VEGF in facilitating extravasation warrants further research.

4T1-induced tumors represent a widely used model system in mice used to study metastasis. The effects of the neutrophilia that we observed in tumor-bearing mice are consistent with clinical data showing that either elevated neutrophil counts or elevated neutrophil/lymphocyte ratios serve as indicators of poor prognoses in a variety of cancers, including lung, pancreatic, ovarian, gastric, and colon carcinomas [63-67]. Furthermore, elevated plasma G-CSF levels have been reported in a variety of solid tumors and found associated with severe leukocytosis and poor prognosis [68-72].

In oncologic practice, G-CSF is often used to overcome chemotherapy-associated neutropenia [73]. Importantly, the present findings and those of others [12, 14] suggest that such G-CSF may, in certain circumstances, actually serve to facilitate tumor metastasis. In particular, our data indicate that G-CSF administration has pro-metastatic effects not only in the case of prolonged exposure to high levels of G-CSF secreted by the primary tumor but even following short-term (5 days) systemic administration of this cytokine. Other reports have shown in experimental mouse models that overexpression of G-CSF by tumors has a deleterious impact on therapeutic outcome, since it mediates tumor refractoriness to anti-VEGF therapy [14]. While it may be necessary to administer G-CSF to overcome the acute neutropenia of certain patients, identifying and eliminating specific tumor-promoting activities induced by G-CSF may eventually yield more beneficial clinical outcomes for cancer patients suffering neutropenia.

Experimental Procedures

Cell Culture

All cells were cultured in 5% CO_2 humidified incubator at 37° C. Mouse mammary carcinoma cell lines 4T1 (ATCC) and D2A1 (gift from F. R. Miller) were grown in RPMI supplemented with 10% heat inactivated fetal bovine serum (FBS), 100 U/ml penicillin, and 100 μg/ml streptomycin (Invitrogen). Murine endothelial, B.end3 cells were grown in Dulbecco's Modified Eagle (DME) medium, supplemented with 10% FBS, 100 U/ml penicillin, and 100 μg/ml streptomycin. Human umbilical vein endothelial cells (HUVECs) were propagated in endothelial cell basal medium (EBM) with 0.1% human epidermal growth factor (hEGF), 0.1% hydrocortisone, 2% FBS, 0.4% bovine brain extract (BBE), 30 μg/ml Gentamicin, and 15 ng/ml Amphotericin. MDA-MB-231 cells were grown in DME/F12 supplemented with 10% FBS, 100 U/ml penicillin, and 100 μg/ml streptomycin. B16-F10 cells were grown in DME medium supplemented with 10% heat inactivated FBS, 100 U/ml penicillin, and 100 μg/ml streptomycin (Invitrogen). YAC-1 cells were grown in RPMI supplemented with 10% FBS, 100 U/ml penicillin, and 100 μg/ml streptomycin (Invitrogen). In experiments testing in vitro extravasation in microvasculature networks, HUVECs stably expressing GFP (Angioprotemie) were cultured in EGM-2MV medium (Lonza) and used at passage 4 to 6. Normal human lung fibroblasts (Lonza) were cultured in complete FGM (Lonza) and used between passages 4 to 8. Cells that were stably infected with GFP or tdTomato were done so as previously described [1]. In order to overexpress G-CSF lentiviral vectors expressing the G-CSF protein coding DNA (MMM1013-99829324; Open

Biosystems) were generated using the pLV-IRES-neo as a backbone. D2A1 and B16-F10 cells were then infected with the lentiviral vectors.

Animals

All research involving animals complied with protocols approved by the MIT Committee on Animal Care. BALB/c mice, C57/BL6 mice and CB6F1 mice (a cross between BALB/c and C57BL/6) were obtained from Jackson Laboratory. A colony of NOD-SCID mice was maintained in-house. The MMP-9 KO mice (Stock # 007084) were originally obtained from the Jackson Laboratory.

Tumor models

For primary tumor formation, 2.5 x 10^5 4T1, D2A1 or B16-F10 tumor cells were injected subcutaneously (s.c.) in their growth medium with 20% Matrigel into 10 to 14-week old female syngeneic BALB/c or C57BL/6 (for B16-F10 cells) mice. For contralateral injections, 2.5 x 10^5 4T1 tumor cells were injected subcutaneously on the right, and at the same time, 2.5 x 10^5 D2A1-Tom$^+$ tumor cells were injected subcutaneously on the left side of the same mouse. For intravenous (i.v.) injections 2 x 10^4 cells were injected in 100 ml volume into mice. Splenectomy was performed as previously described [2]. Five hours after splenectomy tumor cells were injected subcutaneously. The contralateral experiments and the splenectomy experiments were terminated 4-5 weeks after tumor cell implantation, at which time leukocyte mobilization as well as pulmonary metastasis were scored.. In experiments assessing lung macrometastatic formation following i.v. injection D2A1, B16-F10 and MDA-MB-231

cells (2 x 10^4) were injected i.v. into BALB/c mice (for D2A1 cells) or NOD/SCID mice (for B16-F10 and MDA-MB-231 cells) implanted with 4T1 cells 2 weeks earlier (or control non-tumor bearing mice) experiments were terminated and metastasis was scored 14 days later. In experiments testing short term retention of tumor cells (NK clearance and extravasation; 2-24 hours after i.v. injection), the cells were injected into mice implanted with 4T1 cells 4 weeks earlier (or control non-tumor bearing mice). In compliance with veterinary guidelines, experiments in which C57BL/6 mice were implanted with B16-F10-GCSF cells (or B16-F10 cells overexpressing control vector) were terminated 3 weeks post tumor cell implantation.

Splenocyte and neutrophil adoptive transfer

In experiments involving adoptive transfer of splencoytes or $Ly6G^+$ neutrophils, spleens were removed from donor mice and homogenized into a single-cell suspension using a 3 ml syringe plunger and 40 μm cell strainer (BD Falcon). Thereafter, splenocytes were passed through a 40 micron filter basket prior to injection. In experiments involving adoptive transfer of neutrophils, splenocytes were enriched for $Ly6G^+$ neutrophils using the MACS cell separation kit (Miltenyi Biotec) according to manufacturer's instructions. Mice were injected i.v. with 2 injections of splenocytes (2.5-3 × 10^7) or $Ly6G^+$ neutrophils (5-6 x 10^6) suspended in 200 μL medium per injection, 45 minutes apart (control mice were injected with vehicle). D2A1-Tom^+ cells or B16-F10-GFP^+ cells (2 x 10^4 cells in 100 ml medium) were injected i.v. 45 minutes after the last splenocyte or neutrophil injection.

Quantification of Lung Metastases

For visualizing cancer cells that had disseminated in the lung tissue, lungs were harvested from the injected mice, dissected into the five lobes and analyzed under a fluorescence dissection microscope (Leica MZ12) for the presence of tdTomato$^+$- or GFP$^+$-labeled microscopic and/or macroscopic lung metastases. The quantification of cells retained in the lungs 10 minutes, 1 hour, 2 hours, 4 hours or 24 hours after i.v. injection was performed by directly counting the numbers of GFP$^+$ cells or tdTomato$^+$ cells in the lung under a fluorescence dissection microscope (Leica MZ12). For quantification of lung metastases in mice carrying unlabeled 4T1 tumors, lungs were fixed in 10% formalin, embedded in paraffin, sectioned and stained with hematoxylin and eosin. Yac-1 cells were labeled with Cell Trace CFSE (Life Technologies) prior to intravenous injections (2 x 10^4 cells) according to according to manufacturer's instructions.

In vivo imaging

Bioluminescence imaging of luciferase activity was used to monitor cancer cell clearance with a Xenogen IVIS system under 2.5% isoflurane anesthesia at the indicated time points as described. Imaging of mice was performed by injection of D-luciferin (165mg/kg of body weight, intraperitoneal (i.p.) injection; Caliper Life Sciences), 10 minutes before bioluminescence imaging. Images were analyzed using Living Image Software version 4.3.1 (Caliper Life Sciences).

NK and neutrophil depletion

To deplete NK cells, anti-asialo GM-1 (20 μl per mouse, clone Poly21460; Biolegend) or anti NK1.1 (cat # BE0036; Bioxcell) antibodies were injected i.p. one day prior to tumor cell injections. Matching isotype Rabbit polyclonal IgG (AB-105-C; R&D Biosystems) served as control. To deplete neutrophils, anti-Ly6G antibody (200 μg per mouse, clone 1A8; Bioxcell) was injected i.p. one day prior to tumor cell injections. Matching isotype Rat IgG2A (MAB006; R&D Biosystems) served as control.

***In vivo* extravasation**

In vivo extravasation assay was done as previously described [3]. FITC-conjugated anti-human HLA-2 antibody (20 μg/mouse, clone BB7.2; BD Biosciences) was injected i.v. into NOD/SCID mice two hours after i.v. injection of 1×10^5 MDA-MB-231-Tom$^+$ cells. Lungs were harvested 10 minutes after injection of antibody, digested with collagenase A (1.5 mg/ml), hyaluronidase (125 u/ml) and DNAse (0.1 mg/ml) for 1 hr at 37° C. Resulting cell suspensions were filtered through 70 μm pore-size nylon meshes. Cells were incubated in the presence of saturating amounts (10 μg/sample) of unlabeled anti-HLA-A2 Ab for 30 minutes. The percentage of MDA-MB-231-Tom$^+$ cells that were labelled with FITC-HLA-A2 antibodies was determined by flow cytometry.

***In vivo* G-CSF administration**

To assess the effects of G-CSF on metastasis, BALB/c mice were injected s.c. with rhG-CSF (250 mg/kg; Neupogen, Amgen) daily for five consecutive days. Control animals were given PBS as a vehicle. Five hours after the last G-CSF injection, 2×10^4

D2A1 cells were injected i.v.. In other experiments, the effect of adoptive transfer of splenocytes from G-CSF treated mice was tested. Five hours after the last G-CSF injection, spleens were harvested from G-CSF-treated mice (or control PBS-treated mice) and adoptive transfer into recipient BALB/c mice followed by i.v. injection of D2A1 cells was done as previously described in 'splenocyte adoptive transfer' section.

Preparation of splenocyte - conditioned media

Splenocyte-conditioned media were prepared from 1.5 x 10^7 freshly isolated unsorted splenocytes or from the $Ly6G^+$ enriched subpopulation. These freshly isolated cells were plated in the presence of 10 ml RPMI medium (supplemented with 10% heat-inactivated FBS, 100 U/ml penicillin and 100 μg/ml streptomycin) for 48 hours at 37°C, 5% CO_2 in a humidified incubator. Subsequently the conditioned medium was collected and the cells were removed by centrifugation. The supernatant was collected and sterile filtered through a 0.2 μm Acrodisc filter (PALL Biosciences).

ELISA and protein arrays

Plasmas and conditioned media were analyzed for mouse G-CSF (MCS00; R&D Systems), IL-1b (MLB00B; R&D Systems), MMP9 (MMP900B; R&D Systems) and MMP-8 (Uscn Life science Inc.) according to manufacturer's instructions. Conditioned media from splenocytes or tumor cell lines were analyzed for the secretion of various proteins using mouse angiogenesis array (ARY015; R&D Systems) and mouse cytokine array (ARY006; R&D Systems) according to manufacturer's instructions.

***In vitro* transendothelial migration assay**

The upper surface of 8μm polyester Transwells (PET; corning) was coated with 5 × 10^4 mouse endothelial cells for 24 hours at 37° C in complete bEnd.3 mEC media (100 μL in the upper chamber and 500 μL in the lower well). Once the endothelial cell layer had been established, tumor cells (5 × 10^4) were added to the upper chamber. The lower compartments of the wells were filled with RPMI medium (supplemented with 10% FBS) or splenocyte-conditioned media (prepared as described above). In the inhibition experiments, 5 ng/ml IL-1b receptor antagonist (Prospec), 1 μg of anti-MMP-9 antibody (ab38898; Abcam) or anti-MMP-8 antibody (ab53017; Abcam) was added to the upper chamber. MMP-8 inhibition on the transendothelial migration of D2A1 tumor cells was also tested using 10, 50 or 100 μM of MMP-8 inhibitor-1 (Calbiochem); wells supplemented with RPMI containing 0.1 % DMSO were included in the analysis as controls. For the pre-conditioning experiments, D2A1-Tom^+ cells or mouse endothelial cells were treated with conditioned medium from splenocytes obtained from naïve BALB/c or 4T1mice, or RPMI (control) for 4 hours. The pre-treated endothelial cells or D2A1-Tom^+ cells were washed in PBS to remove any residue of the conditioned medium prior to the addition of D2A1 cells to the top chamber of transwells. Migration was assessed after 4h at 37° C in 5% CO_2. The cells from the upper surface of the well were wiped off with PBS, and the number of migrated cells were counted in 4 fields. Experiments were repeated at least 5 times and performed in duplicates or triplicates.

Microvascular network extravasation assay

Perfusable in vitro microvascular networks were generated in microfluidic devices as described previously [4]. Briefly, HUVECs and normal human lung fibroblasts were resuspended in fibrin gels at $6x10^6$ cells/mL and $3x10^6$ cells/mL, respectively, and injected into micro channels. Devices were then cultured in EGM-2MV for 4 days at 37° C in 5% CO_2, after which lumens formed and became perfusable. Four hours prior to tumor cell injection, media in devices were changed to splenocyte conditioned media or control RPMI. Then, MDA-MB-231 Td Tomato were resuspended to $5x10^5$ cells/mL in either conditioned media or RPMI (Company) and perfused into corresponding devices via a hydrostatic pressure drop. Devices were transferred to an environmental chamber equipped confocal microscopy (Olympus FV1000). Time-lapse images were taken every 15 minutes for at least 4 hours at 20X magnification and z-steps of 1.7 um. Images were analyzed using Imaris Bitplane software. A cell is defined as extravasated when the entire cell body has cleared the lumen, based on the orthogonal views given in Imaris. As soon as a cell becomes partially translocated past the lumen, it is defined as "protrusive." The same individual cells were followed over a time period of 4 hours. Data was collected from >150 cells per condition, over 3 independent experiments.

White blood cell counts in peripheral blood

To obtain peripheral white blood cell counts, mice were bled retro-orbitally. For white blood cell counts, an aliquot was diluted 1:10 in 1X PBS and processed at the MIT Division of Comparative Medicine.

Flow cytometry

Cells were labeled for flow cytometry by incubation with the following fluorophore-conjugated antibodies: CD3 perCP-Cy5.5(17A2; Biolegend), Cd49b PE (DX5; Biolegend), NKp46 APC (29A1.4; Biolegend), CD11b FITC (M1/70; eBioscience), Ly6G PE (1A8; BD Pharmingen), G-CSF Receptor (S1390; Abcam), CD107a (1D4B; Biolegend). Flow cytometric analyses were carried out on a fluorescent -activated cell sorting (FACS) Fortessa (BD Biosciences) using BD FACSDiva Software.

Ly6G$^+$ neutrophil Enrichment

Spleens of tumor-bearing and control mice were homogenized with the GentleMACS (Miltenyi Biotech), according to the manufacturer's instructions in order to obtain a single -cell suspension. Splenocytes were counted, and 1-2 x 10^8 cells were enriched for Ly6G$^+$ cells using magnetic beads (130-092-332, Miltenyi Biotech) according to manufacturer's instructions. The purity of the Ly6G$^+$ population was assessed by FACS analysis.

Ex vivo degranulation assay

Wells of flat-bottomed, high-protein binding plates (Thermo Fisher Scientific) were coated with 0.5 μg of anti-NKG2D antibody (MI-6) or with 0.5 μg of anti-NKp46 antibody (29A1.4) or rat IgG2a as a control. 10^6 cells per well were stimulated for 5

hours in the presence of 1 μg of Golgi Plug (BD), 1 μg of Golgi Stop (BD), 100 U of recombinant human IL-2 (Roche), and anti-CD107a (1D4B) mAb antibody.

Immunofluorescence

Serial frozen sections (6 μm) were prepared and immunofluorescence staining was carried out for histological analysis. After blocking the sections with 4% normal goat serum in PBS at room temperature for 30 minutes, MMP9 antibody (ab38898, Abcam) was incubated at 4°C overnight followed by Alexa Fluor 594 goat anti-rabbit IgG or Alexa Fluor 647 anti-rabbit IgG antibody (A11037 and A21245, Life Technologies). For double immunofluorescence staining, anti-Ly-6G antibody (clone: 1A8, BioLegend) was incubated at room temperature for 1 hour followed by Alexa Fluor 488 goat anti-rat IgG (H+L) antibody (A11006, Life technologies). Nuclei were stained with DAPI using VECTASHIELD Mounting Medium (H-1200, Vector Laboratories, Inc.) and images were captured using BX63 (Olympus) equipped with ANDOR Neo sCMOS Monochrome Camera (Andor Technology Ltd.). The images were processed using ImageJ software.

Statistical Analysis

All of the data are presented as the mean ± standard errors of mean (SEM). An unpaired two-tailed Student's t test was used to calculate the p values. A p value of less than 0.05 was considered significant.

REFERENCES

1. Shibue, T. and R.A. Weinberg, *Integrin beta1-focal adhesion kinase signaling directs the proliferation of metastatic cancer cells disseminated in the lungs*. Proc Natl Acad Sci U S A, 2009. **106**(25): p. 10290-5.
2. Cortez-Retamozo, V., et al., *Origins of tumor-associated macrophages and neutrophils*. Proc Natl Acad Sci U S A, 2012. **109**(7): p. 2491-6.
3. Galkina, E., et al., *Preferential migration of effector CD8+ T cells into the interstitium of the normal lung*. J Clin Invest, 2005. **115**(12): p. 3473-83.
4. Chen, M.B., et al., *Mechanisms of tumor cell extravasation in an in vitro microvascular network platform*. Integr Biol (Camb), 2013. **5**(10): p. 1262-71.

References

1. Fidler, I.J., *The pathogenesis of cancer metastasis: the 'seed and soil' hypothesis revisited*. Nat Rev Cancer, 2003. **3**(6): p. 453-8.
2. Wyckoff, J.B., et al., *Direct visualization of macrophage-assisted tumor cell intravasation in mammary tumors*. Cancer Res, 2007. **67**(6): p. 2649-56.
3. Coussens, L.M. and Z. Werb, *Inflammation and cancer*. Nature, 2002. **420**(6917): p. 860-7.
4. de Visser, K.E., A. Eichten, and L.M. Coussens, *Paradoxical roles of the immune system during cancer development*. Nat Rev Cancer, 2006. **6**(1): p. 24-37.
5. Mantovani, A., et al., *Cancer-related inflammation*. Nature, 2008. **454**(7203): p. 436-44.
6. Trinchieri, G., *Cancer and inflammation: an old intuition with rapidly evolving new concepts*. Annu Rev Immunol, 2012. **30**: p. 677-706.
7. Welch, D.R., et al., *Tumor-elicited polymorphonuclear cells, in contrast to "normal" circulating polymorphonuclear cells, stimulate invasive and metastatic potentials of rat mammary adenocarcinoma cells*. Proc Natl Acad Sci U S A, 1989. **86**(15): p. 5859-63.
8. Fridlender, Z.G. and S.M. Albelda, *Tumor-associated neutrophils: friend or foe?* Carcinogenesis, 2012. **33**(5): p. 949-55.
9. Fridlender, Z.G., et al., *Polarization of tumor-associated neutrophil phenotype by TGF-beta: "N1" versus "N2" TAN*. Cancer Cell, 2009. **16**(3): p. 183-94.
10. Galdiero, M.R., et al., *Tumor associated macrophages and neutrophils in cancer*. Immunobiology, 2013. **218**(11): p. 1402-10.

11. Granot, Z., et al., *Tumor entrained neutrophils inhibit seeding in the premetastatic lung*. Cancer Cell, 2011. **20**(3): p. 300-14.

12. Kowanetz, M., et al., *Granulocyte-colony stimulating factor promotes lung metastasis through mobilization of Ly6G+Ly6C+ granulocytes*. Proc Natl Acad Sci U S A, 2010. **107**(50): p. 21248-55.

13. Shojaei, F., et al., *Tumor refractoriness to anti-VEGF treatment is mediated by CD11b+Gr1+ myeloid cells*. Nat Biotechnol, 2007. **25**(8): p. 911-20.

14. Shojaei, F., et al., *G-CSF-initiated myeloid cell mobilization and angiogenesis mediate tumor refractoriness to anti-VEGF therapy in mouse models*. Proc Natl Acad Sci U S A, 2009. **106**(16): p. 6742-7.

15. Sionov, R.V., Z.G. Fridlender, and Z. Granot, *The Multifaceted Roles Neutrophils Play in the Tumor Microenvironment*. Cancer Microenviron, 2014.

16. Scapini, P., et al., *The neutrophil as a cellular source of chemokines*. Immunol Rev, 2000. **177**: p. 195-203.

17. Nozawa, H., C. Chiu, and D. Hanahan, *Infiltrating neutrophils mediate the initial angiogenic switch in a mouse model of multistage carcinogenesis*. Proc Natl Acad Sci U S A, 2006. **103**(33): p. 12493-8.

18. Brinckerhoff, C.E. and L.M. Matrisian, *Matrix metalloproteinases: a tail of a frog that became a prince*. Nat Rev Mol Cell Biol, 2002. **3**(3): p. 207-14.

19. Egeblad, M. and Z. Werb, *New functions for the matrix metalloproteinases in cancer progression*. Nat Rev Cancer, 2002. **2**(3): p. 161-74.

20. Ardi, V.C., et al., *Human neutrophils uniquely release TIMP-free MMP-9 to provide a potent catalytic stimulator of angiogenesis*. Proc Natl Acad Sci U S A, 2007. **104**(51): p. 20262-7.

21. Kessenbrock, K., V. Plaks, and Z. Werb, *Matrix metalloproteinases: regulators of the tumor microenvironment*. Cell, 2010. **141**(1): p. 52-67.

22. Mason, S.D. and J.A. Joyce, *Proteolytic networks in cancer*. Trends Cell Biol, 2011. **21**(4): p. 228-37.

23. Acuff, H.B., et al., *Matrix metalloproteinase-9 from bone marrow-derived cells contributes to survival but not growth of tumor cells in the lung microenvironment*. Cancer Res, 2006. **66**(1): p. 259-66.

24. Hiratsuka, S., et al., *MMP9 induction by vascular endothelial growth factor receptor-1 is involved in lung-specific metastasis*. Cancer Cell, 2002. **2**(4): p. 289-300.

25. Casbon, A.J., et al., *Invasive breast cancer reprograms early myeloid differentiation in the bone marrow to generate immunosuppressive neutrophils*. Proc Natl Acad Sci U S A, 2015. **112**(6): p. E566-75.

26. Joyce, J.A. and J.W. Pollard, *Microenvironmental regulation of metastasis*. Nat Rev Cancer, 2009. **9**(4): p. 239-52.

27. Almand, B., et al., *Increased production of immature myeloid cells in cancer patients: a mechanism of immunosuppression in cancer*. J Immunol, 2001. **166**(1): p. 678-89.

28. Yang, L., et al., *Expansion of myeloid immune suppressor Gr+CD11b+ cells in tumor-bearing host directly promotes tumor angiogenesis*. Cancer Cell, 2004. **6**(4): p. 409-21.

29. Atzpodien, J. and M. Reitz, *Peripheral blood neutrophils as independent immunologic predictor of response and long-term survival upon immunotherapy in metastatic renal-cell carcinoma*. Cancer Biother Radiopharm, 2008. **23**(1): p. 129-34.

30. Joshita, S., et al., *Granulocyte-colony stimulating factor-producing pancreatic adenosquamous carcinoma showing aggressive clinical course*. Intern Med, 2009. **48**(9): p. 687-91.

31. Aslakson, C.J. and F.R. Miller, *Selective events in the metastatic process defined by analysis of the sequential dissemination of subpopulations of a mouse mammary tumor*. Cancer Res, 1992. **52**(6): p. 1399-405.

32. Rak, J.W., D. McEachern, and F.R. Miller, *Sequential alteration of peanut agglutinin binding-glycoprotein expression during progression of murine mammary neoplasia*. Br J Cancer, 1992. **65**(5): p. 641-8.

33. Yan, H.H., et al., *Gr-1+CD11b+ myeloid cells tip the balance of immune protection to tumor promotion in the premetastatic lung*. Cancer Res, 2010. **70**(15): p. 6139-49.

34. Cortez-Retamozo, V., et al., *Origins of tumor-associated macrophages and neutrophils*. Proc Natl Acad Sci U S A, 2012. **109**(7): p. 2491-6.

35. Morris, V.L., et al., *Tumor progression and metastasis in murine D2 hyperplastic alveolar nodule mammary tumor cell lines*. Clin Exp Metastasis, 1993. **11**(1): p. 103-12.

36. Shibue, T. and R.A. Weinberg, *Integrin beta1-focal adhesion kinase signaling directs the proliferation of metastatic cancer cells disseminated in the lungs*. Proc Natl Acad Sci U S A, 2009. **106**(25): p. 10290-5.

37. Daley, J.M., et al., *Use of Ly6G-specific monoclonal antibody to deplete neutrophils in mice*. J Leukoc Biol, 2008. **83**(1): p. 64-70.

38. Shibue, T., et al., *The outgrowth of micrometastases is enabled by the formation of filopodium-like protrusions*. Cancer Discov, 2012. **2**(8): p. 706-21.

39. Barlozzari, T., C.W. Reynolds, and R.B. Herberman, *In vivo role of natural killer cells: involvement of large granular lymphocytes in the clearance of tumor cells in anti-asialo GM1-treated rats*. J Immunol, 1983. **131**(2): p. 1024-7.

40. Riccardi, C., et al., *In vivo natural reactivity of mice against tumor cells*. Int J Cancer, 1980. **25**(4): p. 475-86.

41. Kasai, M., et al., *In vivo effect of anti-asialo GM1 antibody on natural killer activity*. Nature, 1981. **291**(5813): p. 334-5.

42. Kiessling, R., et al., *"Natural" killer cells in the mouse. II. Cytotoxic cells with specificity for mouse Moloney leukemia cells. Characteristics of the killer cell*. Eur J Immunol, 1975. **5**(2): p. 117-21.

43. Fernandez, N.C., et al., *A subset of natural killer cells achieves self-tolerance without expressing inhibitory receptors specific for self-MHC molecules*. Blood, 2005. **105**(11): p. 4416-23.

44. Kim, S., et al., *Licensing of natural killer cells by host major histocompatibility complex class I molecules*. Nature, 2005. **436**(7051): p. 709-13.

45. Labelle, M. and R.O. Hynes, *The initial hours of metastasis: the importance of cooperative host-tumor cell interactions during hematogenous dissemination*. Cancer Discov, 2012. **2**(12): p. 1091-9.

46. Vu, T.H., et al., *MMP-9/gelatinase B is a key regulator of growth plate angiogenesis and apoptosis of hypertrophic chondrocytes*. Cell, 1998. **93**(3): p. 411-22.

47. Chen, M.B., et al., *Mechanisms of tumor cell extravasation in an in vitro microvascular network platform*. Integr Biol (Camb), 2013. **5**(10): p. 1262-71.

48. Erler, J.T., et al., *Hypoxia-induced lysyl oxidase is a critical mediator of bone marrow cell recruitment to form the premetastatic niche*. Cancer Cell, 2009. **15**(1): p. 35-44.

49. Hiratsuka, S., et al., *Tumour-mediated upregulation of chemoattractants and recruitment of myeloid cells predetermines lung metastasis*. Nat Cell Biol, 2006. **8**(12): p. 1369-75.

50. Kaplan, R.N., et al., *VEGFR1-positive haematopoietic bone marrow progenitors initiate the pre-metastatic niche*. Nature, 2005. **438**(7069): p. 820-7.

51. Lu, X. and Y. Kang, *Chemokine (C-C motif) ligand 2 engages CCR2+ stromal cells of monocytic origin to promote breast cancer metastasis to lung and bone*. J Biol Chem, 2009. **284**(42): p. 29087-96.

52. Qian, B.Z., et al., *CCL2 recruits inflammatory monocytes to facilitate breast-tumour metastasis*. Nature, 2011. **475**(7355): p. 222-5.

53. Wolf, M.J., et al., *Endothelial CCR2 signaling induced by colon carcinoma cells enables extravasation via the JAK2-Stat5 and p38MAPK pathway*. Cancer Cell, 2012. **22**(1): p. 91-105.

54. Labelle, M., S. Begum, and R.O. Hynes, *Platelets guide the formation of early metastatic niches*. Proc Natl Acad Sci U S A, 2014. **111**(30): p. E3053-61.

55. Elkabets, M., et al., *IL-1beta regulates a novel myeloid-derived suppressor cell subset that impairs NK cell development and function*. Eur J Immunol, 2010. **40**(12): p. 3347-57.

56. Hoechst, B., et al., *Myeloid derived suppressor cells inhibit natural killer cells in patients with hepatocellular carcinoma via the NKp30 receptor*. Hepatology, 2009. **50**(3): p. 799-807.

57. Liu, C., et al., *Expansion of spleen myeloid suppressor cells represses NK cell cytotoxicity in tumor-bearing host*. Blood, 2007. **109**(10): p. 4336-42.

58. Mundy-Bosse, B.L., et al., *Myeloid-derived suppressor cell inhibition of the IFN response in tumor-bearing mice*. Cancer Res, 2011. **71**(15): p. 5101-10.

59. Gabrilovich, D.I. and S. Nagaraj, *Myeloid-derived suppressor cells as regulators of the immune system*. Nat Rev Immunol, 2009. **9**(3): p. 162-74.

60. Gabrilovich, D.I., S. Ostrand-Rosenberg, and V. Bronte, *Coordinated regulation of myeloid cells by tumours*. Nat Rev Immunol, 2012. **12**(4): p. 253-68.

61. Bergers, G., et al., *Matrix metalloproteinase-9 triggers the angiogenic switch during carcinogenesis*. Nat Cell Biol, 2000. **2**(10): p. 737-44.

62. Lee, S., et al., *Processing of VEGF-A by matrix metalloproteinases regulates bioavailability and vascular patterning in tumors*. J Cell Biol, 2005. **169**(4): p. 681-91.

63. An, X., et al., *Elevated neutrophil to lymphocyte ratio predicts survival in advanced pancreatic cancer*. Biomarkers, 2010. **15**(6): p. 516-22.

64. Cho, H., et al., *Pre-treatment neutrophil to lymphocyte ratio is elevated in epithelial ovarian cancer and predicts survival after treatment*. Cancer Immunol Immunother, 2009. **58**(1): p. 15-23.

65. Liu, H., et al., *The baseline ratio of neutrophils to lymphocytes is associated with patient prognosis in rectal carcinoma*. J Gastrointest Cancer, 2010. **41**(2): p. 116-20.

66. Teramukai, S., et al., *Pretreatment neutrophil count as an independent prognostic factor in advanced non-small-cell lung cancer: an analysis of Japan Multinational Trial Organisation LC00-03*. Eur J Cancer, 2009. **45**(11): p. 1950-8.

67. Ubukata, H., et al., *Evaluations of interferon-gamma/interleukin-4 ratio and neutrophil/lymphocyte ratio as prognostic indicators in gastric cancer patients*. J Surg Oncol, 2010. **102**(7): p. 742-7.

68. Granger, J.M. and D.P. Kontoyiannis, *Etiology and outcome of extreme leukocytosis in 758 nonhematologic cancer patients: a retrospective, single-institution study*. Cancer, 2009. **115**(17): p. 3919-23.

69. Hasegawa, S., et al., *Lung large cell carcinoma producing granulocyte-colony-stimulating factor*. Ann Thorac Surg, 2007. **83**(1): p. 308-10.

70. Hirasawa, K., et al., *Bladder tumor producing granulocyte colony-stimulating factor and parathyroid hormone related protein*. J Urol, 2002. **167**(5): p. 2130.

71. Mabuchi, S., et al., *The first 2 cases of granulocyte colony-stimulating factor producing adenocarcinoma of the uterine cervix*. Int J Gynecol Pathol, 2010. **29**(5): p. 483-7.

72. Yamamoto, S., et al., *Granulocyte-colony-stimulating-factor-producing hepatocellular carcinoma*. J Gastroenterol, 1999. **34**(5): p. 640-4.

73. Crawford, J., et al., *Reduction by granulocyte colony-stimulating factor of fever and neutropenia induced by chemotherapy in patients with small-cell lung cancer*. N Engl J Med, 1991. **325**(3): p. 164-70.

Figure Legends

Figure 1: Tumor metastasis is mediated by neutrophils.

(A) Total leukocyte (WBCs) and neutrophil counts in blood from control non-injected mice or 4-5 weeks post-implantation with murine breast carcinoma 4T1 cells. $n \geq 9$ mice for each group. (B) Representative picture (top) and average weight (bottom) of spleen from naïve BALB/c (control) or 5 weeks after s.c implantation of mice with 4T1 cells. $n \geq 8$ mice for each group. (C) 4T1 tumor weight in sham-operated BALB/c mice (control) or splenectomized mice. $n \geq 17$ for each group. (D) Number of 4T1 lung metastases (per hematoxylin & eosin-stained section comprising all five lobes) in mice implanted with 4T1 cells in sham-operated BALB/c mice (control) or splenectomized mice. $n \geq 12$ for each group. (E) Representative picture of lung lobes from sham surgery or splenectomized mice. Red arrows point to lung metastases. (F) D2A1 primary tumor weight 4-5 weeks after s.c implantation of mice with D2A1 cells contralateral to 4T1 cells or Matrigel (control). $n \geq 19$ for each group. (G) D2A1 lung metastases (fold increase vs D2A1 injected contralaterally to Matrigel) in mice implanted with D2A1 cells contralateral to 4T1 cells or Matrigel (control). $n \geq 14$ for each group. (H) D2A1 lung metastases (fold increase vs D2A1 injected contralaterally to Matrigel) in sham-operated or splenectomized mice implanted with D2A1 cells contralateral to 4T1 cells. $n \geq 8$ for each group. * indicates $p < 0.05$. (I) Total leukocyte (WBCs) and neutrophil counts in blood from mice 4-5 weeks post-implantation with D2A1 cells ectopically expressing empty vector (control) or G-CSF. $n \geq 9$ mice for each group. (J) D2A1 lung metastases spontaneously arising in mice bearing primary tumors of D2A1 cells ectopically expressing G-CSF or empty vector (control). $n \geq 7$ for each group. (K) Number of D2A1-

Tom$^+$ metastases in lungs of mice lacking primary tumors 2 weeks after intravenous injection of D2A-Tom$^+$ cells. Mice were injected with PBS, or anti-Ly6G antibody 24 hours before intravenous injection of cells. $n \geq 7$ for each group. * indicates $p < 0.05$.

Figure 2: Neutrophils facilitate later steps of the invasion-metastasis cascade.

(A) Lung metastasis (non-4T1) in mice injected i.v. with $2x10^4$ D2A1-Tom$^+$, B16-F10-GFP$^+$ or MDA-MB-231-Tom$^+$ cells. Results show fold increase upon injection into 4T1 tumor-bearing mice vs naive non-tumor-bearing mice (control). B16-F10-GFP$^+$ and MDA-MB-231-Tom$^+$ cells were injected into NOD/SCID 4T1 tumor-bearing mice 14 days after implantation of 4T1 cells. Experiment was terminated 2-3 weeks later and lung metastases were quantified. $n \geq 8$ for each group. (B) D2A1 lung metastases in mice (fold increase vs. control PBS injection) following adoptive transfer of splenocytes from non-tumor bearing or 4T1 tumor-bearing mice. $n \geq 9$ for each group. (C) Number of D2A1-Tom$^+$ metastases in lungs of G-CSF-treated mice compared to control (PBS-treated) mice. $n \geq 13$ for each group. (D) Number of D2A1-Tom$^+$ metastases in lungs following adoptive transfer of splenocytes from G-CSF-treated mice (fold increase compared to control mice that were injected with splenocytes from PBS-treated mice). $n \geq 12$ for each group. (E) Number of D2A1-Tom$^+$ cells in lungs of 4T1 (or naïve control) mice 24 hours post i.v. injection of D2A1 cells (left). Representative lung lobe images (right). 4T1 mice had been implanted with 4T1 cells 4 weeks earlier (F) Number of D2A1-Tom$^+$ cells in lungs of mice i.v. injection of D2A1-Tom$^+$ cells into either control naïve mice, or mice bearing primary tumors of D2A1 or B16-F10 cells ectopically

expressing G-CSF (implanted 4 weeks earlier). n ≥ 6 for each group. (G) Number of D2A1-Tom$^+$ cells in lungs of mice (fold increase vs. control PBS injection) following adoptive transfer of Ly6G$^+$-enriched neutrophils from splenocytes from 4T1 tumor-bearing mice. n ≥ 7 for each group. (H) D2A1-Tom$^+$ cells in lungs (fold increase compared to control mice without primary tumors) of 4T1 mice 24 hours post i.v. injection of D2A1 cells. Mice were injected with PBS, IgG antibody or anti-Ly6G (1A8) antibody 24 hours before injection of cells. Non-tumor-bearing mice served as control. n ≥ 10 mice per group. (I) Number of D2A1-Tom$^+$ cells in lungs of non-tumor-bearing mice 24 hours post i.v. injection of D2A1 cells. Mice were injected with PBS, control IgG antibody, or anti-Ly6G antibody 24 hours before i.v.injection of cells. n ≥ 11 for each group. For panels B, C & D - experiment was terminated and D2A1 lung metastases were quantified 2 weeks after i.v. injection of D2A1 cells. For panels E, F, G, H & I - experiment was terminated 24 hours after i.v. injection of D2A1 cells and number of D2A1-Tom$^+$ cells in the lung was assessed. In adoptive transfer experiments (panels B & G) splenocytes were obtained from 4T1 mice that had been implanted with 4T1 cells 4 weeks earlier. * indicates $p < 0.05$.

Figure 3: Neutrophils inhibit NK-mediated clearance of tumor cells.

(A) Representative bioluminescent imaging of BALB/c mice injected with D2A1-Tom$^+$ cells expressing luciferase. (B) Number of D2A1-Tom$^+$ cells detected in large lobes of lungs at the indicated time points after intravenous injection of D2A1-Tom$^+$ cells into control naïve mice or 4T1 mice (implanted with 4T1 cells 4 weeks earlier). n ≥ 6 for each

time point. (C) Number of D2A1-Tom$^+$ cells in lungs of mice 4 hours post i.v. injection of D2A1-Tom$^+$ cells. Mice were injected with PBS (control), IgG2A antibody, or anti-asialo-GM-1 antibody 24 hours before injection of cells. Results show fold increase vs control non-tumor-bearing mice. $n \geq 8$ for each group. (D) D2A1-Tom$^+$ lung metastases in mice (fold increase vs. control PBS treated mice) following injection of anti-asialo-GM-1 antibody 24 hours after injection of cells. $n \geq 5$ for each group. (E) Number of D2A1-Tom$^+$ cells detected in lungs 4 hours after intravenous injection into control non-tumor-bearing mice, 4T1-bearing mice, or 4T1-bearing mice that had been injected with anti-asialo-GM-1 antibody 24 hours before injection of cells. $n \geq 6$ for each group. (F) Left: number of YAC-1 cells in lungs of non-tumor-bearing BALB/c mice 4 hours post intravenous injection of YAC-1 cells. Mice were injected with PBS (control), IgG2A antibody, or anti-asialo-GM-1 antibody 24 hours before injection of cells. $n \geq 8$ for each group. Right: number of YAC-1 cells detected in lungs 4 hours after intravenous injection into control non-tumor-bearing mice or 4T1-bearing mice. $n \geq 6$ for each group. (G) YAC-1 cells in lungs (fold increase compared to control mice without primary tumors) of 4T1 mice 4 hours post i.v. injection of YAC-1 cells. Mice were injected with PBS or anti-Ly6G (1A8) antibody 24 hours before injection of cells. $n \geq 8$ for each group. (H) Percent of IFN-γ^+/CD107a$^+$ NK cells from the spleens (left) and lungs (right) of 4T1 tumor-bearing or non-tumor bearing naive mice following in vitro stimulation of the cells with NK-activating receptor antibodies or IgG control. $n \geq 6$ for each group. In panels B,F,G & H, host 4T1 mice had been implanted with 4T1 cells 4 weeks earlier. * indicates $p < 0.05$.

Figure 4: MMP-8 and MMP-9 facilitate transendothelial migration and metastasis. (A) Intraluminal antibody staining of MDA-MB-231 cells injected i.v. into 4T1-mice (implanted with 4T1 cells 4 weeks earlier) or control naïve mice. Graph shows percent of MDA-MB-231-Tom$^+$ cells found in the lung that also stained positive by i.v. injected anti-HLA-2-FITC antibodies. n $\geq$ 6 for each group. (B) Transendothelial migration of D2A1-Tom$^+$ cells through HUVECs in the presence of the indicated conditioned media. Results present fold increase compared to control RPMI medium. At least 3 experiments were performed in duplicates. (C) Representative images of D2A1-Tom$^+$ cells that migrated through HUVECs in the presence of the indicated conditioned media. (D) Transendothelial migration of D2A1-Tom$^+$ cells or B16-F10-GFP$^+$ cells through mouse endothelial, bEnd.3, cells in the presence of the indicated conditioned media. Results present fold increase compared to control RPMI medium. At least 3 experiments were performed in duplicates. (E) Transendothelial migration of D2A1 cells (fold increase compared to control RPMI medium) through mouse endothelial bEnd.3 cells in the presence of conditioned medium from unfractionated splenocytes or the Ly6G$^+$ enriched subpopulation of splenocytes from 4T1 mice. The number of Ly6G$^+$ cells used to prepare the conditioned medium was equivalent to the number of Ly6G$^+$ cells in 1.5 x10^7 unfractionated splenocytes population.(F) Transendothelial migration of D2A1 cells (fold increase compared to control RPMI medium) in the presence of conditioned medium from the Ly6G$^+$ enriched subpopulation of splenocytes from non-tumor-bearing or 4T1 mice. (G) MMP-8 and MMP-9 secretion by an equal number of splenocytes from naïve BALB/c or 4T1–bearing mice. (H) Transendothelial migration (fold increase compared to control RPMI) of D2A1cells in the presence of the indicated conditioned media, inhibitor

or antibody against MMP-8 or antibody against MMP-9. At least 3 experiments were performed in duplicates. (I) Immunofluorescent staining of MMP-9 (green) and Ly6G (red) in lungs of naïve BALB/c and 4T1 mice (implanted with 4T1 cells 4 weeks earlier). Scale bar 25mm. (J) Adoptive transfer of splenocytes from WT or MMP-9 KO tumor-bearing mice (implanted with B16-F10-GCSF overexpressing cells 3 weeks earlier). Donor splenocytes were injected into WT or MMP9-KO recipient mice, as indicated. Experiment was terminated 2 weeks later, and pulmonary metastases of GFP-labelled B16-F10 cells were quantified. * indicates $p< 0.05$.

Figure 5: Neutrophil-secreted IL-1b activates endothelial cells and facilitates migration (A) Transendothelial migration (fold increase compared to control RPMI medium) of D2A1 cells following pretreatment of bEnd.3 cells with the indicated conditioned media (prepared from equal numbers of splenocytes). The inserts were washed with RPMI medium prior to addition of the D2A1 cells. 5 experiments were performed in duplicates. (B) Transendothelial migration (fold increase compared to control RPMI medium) of D2A1 cells following pretreatment of bEnd.3 cells with the indicated conditioned media (prepared from equal numbers of splenocytes). The inserts were washed with RPMI medium prior to addition of the D2A1 cells. 5 experiments were performed in duplicates. (C) Secretion of MMP-9 by bEnd.3 cells following incubation of the endothelial cells with 4T1-splenocyte-conditioned medium or splenocyte-conditioned medium from control non-tumor-bearing mice (prepared from equal numbers of splenocytes) as determined by ELISA (D) Secretion of IL-1b by splenocytes from naïve BALB/c mice, splenocytes from 4T1mice, or $Ly6G^+$ neutrophils enriched from

splenocytes from 4T1 mice. Levels of IL-1b secreted into the conditioned medium were determined by ELISA. of at least 5 samples per group. (E) Transendothelial migration (fold increase compared to control RPMI) of D2A1 cells following pre-incubation of bEnd.3 cells with the indicated conditioned media and in the presence of IL-1 b receptor antagonist. At least 4 experiments were performed in duplicates. (F) Secretion of MMP-9 by bEnd.3 endothelial cells following incubation of the endothelial cells with splenocyte-conditioned medium from control non-tumor-bearing mice, 4T1 tumor bearing mice or 4T1 tumor bearing mice together with IL-1 receptor antagonist. MMP-9 secretion was determined by ELISA of at least 5 samples per treatment. * indicates $p< 0.05$.

Figure 6: Visualization of protrusion and extravasation dynamics of tumor cells. (A) Left - high resolution time-lapse confocal microscopy (20X) of an extravasating MDA-MB-231 cell (red) immediately after seeding in microvasculature network (HUVEC cells labeled in green). Right - confocal images taken at a single slice tracking a tumor cells as it transmigrates through the endothelium and into the 3D matrix over a period of 3 hours. (B) Protrusion formation (red) and extravasation (blue) rates of MDA-MB-231 cells in HUVEC vessels that had been pre-treated with 4T1 splenocyte conditioned medium or Control (RPMI). (C) Time required for protrusion formation (i.e. partial translocation across the lumen) and (D) time required for complete extravasation (i.e. the entire cell body has cleared the lumen) of MDA-MB-231 cells in HUVEC vessels that had been pre-treated with 4T1 splenocyte conditioned medium or Control (RPMI). Data were collected from >150 cells per condition, over 3 independent experiments. (E) Events leading to metastasis of circulating tumor cells: 1) Primary tumor perturbs distant organs, leading to

neutrophil expansion and mobilization. 2) Neutrophils increase intraluminal survival of circulating tumor cells by inhibiting their clearance by NK cells. 3) Neutrophils increase extravasation of circulating tumor cells through secretion of IL-1b and MMPs. * indicates $p < 0.05$.

Supplementary Figure 1: Systemic neutrophilia in tumor bearing mice.

(A) Total leukocyte (WBCs) and neutrophil counts in blood (left) and weight of spleen (right) from mice implanted with 4T1 cells either orthotopically or subcutaneously 4-5 weeks earlier. $n \geq 6$ mice for each group. (B) Cell surface expression of G-CSF receptor on 4T1 cells. Staining with secondary antibody served as negative control. Staining of $Ly6G^+$ cells served as positive control. (C) Total leukocyte and neutrophil counts in blood from control non-injected mice, mice implanted with 4T1 cells or splenectomized mice implanted with 4T1 cells. (D) G-CSF secretion by D2A1 cells ectopically expressing G-CSF or empty vector (control) or 4T1 cells. Equal number of cells (10^6) were plated in 10 cm dishes and medium was collected 48 hours later. $n \geq 5$ for each group. * indicates $p < 0.05$.

Supplementary Figure 2: Increased metastasis does not result from increased intravasation or post-extravasation events.

(A) Number of D2A1-Tom^+ tumor cells detected in equal volume (100 ml) of blood from mice implanted with D2A1-Tom^+ cells contralateral to 4T1 cells or Matrigel. $n \geq 7$ for each group. Number of circulating tumor D2A1 cells was determined by flow cytometry. (B) Number of D2A1-Tom^+ metastases in lungs following intravenous injection of $2x10^4$

4T1 cells or PBS control) one day prior to injection of the D2A1 tom+ cells. $n \geq 5$ for each group. (C) D2A1 lung metastasis (fold increase vs control PBS injection) following adoptive transfer of splenocytes from 4T1 tumor bearing mice. Splenocytes were injected i.v. 1 day after injection of D2A1 cells. (D) G-CSF secretion by B16-F10 cells ectopically expressing G-CSF or empty vector (control) or 4T1 cells. Equal number of cells (10^6) were plated in 10 cm dishes and medium was collected 48 hours later. * indicates $p < 0.05$.

Supplementary Figure 3: NK-mediated clearance of B16-F10-GFP$^+$ cells

(A) Number of B16-F10-GFP$^+$ cells in lungs of mice 24 hours post i.v. injection of D2A1-Tom$^+$ cells. Mice were injected with PBS (control), IgG antibody, or anti-NK1.1 antibody 24 hours before injection of cells. $n \geq 5$ for each group. * indicates $p < 0.05$.

Supplementary Figure 4: Ly6G$^+$ neutrophils are more abundant in spleens of 4T1 bearing mice.

(A) Representative flow cytometry analysis of CD11b$^+$/Ly6G$^+$ neutrophils in splenocytes from 4T1 tumor bearing mice or control, naïve BALB/c mice.

Supplementary Figure 5: Splenocyte conditioned medium activates endothelial cells and induces MMP-9 secretion.

Expression of MMP-9 in bEnd.3 cells following incubation with 4T1-splenocyte-conditioned medium or splenocyte-conditioned medium from control non-tumor-bearing mice (prepared from equal numbers of splenocytes). (B) Secretion of MMP-9 by bEnd.3

cells following incubation of the endothelial cells with 4T1-splenocyte-conditioned medium or splenocyte-conditioned medium from control non-tumor-bearing mice (prepared from equal numbers of splenocytes) as determined by western blotting (C) Transendothelial migration (fold increase compared to control RPMI) of D2A1 cells when IL-1b (1 ng/ml) was added to RPMI. 4 experiments were performed in duplicates. * indicates $p < 0.05$.

Figure 1

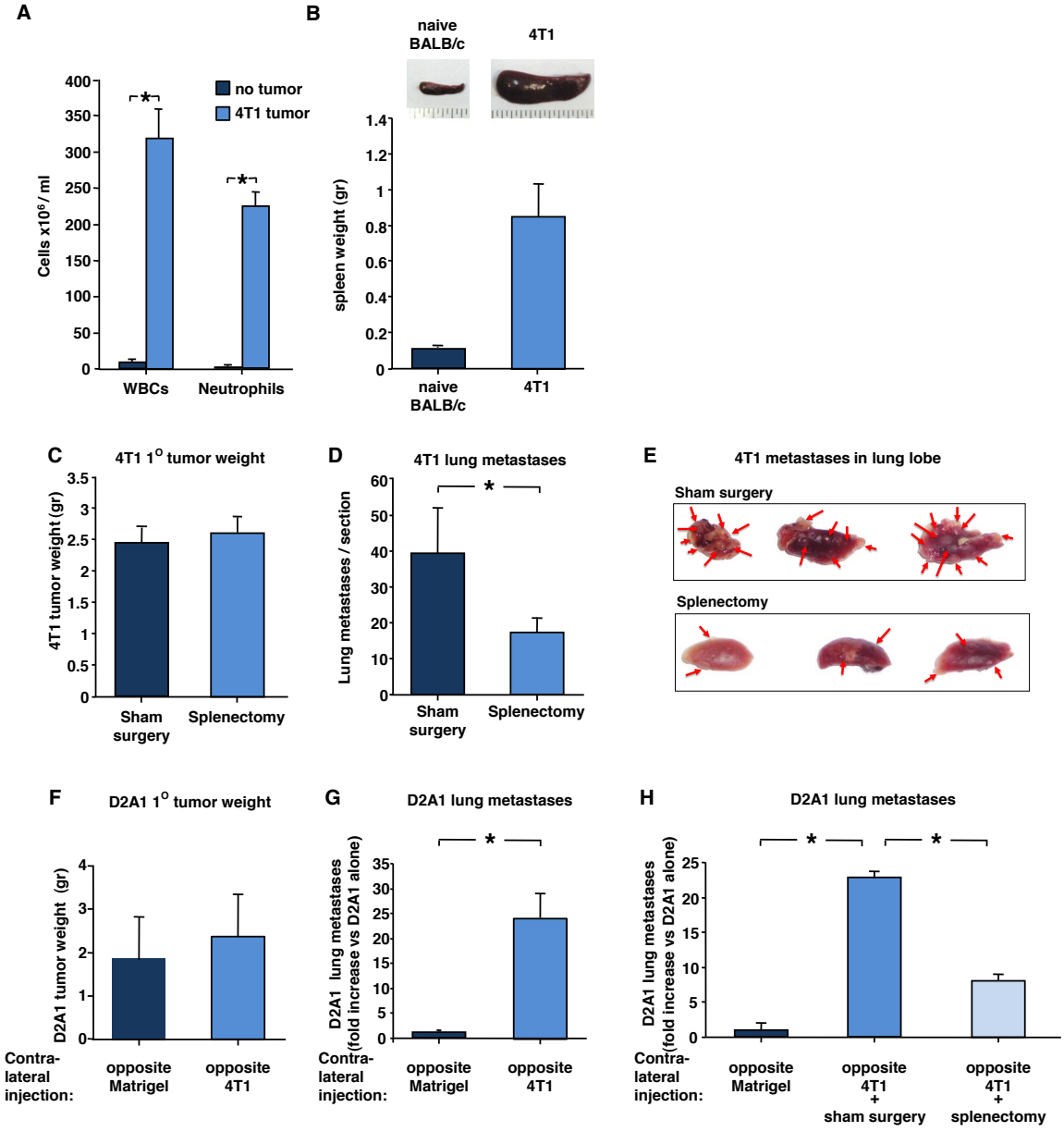
A
Cells x10⁶ / ml
no tumor
4T1 tumor
WBCs
Neutrophils
B
naive BALB/c
4T1
spleen weight (gr)
C
4T1 1° tumor weight
4T1 tumor weight (gr)
Sham surgery
Splenectomy
D
4T1 lung metastases
Lung metastases / section
E
4T1 metastases in lung lobe
Sham surgery
Splenectomy
F
D2A1 1° tumor weight
D2A1 tumor weight (gr)
Contra-lateral injection:
opposite Matrigel
opposite 4T1
G
D2A1 lung metastases
D2A1 lung metastases (fold increase vs D2A1 alone)
H
opposite 4T1 + sham surgery
opposite 4T1 + splenectomy

Figure 1 (con't)

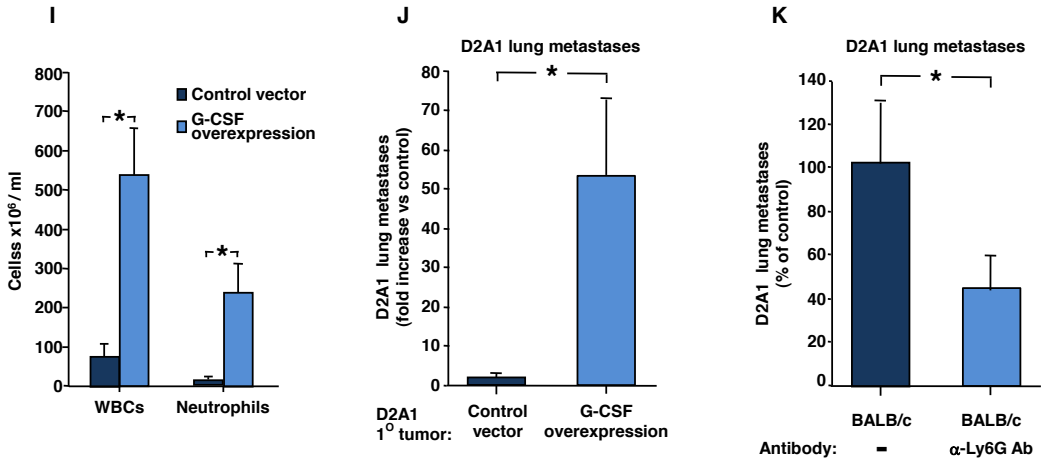

Figure 2

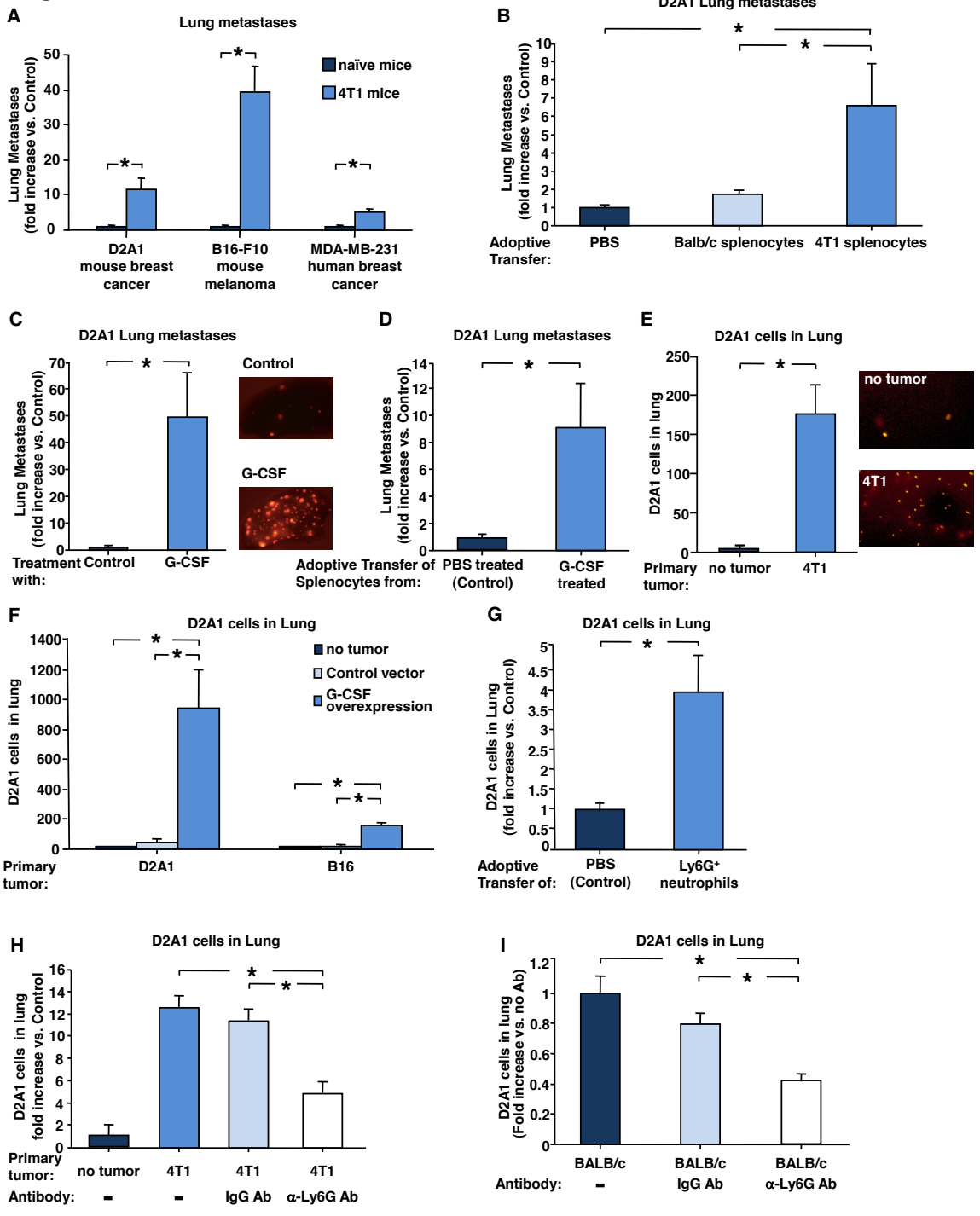
A
Lung metastases
Lung Metastases (fold increase vs. Control)
naïve mice
4T1 mice
D2A1 mouse breast cancer
B16-F10 mouse melanoma
MDA-MB-231 human breast cancer
B
D2A1 Lung metastases
Lung Metastases (fold increase vs. Control)
Adoptive Transfer:
PBS
Balb/c splenocytes
4T1 splenocytes
C
D2A1 Lung metastases
Lung Metastases (fold increase vs. Control)
Control
G-CSF
Treatment with:
Control
G-CSF
D
D2A1 Lung metastases
Lung Metastases (fold increase vs. Control)
Adoptive Transfer of Splenocytes from:
PBS treated (Control)
G-CSF treated
E
D2A1 cells in Lung
D2A1 cells in lung
no tumor
4T1
Primary tumor:
no tumor
4T1
F
D2A1 cells in Lung
D2A1 cells in lung
no tumor
Control vector
G-CSF overexpression
Primary tumor:
D2A1
B16
G
D2A1 cells in Lung
D2A1 cells in Lung (fold increase vs. Control)
Adoptive Transfer of:
PBS (Control)
Ly6G+ neutrophils
H
D2A1 cells in Lung
D2A1 cells in lung fold increase vs. Control
Primary tumor:
no tumor
4T1
4T1
4T1
Antibody:
-
-
IgG Ab
α-Ly6G Ab
I
D2A1 cells in Lung
D2A1 cells in lung (Fold increase vs. no Ab)
BALB/c
BALB/c
BALB/c
Antibody:
-
IgG Ab
α-Ly6G Ab

Figure 3

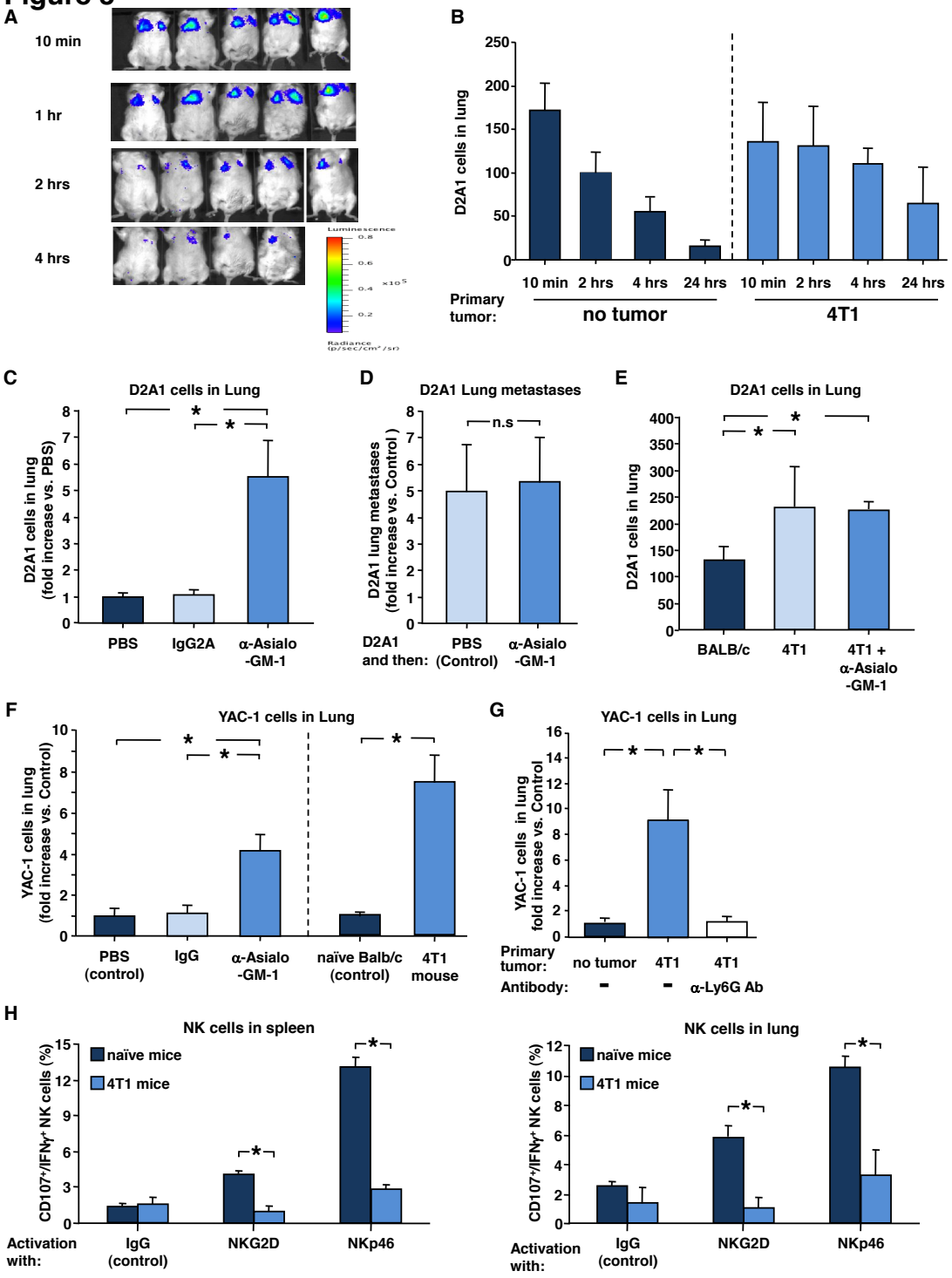
A
10 min
1 hr
2 hrs
4 hrs
Luminescence
Radiance (p/sec/cm²/sr)
B
D2A1 cells in lung
10 min 2 hrs 4 hrs 24 hrs 10 min 2 hrs 4 hrs 24 hrs
Primary tumor:
no tumor
4T1
C
D2A1 cells in Lung
D2A1 cells in lung (fold increase vs. PBS)
PBS
IgG2A
α-Asialo -GM-1
D
D2A1 Lung metastases
D2A1 lung metastases (fold increase vs. Control)
n.s
D2A1 and then:
PBS (Control)
α-Asialo -GM-1
E
D2A1 cells in Lung
D2A1 cells in lung
BALB/c
4T1
4T1 + α-Asialo -GM-1
F
YAC-1 cells in Lung
YAC-1 cells in lung (fold increase vs. Control)
PBS (control)
IgG
α-Asialo -GM-1
naïve Balb/c (control)
4T1 mouse
G
YAC-1 cells in Lung
YAC-1 cells in lung fold increase vs. Control
Primary tumor:
no tumor
4T1
4T1
Antibody:
α-Ly6G Ab
H
NK cells in spleen
CD107⁺/IFNγ⁺ NK cells (%)
naïve mice
4T1 mice
Activation with:
IgG (control)
NKG2D
NKp46
NK cells in lung
CD107⁺/IFNγ⁺ NK cells (%)
naïve mice
4T1 mice
Activation with:
IgG (control)
NKG2D
NKp46

Figure 4

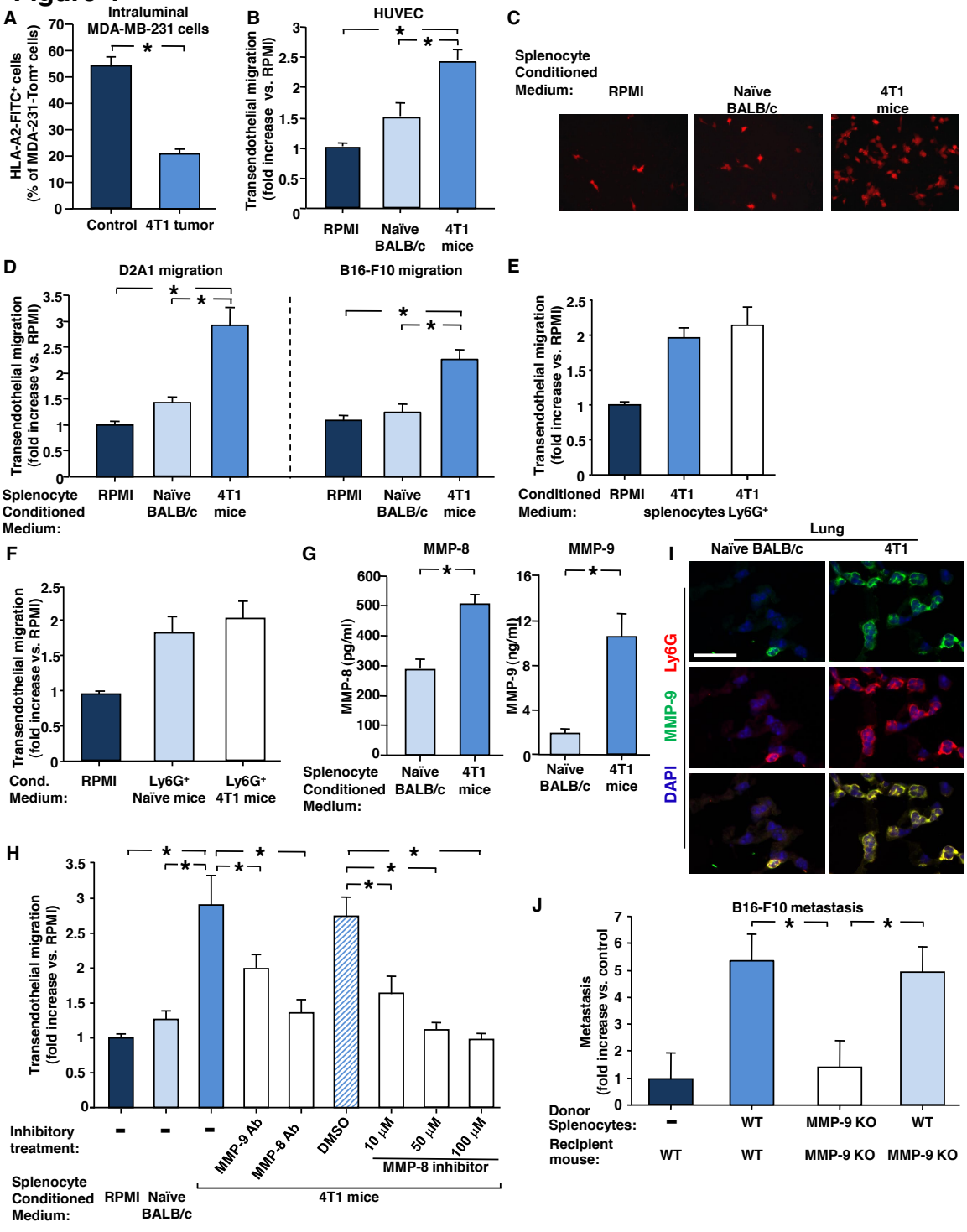
A
Intraluminal MDA-MB-231 cells
HLA-A2-FITC+ cells (% of MDA-231-Tom+ cells)
Control
4T1 tumor
B
HUVEC
Transendothelial migration (fold increase vs. RPMI)
RPMI
Naïve BALB/c
4T1 mice
C
Splenocyte Conditioned Medium:
RPMI
Naïve BALB/c
4T1 mice
D
D2A1 migration
B16-F10 migration
Transendothelial migration (fold increase vs. RPMI)
Splenocyte Conditioned Medium:
RPMI
Naïve BALB/c
4T1 mice
E
Transendothelial migration (fold increase vs. RPMI)
Conditioned Medium:
RPMI
4T1 splenocytes
4T1 Ly6G+
F
Transendothelial migration (fold increase vs. RPMI)
Cond. Medium:
RPMI
Ly6G+ Naïve mice
Ly6G+ 4T1 mice
G
MMP-8
MMP-8 (pg/ml)
MMP-9
MMP-9 (ng/ml)
Splenocyte Conditioned Medium:
Naïve BALB/c
4T1 mice
I
Lung
Naïve BALB/c
4T1
Ly6G
MMP-9
DAPI
H
Transendothelial migration (fold increase vs. RPMI)
Inhibitory treatment:
MMP-9 Ab
MMP-8 Ab
DMSO
10 μM
50 μM
100 μM
MMP-8 inhibitor
Splenocyte Conditioned Medium:
RPMI
Naïve BALB/c
4T1 mice
J
B16-F10 metastasis
Metastasis (fold increase vs. control)
Donor Splenocytes:
WT
MMP-9 KO
WT
Recipient mouse:
WT
WT
MMP-9 KO
MMP-9 KO

Figure 5

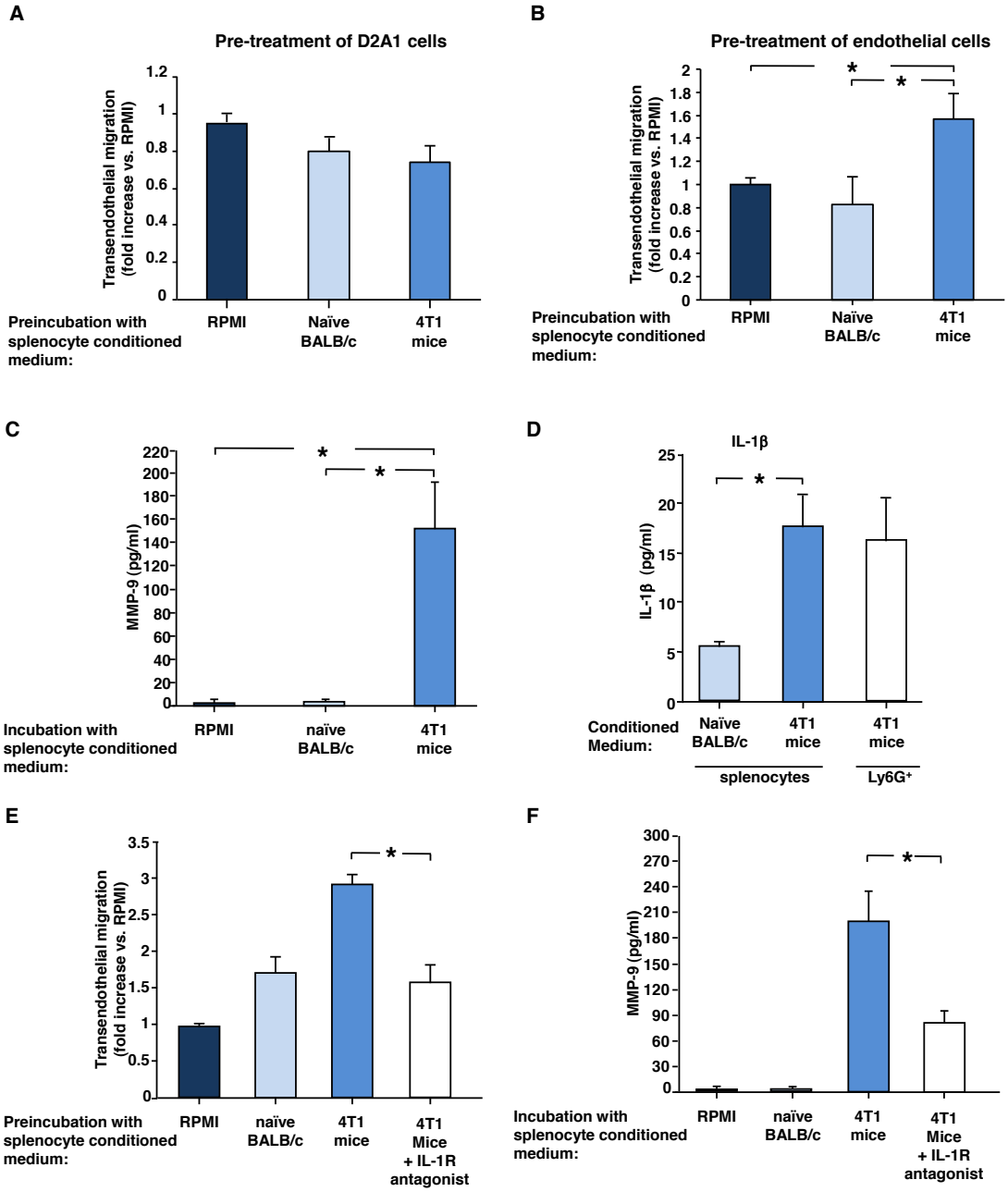
A
Pre-treatment of D2A1 cells
Transendothelial migration (fold increase vs. RPMI)
1.2
1
0.8
0.6
0.4
0.2
0
Preincubation with splenocyte conditioned medium:
RPMI
Naïve BALB/c
4T1 mice
B
Pre-treatment of endothelial cells
Transendothelial migration (fold increase vs. RPMI)
2
1.8
1.6
1.4
1.2
1
0.8
0.6
0.4
0.2
0
*
*
Preincubation with splenocyte conditioned medium:
RPMI
Naïve BALB/c
4T1 mice
C
MMP-9 (pg/ml)
220
200
180
160
140
120
100
80
60
40
20
0
*
*
Incubation with splenocyte conditioned medium:
RPMI
naïve BALB/c
4T1 mice
D
IL-1β
IL-1β (pg/ml)
25
20
15
10
5
0
*
Conditioned Medium:
Naïve BALB/c
4T1 mice
4T1 mice
splenocytes
Ly6G+
E
Transendothelial migration (fold increase vs. RPMI)
3.5
3
2.5
2
1.5
1
0.5
0
*
Preincubation with splenocyte conditioned medium:
RPMI
naïve BALB/c
4T1 mice
4T1 Mice + IL-1R antagonist
F
MMP-9 (pg/ml)
300
270
240
210
180
150
120
90
60
30
0
*
Incubation with splenocyte conditioned medium:
RPMI
naïve BALB/c
4T1 mice
4T1 Mice + IL-1R antagonist

Figure 6

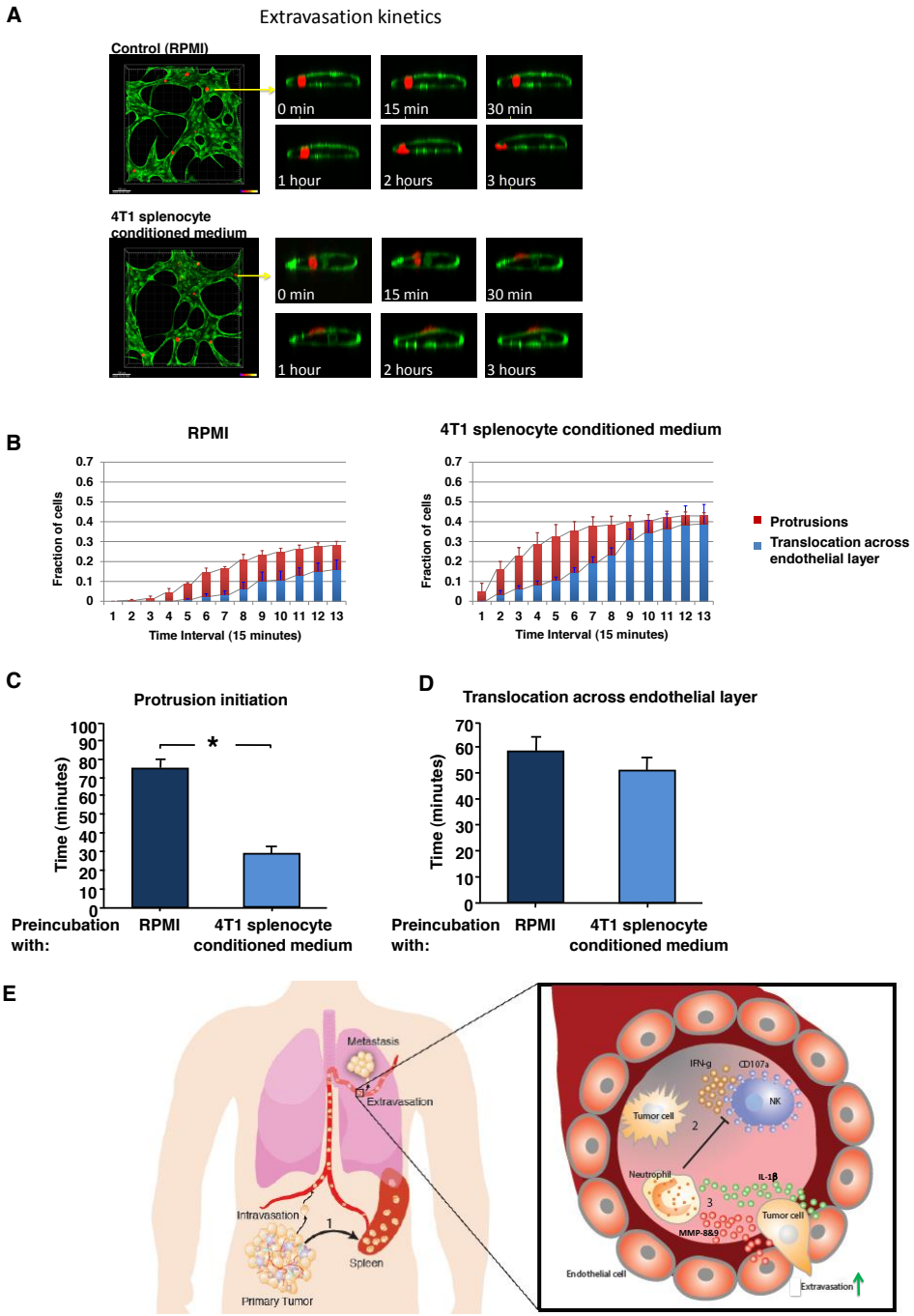
A
Extravasation kinetics
Control (RPMI)
0 min
15 min
30 min
1 hour
2 hours
3 hours
4T1 splenocyte conditioned medium
0 min
15 min
30 min
1 hour
2 hours
3 hours
B
RPMI
4T1 splenocyte conditioned medium
Fraction of cells
Time Interval (15 minutes)
Protrusions
Translocation across endothelial layer
C
Protrusion initiation
Time (minutes)
Preincubation with:
RPMI
4T1 splenocyte conditioned medium
D
Translocation across endothelial layer
Time (minutes)
Preincubation with:
RPMI
4T1 splenocyte conditioned medium
E
Metastasis
Extravasation
Intravasation
Spleen
Primary Tumor
IFN-g
CD107a
NK
Tumor cell
Neutrophil
IL-1β
MMP-8&9
Endothelial cell
Extravasation

Appendix II:

LACTB, a novel tumor suppressor that modulates mitochondrial lipid metabolism and cancer cell differentiation

Zuzana Keckesova[1]*, Joana Liu Donaher[1], Jasmine De Cock[1], Elizaveta Freinkman[1], Susanne Lingrell[6], Daniel A. Bachovchin[2], Brian Bierie[1], Verena Tischler[3], Aurelia Noske[3], Ferenc Reinhardt[1], Prathapan Thiru[1], Todd R. Golub[2], Jean E. Vance[6] and Robert A. Weinberg [1,4,5,]*

[1]Whitehead Institute for Biomedical Research, 9 Cambridge Center, Cambridge, MA 02142, USA

[2]Broad Institute, Massachusetts Institute of Technology, Cambridge, MA 02142, USA

[3]Institute of Surgical Pathology, University Hospital Zurich, Zurich, Switzerland

[4]Department of Biology, Massachusetts Institute of Technology, Cambridge, MA 02139, USA

[5]MIT Ludwig Center for Molecular Oncology, Cambridge, MA 02139, USA

[6]Department of Medicine and the Group on Molecular and Cell Biology of Lipids, University of Alberta, Edmonton, Alberta T6G 2S2, Canada

Personal Contribution to the Project

This chapter is the result of collaboration with Zuzana Keckesova on work that is currently under review with *Nature*. Zuzana requested assistance in molecular biology techniques. I conducted *in vitro* cell viability assays, aided in bioluminescent imaging experiments, and the results are described in this appendix.

Abstract

Post-mitotic, differentiated cells exhibit a variety of characteristics that contrast with those of actively growing neoplastic cells, such as expression of cell-cycle inhibitors and differentiation factors. We hypothesized that the gene expression profiles of such cells would reveal the identities of genes that function as novel tumor suppressors. Here we show using *in vitro* and *in vivo* studies, that mitochondrial protein LACTB is a potent inhibitor of the proliferation of breast cancer cells but not of corresponding normal cells. Its mechanism of action involves alteration of mitochondrial lipid metabolism and differentiation of cancer cells. This is achieved, at least in part, through reducing the levels of mitochondrial phosphatidylserine decarboxylase (PISD), which is involved in the synthesis of mitochondrial phosphatidylethanolamine. These observations have uncovered a novel mitochondrial tumor suppressor and demonstrate an interconnection between mitochondrial lipid metabolism and the differentiation program of cancer cells, thereby revealing a previously undescribed mechanism of tumor suppression.

Cancer cells can be distinguished from their normal counterparts by alterations in cell cycle regulation, differentiation and metabolism. In general, cancer cells are proliferative, tend to be relatively undifferentiated, and prefer glycolysis over oxidative phosphorylation. Wishing to identify novel tumor suppressor genes, we hypothesized that the best cellular models to search for these genes would be in the cells/tissues that differ most in their cell-biological state from cancer cells. Accordingly, we asked whether there are cells/tissues within living organisms whose traits are directly opposed to those of cancer cells, i.e., whether there are cells that are non-proliferative, differentiated, and prefer oxidative phosphorylation.

Skeletal muscle cells represent one such class of cells, in that they are maintained in post-mitotic differentiated states, express elevated numbers of various cell-cycle inhibitors[1,2], and rarely undergo neoplastic transformation in adults[3] (http://sarcomahelp.org/learning_center/rhabdomyosarcoma.html). Accordingly, we reasoned that terminally differentiated muscle cells are likely express many factors that induce or maintain them in their non-proliferative, differentiated state, and that the forced expression of some of these factors in cancer cells might have a negative effect on the latter. This approach allowed us to identify a novel tumor suppressor that operates within mitochondria and negatively affects the growth of a variety of tumor cells *in vivo* and *in vitro* while leaving non-tumorigenic cells minimally affected. Its mechanism of action involves, in significant part, alterations of mitochondrial lipid metabolism that are accompanied by differentiation of cancer cells and their loss of tumorigenicity.

LACTB as a tumor suppressor

C2C12 mouse muscle progenitors and primary human muscle progenitors were differentiated *in vitro* according to standard protocols (see Methods). The extent of proper differentiation of these cells into myotubes was gauged by monitoring cellular morphology and by immunofluorescence staining (Extended Data Fig. 1a, b). In addition, the mRNAs encoding a cohort of well-studied tumor-suppressing proteins, namely CDKN1A, CDKN1B, CDKN2A, CDKN2B, pRB, RBL2, p53 and ATM, were upregulated 4-60 fold in the differentiated human muscle cells relative to their less differentiated precursors (Extended Data Fig. 1c), showing that these cells abundantly express a variety of well-characterized tumor suppressors. We performed gene expression microarray analyses of the differentiated and undifferentiated human and mouse skeletal muscle cells as a means of identifying additional genes possibly involved in imposing cell-

cycle inhibition and/or differentiation. We focused our attention on mRNAs that were significantly up-regulated in differentiated post-mitotic muscle cells of both species relative to their undifferentiated, actively cycling counterparts. This list of genes was filtered to include genes that exhibited at least two-fold changes in expression level with p values < 0.01. A total of 87 genes met these criteria (Extended Data Fig. 1d and Supplementary Table S1).

Five genes from this list were chosen for functional validation following RT-PCR measurements of the levels of their respective mRNAs, which confirmed their upregulated expression in differentiated human muscle cells: adenylate cyclase-associated protein 2 (CAP2), beta-lactamase-like protein (LACTB), receptor accessory protein 1 (REEP1), PDZ and LIM domain protein 3 (PDLIM3), and small muscle protein X-linked (SMPX) (Extended Data Fig. 1e). The cDNA of each was cloned into a doxycycline-inducible Tet-ON vector and expressed in a derivative of the MCF7 human breast cancer cell line that carries an introduced *H-RAS* (G12V) oncogene (MCF7ras)[4]. Upon doxycycline induction, as judged by monitoring cellular behavior and proliferation rate, LACTB exerted a profoundly negative effect on these cells' ability to proliferate, SMPX exhibited a modest effect, while no significant effect on cell proliferation resulted from over-expression of CAP2, REEP1 or PDLIM3 (Extended Data Fig. 1f and Fig. 2a). Consequently, we focused our attention on characterizing the functional role of the LACTB protein in cancer cells.

LACTB is a mitochondrial protein that is related evolutionarily to bacterial penicillin-binding/B-lactamase proteins[5,6]. Homologs of the *LACTB* gene are present in the genomes of all chordates examined thus far as well as those of certain non-chordates, such as *Caenorhabditis*

elegans; LACTB is absent, however, from the genomes of *Drosophila melanogaster* and *Saccharomyces cerevisae*[5,6]. In mammals LACTB appears to be ubiquitously expressed, being most prominent in skeletal muscle, heart and liver[5,7]. Such evolutionary conservation points to an essential, albeit still-unknown, cellular function.

In bacteria, β-lactamase enzymes are involved in the synthesis of peptidoglycans, major components of the bacterial cell wall. Metazoan cells, however, possess neither cell wall structures nor the machinery for peptidoglycan synthesis, which points to an alternative biochemical and cell-physiologic function for LACTB. The presence of a highly conserved catalytic serine residue in metazoan LACTB has suggested that it possesses either peptidase or esterase activity[6]. LACTB has been found to undergo polymerization into filaments within the mitochondrial inter-membrane space, suggesting that this protein might promote intra-mitochondrial membrane organization[8]. LACTB was also suggested to be involved in the regulation of complex I of the mitochondrial electron transport chain, since down-regulation of LACTB led to decreased activity of this complex[9]. Through gene co-expression analysis and transgenic mice validation, LACTB function has been linked to obesity[10] and fatty acid metabolism[11], hinting at a possible role in regulating cellular metabolic processes.

We performed quantitative RT-PCR analyses in order to compare the levels of *LACTB* mRNA in various non-tumorigenic and tumorigenic mammary cell lines. This analysis failed to show any correlation between LACTB mRNA expression and the neoplastic cell state (Extended Data Fig. 2a). However, since LACTB protein expression has also been shown to be frequently regulated at the post-transcriptional level[12,13,8], we compared the levels of LACTB protein in

normal and neoplastic cells and tissues. Immunoblot analysis of a panel of non-tumorigenic cell lines and tumorigenic breast cancer cell lines showed a marked reduction of LACTB protein levels in breast cancer cell lines relative to non-tumorigenic mammary epithelial, endothelial and mesenchymal cells (Fig. 1a). Out of 18 breast cancer cell lines analyzed 15 showed decreased LACTB protein levels while 3 cell lines (MCF7ras, SUM159, MDA-MB-231) cells) exhibited LACTB protein levels comparable to those found in non-tumorigenic cell lines (Fig. 1a). We therefore examined whether the LACTB protein in MCF7ras cells was correctly localized to mitochondria. While immunofluorescence analysis of LACTB in non-tumorigenic MCF10A mammary cell lines confirmed the mitochondrial localization of LACTB, as indicated by its co-localization with a mitochondrial marker, LACTB in MCF7ras cancer cells displayed a punctate, largely non-mitochondrial staining pattern (Extended Data Fig. 2b). This suggested its localization to an ectopic intracellular site where it might not be able to carry out its normal function(s). We sequenced the endogenous LACTB gene from MCF7ras cells and noticed the presence of R469K mutation in the C-terminus of LACTB, which is closely adjacent to one of the three important catalytic domains[6]. Surprisingly, the same mutation was found in the endogenous LACTB sequence in SUM159 cells, while the sequence of endogenous LACTB in MDA-MB-231 cells harbored no apparent somatic mutations (Extended Data Fig. 9b).

We proceeded to extend our findings with cell lines to clinical samples by examining the expression of LACTB protein in normal human breast tissues (n=120) and in a panel of 714 clinically defined human breast cancer samples. H&E staining of normal human breast tissue showed that LACTB is expressed in both myoepithelial and luminal mammary epithelial layers with stronger staining in the myoepithelial layer (Extended Data Fig. 2c). While LACTB was

expressed in 100% of normal mammary glands analyzed, its expression was significantly down-regulated in 36% of breast cancer tissues (Fig. 1b). A representative H&E image of LACTB expression levels in neoplastic mammary tissue adjacent to normal mammary gland tissue shows the relative down-regulation of LACTB levels in breast cancer cells relative to adjacent normal mammary epithelial cells (Fig. 1c). This down-regulation did not correlate with any particular tumor type, grade or size (Fig. 1b and Extended Data Fig. 2d). While these analyses did not address the intracellular localization of LACTB in these breast cancer tissues, they did confirm the frequent down-regulation of LACTB levels in clinical breast cancers.

In order to gauge the cell-biological effects of LACTB expression, we introduced a doxycycline-inducible LACTB (Tet/ON-LACTB) expression vector into a panel of tumorigenic and non-tumorigenic cell lines and measured subsequent cell proliferation over the course of nine to eleven days of LACTB induction. Of note, since doxycycline has been reported to modulate mitochondrial function via its effects on the mitochondrial translation machinery[14-16], experiments in this study were always performed by adding doxycycline to control cells unless otherwise noted. LACTB over-expression decreased the rate of proliferation (between 2.5 and 10 fold) in the three breast cancer cell lines tested (HMLER, MCF7ras, HCC1806), while proliferation of the three non-tumorigenic cell lines (HME, MCF10A, and BJ1) was only minimally affected by LACTB over-expression (Fig. 2a). Immunoblotting confirmed that comparable levels of LACTB protein were expressed following doxycycline-mediated induction in all cell lines tested (Extended Data Fig. 2e).

The results of the proliferation experiments were further confirmed by EdU (5-ethynyl-2'-deoxyuridine) staining, which gauges DNA synthesis and revealed that all three cancer cell lines tested exhibited reduced EdU incorporation (1.5-13 fold) following induction of LACTB expression for 3 days (Fig. 2b). Annexin V staining, which reflects apoptosis, showed an increase (over 7-fold) in the number of apoptotic cells in MCF7ras cell line, but not in HCC1806 or HMLER cells, in response to induced LACTB expression (Extended Data Fig. 2f). Moreover, immunofluorescence studies showed that expression of the Ki-67 proliferation marker in MCF7ras cells expressing LACTB for 3 days was markedly reduced compared to that in the co-mixed control cells (Extended Data Fig. 2g). Since the Ki-67 marker is present during all phases of the active cell cycle (G1, S, G2, and mitosis) but is absent from resting cells (G0), this result provided support for the notion that expression of LACTB caused responding cells to withdraw from the active cell cycle. Of the three non-tumorigenic cell lines tested (MCF10A, BJ-1, HME), only HME cells showed small but measureable (1.8 fold) decrease in EdU incorporation upon LACTB induction, while the two other cell lines were unaffected, showing that the LACTB-induced negative effect on cell proliferation is largely manifested in neoplastic cells (Fig. 2b).

We proceeded to introduce the mutant *R469K LACTB* allele that was discovered in MCF7ras cells into a doxycycline-inducible Tet/ON vector and monitored its effect on the growth of MCF7r and HMLER cells. R469K LACTB did not display any negative effect on growth of these cancer cells (Extended Data Fig. 3a). Of note, when wild-type LACTB was expressed in SUM159 and MDA-MB-231 cells, it had a negative effect on growth of SUM159 cells but not on the growth of MDA-MB-231 cells (Extended Data Fig. 3b). In summary, these and previous results showed that while a substantial majority of breast cancer cell lines exhibit down-regulated,

mutated and/or mis-localized LACTB, there are some breast cancer cell lines (such as MDA-MB-231) that seem to be immune to LACTB expression.

We then redirected our attention toward determining whether expression of LACTB in already-formed tumors exerted a negative effect on further tumor growth. To do so, we implanted MCF7ras, HCC1806 and HMLER cells orthotopically into fat pads of NOD/SCID mice and allowed the tumors to grow until they reached the exponential phase of growth with diameters of ~5-10mm. LACTB was then induced by the addition of doxycycline and tumor growth was monitored by *in vivo* imaging and by direct measurements. Tumors in which LACTB had been induced decreased significantly in size within 2-3 weeks of LACTB induction, with some tumors completely disappearing by 4 weeks of LACTB induction (Fig. 2c and Fig. 2d). In contrast, the control tumors in which LACTB was not induced showed no regression in size but instead continued to grow at a steady rate (Fig. 2c and Fig. 2d). Immunofluorescence studies of tissue sections showed a high proliferation index of the MCF7ras control tumor cells, as gauged by Ki-67 staining (80% positive), while cells expressing LACTB exhibited markedly lower Ki-67 expression (15% of cells staining positive) (Fig. 2e). This decrease in proliferation was accompanied by an increase in cleaved caspase-3 staining, indicative of apoptosis (Extended Data Fig. 3c).

Interestingly, H&E staining of these LACTB-exposed tumors showed a staining pattern that was very different from that of control tumors, particularly for the HMLER and MCF7ras tumors and to a lesser degree for the HCC1806 tumors. Control tumors contain large, poorly differentiated cells with little cytoplasm, relatively little stroma, and small areas of central

necrosis. In contrast, tumors expressing induced LACTB consisted of large areas of necrosis extending throughout the entire tumor, abundant stroma, and residual cancer cells that were smaller with a more differentiated, epithelial appearance (Extended Data Fig. 3d).

In order to extend the evidence that LACTB can play an active role in hindering tumorigenesis, we employed shRNA to down-regulate LACTB expression in the non-tumorigenic, hTERT-immortalized HME human mammary epithelial cells[17]. Two different *LACTB* shRNAs (L-3 and B-3) were chosen based on their LACTB knockdown efficiencies (86% and 90% respectively; Fig. 3a and Extended Data Fig. 4a). Decreased levels of LACTB in these HME cells (termed HME-shLACTB) resulted in a 2-fold reduction in proliferation relative to unmodified HME cells propagated in parallel (Fig. 3b). The tumorigenic abilities of the two resulting cell populations (denoted HME-shLACTB-L-3 and B-3) were gauged by orthotopic implantation into NOD/SCID hosts. Both cell populations failed to form tumors by 12 weeks post-implantation, indicating that LACTB down-regulation did not suffice, on its own, to transform these cells to a tumorigenic state (Fig. 3c).

Since loss of tumor suppressor gene function often requires concomitant expression of an oncogene in order for transformation to occur[17-21], we tested whether the concomitant knockdown of LACTB and introduction of an *H-RAS* (G12V) oncogene would make HME cells tumorigenic. Indeed, following orthotopic implantation, these cells formed tumors at 6 weeks post-injection (8/12 for L-3 shRNA and 4/12 for B-3 shRNA), whereas HME cells expressing only the introduced *H-RAS* (G12V) oncogene failed to form tumors by 12 weeks post-injection (Fig. 3c).

We also tested whether decreased levels of LACTB caused tumorigenesis when introduced together with an alternative oncogene. As seen in Fig. 3d and Fig. 3e, robust tumor growth was also observed when down-regulation of LACTB was coupled with up-regulation of an active *c-MYC* (T58A) oncogene but not when the decrease in LACTB was coupled with wild-type human HER2 over-expression. Moreover, expression of this *MYC* oncogene in HME cells without concomitant LACTB-down-regulation did not yield tumorigenic cells (Fig. 3d). The efficient knock-down of LACTB and forced expression of *H-RAS* (G12V), *c-MYC* (T58A) and *HER2* were confirmed by RT-PCR and Western blot analyses (Extended Data Fig. 4b, c). Hence, loss of LACTB can collaborate with a co-introduced activated oncogene to transform hTERT-immortalized human mammary epithelial cells to a tumorigenic state -- a stringent test for oncogenic activity.

LACTB mechanism

Our *in vitro* experiments revealed that carcinoma cells (HMLER, MCF7ras) that experienced and survived forced LACTB expression (for 3 days or more) exhibited a morphology that was quite different from their initial appearance. In particular, relative to control HMLER cells, HMLER cells in which LACTB was induced for either 3 days (acute stage of LACTB expression) or for two weeks (chronic LACTB expression) showed a more differentiated morphology characterized by tight epithelial cobblestone islands (Extended Data Fig. 5a). Staining for CD24 and EPCAM (markers of epithelial differentiation) and CD44 (a marker of more mesenchymal, stem-like cells[22-25]) revealed that those cells that experienced LACTB induction exhibited increased expression of markers of epithelial differentiation and decreased CD44 expression (Fig. 4a). RT-PCR-analysis confirmed that the cancer stem-cell marker ZEB1[26,27], as

well as the vimentin, fibronectin and N-cadherin mesenchymal markers, were all down-regulated in HMLER cells in which LACTB was induced (Fig. 4b). In contrast, epithelial markers, notably E-cadherin, ZO-1, as well as cytokeratins 8 and 14, were upregulated in these cells (Fig. 4b). These observations were further supported by immunofluorescence analyses confirming the up-regulation of epithelial markers and down-regulation of the ZEB1 and mesenchymal markers in HMLER cells in which LACTB expression was chronically induced (Fig. 4c).

Together, these observations converge on the notion that carcinoma cells that survive the induction of LACTB expression exit a more mesenchymal state and enter into a more differentiated, epithelial state, a transition that has previously been associated with lower representation of tumor-initiating/cancer stem cells (CSCs) and reduced tumorigenicity[28,29]. Of note, and as before, forced overexpression of LACTB in non-tumorigenic HME cells had no discernible effect on their morphology (Extended Data Fig. 5a), the levels of the CD24, CD44 and EPCAM markers (Fig. 4a), and a gene expression profile that monitored the mRNA expression levels of mesenchymal, epithelial and cancer stem-cell markers (Fig. 4b). When injected at limiting dilutions into fat pads of NOD/SCID mice, a decrease in tumor formation and tumor weight was seen in the more differentiated HMLER cells that experienced chronic LACTB induction relative to control HMLER cells in which LACTB had not been induced (Fig. 4d). Of note, the *in vitro* proliferation rates of these two cell lines were comparable (Extended Data Fig. 5b).

To distinguish whether LACTB expression led directly to the induction of epithelial differentiation, we used FACS to collect and single-cell clone the more mesenchymal, cancer stem

cell (CSC)-enriched $CD44^{high}/CD24^{low}$ cells from a population of HMLER-Tet/ON LACTB cells. LACTB expression was then induced in two of the resulting single-cell clones (HMLER-CD44+ cl.1 and cl.2) and effects on cells morphology and proliferation were monitored by live time-lapse imaging. In both clonal cell populations, those cells in which LACTB was induced proliferated more slowly and formed small epithelial islands within 3-4 days of LACTB expression, whereas the control cells retained their mesenchymal morphology (Fig. 4e, Extended Data Fig. 5c, Supplemental Movies 1-4). We then orthotopically implanted 10^6 control HMLER $CD44^{high}/CD24^{low}$ cells (in which LACTB expression had not been induced) as well as 10^6 HMLER-CD44+ cl.1 and cl.2 cells which had experienced chronic LACTB expression. Control tumors formed in these NOD/SCID hosts with 100% incidence (8/8), whereas HMLER-CD44+ cl.1 and cl.2 either failed to form tumors (0/8 for clone 1) or formed fewer tumors (4/8 for clone 2)(Fig. 4e). Similar effects on epithelial differentiation coupled with the loss of tumorsphere-forming and tumor-initiating ability were observed in MCF7ras cells forced to express LACTB (Extended Data Fig. 6a-e). Hence, LACTB was capable of inducing epithelial differentiation in carcinoma cells, which was associated with a decrease in their tumor-initiating ability.

We also tested expression of LACTB in other differentiating cell types; such as mesenchymal stem cells that were induced into osteocytic differentiation, and HME cells that were separated into $CD44^{high}/CD24^{low}$ stem-cell enriched population and $CD44^{low}/CD24^{high}$ differentiated epithelial population. In these differentiation models LACTB was increased in differentiated cells versus their non-differentiated counterparts (Extended Data Fig. 6f, g). This gives another support to our observation of involvement of LACTB in cellular differentiation.

As a further approach to discover more direct mechanism(s) of action of LACTB, we concentrated our attention on early time points (within 1 day) of LACTB induction. We reasoned that such time points would lead us to the immediate roles for LACTB in cancer cells while more delayed responses might represent secondary or tertiary effects of LACTB expression. Its mitochondrial localization suggested that it might constrain cancer cell proliferation either by suppressing ATP synthesis or modulating mitochondrial membrane potential, reactive oxygen species (ROS) production or mitochondrial biogenesis (mitogenesis). As shown in Extended Data Fig. 7a-c, we failed to detect any significant changes in ATP or ROS production or mitochondrial membrane potential in MCF7ras cells in which LACTB expression had been induced for up to 24 hours. We proceeded to co-mix wild type MCF7ras cells with MCF7ras-Tet/ON-LACTB cells and treated these cells for 24 hours with doxycycline to induce LACTB expression. Confocal microscopy was then used to monitor changes in mitochondrial numbers and localization within these cells. In fact, neither was observed to change in cells forced to over-express LACTB for 24 hours (Extended Data Fig. 7d). Moreover, during this period of time, the protein levels and localization of markers of mitochondrial fusion (OPA1, Mfn1 and Mfn2) and fission (Fis1, Drp1) did not change (Extended Data Fig. 7d). Similarly, the levels of individual components of the mitochondrial electron transport chain complexes did not appear to change with the possible exception of a slight increase in component NDUFB8 of Complex I in cells in which LACTB had been induced (Extended Data Fig. 7d). This is in agreement with the published observation that LACTB might affect the stability of mitochondrial Complex I[9]. However, since we observed no significant effects on mitochondrial membrane potential or ATP production, this change in NDUFB8 did not appear to signal an overall change in mitochondrial function including energy production. These results indicated that LACTB, at least during the initial periods of induced over-

expression in MCF7ras cells, did not appear to be directly involved in regulating ATP or ROS production, mitochondrial membrane potential or mitochondrial biogenesis. However, when these processes were assessed at later time points (3-6 days) they showed marked changes when compared to the control cells (Extended Data Fig. 7a-c and data not shown). We concluded these are the secondary, indirect effects of LACTB induction.

Since bioinformatics and transgenic mice studies have also linked LACTB to obesity and fatty acid metabolism[10,11], we also turned our attention to mitochondrial lipids. Liquid chromatography-tandem mass spectrometry (LC-MS) analysis of mitochondrial lipids showed significant changes in the quantities of lysophosphatidylethanolamines (LPE) and phosphatidylethanolamines (PE) during the initial induction of LACTB expression (24 hours) in the tumorigenic MCF7ras cells but not in non-tumorigenic HME cells (Fig. 5a, b; Table S2). The levels of other lipid classes, such as ceramides, di- and tri-acylglycerols and sphingomyelins, did not change in any of these cell lines (Fig. 5a, b; Supplemental Table S2). In particular, induction of LACTB for one day in MCF7ras cells led to decreased amounts of the 16:0, 18:0, 16:0/18:1 molecular species of LPE and PE, which are among the most abundant forms of LPE and PE in mitochondria, by 30-50%.

In order to determine whether the lower levels of LPE and/or PE species were physiologically consequential and whether they contributed to LACTB's negative effect on the proliferation of MCF7ras cells, we supplemented the culture medium of LACTB-exposed MCF7ras cell individually with these two lipids. Previous publications[30-32] showed that extracellular LPE, but not PE, can be efficiently transported into mitochondria where the LPE is

acylated to PE. Supplementation of the growth medium of LACTB-expressing MCF7ras cancer cells with 20μM LPE increased cell proliferation by 5-fold, thus partially reversing the reduction in cell proliferation imposed by LACTB (Fig. 5c). In contrast, cells supplemented with 50μM phosphatidylethanolamine, phosphatidylglycerol (PG) or lysophosphatidylcholine (LPC) failed to exhibit this effect (Extended Data Fig. 8a). Cancer cell proliferation did not increase when control MCF7ras cells, in which LACTB had not been induced, were supplemented with 20μM LPE, ruling out the possibility that LPE is a general growth stimulant in these cells (Fig. 5c). Moreover, EdU staining of MCF7ras cells in which LACTB had been induced in the presence of 20μM LPE exhibited a 50% higher proliferative capacity relative to control MCF7ras (Fig. 5d). These data provide support for the notion that a significant part of LACTB-induced negative proliferative effects on MCF7ras cells is mediated by decreased levels of LPE and/or PE.

We proceeded to determine whether LACTB-induced cancer cell differentiation and LACTB-induced modulation of lipid metabolism are two independent events or whether they are interconnected. Consequently, we induced LACTB expression in MCF7ras and HMLER cells that were supplemented with 20μM LPE and monitored the level of CD24 as a marker of cellular differentiation. As seen in Fig. 5e, MCF7ras and HMLER cancer cells in which LACTB was induced in the presence of supplemented LPE failed to increase the level of the CD24- differentiation marker relative to that in control cells in which LACTB was induced without LPE addition. These observations indicate that supplementation of these cancer cell lines with LPE upon LACTB expression can counteract the differentiation-inducing ability of LACTB.

In order to further identify downstream targets of LACTB's activity we hypothesized that mitochondrial proteins that are involved in phospholipid metabolism, notably LPE and PE, were involved in the anti-proliferative effects of LACTB. One such candidate was mitochondrial phosphatidylserine decarboxylase (PISD), an inner-mitochondrial-membrane enzyme that converts phosphatidylserine (PS) to phosphatidylethanolamine (PE)[33]. Wishing to examine the involvement of PISD in the mechanism-of-action of LACTB, we fractionated control MCF7ras cells and MCF7ras cells in which LACTB had been induced for 24 h into mitochondrial and cytosolic fractions and analyzed the amounts of PISD protein by immunoblotting. Fig. 6a and Extended Data Fig. 8b show that induced expression of LACTB was associated with strongly decreased levels of the PISD protein (by 60-95%) in mitochondria. The levels of several other mitochondrial membrane-localized lipid-metabolizing enzymes, such as phosphatidylglycerophosphate synthase 1 (PGS1) and phosphatidylglycerophosphatase (PGP), which are involved in the biosynthesis of cardiolipin, were not reduced by LACTB expression (Fig. 6a). This effect was the result of a post-transcriptional event, since PISD mRNA levels were not reduced upon LACTB induction (Extended Data Fig. 8c). Kinetic experiments, in which doxycycline was added to MCF7ras-Tet/ON-LACTB cells for different lengths of time, showed that PISD levels began to decrease at 24 hours of induced LACTB expression (Extended Data Fig. 8d).

In order to determine whether LACTB expression directly reduced PISD function in cells, we supplemented MCF7ras cells with [^{3}H] serine for up to 6 h and monitored the conversion of phosphatidylserine to phosphatidylethanolamine by PISD in both control MCF7ras cells and in MCF7ras cell in which LACTB was induced for 2 days. The cells in which LACTB had been induced showed a significantly reduced (by 60-80%) production of [^{3}H]PE from [^{3}H]PS, consistent

with our previous conclusion that the activity/stability of PISD is influenced by LACTB (Fig. 6b and Extended Data Fig. 8e). Of note, the amount of [^{3}H]PS was not altered by LACTB expression (Fig. 6b). This is in agreement with numerous reports showing that the overall phospholipid levels of cells, including those of PS, are very tightly regulated[34,35]. As such, when exogenous PS is added to cells, the rate of endogenous PS biosynthesis is quickly reduced in a compensatory manner.

In order to determine whether down-regulation of PISD exerted similar effects on MCF7ras cell biology as induction of LACTB, we designed four small interfering RNA duplexes (siRNA) to target PISD. All four siRNAs efficiently decreased the amount of PISD protein, as judged by Western blot analysis (Extended Data Fig. 8f). Transfection of the PISD-directed siRNA individually, but not the control siRNA, into MCF7ras cells significantly reduced (3-7 fold) the proliferative ability of MCF7ras cells as judged by EdU staining (Fig. 6c), as was also observed upon LACTB induction in MCF7ras cells. Moreover, LACTB induction coupled with siRNA-imposed PISD down-regulation did not lead to any further significant decreases in EdU staining when compared to cells in which LACTB was induced in the absence of siRNA silencing of PISD (Fig. 6d). This implied that the two effects were neither additive nor multiplicative, and that these two agents might operate in the same linear pathway. We concluded that the effects of LACTB on mitochondrial lipid metabolism derived largely from its effect on the PISD enzyme. Nonetheless, it is plausible that LACTB acts on more than one substrate and thus has more than one downstream effector. Down-regulation of PISD by DsiRNA (for 48 and 72 hours) was previously reported to lead to significant reductions in cellular proliferation and in ATP-synthesis[32]. This is in agreement

with our results shown in Fig. 2a and Extended Data Fig. 7a, confirming that LACTB induction phenotypically mimics down-regulation of PISD.

While LACTB is predicted from its structure to be a serine protease, its proteolytic activity has not been directly confirmed. LACTB is inhibited by Z-AAD-CMK[36], a known granzyme B inhibitor, which led us to predict that it might cleave peptide bonds adjacent to aspartic acid residues. Indeed, LACTB efficiently cleaved the fluorogenic peptide Ac-YVAD-AMC, but not the A-AMC or VP-AMC peptides, indicating that LACTB possesses proteolytic activity and can cleave peptide bonds adjacent to aspartic acid residues (Fig. 6e and Extended Data Fig. 9a). Based on this finding, we set out to examine whether the proteolytic function of LACTB and its mitochondrial localization were important for its tumor-suppressing effect. Accordingly, we generated one mutant form of LACTB protein in which a critical serine residue within its catalytic site was replaced by an isoleucine (dS-LACTB) and another mutant form of LACTB protein lacking mitochondrial localization sequence (d1-97 LACTB, partial aminoacid sequence in Extended Data Fig. 9b and as described in ref. 8). Immunofluorescence analysis showed the mislocalization of d1-97 mutant from mitochondria, while the catalytic serine mutant was still correctly localized to mitochondria (Extended Data Fig. 9c). Western blot analysis showed that these mutants were stably expressed upon doxycycline addition (Extended Data Fig. 9d). Expression of the d1-97 and the dS-LACTB mutant in tumorigenic MCF7ras cells showed 100% and 85% reduction in the ability of LACTB to negatively affect the growth of these cancer cells, respectively (Extended Data Fig. 9e). This indicated the importance of mitochondrial localization and of an active catalytic site for the efficient LACTB-induced negative effect on cancer cell proliferation.

We proceeded to test whether PISD down-regulation in the presence of induced LACTB was dependent on the intact catalytic activity of LACTB. Extended Data Fig. 9f demonstrates that PISD protein levels were unchanged when we induced expression of the catalytically inactive dS-LACTB in MCF7ras cells, indicating that the observed LACTB-induced down-regulation of PISD depends on a functional catalytic site of LACTB. Based on these findings, we mixed recombinant LACTB produced in HEK293 cells with permeabilized mitochondria isolated from MCF7ras cells to determine if LACTB cleaved PISD protein *in vitro*. We failed to see any direct degradation of PISD by LACTB (Extended Data Fig. 9g). However, the absence of an effect of LACTB on PISD protein was difficult to interpret, given our inability to know the precise conditions in which these proteins interact *in vivo.*

We proceeded to examine whether the LACTB-induced decrease in PISD was specific for MCF7ras cells or whether a similar reduction occurred in other non-tumorigenic and breast cancer cell lines. Fig. 6f shows that PISD levels were similarly reduced in response to LACTB induction in tumorigenic HMLER, HCC38, HS578t and to a lesser degree HCC1806 cell lines, but not in the SUM149 breast cancer and the non-tumorigenic HME and MCF10A mammary cell lines. These data indicate that the decrease in the amount of PISD by LACTB might represent a mechanism-of-action of LACTB shared by several, but perhaps not all, cancer cells and that this reduction in PISD does not occur in the non-tumorigenic cell lines tested.

DISCUSSION

Our report describes a novel tumor suppressor gene and protein and a novel mechanism of the control of the neoplastic state. We show using *in vivo*, *in vitro* and clinical

studies, that LACTB which normally resides within the intermembrane space of mitochondria, is a potent inhibitor of the proliferation of breast cancer cells. We show that LACTB has the ability to perturb mitochondrial lipid metabolism and, through such reprogramming, to modulate the differentiation state of cancer cells. This is achieved via the novel LACTB-PISD-LPE/PE axis (Extended Data Fig.10 Graphical Abstract).

Mitochondrial phospholipids are important building blocks of mitochondrial membranes and perturbation of PE/LPE might influence many processes dependent on the proteins and receptors within these membranes. Since LPE is a precursor of PE within mitochondria, our work does not distinguish between the reduction in PE, LPE, or both as inciting cause(s) for cancer cell differentiation. In fact, some reports have linked LPE to cell differentiation. For example, LPE-acyltransferase, the mitochondrial enzyme responsible for synthesis of PE from LPE, has been reported to have a role in cardiac muscle differentiation[37]. LPE also appears to modulate differentiation of neuronal PC12 cells[38]. It is plausible that changes in the representation of various mitochondrial phospholipids are required for the differentiation of dedifferentiated epithelial cells and that a transient change in the ratio of these mitochondrial phospholipids might initiate the process of differentiation. Our study has identified new vulnerabilities in cancer biology and opened new windows of exploration, the research of which might ultimately lead to the development of novel cancer therapeutics.

Experimental Procedures

Cell Culture and reagents

All cells were cultured in a 5% CO2 humidified incubator at 37° C. Cell lines, growth media and sources are described in Table S3. For activating tetracycline-inducible gene expression, the cells were treated with 1μg/ml doxycycline hyclate (Sigma-Aldrich) in media. Fresh doxycycline was added every 3 days.

Muscle Progenitor Cell and Mesenchymal Stem Cell (MSC)

C2C12 mouse myoblast cells (ATCC) were cultured in DMEM+15% FBS. For differentiation of C2C12 cells media were changed to DMEM+2% horse serum. Media was changed every 3 days and differentiation occurred around days 4-6. Human progenitor muscle cells (Cell Applications 151-25a) were grown and differentiated according to manufacturer's protocol.

MSCs were obtained from reduction mammoplasty samples, where the adipose tissue was separated from the dense collagen fibers containing the mammary epithelium, using modified protocol based on[39]. Briefly, 1g pieces of adipose tissue were suspended in HBSS containing 2 mg/ml collagenase type I (Invitrogen) and 4 mg/ml BSA and agitated for 1 hour at 37°C. The suspension was filtered through a 200-μm sieve and allowed to stand for 15 minutes to permit adipocytes to rise to the top of the solution. Cell suspensions were then centrifuged at 500 *g* for 5 minutes to pellet the stromal/vascular cells. Adipocytes and supernatant were removed by aspiration. The stromal vascular fraction was washed three times with HBSS/3%BSA and then plated in Mesenchymal Stem Cell Medium (Sciencell Research Laboratories # 7501) at a density of 2 × 106 cells/ml. MSCs were differentiated for 18 days (media changed every 3 days) in DMEM+10% IFS supplemented with 1 μM dexamethasone (Sigma **D4902)**, 10 mM β-glycerophosphate (Westnet # BP-435), 200 μM

ascorbic acid (Sigma Aldrich # A4544). The osteogenic differentiation was examined by staining with Alizarin Red reagent (Sciencell Research Laboratories # 0223) according to manufacturer's protocol. The efficiency of osteocytic differentiation was around 40%.

Animals

All animal experiments were performed with female virgin NOD/SCID mice (non-obese diabetic/severe combined immunodeficiency). Mice were 2-4 months of age at time of injections. A colony of NOD-SCID mice was maintained in-house. All research involving animals complied with protocols approved by the MIT Committee on Animal Care.

Viral vectors and infection

Human LACTB cDNA was purchased from Open Biosystems # MHS1010-98051227. REEP1 cDNA was purchased from Open Biosystems # MHS1010-98051276. CAP2, SMPX and PDLIM3 cDNAs were obtained by reverse transcription PCR from differentiated human muscle cells using primers described in Table S4. R469K-LACTB cDNA was obtained by reverse transcription PCR from MCF7ras cells using primers for LACTB described in Table S4. All cDNAs were then subcloned into the FUW-LPT2 tetracycline-inducible lentiviral vector (modified from FUW-tetO by Kong-Jie Kah) with puromycin resistance gene. dS-LACTB was generated by mutating the serine residue in position 164 to isoleucine using primers described in Table S4 and then subcloned into FUW-LPT2 tetracycline-inducible lentiviral vector. d1-97-LACTB was generated by PCR using primers described in Table S4; it is starting with methionine as amino-acid position number 97. c-MYC T58A was purchased from Addgene #18773. RAS-IRES-GFP was purchased from Addgene #18780. Human pWPXL-HER2 plasmid was a kind gift from Wenjun Guo (Albert Einstein College of Medicine, New

York). pMMP-LucNeo, carrying coding sequences for luciferase and neomycin phosphotransferase, were obtained from Dr. Segal[40]. To down-regulate LACTB expression we used shLACTB L-3 (Open Biosystems # TRCN0000046625) and shLACTB B-3 (Broad Institute TRC shRNA library # TRCN0000296726). Both shRNAs are cloned in pLKO.1 lentiviral vector with puromycin selection marker. Empty pLKO.1 vector was used as a control.

For lentiviral infection, cells were seeded at 30% confluency in 10cm dish and transduced 24 hours later with virus in the presence of 5 μg/ml polybrene (EMD Millipore # TR-1003-G). Cells were then selected by relevant selection marker.

We found the doxycycline-inducible FUW-LPT2 vector to be a little leaky; minimal amounts of cloned gene were expressed even in the absence of doxycycline (as judged by RT-PCR analysis). While this leakiness never had any physiological significance for short term experiments, keeping such cells for a long time in tissue culture might lead to a change in physiology of these cells. Therefore, as a precaution, we never kept cell lines transduced with FUW-LPT2+cloned factor in tissue culture for longer than two months. After two months, the cell lines were discarded and the new ones were freshly transduced with FUW-LPT2+cloned factor vector and selected with proper selection marker.

siRNA and transfection

Four dsiRNA duplexes against human *PISD* gene were designed and purchased from Integrated DNA Technologies.

dsiRNA-PISD-1sense: rCrCrArCrCrArUrCrGrUrGrCrUrCrArUrCrUrUrCrGrArGGC

dsiRNA-PISD-2sense: rCrCrUrArCrArArUrGrArCrUrUrCrArGrCrUrUrCrGrUrGAC

dsiRNA-PISD-3sense: rCrArArUrCrArGrGrUrGrGrArGrCrUrGrCrCrArCrArCrUGG

dsiRNA-PISD-4sense: rGrCrArGrGrGrUrGrGrCrUrUrUrGrUrArCrArArGrUrCrAGT

Premade negative control dsiRNA was purchased from Integrated DNA Technologies (DS NC1, 180683394). Cells were plated in 10-cm dishes and next day transfected with Lipofectamine 2000 (ThermoFisher) according to manufacturer's protocol. Analyses were performed 48 hours after transfection.

Tumor cell injections

For orthotopic tumor transplantations, cells were resuspended in 20µl of 50%Matrigel and injected into mammary fat pads of female NOD-SCID mice. The *in vivo* doxycycline treatment was administered through drinking water containing 2 mg/ml doxycycline and 10 mg/ml sucrose. The tumor incidence and weight were measured 2-3 months post injection. For limiting dilution analyses, the frequency of cancer stem cells in the cell population being transplanted was calculated using the Extreme Limiting Dilution Analysis Program (http://bioinf.wehi.edu.au/software/elda/index.html)

***In vivo* mouse imaging**

Bioluminescence imaging of luciferase activity was used to monitor tumor growth with a Xenogen IVIS system under 2.5% isoflurane anesthesia at the indicated time points. Imaging of mice was performed by injection of D-luciferin (165mg/kg of body weight, intraperitoneal injection; Caliper Life Sciences) 10 minutes before bioluminescence imaging. Images were analyzed using Living Image Software version 4.3.1 (Caliper Life Sciences).

Immunofluorescence (tissues, cells)

Tumors were fixed in 10% neutral buffered formalin overnight and embedded in paraffin for sectioning. Sections were cut at 5µm. Tumor sections were deparaffinized in Xylene and antigen retrieval was performed in Target Retrieval Solution (Dako # S1700) using a microwave. Background was ten reduced using ImmunoStain Blocker Solution (GeneTex # GTX73323) for one hour at room temperature. Sections were then blocked with 2% normal horse serum in PBS for one hour at room temperature. Sections were incubated with primary antibody at 4^0C overnight. The type, source and dilution of antibodies are described in Table S5. After three washes with PBS, sections were incubated with secondary antibodies (AlexaFluor, Invitrogen, 1:500) for one hour at room temperature, washed three times with PBS, and mounted on glass microslides (VWR#48312-002) in Prolong gold antifade reagent with DAPI (Life Technologies # P36931) and let dry overnight at room temperature in dark.

Cultured cells were seeded on sterilized glass round slides inside 10-cm Petri dishes with cell culture media. Once cells reached a sufficient density, glass slides were transferred into individual wells of 6-well dish and subsequent processing was done in this format at room temperature unless otherwise stated. Cells were washed in PBS, fixed in 10% formalin for 10 minutes, washed once in PBS, permeabilized with PBS+0.1% Triton-X for 10 minutes, washed 3x10 minutes in PBS and incubated in 5% horse serum for 1 hour. Cells were then incubated in specific primary antibodies at 4^0C overnight, washed three times with PBS, then incubated with secondary antibodies for 1 hour at room temperature. After three washes with PBS, stained cells were mounted on glass microslides (VWR#48312-002) in Prolong gold antifade reagent with DAPI (Life Technologies # P36931) and let dry overnight at room temperature in dark. The type, source and dilution of antibodies are described in Table S5.

Immunostained samples were imaged and analyzed using Zeiss RPI Spinning Disc Confocal microscope with MetaMorph Software or Perkin Elmer Spinning Disc Confocal microscope with Volocity software.

Western Blot

Proteins were extracted from cells using RIPA buffer (Sigma Aldrich # R0278) always in the presence of Protease (Roche Diagnostics # 11836153001) and Phosphatase (Roche Diagnostics # 04906845001) Inhibitors. Human Skeletal Myoblast lysate was purchased from ZenBio # TCE-SKB and lysate from differentiated human skeletal myotubes was purchased from ZenBio # TCE-SKM. Approximately 10-20µg of protein lysate was loaded on the gels. Western blots and transfers were done using standard protocols. Horseradish peroxidase-conjugated secondary antibodies were used (Cell Signaling, 1:5000). Blots were developed using ECL (Dura or Femto, Thermo Scientific). The type, source and dilution of antibodies are described in Table S5.

Western Blot analysis related to [^{3}H]serine labeling of phospholipids was performed by loading sample proteins on a 10% gel, then transferring the proteins to polyvinylidene difluoride membranes and blocking in 1% milk. The antibodies and their dilutions are described in Table S5. HRP substrate is Luminata Forte (Millipore) and images were collected on G:BOX with Syngene software.

Quantitative RT-PCR

Total RNA was isolated directly from cultured cells using the RNeasy Plus Mini kit (Qiagen # 74136). Reverse transcription was performed with High Capacity cDNA Reverse Transcription Kit (Life Technologies # 4368814). mRNA levels were measured with gene-specific primers using the SYBR

Green I master mix (Roche) on a Roche LightCycler 480 system (Roche). Relative expression levels were normalized to GAPDH. The PCR primer sequences are listed in Table S4.

Clinical data in human breast tissues

LACTB expression was studied on 808 patient samples assembled on a tissue microarray as previously described[41]. The study was approved by the ethical committee of the Kanton Zürich under reference number KEK-ZH-Nr. 2014-0604. Tumor tissue was immunohistochemically stained using the LACTB polyclonal antibody (Proteintech Group, dilution 1:200) on an automated immunostaining platform (Leica BOND, Wetzlar, Germany). Immunohistochemical intrinsic subtyping of the cohort was performed as previously described[42]. LACTB expression was analyzed as no expression or lower than in normal tissues (scores 0, 1) and normal expression in the luminal or basal compartment (scores 2, 3). Statistical analysis was performed with SPSS statistical package version 21 (IBM P-values < 0.05 were considered statistically significant).

Flow Cytometry (Edu, Annexin, ROS and Mitochondrial Membrane Potential)

Cells were trypsinized and filtered through 40μm cell strainers to obtain single cells. Cells were then labeled for flow cytometry by 1 hour incubation with dye-conjugated antibodies and washed once in PBS. The list of antibodies, their source and dilution is in Table S5. Samples were sorted on a BD FACSAriaII sorter and analyzed using BD FACSDiva Software (BD Biosciences).

Click-iT EdU Alexa Fluor 647 Flow Cytometry Assay Kit (Life Technologies # C10424) was used for Edu staining according to manufacturer's protocol.

ANXN V-PE Apoptosis Detection Kit (BD Biosciences # 559763) was used for annexinV staining according to manufacturer's protocol.

MitoProbe DiIC 1 (5) Assay Kit (Life Technologies # M34151) was used for mitochondrial membrane potential staining according to manufacturer's protocol.

DCFDA - Cellular Reactive Oxygen Species Detection Assay Kit (Abcam # ab113851) was used for ROS measurement according to manufacturer's protocol.

ATP measurement

ATP levels within cells were assessed using the CellTiter-Glo Luminescent Cell Viability Assay (Promega # G7572) according to manufacturer's protocol. 1000-3000 cells were seeded in a flat bottom 96-well plate. Four replicates were plated for each time point.

Soft agar colony formation assay (tumorspheres)

Growth in soft agar was performed as described in[43].

Subfractionation and Mitochondrial Isolation

Cells were harvested and mitochondria isolated using the Qproteome Mitochondria Isolation Kit (Qiagen # 37612) for mitochondrial lipid composition analysis or Cell Fractionation Kit (Abcam # ab109719) for Western Blot subfractionation experiments. Isolated mitochondria were frozen at -80°C. The Cell Fractionation Kit was also used for isolating cytosolic fractions.

Permeabilized Mitochodria: Mitochondria isolated using Qproteome Mitochondria Isolation Kit were incubated in hypotonic 100 mM HEPES (pH 7.0-7.6) solution (Sigma # H0887) with or without 150 mM NaCl.

Mitochondrial Lipid Extraction

Frozen mitochondria in eppendorf tubes were thawed on ice, after which 600µl LC/MS grade 100% methanol, 300µl LC/MS grade water, 400µl chloroform (without amylenes) were added in this order. Samples were vortexed for 10 min at 4°C and centrifuged at 13000 RPM for 10 min at 4°C. The lower lipid-containing layer was then carefully collected and dried for 1 h. Lipid extracts were stored at -80°C.

Liquid Chromatography/Mass Spectrometry

Lipid extracts were separated on an Ascentis Express C18 2.1 x 150 mm 2.7µm column (Sigma-Aldrich, St. Louis, MO) connected to a Dionex UltiMate 3000 UPLC system and a QExactive benchtop orbitrap mass spectrometer (Thermo Fisher Scientific, San Jose, CA) equipped with a heated electrospray ionization (HESI) probe. Dried lipid samples were typically dissolved in 50µl 65:30:5 acetonitrile:isopropanol:water (v/v/v) and 5µl was injected into the LC/MS, with separate injections for positive and negative ionization modes. Mobile phase A in the chromatographic method consisted of 60:40 water/acetonitrile in 10mM ammonium formate and 0.1% formic acid, and mobile phase B consisted of 90:10 isopropanol/acetonitrile, also with 10 mM ammonium formate and 0.1% formic acid. The chromatographic gradient was described previously[44]. The column oven and autosampler tray were held at 55°C and 4°C, respectively. The MS instrument parameters were as described previously[45] and modified by[46]. The spray voltage was set to 4.2 kV, and the heated capillary and the HESI were held at 320°C and 300°C, respectively. The S-lens RF level was set to 50, and the sheath and auxiliary gas were set to 35 and 3 units, respectively. These conditions were held constant for both positive and negative ionization mode acquisitions. External mass calibration was performed using the standard calibration mixture every 7 days. MS spectra of lipids were acquired in full-scan /

data-dependent MS^2 mode. For the full scan acquisition, the resolution was set to 70,000, the AGC target was 1e6, the maximum integration time was 50 msec, and the scan range was m/z = 133.4-2000. For data-dependent MS^2, the top 10 ions in each full scan were isolated with a 1.0 Da window, fragmented at stepped normalized collision energy of 15, 25, and 35 units, and analyzed at a resolution of 17,500 with an AGC target of 2e5 and a maximum integration time of 100 msec. The underfill ratio was set to 0. The selection of the top 10 ions was subject to isotopic exclusion, a dynamic exclusion window of 5.0 sec, and an exclusion list of background ions based on a solvent blank.

High-throughput identification and relative quantification of lipids was performed separately for positive and negative ionization mode data, using LipidSearch software (Thermo Fisher Scientific / Mitsui Knowledge Industries) with the default parameters for QExactive Product Search and Alignment. After alignment, raw peak areas for all identified lipids were exported to Excel and filtered according to the following pre-determined quality control criteria: Rej ("Reject" parameter calculated by LipidSearch software) equal to 0; PQ ("Peak Quality" parameter calculated by LipidSearch software) greater than 0.85; CV (standard deviation / average peak area across triplicate injections of a representative [pooled] biological sample) below 0.4; R (linear correlation across a three-point dilution series of the representative [pooled] biological sample) greater than 0.9. Typically ~70% of identified lipids passed all four quality control criteria. Raw peak areas of the filtered lipids were added to generate a "total lipid signal" for each sample, and individual lipid peak areas were normalized to this total signal as a control for extraction efficiency and sample loading. These normalized lipid abundances from control and LACTB-expressing cells were used to calculate fold changes and p-values (Student's t-test, two-tailed, unequal variance) upon LACTB expression. After

this calculation, positive and negative ionization mode data were combined to generate Fig. 6A and 6B.

Lipid Supplementation

All lipids were purchased from Avanti Polar Lipids: lysophosphatidylethanolamine (LPE, VWR # 100123-538), lysophosphatidylcholine (LPC, Avanti Polar Lipids # 830071P), phosphatidylethanolamine (PE, VWR # 100127-544), phosphatidylglycerol (PG, VWR # 100123-722). A stock solution (25mM) of LPE was prepared either by dissolving LPE powder in distilled water and subsequent sonication as described in[47], or by dissolving LPE in chloroform:methanol:water (65:35:8, v:v) as advised by Avanti Lipids. Stock solutions of LPC, PE and PG (25-100nM) were made by dissolving these lipids in chloroform:methanol:water (65:35:8) (v:v) as advised by Avanti Lipids. The lipids were replenished every 1 to 3 days.

Time lapse imaging

Cells were plated sparsely in 12-well plates. If doxycycline was added, it was added 1 h before imaging. Cells were monitored with 10x objective using Nikon TE2000 automated inverted microscope with incubation enclosure (37^0C, 5%CO2). MetaMorph acquision software was used to analyze the data.

Recombinant LACTB preparation

The open-reading frame encoding LACTB was transferred into a Gateway-compatible version of the pCLNCX vector (Imgenex) containing C-terminal FLAG and His tags, and HEK293T cells were infected according to the manufacturer's instructions. Cells were grown in DMEM with 10% fetal

bovine serum at 37°C with 5% CO_2. Infected cells were selected with media containing hygromycin (100μg/mL) and grown to 100% confluency (10 × 15 cm plates total). For isolation of LACTB, cells were washed two times with PBS and scraped. Cell pellets were then isolated by centrifugation at 1,400 × *g* for 3 min. The pellets were resuspended in RIPA buffer (5mL, Cell Signaling Technology), sonicated, and debris was removed by centrifugation at 12,000 × *g* for 15 min. LACTB was then captured by incubation overnight with 300μL of Anti-FLAG M2 affinity gel (Sigma). The agarose gel was washed three times with PBS (5mL), and LACTB was eluted with 1mL of 150ng/μL solution of 3X FLAG peptide (Sigma) in PBS. Protein was then concentrated (and FLAG peptide removed) using an ultra-centrifugal filter unit (Amicon, 30kDa cut-off) according to manufacturer's instructions. Protein concentration was determined using a protein assay kit (Bio-Rad). Glycerol was added to a final concentration of 10%, and proteins were aliquoted stored at -80 °C until use.

LACTB *in vitro* substrate assay

LACTB (15nM final concentration) was added to 96-well black, clear-bottom plate (Costar # 3603) in 99μL PBS. Substrates were dissolved in DMSO at 100x indicated concentration (see below) and 1μL was added to each well. Reactions were incubated for 1 h at 25°C while been read on a Spectramax M5 plate reader (Molecular Devices) using an excitation wavelength of 380 nm and an emission wavelength of 460nm. To test for cleavage of the substrates Ac-YVAD-AMC, A-AMC, and VP-AMC, a final concentration of 100μM of each substrate was used. To assess kinetics of Ac-YVAD-AMC cleavage, final substrate concentrations of 100, 33, 11, 3.7, 1.23, 0.41, and 0.14μM were used. The initial reaction velocities for each concentration were fit to a nonlinear regression (Prism software).

Related to Extended Data Fig. 9g: Recombinant LACTB (0.2 µg) was mixed with perforated mitochondria (1 µg) in PBS and incubated at 25°C for 2 hours.

[^{3}H]serine labeling of phospholipids in cells

MCF7ras and MCF7ras-Tet/ON-LACTB cells were plated on 6-cm dishes and treated with doxycycline for 48 hours. Pulse medium (20ml DMEM + 10µl dox + 100µl [^{3}H]serine) was then added for 2, 4 and 6 h. The [^{3}H-serine] was purchased from Perkin Elmer (250uCi/ 250 µl). Cells were harvested, lysed and lipids were extracted and dried. The resuspended lipid extract (50/75µl) was applied to thin-layer chromatography plates (Millipore) and separated in the solvent system chloroform:methanol:acetic acid:formic acid:water (70:30:12:4:1, v:v). Bands corresponding to standard PS and PE were scraped from the plates and radioactivity was measured by scintillation counting after overnight incubation at room temperature. The experiment was performed in triplicate.

Microarray analysis

The microarrays used were Human and Mouse Agilent 4x44k arrays. Arrays were scanned using an Agilent scanner and the data was extracted using Agilent's Feature Extraction software. Agilent two-color arrays were normalized within-array by loess and between-arrays by quantile normalization of average intensities (Aquantile), as implemented by the limma package in Bioconductor. Replicate spots were averaged and then mean-centered to obtain log ratios. Human and mouse orthologs were obtained from Ensembl BioMart and Homologene.

Proliferation assay

Proliferation of cells was assessed using the WST-1 Cell Proliferation Reagent (Roche Diagnostics # 11644807001) according to manufacturer's protocol. Cells (1000-3000) were seeded in a flat bottom 96-well plate. Four replicates were plated for each time point.

Proliferation of cells was also assessed by seeding cells in 10-cm Petri dishes and trypsinization and manual counting of cells, using either haemocytometer or Vi-CELL XR Cell Viability analyzer (Beckman Coulter), at indicated time points.

Statistical analysis

All the data are presented as the mean ± standard errors of mean (SEM) unless otherwise specified. An unpaired two tailed Student's t-test was used to calculate the p values except as otherwise specified. $p<0.05$ was considered significant.

Abbreviations are described in Table S6.

EXTENDED REFERENCES (related to Methods)

39. Crossno, J.T. Jr, Majka, S.M., Grazia, T., Gill, R.G., & Klemm, D.J. (2006). Rosiglitazone promotes development of a novel adipocyte population from bone marrow-derived circulating progenitor cells. *J Clin Invest.* **116(12)**, 3220-3228.
40. Rubin, J.B. *et al* (2003). A small-molecule antagonist of CXCR4 inhibits intracranial growth of primary brain tumors. *Proc Natl Acad Sci U S A* **100(23)**, 13513-13518.
41. Theurillat, J.P. *et al* (2007). NY-ESO-1 protein expression in primary breast carcinoma and metastases: correlation with CD8+ T-cell and CD79a+ plasmacytic/B-cell infiltration. *Int J Cancer* **120(11)**, 2411-2417.

42. Goldhirsch, A. *et al* (2011). Strategies for subtypes--dealing with the diversity of breast cancer: highlights of the St. Gallen International Expert Consensus on the Primary Therapy of Early Breast Cancer 2011. *Ann Oncol.* **22(8)**, 1736-1747.

43. Cifone, M.A., & Fidler, I.J (1980). Correlation of patterns of anchorage-independent growth with in vivo behavior of cells from a murine fibrosarcoma. *Proc Natl Acad Sci U S A*, **77(2)**, 1039-1043.

44. Hu, C. *et al* (2008). RPLC-ion-trap-FTMS method for lipid profiling of plasma: method validation and application to p53 mutant mouse model. *J Proteome Res.* **7(11)**, 4982-4991.

45. Bird, S.S., Marur, V.R., Sniatynski, M.J., Greenberg, H.K., & Kristal, B.S. (2011). Serum lipidomics profiling using LC-MS and high-energy collisional dissociation fragmentation: focus on triglyceride detection and characterization. *Anal Chem* **83(17)**, 6648-6657.

46. Ruzicka, J., McHale, K.J., & Peake, D.A. Data acquisition parameters optimization of quadrupole orbitrap for global lipidomics on LC-MS/MS time frame. Poster MP243 presented at 2014 American Society for Mass Spectrometry Annual Meeting, Baltimore, MD, June 15-20, 2014.

47. Park, K.S. *et al* (2007). Lysophosphatidylethanolamine stimulates chemotactic migration and cellular invasion in SK-OV3 human ovarian cancer cells: involvement of pertussis toxin-sensitive G-protein coupled receptor. *FEBS Lett.* **581(23)**, 4411-4416.

REFERENCES

1. Lassar, A.B., Skapek, S.X., & Novitch, B. (1994). Regulatory mechanisms that coordinate skeletal muscle differentiation and cell cycle withdrawal. *Curr Opin Cell Biol.* **6(6),** 788-794.
2. Walsh, K., & Perlman, H. (1997). Cell cycle exit upon myogenic differentiation. *Curr Opin Genet Dev.* **7(5)**, 597-602.
3. Seely, S. (1980). Possible reasons for the high resistance of muscle to cancer. *Med Hypotheses.* **6(2)**, 133-137.
4. Kasid, A., Lippman, M. E., Papageorge, A. G., Lowy, D. R. & Gelmann, E. P. (1985). Transfection of v-rasH DNA into MCF-7 human breast cancer cells bypasses dependence on estrogen for tumorigenicity. *Science* **228**, 725-728.
5. Smith, T.S. *et al* (2001). Identification, genomic organization, and mRNA expression of LACTB, encoding a serine beta-lactamase-like protein with an amino-terminal transmembrane domain. *Genomics* **78(1-2)**, 12-14.
6. Peitsaro, N. *et al* (2008). Evolution of a family of metazoan active-site-serine enzymes from penicillin-binding proteins: a novel facet of the bacterial legacy. *BMC Evol Biol.* **8**, 26.
7. Mootha, V.K. *et al* (2003). Integrated analysis of protein composition, tissue diversity, and gene regulation in mouse mitochondria. *Cell* **115(5)**, 629-640.
8. Polianskyte, Z. *et al* (2009). LACTB is a filament-forming protein localized in mitochondria. *Proc Natl Acad Sci U S A.* **106(45)**, 18960-18965.
9. Pagliarini, D.J. *et al* (2008) A mitochondrial protein compendium elucidates complex I disease biology. *Cell* **134(1)**, 112-123.
10. Chen, Y. *et al* (2008). Variations in DNA elucidate molecular networks that cause disease. *Nature* **452(7186)**, 429-435.

11. Yang, X. *et al* (2009) Validation of causal genes for obesity that affect shared metabolic pathways and networks. *Nat Genet* **41**, 415-423.

12. Kim, S.C. *et al* (2006). Substrate and functional diversity of lysine acetylation revealed by a proteomics survey. *Mol Cell* **23**, 607-618.

13. Lee, J. *et al* (2007). Mitochondrial Phosphoproteome Revealed by an Improved IMAC Method and MS/MS/MS. *Mol Cell Proteom* **6**, 669-676.

14. Bogert van den, C., Holtrop, M., Melis, T.E., Roefsema, P.R., & Kroon, A.M. (1987). Different effects of oxytetracycline and doxycycline on mitochondrial protein synthesis in rat liver after long-term treatment. *Biochem Pharmacol* **36(9)**, 1555-1559.

15. Ahler, E. *et al* (2013). Doxycycline alters metabolism and proliferation of human cell lines. *PLoS One **8(5)***, e64561.

16. Moullan, N. *et al* (2015). Tetracyclines Disturb Mitochondrial Function across Eukaryotic Models: A Call for Caution in Biomedical Research. *Cell Rep.* **15** 180-181.

17. Elenbaas, B. *et al* (2001). Human breast cancer cells generated by oncogenic transformation of primary mammary epithelial cells. *Genes Dev.* **15(1)**, 50-65.

18. Hahn, W.C. *et al* (1999). Creation of human tumour cells with defined genetic elements. *Nature* **400(6743)**, 464-468.

19. DuPage, M., Dooley, A.L., & Jacks, T. (2009). Conditional mouse lung cancer models using adenoviral or lentiviral delivery of Cre recombinase. *Nat Protoc.* **4(7)**, 1064-1072.

20. Feldser, D.M. *et al* (2010). Stage-specific sensitivity to p53 restoration during lung cancer progression. *Nature* **468(7323)**, 572-575.

21. McFadden, D.G. *et al* (2014). p53 constrains progression to anaplastic thyroid carcinoma in a Braf-mutant mouse model of papillary thyroid cancer. *Proc Natl Acad Sci U S A*. **111(16)**, E1600-1609.

22. Al-Hajj, M., Wicha, M.S., Benito-Hernandez, A., Morrison, S.J., & Clarke, M.F. (2003). Prospective identification of tumorigenic breast cancer cells. *Proc Natl Acad Sci U S A* **100**,
3983-3988.

23. Mani, S.A. *et al* (2008). The epithelial-mesenchymal transition generates cells with properties of stem cells. *Cell* **133**, 704-715.

24. Blick, T. *et al* (2010). Epithelial mesenchymal transition traits in human breast cancer cell lines parallel the CD44(hi/)CD24 (lo/-) stem cell phenotype in human breast cancer. *J Mammary Gland Biol Neoplasia* **15(2)**, 235-252.

25. Chaffer, C.L. *et al* (2011). Normal and neoplastic nonstem cells can spontaneously convert to a stem-like state. *Proc Natl Acad Sci U S A* **108**, 7950-7955.

26. Wellner, U. *et al* (2009). The EMT-activator ZEB1 promotes tumorigenicity by repressing stemness-inhibiting microRNAs. *Nat Cell Biol.* **11(12)**, 1487-1495.

27. Chaffer, C.L. *et al* (2013). Poised chromatin at the ZEB1 promoter enables breast cancer cell plasticity and enhances tumorigenicity. *Cell* **154**, 61-74.

28. Thiery, J.P., Acloque, H., Huang, R.Y., & Nieto, M.A. (2009). Epithelial-mesenchymal transitions in development and disease. *Cell* **139**, 871–890.

29. Biddle, A., & Mackenzie, I.C. (2012). Cancer stem cells and EMT in carcinoma. *Cancer Metastasis Rev.* **Feb 3**.

30. Riekhof, W. R., & Voelker, D. R. (2006). Uptake and utilization of lysophosphatidylethanolamine by Saccharomyces cerevisiae. *J. Biol. Chem.* **281**, 36588-36596.

31. Riekhof, W. R., Wu, J., Jones, J. L., & Voelker, D. R. (2007). Identification and characterization of the major lysophosphatidylethanolamine acyltransferase in Saccharomyces cerevisiae. *J. Biol. Chem.* **282**, 28344-28352.

32. Tasseva, G. *et al* (2013). Phosphatidylethanolamine deficiency in Mammalian mitochondria impairs oxidative phosphorylation and alters mitochondrial morphology. *J Biol Chem.* **288(6)**, 4158-4173.

33. Vance, J.E., & Tasseva, G. (2013). Formation and function of phosphatidylserine and phosphatidylethanolamine in mammalian cells. *Biochim Biophys Acta.* **1831(3)**, 543-554.

34. Nishijima, M., Kuge, O., & Akamatsu, Y. (1986). Phosphatidylserine biosynthesis in cultured Chinese hamster ovary cells. I. Inhibition of de novo phosphatidylserine biosynthesis by exogenous phosphatidylserine and its efficient incorporation. *J Biol Chem.* **261(13)**, 5784-5789.

35. Kuge, O., Hasegawa, K., Saito, K., & Nishijima, M. (1998). Control of phosphatidylserine biosynthesis through phosphatidylserine-mediated inhibition of phosphatidylserine synthase I in Chinese hamster ovary cells. *Proc Natl Acad Sci U S A.* **95(8)**, 4199-4203.

36. Bachovchin, D.A. *et al* (2014). A high-throughput, multiplexed assay for superfamily-wide profiling of enzyme activity. *Nat Chem Biol.* **10(8)**, 656-663.

37. Fotheringham, J. *et al* (2000). Lysophosphatidylethanolamine acyltransferase activity is elevated during cardiac cell differentiation. *Biochim Biophys Acta.* **1485(1)**, 1-10.

38. Nishina, A. *et al* (2006). Lysophosphatidylethanolamine in Grifola frondosa as a neurotrophic activator via activation of MAPK. *J Lipid Res.* **47(7)**, 1434-1443.

FIGURE LEGENDS

Figure 1: LACTB down-regulation in cancer cells.

(a) Detection of endogenous LACTB protein levels by Western Blot in various non-tumorigenic and breast cancer cell lines. NT=non-tumorigenic, BC-L=breast cancer luminal, BC-B=breast cancer basal. (b) Examination of endogenous LACTB protein levels (brown) by immunohistochemistry in a panel of 714 clinically-defined human breast cancer samples. Scores 2 & 3 represent LACTB staining that was considered normal (not downregulated), while scores 0 & 1 represent LACTB staining that was considered downregulated. (c) Detection of endogenous LACTB expression levels (brown) by immunohistochemistry in human breast cancer tissue sections. Shown is the amount of LACTB in normal mammary gland and in the adjacent neoplastic mammary gland. DCIS=ductal carcinoma in situ; Invasive=invasive carcinoma (red circles), M=macrophages (yellow circles); BV=blood vessel.

Figure 2: LACTB-induced effects on proliferation of breast cancer cells.

(a) Proliferation rates of non-tumorigenic (HME, MCF10A, BJ-1) and tumorigenic (HMLER, MCF7ras, HCC1806) cell lines in the presence and absence of induced LACTB. Doxycycline was added to all cells. Three independent experiments were performed. (b) DNA synthesis was measured by EdU incorporation and by flow cytometry in non-tumorigenic (HME, MCF10A, BJ-1) and tumorigenic (HMLER, MCF7ras, HCC1806) cell lines in the presence and absence of induced LACTB. Numbers within the graphs represent percentages of gated cells. Doxycycline was added to all cells. The experiment was repeated twice. (c) Induction of LACTB in formed MCF7ras tumors *in vivo*. Control and Tet/ON LACTB MCF7ras cell were injected (10^5 cells per injection) into fat pads of female NOD/SCID mice. When the tumors reached approximately 10mm in diameter

doxycycline was added to both groups and tumor growth rate was monitored *in vivo* by whole mouse imaging and tumor measurements. P value < 0.05 is considered significant. The experiment was performed 3 times. (d) LACTB induction in formed HCC1806 and HMLER tumors *in vivo*. Tet/ON LACTB cells were injected (10^5 cells per injection for HCC1806 cells and 10^6 cells per injection for HMLER cells) into fat pads of female NOD/SCID mice. When the tumors reached approximately 5mm in diameter, mice were randomly divided into two groups and doxycycline was added to one group. *In vivo* whole mouse images are shown for HCC1806 tumors. Tumor weight and number of resulting tumors was measured at 3 weeks of doxycycline treatment. P values < 0.05 are considered significant. (e) Immunofluorescence analysis of tissue sections of control and Tet/ON LACTB MCF7ras tumors with 1 week (Tet/ON LACTB) or two weeks (control and Tet/ON LACTB) of doxycycline induction. Tissues were stained with the cell proliferation marker KI-67 (green), LACTB (red), and DAPI (blue). In the middle panel, where LACTB was induced in MCF7ras tumors for 1 week, a representative image was chosen that shows the two adjacent fields in one tissue section. In one field, LACTB was up-regulated and in the other it was not, allowing for the direct comparison of the mutually exclusive effects of LACTB induction on KI-67 staining and thus cancer cell proliferation. Scale bar 30μm.

Figure 3: Collaboration between down-regulated LACTB and oncogene expression in cellular transformation.

(a) Immunoblotting of endogenous LACTB protein in HME cells transduced with different short hairpin (sh) RNA vectors directed against LACTB. Non-tumorigenic HME cells are included as a positive control and tumorigenic HMLER cells as a negative control for LACTB expression. Highlighted in red are two shRNAs directed against LACTB that were selected for further study. (b)

Proliferation rates of control HME cells and HME cells transduced with different shRNA vectors directed against LACTB. (c, d, e) Tumor incidence was monitored, by *in vivo* imaging, in non-tumorigenic control HME cells and in HME cells transduced with shLACTB vectors (L-3 or B-3) with or without concominant expression of *H-RAS* (G12V)(c), *c-MYC* (T58A)(d) or wild type human *Her2*(e) oncogene. Mice were monitored 6, 9 and 12 weeks post-injection. IN=small indolent tumors which spontaneously regressed.

Figure 4: LACTB-induced effects on cancer cell differentiation.

(a) Levels of marker of stem cells (CD44) and markers of epithelial differentiation (CD24, EPCAM) by flow cytometry in control tumorigenic HMLER and control non-tumorigenic HME cells and in HMLER and HME cells, in which LACTB was induced for 3 days or two weeks. Doxycycline was added to all cells. Numbers within the graphs represent percentages of gated cells. (b) qRT-PCR analysis of relative mRNA levels of mesenchymal, stem cell and epithelial markers in tumorigenic HMLER and non-tumorigenic HME cells in which LACTB was induced for 3 days or two weeks. All the values are relative to control HMLER or HME cells in which LACTB was not induced. Doxycycline was added to all cells. GAPDH expression was used as a normalization control. (c) Immunofluorescence staining of control HMLER cells and HMLER cells in which LACTB had been induced for 2 weeks. Cells were stained with antibodies directed against epithelial markers: E-cadherin (white), β-catenin (white), cytokeratin 8 (CK8, white); mesenchymal markers: vimentin (white), fibronectin (white), stem cell marker Zeb1 (white) and DAPI (blue). Scale bar 30μm. (d) Frequency of cancer stem cells in control HMLER cells and in HMLER cells in which LACTB was induced *in vitro* for two weeks and displayed a more differentiated phenotype (Tet/ON LACTB diff). Cells were injected in limiting dilutions ($1x10^6$, $5x10^5$, $1x10^5$) into fat pads of female

NOD/SCID mice. 8 weeks post-injection mice were euthanized and tumor frequency and tumor diameter calculated and measured. Diameters of tumors arising in $1x10^6$ group are shown. $p<0.05$ is considered significant. (e) Cancer-stem cell enriched population of HMLER-Tet/ON LACTB cells was isolated by flow cytometry based on their $CD44^{high}CD24^{low}$ expression profile. Two single cell clones were prepared from this population and treated with doxycycline to induce LACTB expression or left untreated. Their growth and morphology were monitored by live time lapse imaging. Shown is a representative image of clone n.1. Movies of clones n.1 and n.2 are shown in supplemental material. Scale bar 200µm. $1x10^6$of control HMLER-$CD44^{high}$/$CD24^{low}$ cells and HMLER-CD44+ cl.1 and cl.2 cells in which LACTB was induced for 2 weeks were injected into fat pads of female NOD/SCID mice. 8 weeks post-injection mice were euthanized and tumor frequency calculated.

Figure 5: LACTB-induced changes in mitochondrial phospholipids.

(a,b) Liquid chromatography-tandem mass spectrometry analysis of mitochondrial lipid content of control HME (a) and control MCF7ras (b) cells, as well as HME-Tet/ON LACTB (a) and MCF7ras-Tet/ON LACTB (b) cells. All cells were treated with doxycycline for 24 h. Red dots depict the presence of lysophosphatidylethanolamines (LPEs), blue dots the presence of other lysophospholipids such as lysophosphatidylcholines and lysophosphatidylinositols. Green dots show the presence of phosphatidylethanolamines (PEs). The blue perforated line shows the p value of 0.05. Signals above this line have $p<0.05$. The experiment was repeated twice. (c) Proliferation rates of MCF7ras and MCF7ras-Tet/ON LACTB cells in the presence of doxycycline with or without supplementation with 20µM lysophosphatidylethanolamine (LPE). Images are of MCF7ras-Tet/ON LACTB cells in which LACTB was not induced or induced by addition of doxycycline for 3 days

with or without supplementation of growth media with 20μM lysophosphatidylethanolamine (LPE). The experiment was repeated twice. Scale bar 200μm. (d) Measurement of new DNA synthesis (through EdU incorporation) by flow cytometry in control MCF7ras-Tet/ON LACTB cells (absence of doxycycline) and MCF7ras-Tet/ON LACTB cells in which LACTB was induced by addition of doxycycline for 1 or 3 days with or without supplementation of growth media with 20μM lysophosphatidylethanolamine (LPE). (e) LEFT: Control MCF7ras cells and MCF7ras-Tet/ON-LACTB cells were treated with doxycycline for 6 days in the presence or absence of 20μM LPE and level of the CD24-differentiation marker was measured by FACS. RIGHT: Control HMLER cells (without doxycycline addition) and HMLER-Tet/ON-LACTB cells (with 9 days of doxycycline addition) were incubated in the presence or absence of 20μM LPE and level of the CD24-differentiation marker was measured by FACS.

Figure 6: The role of phosphatidylserine decarboxylase (PISD) in LACTB mechanism. (a) Western blot analysis of control MCF7ras cells and MCF7ras-Tet/ON LACTB-expressing cells in which doxycycline (DOX) had been added to both groups for 24 h. The cells were sub-fractionated into cytosolic and mitochondrial fractions. Mitochondrial membranes were probed for enzymes involved in mitochondrial lipid metabolism (PGS1, PGP, PISD). The membranes were also immunoblotted for LACTB (to show induction and mitochondrial localization of LACTB), actin (cytosolic marker) and COX4 (mitochondrial marker). (b) MCF7ras cells and MCF7ras-Tet/ON LACTB cells were incubated in the presence of doxycycline for 48 h. [^{3}H]serine-containing media was then added for 2, 4 or 6 h and the conversion of PS into PE was monitored by scintillation counting. The experiment was performed in triplicate. P value<0.01 is considered significant. (c) MCF7ras cells were transfected for two days with control siRNA, as

well as 4 different PISD-directed siRNAs or left untreated. The proliferation ability of the cells was measured by EdU staining using FACS. (d) Control MCF7ras and MCF7ras-Tet/ON-LACTB cells were treated with doxycycline for 2 days with or without concominant transfection with 4 different PISD siRNAs. The proliferation ability of the cells was measured by EdU staining using FACS. The rectangle represents the gate containing proliferative cells. (e) Peptides of indicated amino-acid compositions fused to a quenched fluorescent tag (AMC) were incubated in the presence or absence of recombinant LACTB. Only peptides that were cleaved by LACTB activated the fluorescent tag. Fluorescence absorbance was monitored over time as a measure of active peptidase activity of LACTB. (f) Western blot analysis of PISD levels in mitochondria isolated from a panel of control and Tet/ON LACTB non-tumorigenic (HME and MCF10A) and tumorigenic (HMLER, MCF7ras, HCC1806, SUM149, HS578t, HCC38) cell lines to which doxycycline had been added for 24 h.

Extended Data Figure 1: Identification of potential tumor suppressors.

(a) Light microscope images of undifferentiated and differentiated human muscle progenitor cells and mouse C2C12 muscle progenitor cells. Scale bar 200μm. (b) Immunofluorescence analysis of mouse C2C12 cells undergoing differentiation. Cells were stained with marker of skeletal muscle differentiation α–actinin (green), actin-staining agent phalloidin (red) and DAPI (blue). Scale bar 30μm. (c) qRT-PCR analysis of relative expression levels of a panel of known tumor suppressors and cell-cycle inhibitors in differentiated human skeletal muscle cells. All the values are relative to undifferentiated human skeletal muscle progenitor cells. GAPDH expression was used as a normalization control. Experiment was performed in duplicate. (d) Microarray analysis of undifferentiated (UD) and differentiated (D) skeletal muscle cells of human and mouse origin

($p<0.01$, fold change>2). Fold change and p value are shown for five factors that were further chosen for functional validation for tumor-suppressive ability. (e) qRT-PCR analysis of mRNA levels of several genes from microarray analysis in differentiated human skeletal muscle cells. All the values are relative to undifferentiated human skeletal muscle progenitor cells. GAPDH expression was used as a normalization control. Experiment was performed in duplicate. (f) Light microscope images of control MCF7ras cells and MCF7ras cells transduced with five doxycycline-inducible factors in the absence or presence of doxycycline (DOX). Images were taken after 12 days of DOX treatment in all groups except for the LACTB cells which were treated for 6 days with DOX. Scale bar 200μm.

Extended Data Figure 2: LACTB expression in normal and neoplastic cells.

(a) qRT-PCR analysis of endogenous LACTB mRNA levels in non-tumorigenic (HME, MCF10A) and neoplastic breast cell lines. All values are relative to those in the non-tumorigenic human mammary epithelial cell line (HME). GAPDH expression was used as a normalization control. Experiment was performed in duplicate. (b) Immunofluorescence staining of LACTB expression in non-tumorigenic (MCF10A) and tumorigenic (MCF7ras) cell lines. Cells were stained with mitochondrial marker (green), LACTB (red) and DAPI (blue). The experiment was performed in triplicate. Scale bar 30μm. (c) Detection of endogenous LACTB protein levels (brown) by immunohistochemistry in normal human mammary glands. (d) Stratification of low and high levels of LACTB in human breast cancer clinical samples of different grade, size and nodal stage. (e) Immunoblotting of exogenous LACTB protein in control cells (C) and cells in which LACTB was induced by doxycycline (DOX) for 2 days (L). GAPDH was used as a normalization control. (f) Measurement of apoptosis through AnnexinV staining and flow cytometry in non-tumorigenic (HME) and tumorigenic (HMLER, MCF7ras, HCC1806) cell lines in the presence and absence of

induced LACTB. Doxycycline was added to all cells. Numbers within the graphs represent percentages of gated cells. (g) Immunofluorescence analysis of control MCF7ras cells mixed with MCF7ras-Tet/ON LACTB cells, in which LACTB was induced for 3 days. Cells were stained with antibodies against the proliferation marker KI-67 (green), LACTB (red), and DAPI (blue). Note the mutually exclusive KI-67 and LACTB staining in these cells; cells in which LACTB was induced do not express KI-67. Doxycycline was added to all cells. Scale bar 30μm.

Extended Data Figure 3: LACTB-induced effects on proliferation of breast cancer cells.

(a) Proliferation curves of control MCF7ras and HMLER cells, and MCF7ras and HMLER cells over-expressing wild type (wt) and R469K LACTB. (b) Proliferation curves of SUM159 and MDA-MB-231 cells with or without exogenous wild type LACTB over-expression. (c) Immunofluorescence analysis of tissue sections of MCF7ras, and MCF7ras-Tet/ON LACTB tumors in which doxycycline (DOX) was added to both groups for 1 or 2 weeks. Tissues were stained with antibodies against a marker of apoptosis (cleaved caspase 3, CCP3, white), and DAPI (blue). Staining was quantified in 8-15 images for each group. “ns” not significant, “*”significant ($0.05 > p > 0.01$), “***”very significant ($p < 0.01$). Scale bar 30μm. (d) H&E staining of MCF7ras, HCC1806, and HMLER tumors without or with 2- or 3- weeks of *in vivo* LACTB induction. Scale bar 200μm.

Extended Data Figure 4: Collaboration between down-regulated LACTB and oncogene expression in cellular transformation.

(a) qRT-PCR analysis of mRNA levels of endogenous LACTB in control HME cells and in HME cells expressing different LACTB-directed shRNA vectors. GAPDH expression was used as a normalization control. (b) Western Blot analysis of H-Ras expression levels in HME-derived cell lines compared to control HME cells. GAPDH expression was used as a normalization control. (c) qRT-PCR analysis of mRNA levels of endogenous LACTB and exogenous c-myc (T58A) and wild type human HER2 levels in HME-derived cell lines compared to control HME cells. GAPDH expression was used as a normalization control.

Extended Data Figure 5: LACTB-induced effects on HMLER cell differentiation.

(a) Light microscope images of control HMLER and HME cells and HMLER and HME cells in which LACTB was induced with doxycycline for 3 days or 2 weeks. Scale bar 200μm. (b) Proliferation curves of control HMLER cells and HMLER cells in which LACTB was induced and that displayed more differentiated features. (c) Time lapse images of HMLER-Tet/ON LACTB $CD44^{high}CD24^{low}$ single cell clone 2 with (+DOX) or without (NO DOX) LACTB induction. Scale bar 200μm. Movies of clones n.1 and n.2 are shown in supplemental material.

Extended Data Figure 6: LACTB-induced effects on MCF7ras cell differentiation.

(a) Light microscope images of control MCF7ras cells and two independently derived MCF7ras bulk populations that survived 2-weeks long LACTB induction and re-entered their proliferation cycle (LACTB survivor 1 and 2). LACTB survivor cells displayed more epithelial-like, differentiated morphology, characterized by tight cobblestone epithelial features. Scale bar 200μm. (b) Flow cytometry analysis of levels of the epithelial differentiation marker (CD24) in control MCF7ras cells,

MCF7ras cells in which LACTB was induced for 3 days and two independently derived MCF7ras bulk populations that survived 2-weeks long LACTB induction and re-entered their proliferation cycle (LACTB survivor 1 and 2). (c) Proliferation curves of control MCF7ras cells and two independently derived MCF7ras bulk populations that survived 2-weeks long LACTB induction and re-entered their proliferation cycle (LACTB survivor 1 and 2). (d) Quantification of *in vitro* tumor sphere formation of control MCF7ras cells and two independently-derived MCF7ras-LACTB survivor populations. Scale bar 200μm. (e) *In vivo* tumor formation and cancer stem cell frequency of control MCF7ras cells and two independently-derived MCF7ras-LACTB survivor populations. Cells were injected at limiting dilutions ($1x10^3$, $1x10^2$) into fat pads of female NOD/SCID mice and tumor formation was monitored by *in vivo* imaging 8-weeks post-injection. (f) Western blot analysis of endogenous LACTB levels in bulk HME cells and in HME cells that were separated into stem-cell-enriched $CD44^{high}CD24^{low}$ and differentiated $CD44^{low}CD24^{high}$ populations. (g) Western blot analysis of endogenous LACTB levels in mesenchymal stem cells (MSCs) and their differentiated osteocytic derivatives. Of note, the efficiency of osteocytic differentiation was around 40%.

Extended Data Figure 7: LACTB-induced effects on mitochondrial functions.

(a) Measurements of ATP levels in control MCF7ras cells and MCF7ras-Tet/ON LACTB cells, where doxycycline was either not added or added for short term (6, 12 or 24 hours) or longer term (3 and 6 days) time points. (b) Measurements of ROS levels by flow cytometry in MCF7ras-Tet/ON LACTB cells with (6 hrs, 1 day, 5 days) or without DOX induction. Numbers within the graphs represent percentages of gated cells. (c) Measurements of mitochondrial membrane potential, through incorporation of cyanine dye $DiIC_1(5)$, by flow cytometry in control MCF7ras cells and MCF7ras-Tet/ON LACTB cells, where doxycycline was either not added or added for 1 day or 3 days.

Numbers within the graphs represent percentages of gated cells. (d) Immunofluorescence analysis of control MCF7ras cells mixed with MCF7ras-Tet/ON LACTB cells, where LACTB was induced by addition of doxycycline for 1 day. Cells were stained with mitochondrial marker (green), LACTB (red), and DAPI (blue). Mitochondrial signal per area in control cells (n=16) and in LACTB-expressing cells (n=17) was calculated by ImageJ software. p value > 0.05 is considered not significant. Scale bar 30μm. (e) Western blot analysis of control MCF7ras cells and MCF7ras-Tet/ON LACTB cells where doxycycline was added for 24 hours to both groups and cells were then sub-fractionated into cytosolic and mitochondrial fractions. Membrane was probed for proteins involved in mitochondrial fusion (Opa1, Mfn1, Mfn2), fission (Fis1, Drp1), composition of respiratory chain (individual OXPHOS components) and control antibodies: LACTB (to show the proper induction and localization of LACTB), actin (cytosolic marker) and COX4 (mitochondrial marker). The membrane in this Extended Data Figure was also used in Fig. 6a, where it was probed with different set of antibodies. Therefore the signal for the control antibodies is shared between these two Figures.

Extended Data Figure 8: LACTB-induced changes in mitochondrial phospholipids.

(a) Proliferation rates of MCF7ras and MCF7ras-Tet/ON LACTB cells without or with addition of doxycycline and supplementation of growth media with 50μM lysophosphatidylcholine (LPC), 50μM phosphatidylethanolamine (PE) or 50μM phosphatidylglycerol (PG). Experiment was repeated twice. (b) Raw western blot image showing PISD subcellular location and levels in subfractionated MCF7ras and MCF7ras-Tet/ON LACTB cells (related to Fig. 6a). Doxycycline was added to both cell lines for 24 h. (c) qRT-PCR analysis of mRNA levels of LACTB and PISD in control MCF7ras

cells and MCF7ras cells in which LACTB was induced for 3 days. GAPDH expression was used as a normalization control. (d) Western blot analysis of time course of levels of LACTB and PISD in control MCF7ras and MCF7ras-Tet/ON LACTB cells in which LACTB was induced by addition of doxycycline (DOX) for the indicated times. In control MCF7ras cells doxycycline was added for 3 days. (e) Related to Fig. 6b. MCF7ras cells (C) and MCF7ras-Tet/ON LACTB cells (L) were incubated in the presence of doxycycline for 48 h. [^{3}H]serine-containing media was added for 2, 4 or 6 h. A portion of cell lysate was analyzed by immunoblotting to confirm expression of LACTB, down-regulation of PISD and equal protein levels in the samples (by calnexin). (f) Western Blot analysis of control MCF7ras cells and MCF7ras cells transfected for 48 h with four different PISD-siRNAs.

Extended Data Figure 9: LACTB mutagenesis.

(a) Related to Fig. 6e. Velocity of the ac-YVAD-AMC enzymatic reaction in relation to substrate concentration. (b) Comparison of amino-acid sequence of wild type (wt) LACTB, dS-LACTB and d1-97-LACTB. Only partial sequence of LACTB is shown. The points of mutation of dS- and d1-97 LACTB are highlighted in red and marked by red star symbol. Blue star symbol marks the site of R469K mutation in endogenous LACTB from MCF7ras and SUM159 cells. Green star symbol marks the site of important catalytic motif of LACTB. (c) Immunofluorescence analysis of MCF7ras-Tet/ON dS-LACTB and MCF7ras-Tet/ON d1-97-LACTB cells, where doxycycline was added for 24 hours. Cells were stained with mitochondrial marker (green), LACTB (red), and DAPI (blue). Scale bar 30μm. (d) Western blot analysis of expression levels of LACTB in control MCF7ras cells and MCF7ras-Tet/ON LACTB (wild type, dS, d1-97, dSISK) cells where doxycycline was added for 24 hours. dSISK-LACTB mutant is mutated in catalytic serine and 3 adjacent amino-acids. The

expression level of this mutant was unstable therefore we did not include this mutant in our study. (e) Proliferation rates of control MCF7ras cells and MCF7ras-Tet/ON LACTB (wt, dS, d1-97) cells upon addition of doxycycline for indicated number of days. Pictures were taken at 6 days of doxycycline induction. Scale bar 200μm. (f) Western blot analysis of PISD expression in mitochondria isolated from MCF7ras and MCF7ras-Tet/ON LACTB (wt and dS) cells where doxycycline was added for 24 hours to all groups. (g) Western blot analysis of PISD levels from *in vitro* incubation of permeabilized mitochondria (isolated from MCF7ras cells) with or without recombinant LACTB (isolated from HEK293 cells).

Extended Data Figure 10: Graphical Abstract.

LACTB induction leads to a change in cancer cell state. As such, a proliferative, mainly un-differentiated cancer cell turns into a non-proliferative differentiated cancer cell upon LACTB induction. This is manifested by a disappearance of Ki-67 proliferation marker and CD44 stem-cell marker and increased expression of CD24 and EPCAM differentiated epithelial marker. This is achieved via the ability of LACTB to decrease the protein expression levels of mitochondrial PISD enzyme and the subsequent changes in mitochondrial phosphatidylethanolamine and/or lyso-phosphatidylethanolamine levels.

Fig. 1: LACTB down-regulation in cancer cells

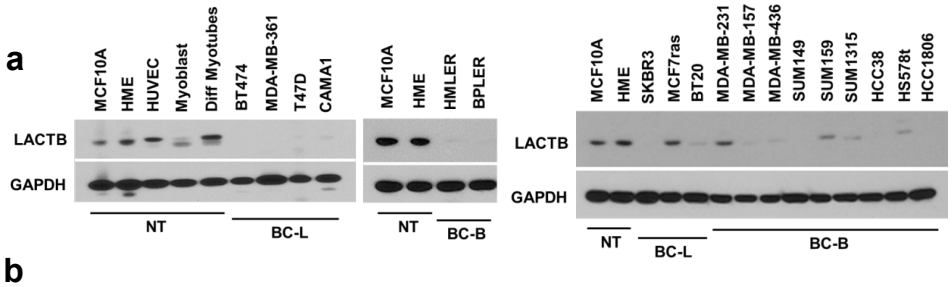

b

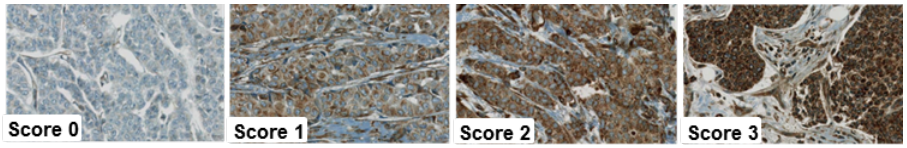

		Luminal A	Luminal B (Her2 negative)	Luminal B (Her2 positive)	Her2 positive (non-luminal)	Triple negative (ductal)	Total
LACTB	no expression or lower than normal (score 0,1)	112	67	25	14	38	256
	normal expression luminal or basal (score 2,3)	217	130	35	23	53	458
Total		329	197	60	37	91	714
Ratio		34%	34%	42%	38%	42%	**36%**

c

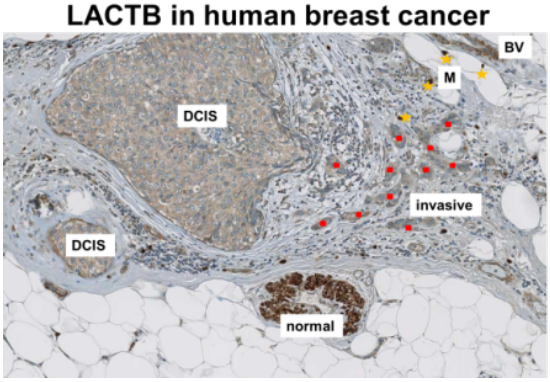

Fig. 2: LACTB-induced effects on proliferation of breast cancer cells

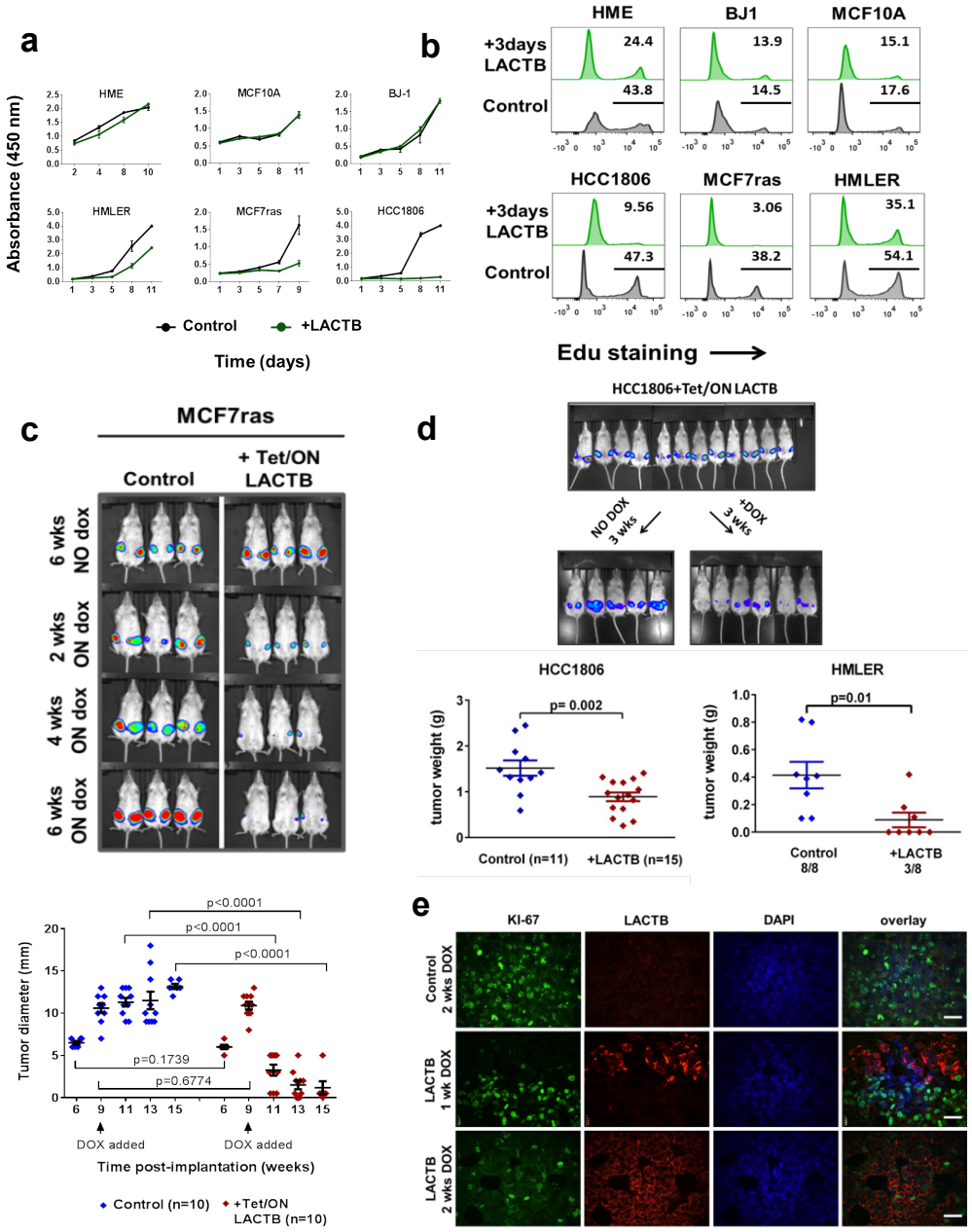

Fig. 3: Collaboration between down-regulated LACTB and oncogene expression in cellular transformation

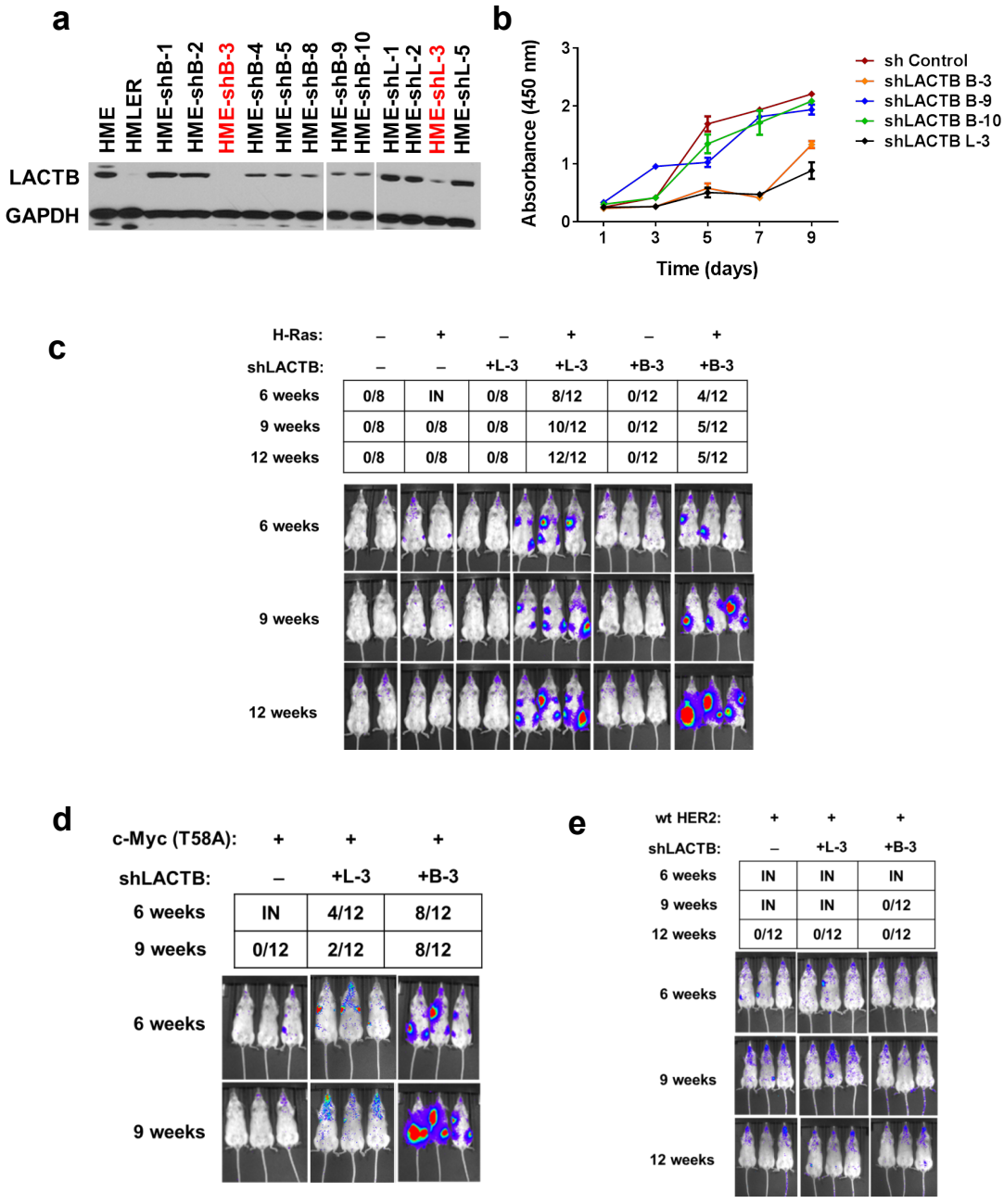

Fig. 4: LACTB-induced effects on cancer cell differentiation

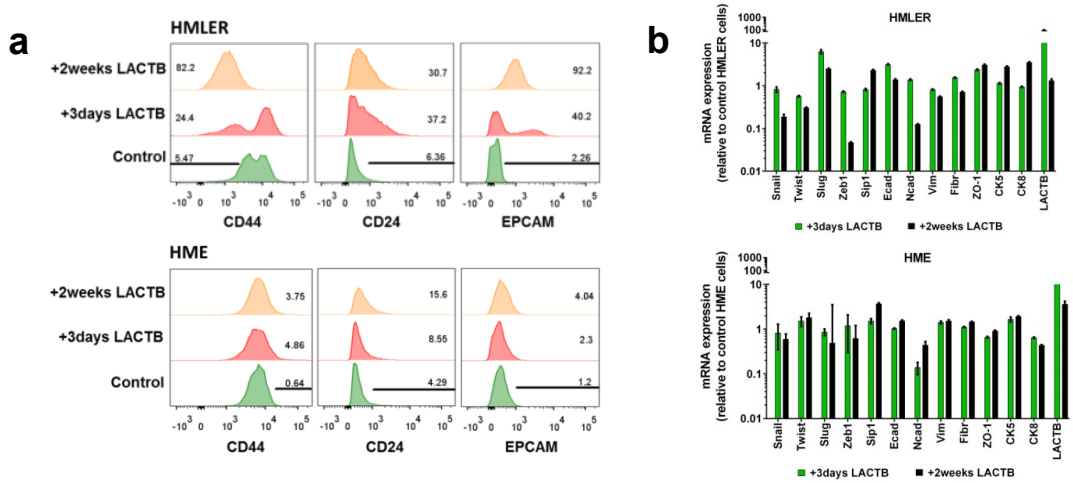

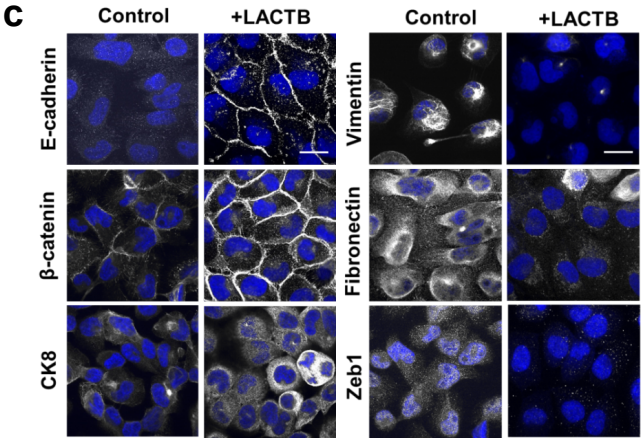

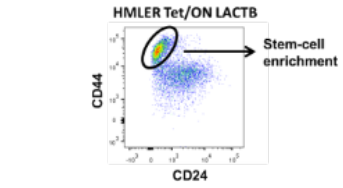

HMLER (Tet/ON LACTB) CD44+ cl.1

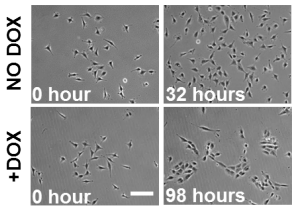

HMLER cells	Control	HMLER-CD44+ cl.1	HMLER-CD44+ cl.2
10^6	8/8	0/8	4/8

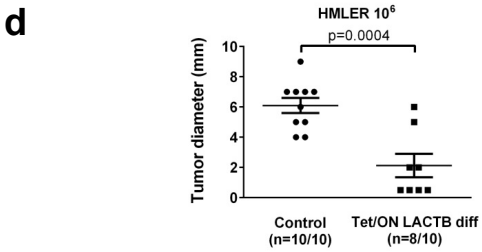

HMLER cells	$1x10^6$	$5x10^5$	$1x10^5$	Cancer Stem Cell frequency
Control	10/10	9/10	4/10	1/201181
Tet/ON LACTB diff	8/10	2/10	0/10	1/1085618

Fig. 5: LACTB-induced changes in mitochondrial phospholipids

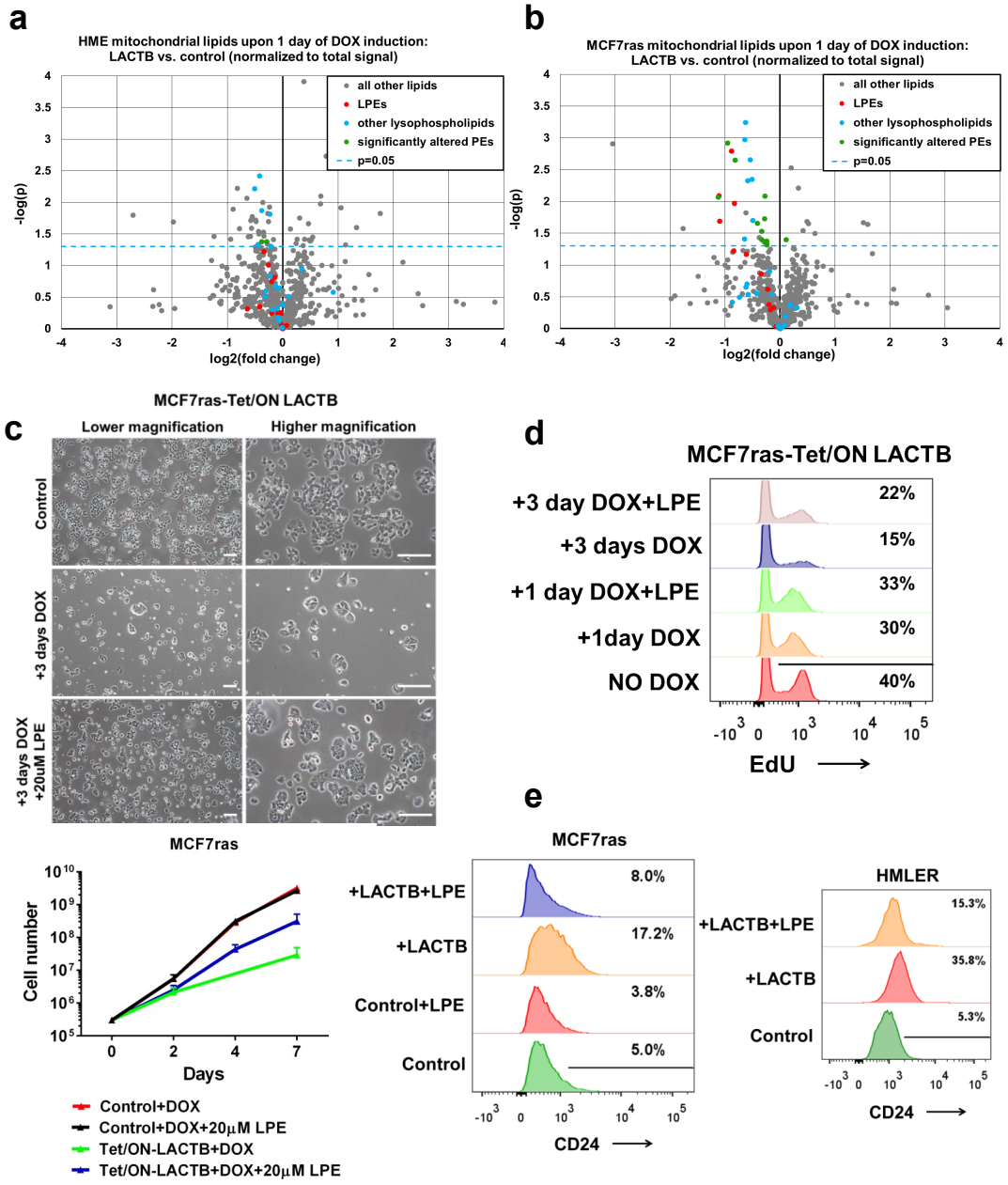

Fig. 6: The role of phosphatidylserine decarboxylase (PISD) in LACTB mechanism

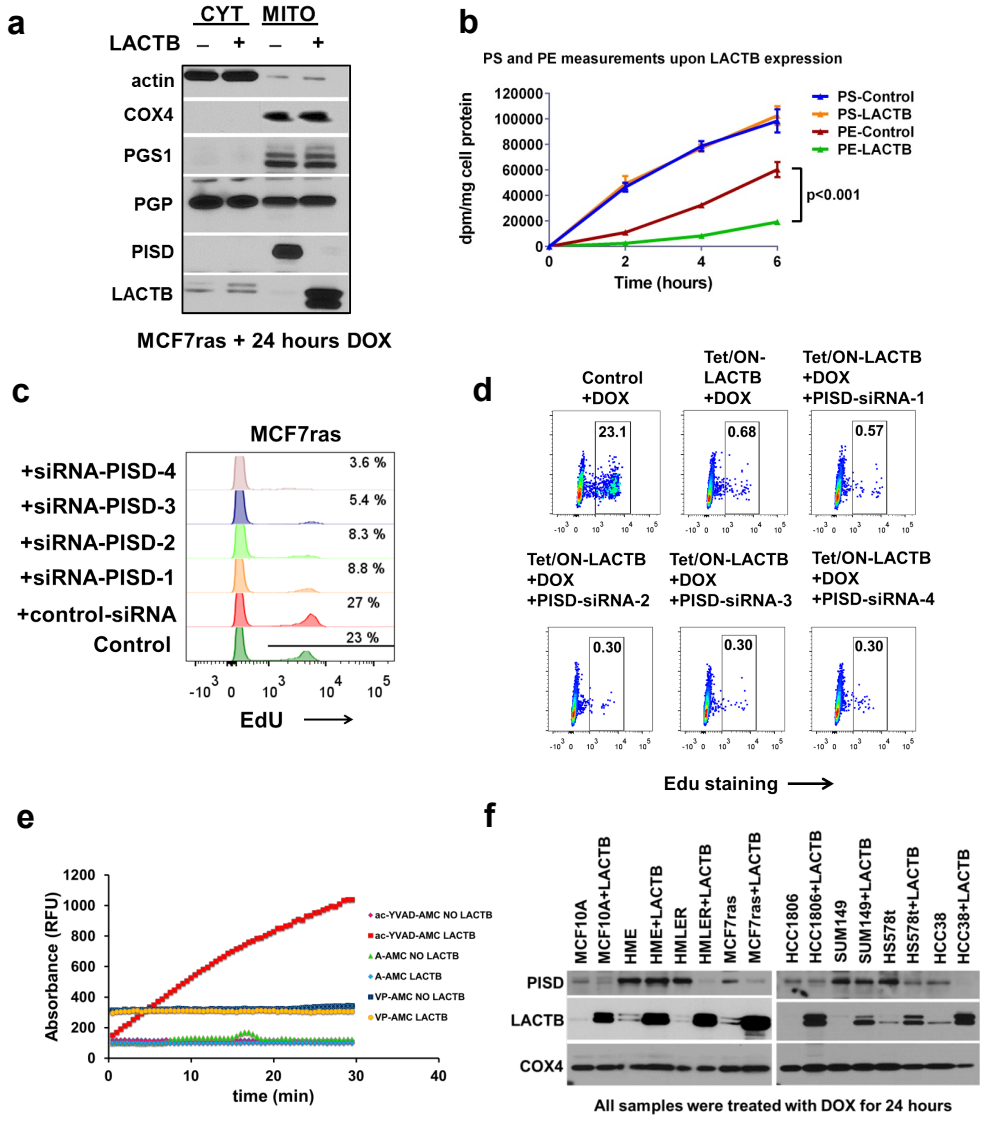

Extended Data Fig. 1: Identification of potential tumor suppressors

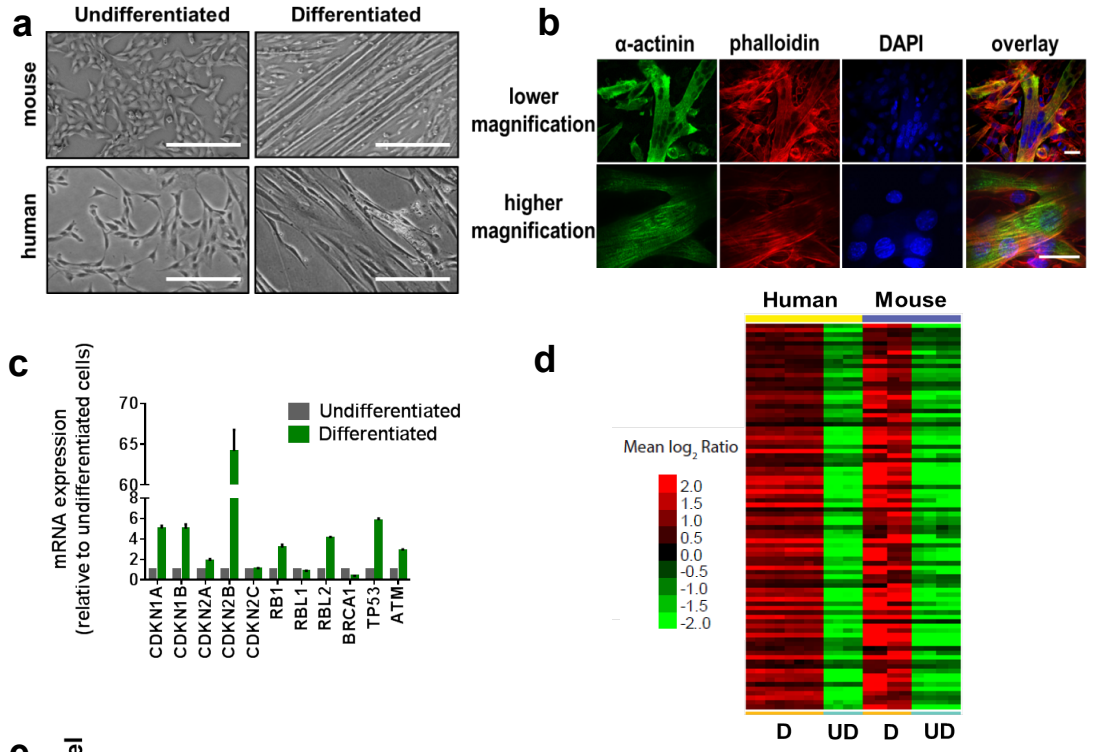

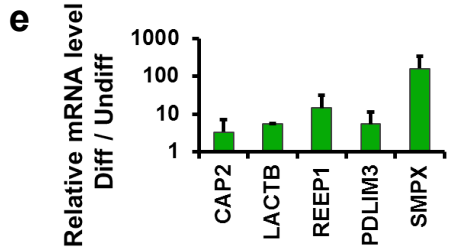

human			mouse		
SYMBOL	log2(D/UD)	pvalue.adj	SYMBOL	log2(D/UD)	pvalue.adj
CAP2	1.925	8.64E-06	**CAP2**	3.181	0.002
LACTB	1.004	6.10E-05	**LACTB**	1.783	0.005
REEP1	1.977	7.63E-05	**REEP1**	4.485	0.009
PDLIM3	2.146	0.0002	**PDLIM3**	4.08	0.003
SMPX	4.024	0.00355	**SMPX**	8.139	0.001

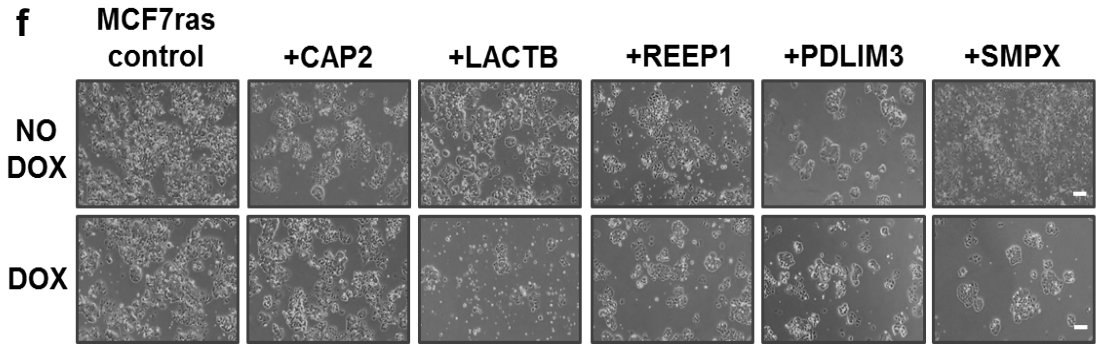

Extended Data Fig. 2: LACTB expression in normal and neoplastic cells

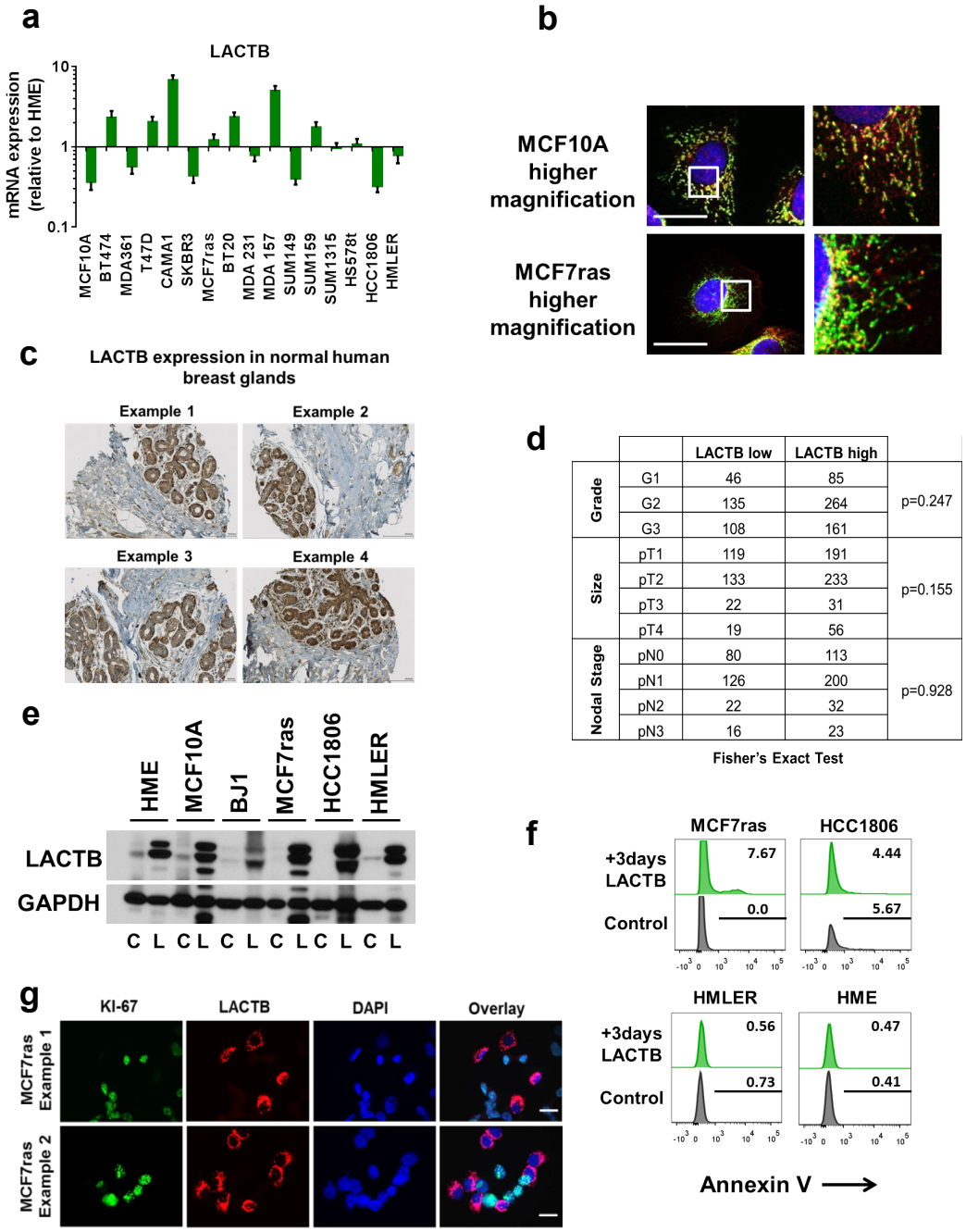

Extended Data Fig. 3: LACTB-induced effects on proliferation of breast cancer cells

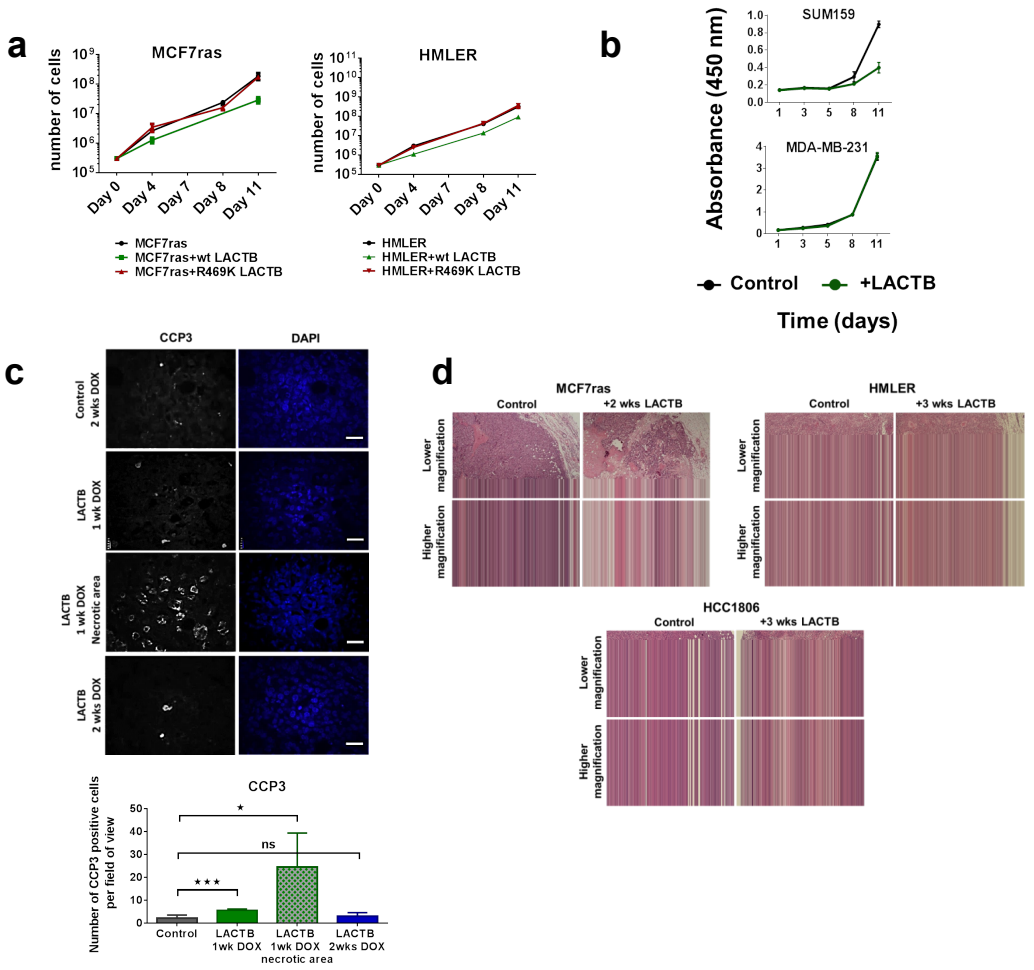

Extended Data Fig. 4: Collaboration between down-regulated LACTB and oncogene expression in cellular transformation

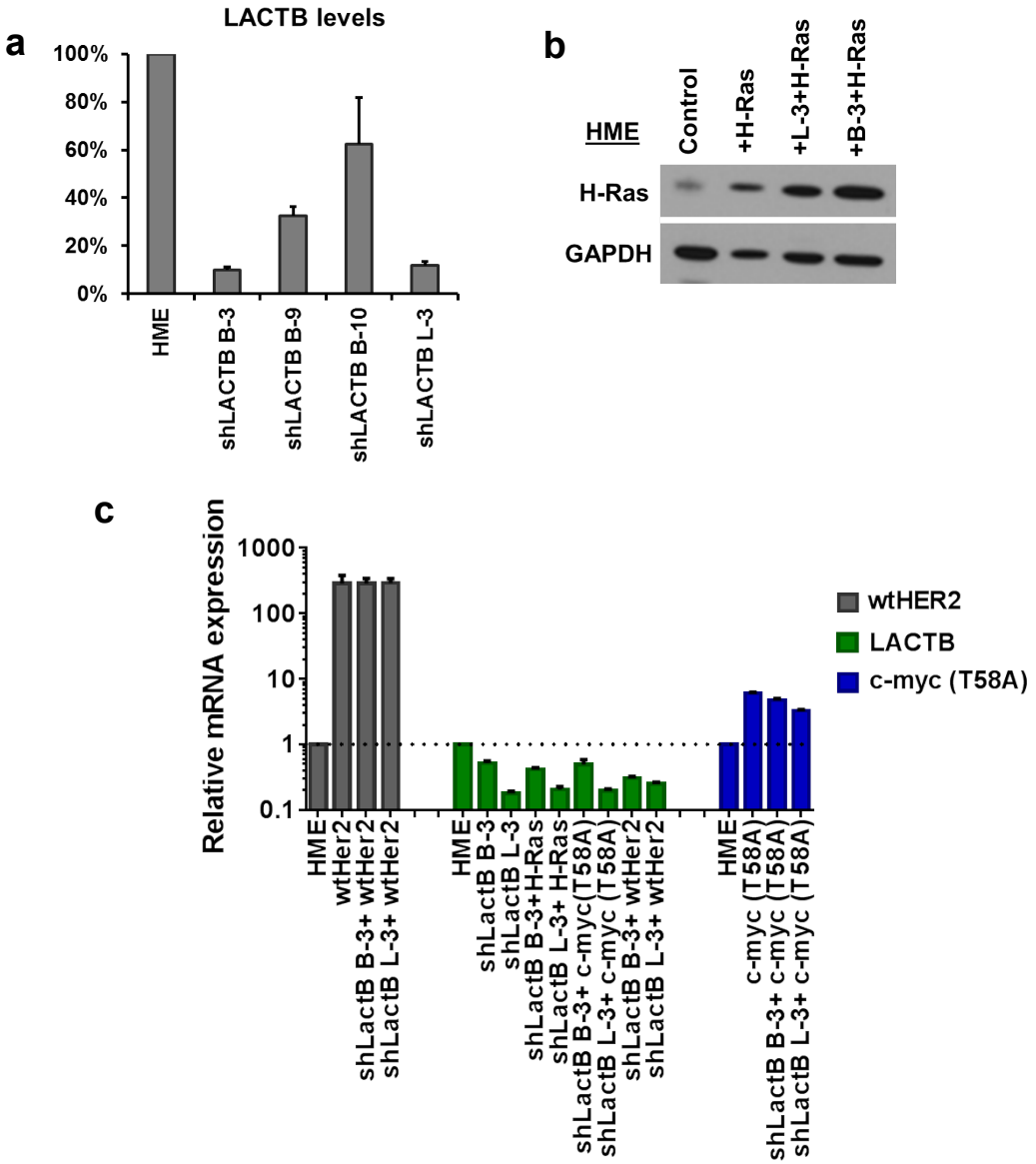

Extended Data Fig. 5: LACTB-induced effects on HMLER cell differentiation

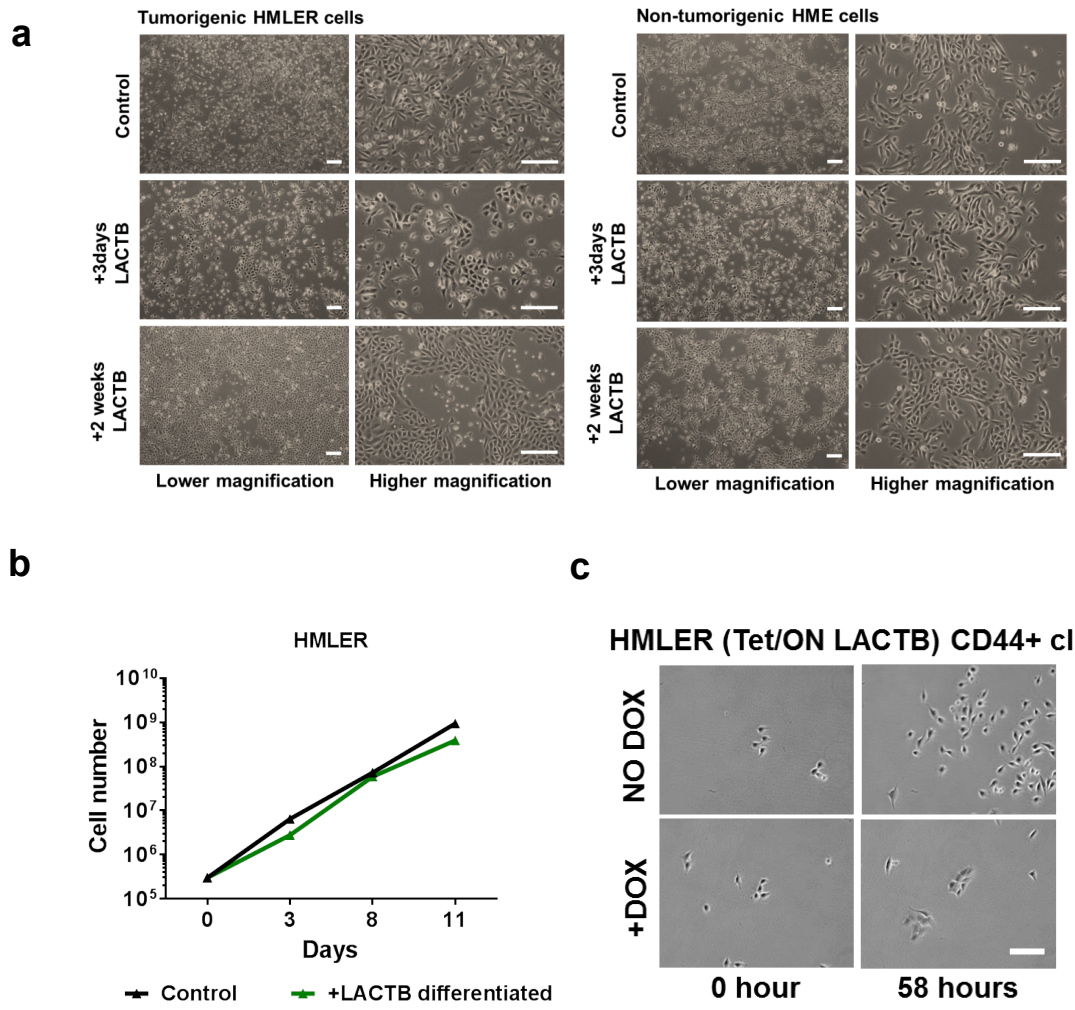

Extended Data Fig. 6: LACTB-induced effects on MCF7ras cell differentiation

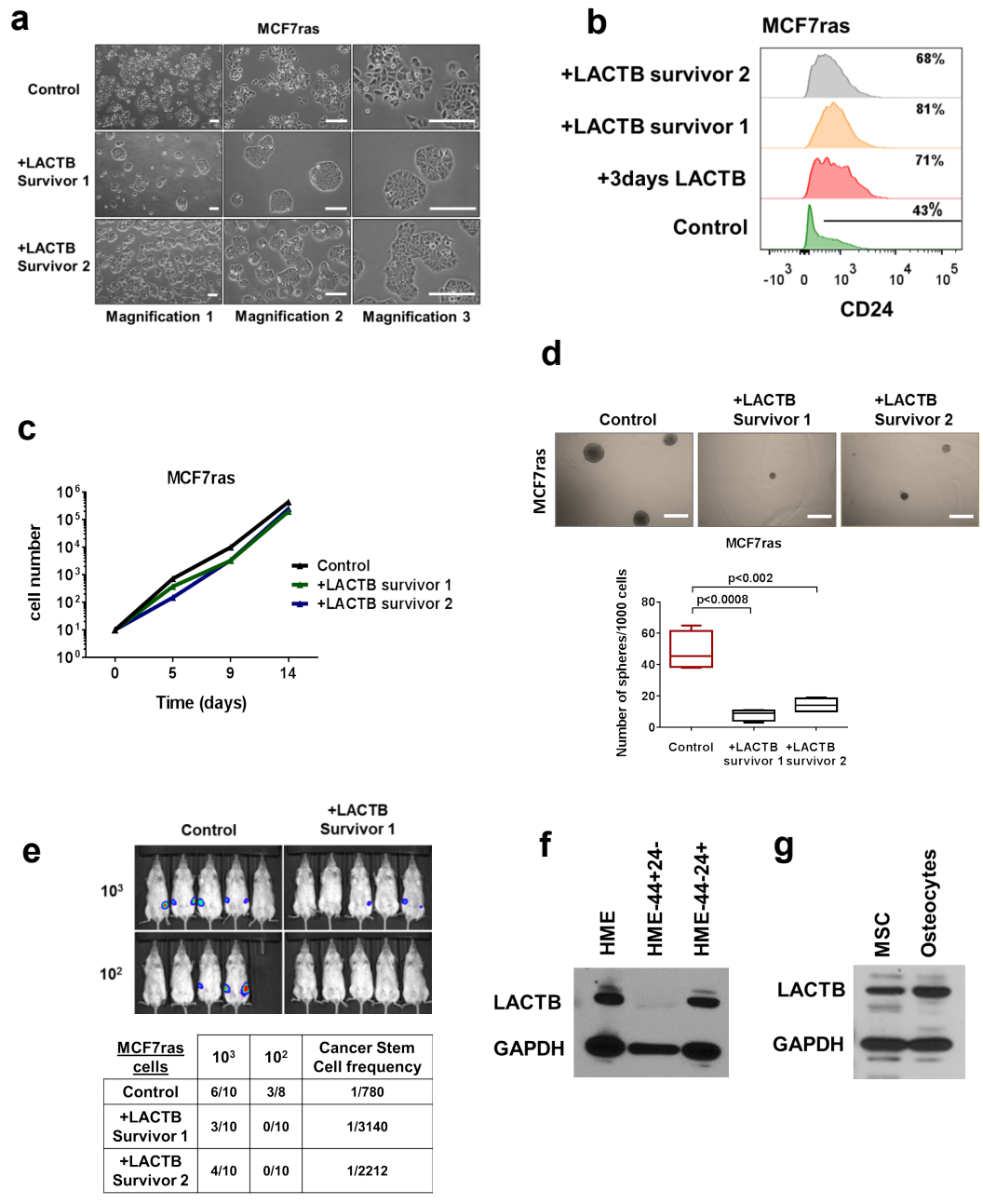

MCF7ras cells	10^3	10^2	Cancer Stem Cell frequency
Control	6/10	3/8	1/780
+LACTB Survivor 1	3/10	0/10	1/3140
+LACTB Survivor 2	4/10	0/10	1/2212

Extended Data Fig. 7: LACTB-induced effects on mitochondrial functions

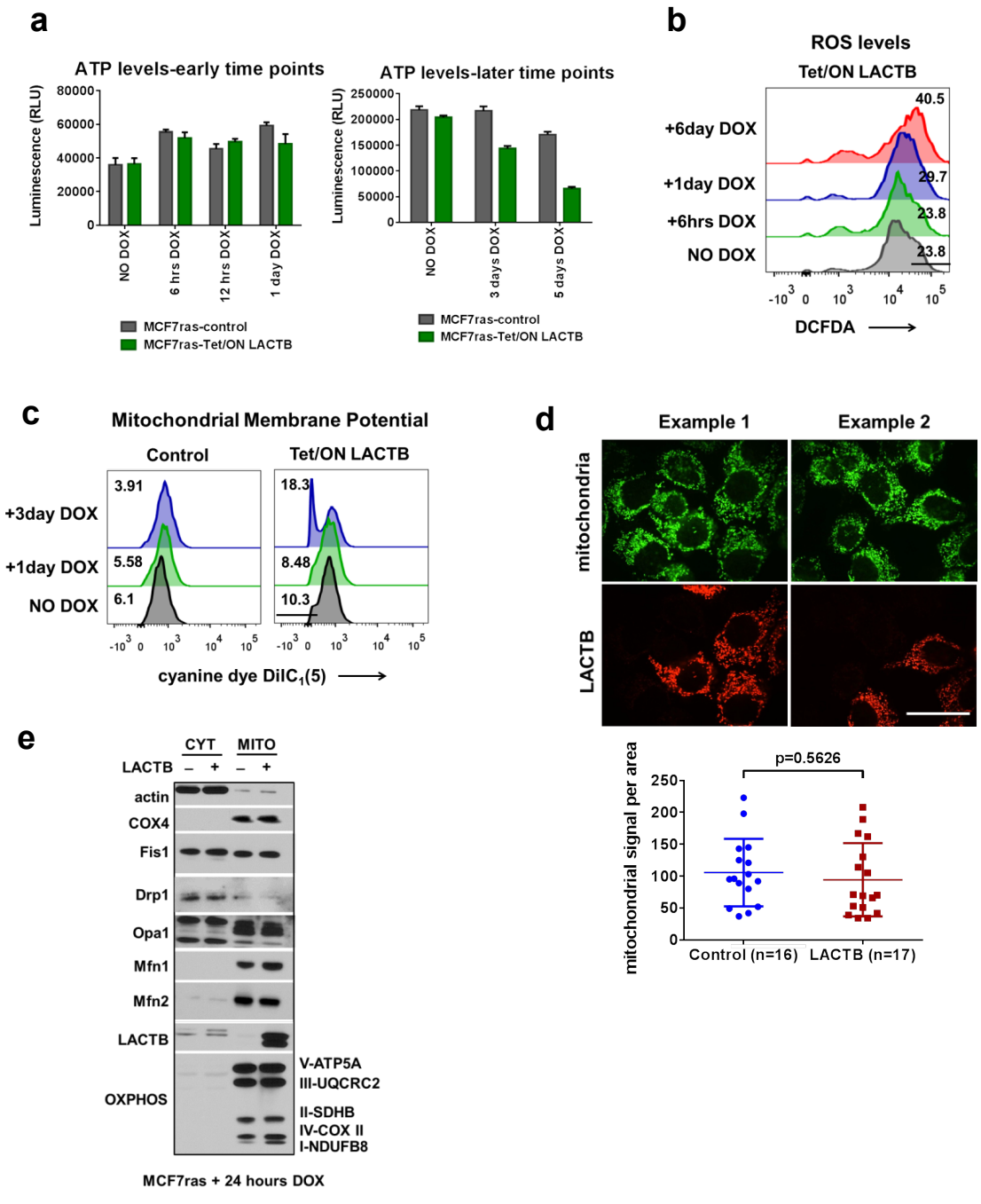

Extended Data Fig. 8: LACTB-induced changes in mitochondrial phospholipids

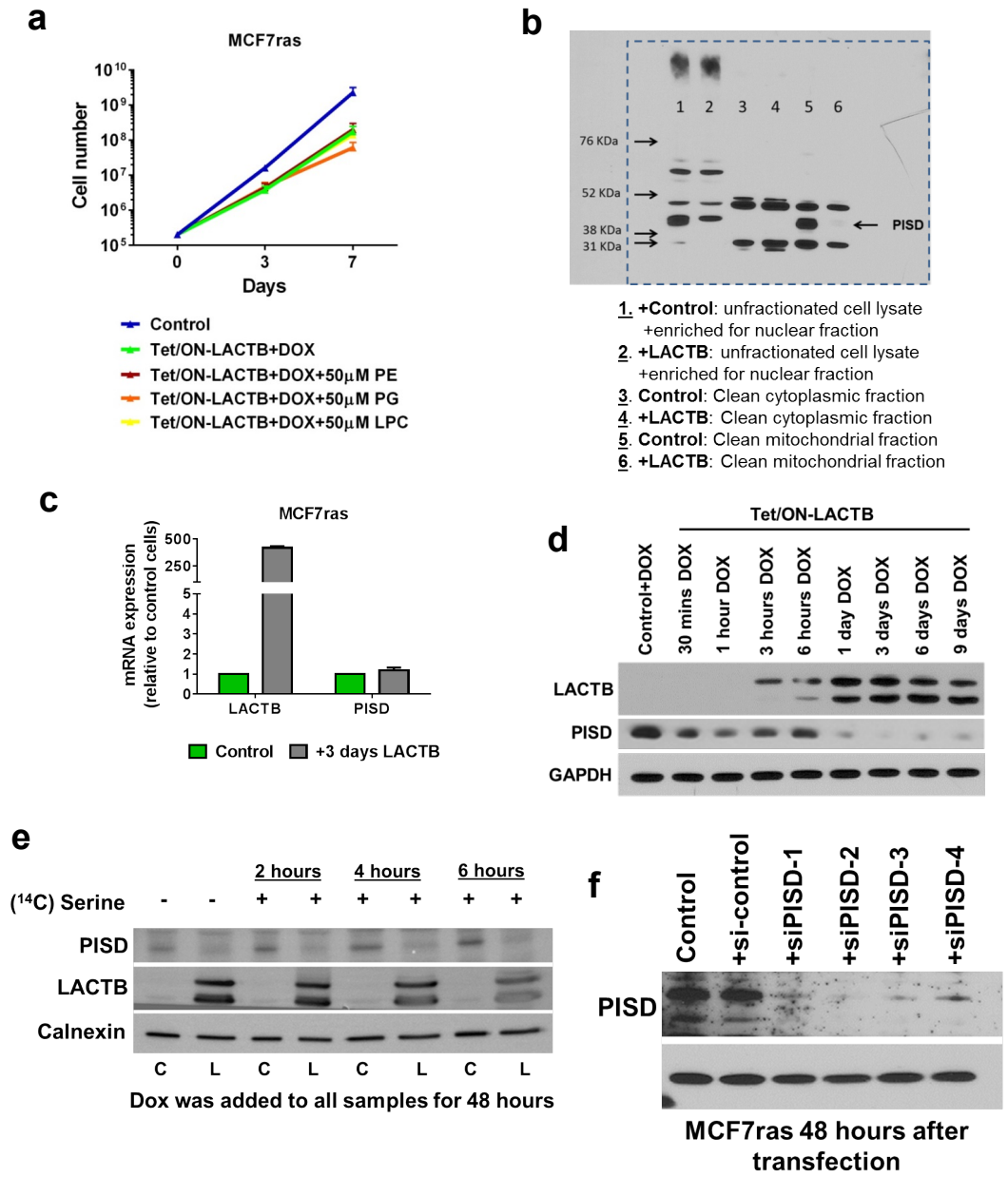

Extended Data Fig. 9: LACTB mutagenesis

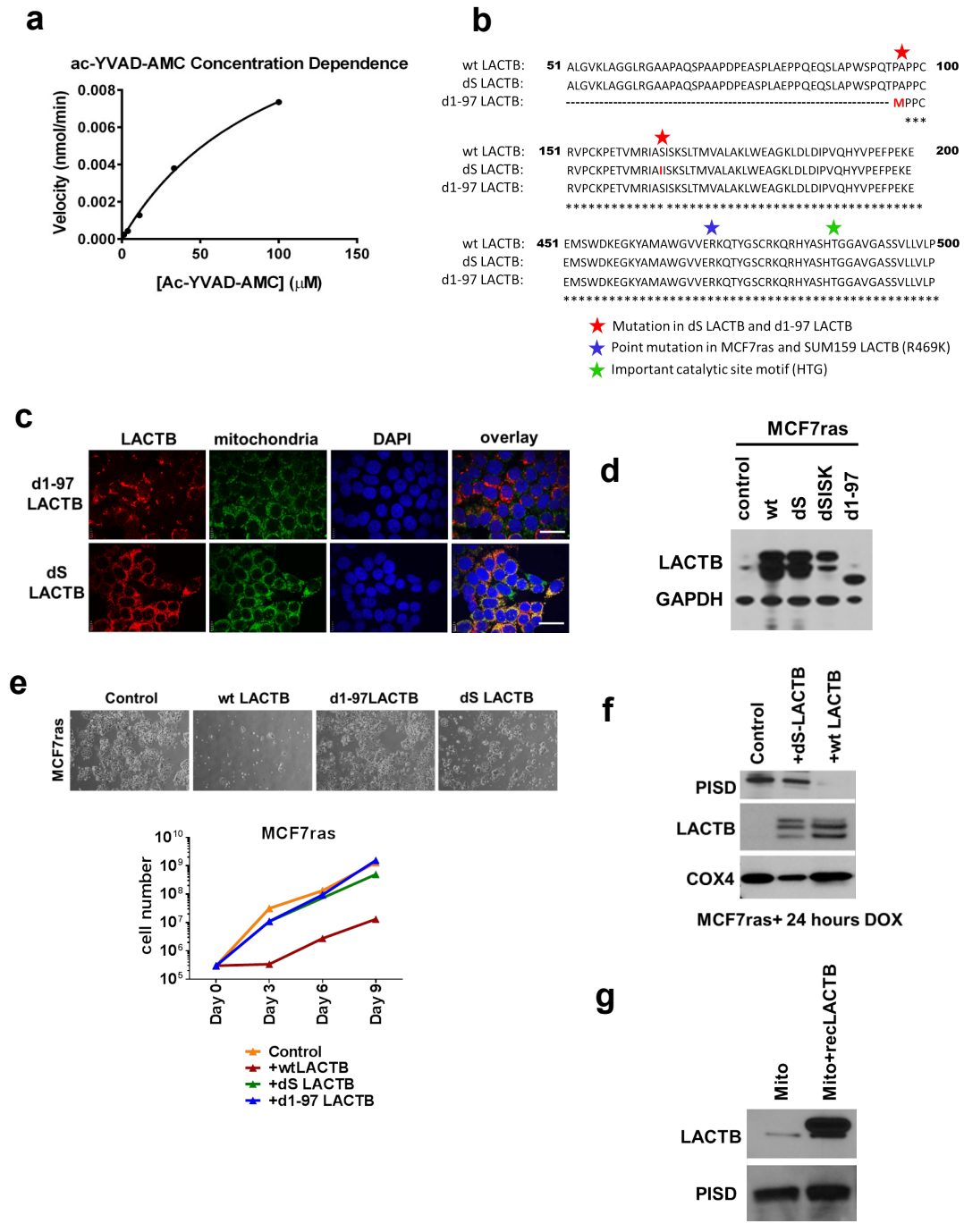

Extended Data Fig. 10: Graphical Abstract